Author/s:
Ing, Keith

Title:
Efficient scheduling for radar resource management

Date:
2019

Efficient scheduling for radar resource management

Keith Ing

ORCID 0000 – 0003 – 1328 – 2118

Submitted in partial fulfilment of the requirements of the degree of

Doctor of Philosophy

Department of Electrical & Electronic Engineering
The University of Melbourne

September, 2020

Abstract

Sensor scheduling and its application in radar has stemmed from the desire to achieve continued improvement in radar capability, particularly for multi-function radar technologies. Adaptive and cognitive radar represent the latest stage in radar evolution, invoking a closed-loop scheduling to replicate the perception-action cycle of cognition. Radar resources are dynamically selected to interrogate the scene before the reflected signals are analysed to inform action in future epochs. Whilst many authors have proposed systems for adaptive and cognitive sensing, the signal processing and computing aspects of modern radar make closed-loop scheduling schemes challenging to realise on the time scales of which radar operates.

This thesis is focused on the implementation aspect of the sensor scheduling problem for radar. The work is presented in three parts that investigate problems related to this issue. In the first part, we consider the linear frequency modulation (LFM) range-Doppler coupling in radar and the associated range bias in measurements using this waveform. A maximum likelihood based estimator that exploits this error is proposed to jointly estimate target range and range-rate using a train of diverse LFM pulses. Efficient methods to select diverse pulse trains based on established adaptive radar waveform cost functions are provided.

Pipeline computing architectures provided by high bandwidth solutions comprising of multiple parallel processors are well suited to complex independent processing applications. Pipeline processing for radar has been previously utilised for computationally intensive applications such as space-time adaptive processing (STAP). In the second problem, we investigate the time costs of radar signal processing and closed-loop sensor scheduling for a knowledge based diversity scheme. A universal cost for the processing and scheduling activities is defined, recognising the delay and subsequent repercussion it can have on the feedback cycle of an adaptive system. We propose two alternate parallel processing architectures that alleviate the narrow time burden between measurement epochs for a sequential feedback loop. The performance degradation of the proposed architectures are investigated in an adaptive radar scenario for various time costs.

Clutter represents the unwanted signals reflected from a radar scene. Efficient clutter modelling is important in implementation of adaptive radar to minimise delay in the target detection process. In the open ocean, sea clutter can be represented using a compound-Gaussian clutter model. In the third problem, we propose a parsimonious parametric model for sea clutter texture that is suitable for high-resolution radar backscatter at low grazing angles in the open ocean. By relating the clutter to its physical source, we exploit spatio-temporal relationships to propose an efficient algorithm for the estimation of the spectral components for the parametric texture model. Validation is performed by comparing the predictive fit for our estimator with a series of temporal estimators and a non-parametric estimator using measured sea clutter data from the Atlantic Ocean.

Declaration

This is to certify that

1. the thesis comprises only my original work towards the PhD,
2. due acknowledgement has been made in the text to all other material used,
3. the thesis is fewer than 100,000 words in length, exclusive of tables, maps, bibliographies and appendices.

Keith Ing

Date

"The life given by us, by nature is short, but the memory of a well-spent life is eternal"

— Marcus Tullius Cicero

Preface

The work in this thesis has been prepared during the course of an approved research program with the following collaborations:

- The work in Chapter 4 was performed under the supervision of Bill Moran and Sofia Suvorova,
- Chapter 5 was carried out under the guidance and oversight of Bill Moran and Robin Evans, and
- Chapter 6 was carried out in collaboration with Bill Moran and Mark Morelande who provided guidance and insight. Work included in this chapter has been published in Ing *et al.* (2016) by IET Radar, Sonar and Navigation on 26 August 2015.

Contributions from the above mentioned collaborators do not exceed 10% of the work in this thesis. All remaining work is the original work of the author alone, except where due acknowledgement has been made. This research was undertaken with support of the Australian Government Research Training Program (RTP) Scholarship, Australian Research Council's *Linkage Projects* funding scheme with industry partner BAE Systems Australia (project number LP120100706) and US Air Force Office of Science Research through AOARD (grant number FA2386-13-1-4080).

Acknowledgements

I received enormous support during the course of this thesis from a number of people to whom I am indebted for their help. Without their assistance and encouragement, I would not have been able to reach this point.

First and foremost, I would like to thank my supervisors, Prof. Bill Moran, Prof. Robin Evans, Dr. Mark Morelande and Dr. Sofia Suvorova for guidance and support through this challenging journey. Their insight and guidance was important in steering the direction of my studies and overcoming crucial hurdles encountered during my candidature.

My loving family, Amanda, Dylan and Bailey who have always provided steadiness during the challenging periods encountered and supported me tremendously throughout the course of my candidature in countless ways, and my parents Frank and Kathy Ing, who remained a foundation for me.

I have met many dedicated students, faculty and staff members who have made my Ph.D. studies a truly memorable experience. I especially grateful to all the students of the Department of Electrical and Electronic Engineering, many who have become close friends during the course of this candidature, provided a pillar of support, a source encouragement and brightened the mood. In no particular order, those who started the journey with me in Walter Boas; Alex Ira, Senaka Samarasekera, Amir Neshastehriz, Laven Soltanian, Michelle Chong, Hasan Arshad Nasir and Muhammad Amjad Raza and those who continued on with me afterwards; Saeed Ahmadizadeh, Omid Monfared, Sasan Gholami, Ehsan Ul Haq, Meraj Ghanbari, David Whittle, Sachintha Karunaratne and Jeffery Spencer.

My current and former work colleagues from BAE Systems Australia who championed and supported me in addition to providing a sounding board for my research, particularly Peter Camilleri, Jerome Vethecan, Adam Billards, Steve Drury, Jon Nasser, Mark Berry, Steve Chapman, Paul Riseborough and Ankit Kaushik. My long-time friends, Adam Pepper and Dave Walls for their light-hearted banter throughout the years and for checking in on me continuously, Ajendra Dwivedi and Rudaba Khan particularly as this thesis was being revised during a difficult period. Finally, Carmel Tom for her moral support, friendship and candour throughout this journey.

Lastly, I wish to acknowledge The University of Melbourne and RMIT University for their support and assistance during my studies.

Contents

List of Figures

List of Abbreviations

AESA Active Electronically Scanned Array

AF Ambiguity Function

AR AutoRegressive

B&B Branch-And-Bound

CCPI Cumulative Coherent Processing Interval

CDAPS Continuous Double Auction Parameter Selection

CFAR Constant False Alarm Rate

CoFAR Cognitive Fully Adaptive Radar

CPI Coherent Processing Interval

CPU Central Processing Unit

CR Cognitive Radar

CRLB Cramér-Rao Lower Bound

CT Coordinated Turn

CV Constant Velocity

CW Continuous Wave

DARPA Defense Advanced Research Projects Agency

EDDB Environmental Dynamic DataBase

EKF Extended Kalman Filter

EM Electromagnetic

ESA Electronically Scanned Array

FAR Fully Adaptive Radar

FFT Fast Fourier Transform

FIM Fisher Information Matrix

FM Frequency Modulation

FrFT Fractional Fourier Transform

GLRT Generalised Likelihood Ratio Test

GNSS Global Navigation Satellite System

HF High Frequency

HMM Hidden Markov Model

i.i.d. Independent and Identically Distributed

ICM Integrated Clutter Measure

IMM Interacting Multiple Model

JDL Joint Directors of Laboratories

KKT Karush–Kuhn–Tucker

KL Kullback-Leibler

LFM Linear Frequency Modulation

LMIPDA Linear Multitarget Integrated Probabilistic Data Association

MAP-PWE Maximum a Posteriori Probability Weighted Eigenwaveform

MDP Markov Decision Process

MF-PWE Match-Filtered Probability Weighted Eigenwaveform

MFR Multi-Function Radar

MIESV Mutual Information Based on Energy Spectral Variance

MIMO Multiple-Input Multiple-Output

MLE Maximum Likelihood Estimation

MOE Measures Of Effectiveness

MSE Mean Square Error

MW Moving Window

NP Nondeterministic Polynomial time

PAR Phased Array Radar

PBR Passive Bistatic Radar

PCL Passive Coherent Location

PCRB Posterior Cramér-Rao Bound

PDA Probabilistic Data Association

PDF Probability Density Function

PM Phase Modulation

POMDP Partially Observable Markov Decision Process

PRF Pulse Repetition Frequency

PRI Pulse Repetition Interval

PWE Probability Weighted Eigenwaveform

Q-RAM Q-Resource Allocation Model

QoS Quality of Service

RBF Radial Bias Function

RCS Radar Cross Section

RF Radio Frequency

RFI Radio Frequency Interference

RMSD Root Means Square Deviation

RMSE Root Mean Square Error

ROC Receiver Operating Characteristic

RRM Radar Resource Manager

SAR Synthetic Aperture Radar

SAW Surface Acoustic Wave

SCR Signal-to-Clutter Ratio

SHT Sequential Hypothesis Testing

SINR Signal-to-Interference-plus-Noise Ratio

SIR Signal-to-Interference Ratio

SIRP Spherically Invariant Random Process

SIRV Spherically Invariant Random Vector

SISO Single Input Single Output

SNR Signal-to-Noise Ratio

SPRT Sequential Probability Ratio Test

STAP Space-Time Adaptive Processing

STAR Simultaneous Transmit and Receive

TCR Target-to-Clutter Ratio

TV TeleVision

UAV Unmanned Aerial Vehicle

Chapter 1

Introduction

Radio Dectection and *Ranging* or radar has traditionally been a technology limited to military and specialist civilian applications such as aerospace, maritime, meteorology and law enforcement because of its complexity, cost and difficulty of operation. From Christian Hülsmeyer's *Telemobiloskop* design in 1904, the function of radar has expanded from simply target detection and range determination to include target tracking, imaging and classification of targets amidst clutter in an increasingly crowded electromagnetic spectral space. Radar's ability to operate under a variety of environmental conduction such as darkness, smoke and rain and travel through various mediums including air, vacuum, foliage, shallow waters and selected solids make it a dominant form of remote sensing. Whilst the basic principles of radar — the illumination of a scene with radio waves and the subsequent reception and processing of the reflected signals remain largely unchanged, the technology and emphasis on its advance has shifted in focus. Fuelled by consumer appetites, major investment and advances from the telecommunications, consumer electronics and computing industries, have spurred increasing hardware capability and falling product costs in these markets. This has lead to the accelerated development of low cost, high capability hardware, synonymous with today's computers, smart phones and processors.

As the production and operating costs of such devices has fallen, the flow has allowed adjacent markets occupied by similar technologies, including radar, to benefit from these advances. As the ubiquity of radar expands, innovative applications are being developed across new areas such as automotive navigation, subsurface imaging, pollutant and health monitoring and even gesture detection for human-machine interactions. The maturity of phased array radar (PAR) and active electronically scanned array (AESA) technology has led to the advance of multi-function radar systems capable of performing multiple tasks such as target tracking, surveillance, guidance and communications — previously executed by individual radars that were limited by their hardware configurations. Void of the constraints and inertia of traditional systems, the agility offered by modern radar provides the ability to instantaneously designate transmission characteristics in space, time, frequency and polarisation and subsequent processing of the received signals.

Until recently, radar resource management attempted to emulate the activities of traditional radar, albeit in a more sophisticated manner, achieving increased radar utility by interleaving disparate tasks in accordance with operational objectives. As technology pushes the bounds of the performance envelopes of these modern radar, capability is limited by the finite budgets of time, energy and computational resources. This thesis is concerned with resourcing scheduling and implementation of the next bound in radar resource management, adaptive radar. Often termed cognitive radar, this area has received considerable attention from the research community over the past two decades. Despite the volume of research, formidable challenges remain to be addressed in the practical application of adaptive radar. The intent of this thesis is to focus on the signal processing aspects related to implementation aspects of adaptive radar. This is achieved by the examination of a series of problems related to optimal resource selection for radar, time costs associated with the implementation of closed-loop sensor scheduling and the efficient representation of clutter.

1.1 Efficient scheduling for radar resource management

Adaptive sensing is motivated by the prospect that the closed-loop control of sensors in an agile manner can improve their utility through the use of resource selection strategies that optimise the available sensor budget. This kind of process is referred to as the perception-action cycle and is often inspired by the neurobiological echolocation systems of species of bats and dolphins. Adaptive radar is a form of adaptive sensing operating in the radio frequency (RF) spectrum. However, many of the problems associated with its implementation are applicable to the wider adaptive sensing problem. The three problems structures presented are intended to categorise and provide some context about the issues addressed within this thesis. Whilst they are directed toward the application of pulse and pulse-Doppler radar, the problem structures are in a wider sense related to the implementation of adaptive sensing as a whole.

1.1.1 Optimal resource selection for adaptive radar

The optimal selection of sensor resources has been an intense area of interest for adaptive radar research for over two decades. As the constraints of conventional radar were lifted with AESA and digital technology, the optimal selection or scheduling of sensor resources for each epoch has become vital to realising the full potential of these highly configurable systems. For multi-function PAR, the radar is generally managed by an adjacent scheduler according to the radar task objectives and load by controlling parameters including beam steering and target revisit intervals, with many of the other parameters predetermined. The dynamic role of multi-function radar (MFR) and modern RF hardware including flexible waveform generators and high duty transmitters add to the number of controllable degrees of freedom that must be addressed by the scheduler. Particular waveforms such as linear frequency modulation (LFM) chirp are prone to measurement errors when used in optimal receiver processing algorithms such a matched filter receivers. Given the expense and logistical challenge of radar installation, providing low cost or existing radars the opportunity to adaptive schedule waveforms has the potential to improve target track performance without costly RF hardware upgrades.

The perception-action cycle is modelled by the adaptive radar by the scheduling of optimal resources to interrogate the scene and processing of the received signals using feedback in a closed-loop cycle. Resource diversity can typically include waveforms, transmit frequency, polarisation and signal processing aspects selected within the constraints of the radar budget on an interpulse basis. The combination of the various attributes that comprise of the transmitted signal and subsequent processing can be used to enhance features of interest, areas of uncertainty or suppress unwanted responses such as clutter. A frequently referred to example of this process is the neurobiological echolocation system of species of bats, dolphins and whales. Using feedback and learning from previous actions, these animals are able to vary the pitch, frequency and repetition of signals emitted from their bio-sonars in accordance with their environment whilst navigating and hunting for prey Vespe *et al.* (2009). Machine based forms of cognitive learning are becoming more prevalent as technologies such as artificial intelligence and machine learning are adopted. Bayesian inference methods represent the most popular form of learning in radar applications, particularly for target tracking when target dynamics can be well represented by Markovian models. The framework is frequently adopted as a structure for resource scheduling problems. By selecting an appropriate estimation performance measure, the scheduler can optimise over the resource library for future epochs.

1.1.2 Time costs associated with adaptive radar processing architectures

In a sequential closed-loop scheduling process, received signals are processed before the scheduler makes an informed decision about the optimal action to select for the epoch(s) in the immediate future. Given the time scales involved in radar operation are so short, this process cannot be easily achieved without incurring some delay penalty using commonly available computing hardware. This makes on-line resource scheduling on any practical scale impossible on an epoch to epoch basis, much less pulse to pulse without massive oversimplification of the scene or scheduling process.

As the inertial lag from mechanical radar systems has been replaced with near instantaneous performance of AESA, the update rate of adaptive radar has become bound by the time required to process received signals and execute scheduling operations. With the transition to more digitally oriented hardware, we can delineate radar into a RF front end coupled with a flexible digital back end or ‘processor’. This then becomes a balance between front end throughput and the computational resources of the radar, matched to prevent bottlenecking by either end of the radar.

The computational effort required to process received signals and optimise radar resources between measurement epochs is not a trivial task. The sheer volume of data gathered by the front end, intricacy of modern receiver processing algorithms and ideally, a rich resource library add to the complexity of an already time limited cycle. Being able to budget the computational resources necessary to deliver a specified capability within the operating interval of an adaptive scheme to successfully function is an outstanding problem that hampers the implementation of adaptive radar.

The definition of a cost for computing aspects of adaptive radar combined with an understanding the performance degradation that is likely to be induced by a scheduling delay or lag will help define the computational performance bounds that need to be achieved for on-line adaptive scheduling scheme to be of value. This differs from established radar resource manager (RRM) methods that function as an adjacent operation to the target update loop, on a slower timescale. The definition of a performance degradation will allow the radar designer to identify relationships between permissible time for the signal processing, scheduling update rates, front-end throughput and computational resource budgets.

1.1.3 Environment representation

The efficient modelling of the scene environment and particularly clutter is an important aspect for adaptive radar. Radar clutter is inherently difficult to model due to the variety of physical structures that make up its source. Whilst clutter can be simply defined as unwanted echoes or returns from adjacent objects in the scene, this definition can vary significantly depending on the radar application. For example, an air surveillance radar may consider weather and precipitation as volume clutter whilst a meteorological radar may consider passing aircraft as interference in a weather pattern. In the maritime environment, sea clutter is a form of surface clutter associated with wave motion that is exhibited as Doppler.

Accurate modelling of the clutter can improve the quality of measurements and the ability of the detector to distinguish targets from clutter. For a varying clutter environment in radar, a constant false alarm rate (CFAR) type algorithm is often employed to discriminate genuine targets. In cell-averaging CFAR, it is assumed that the majority of the radar returns are the result of clutter and that true targets are sparse. The CFAR algorithm tests each cell in the radar range-Doppler space for targets by comparing it with the power received in the surrounding cells. Target detection thresholds are selected based on the quantity of Type I errors or false positives (alarms) we wish to tolerate.

The efficient modelling of clutter can reduce the computational expense associated with performing target detection and classification, particularly in the vast open ocean which is known to be an extremely clutter dense environment. Furthermore, the efficient prediction of the clutter response enables the detection thresholds to be selected prior to scene interrogation. Predictive clutter models can used as part of a closed-loop resource scheduling process such as adaptive radar. Selection of scene illumination and received signal processing methods can be performed with regard to a predicted clutter response. The scheduler can optimise the radar resources with regard to the specified cost that includes the predicted clutter response.

1.2 Summary of contributions and thesis outline

Within this thesis, we address some of the issues regarding the implementation of adaptive radar through the consideration of a selection of topics related to aspects involving signal processing and resource scheduling. We begin by motivating the problem through a small example that seeks to demonstrate the benefits of resource scheduling in a target tracking context.

The contributions in this thesis comprise of the examination of three discrete problems, each related to the implementation of adaptive radar. These problems encompass optimal resource selection, time costs associated with the implementation of closed-loop sensor scheduling for adaptive radar and the efficient representation of clutter.

1.2.1 Waveform diversity for LFM radar

The use of LFM waveforms, common in pulse compression for radar, is because of ease of implementation and their ability to improve measurement resolution under power constraints. When used in conjunction with matched filter receivers, a phenomenon known as range-Doppler coupling occurs for moving targets, creating an error in the range measurement relative to the target motion. In Chapter 4, by exploiting these errors, a joint target range and range-rate estimator is proposed for a train of LFM pulses for pulsed radar systems based on maximum likelihood estimation.

Efficient optimal selection strategies are proposed for pulse trains of diverse LFM waveforms for target interrogation and tracking. The Cramér-Rao lower bound for Gaussian weighted LFM pulses and pulse trains is used to model the accuracy of the pulse trains for the joint estimator and pulse-Doppler processing. Evaluation of the joint estimator is compared with conventional incoherent and pulse Doppler radar with and without range-bias compensation for a manoeuvring target tracking scenario.

1.2.2 Concurrent processing for adaptive radar

In Chapter 5, we consider the requisite tasks required to implement an adaptive sensor system, particularly for a target tracking scenario. By formulating the time costs associated with adaptive radar, decision time is used as a metric for the cost associated with the signal processing aspects of a radar system that includes a closed-loop scheduling process.

With the collapse of Moore's law, to take advantage of the CPU development trend towards more parallel processors, a pipelined radar signal processing architecture is proposed. Two concurrent adaptive radar signal processing architectures are outlined; delayed pipeline processing and concurrent pipeline processing as a means to increase the available decision time between updates without impacting front-end duty. Decision costs commensurate with radar PRIs for the alternate adaptive radar architectures are simulated for tracking scenario for multiple manoeuvring targets. Investigation into the impact of decision time and the effectiveness of the concurrent adaptive radar architectures is evaluated using target track performance and radar task allocation.

1.2.3 Sea clutter texture modelling and estimation

Sea clutter is a prevalent form of unwanted surface clutter for radar operating within a maritime environment. This form of clutter is commonly described using the compound-Gaussian sea clutter model for radars operating at low grazing angles. In Chapter 6, we propose a deterministic parametric sea clutter texture model for high-resolution radar backscatter operating in the open ocean.

A novel method for texture estimation is proposed that exploits the spatio-temporal relationship in the clutter by relating it to its physical source; sea swell. Novel spectral estimation techniques are used to identify tones in the clutter spectrum. Prevalent tones across contiguous range bins are clustered to form a parsimonious joint estimator of the texture travelling across the sea surface. The identified tones are compared with an established physical model for the sea swell. Texture estimation results are validated by comparing the predictive fit for the spatio-temporal estimator with a series of temporal estimators and a non-parametric estimator using measured sea clutter data from the Atlantic Ocean recorded by the IPIX radar of McMaster University in Canada.

1.2.4 List of publications

This thesis has resulted in the following publications:

- Ing K., Morelande M.R., Suvorova S., and Moran B. (**2016**) "Parametric texture estimation and prediction using measured sea clutter data" IET Radar, Sonar & Navigation **10**(3), 449-458.

In addition, the following scholarly papers are either in preparation or have been submitted for publication:

- Ing K., Suvorova S., Moran B. and Evans R. "Joint estimation of range and Doppler using LFM chirp diversity for non-coherent radar systems"

- Ing K., Suvorova S., Moran B. and Evans R. "Radar scheduling using serial and parallel processing for tracking of manoeuvring targets with decision costs"

Chapter 2

Background

In this chapter, we present background information on radar preliminaries and sensor resource management relevant to the topic of thesis. The chapter begins by introducing radar fundamentals with an emphasis on technologies relevant to modern radar systems such as electronically scanned array multi-function radar. We then review radar resource manager and the various algorithms used to perform this important function. The final part of this chapter presents a description of adaptive radar with an emphasis on cognitive radar and some of the challenges associated with its implementation.

2.1 Radar fundamentals

Radar systems were initially developed to exploit the use of electromagnetic (EM) radiation in the radio spectrum for the detection and range determination of targets. The operation of radar primarily comprises of radio waves emanating from a transmitting source to illuminate a scene before being reflected from objects to a receiver. Modern radars have evolved from this early function to incorporate sophisticated transducer and computing resources. This has significantly improved radar capability to include the detection, classification and tracking of targets whilst suppressing unwanted returns or clutter from the scene. This has lead to a diverse spread of specialised applications ranging from air, maritime and terrestrial traffic control, collision avoidance, meteorological monitoring, altimetry and flight control, surveillance systems, imaging and military applications such as missile guidance and air-defence. Although radar systems can vary, in principle they comprise a transmitter, receiver, antenna(s), a signal processor and some form of system clock as shown in Figure 2.1. In this system, the transmitter generates the incident signal that radiates from the antenna. The signal propagates through the environment illuminating the target with a portion of the signal from the target reflected and received by the radar.

For a pulsed monostatic (collocated transmitter and receiver) system such as pulse-Doppler radar, the range from the radar to the target is a function of the time delay τ between when the signal is transmitted and received by the radar

$$R = \frac{c\tau}{2} \tag{2.1}$$

where c is the propagation velocity of the EM wave through the transmission medium, typically $c \approx 3 \times 10^8\,\mathrm{m\,s^{-1}}$ the speed of light. For targets that exhibit radial motion relative the radar, the shift in distance during the pulse results in an apparent frequency shift in the reflected signal known as Doppler. For a narrowband signal, the Doppler shift in the observed frequency of the reflected signal is

$$f_d = \frac{2vf_0}{c - v} \approx \frac{2v}{\lambda_0}, \quad v \ll c \tag{2.2}$$

where v is the target radial velocity relative to the radar, f_0 the carrier frequency of the transmitted signal and wavelength $\lambda = {}^{c}/_{f}$.

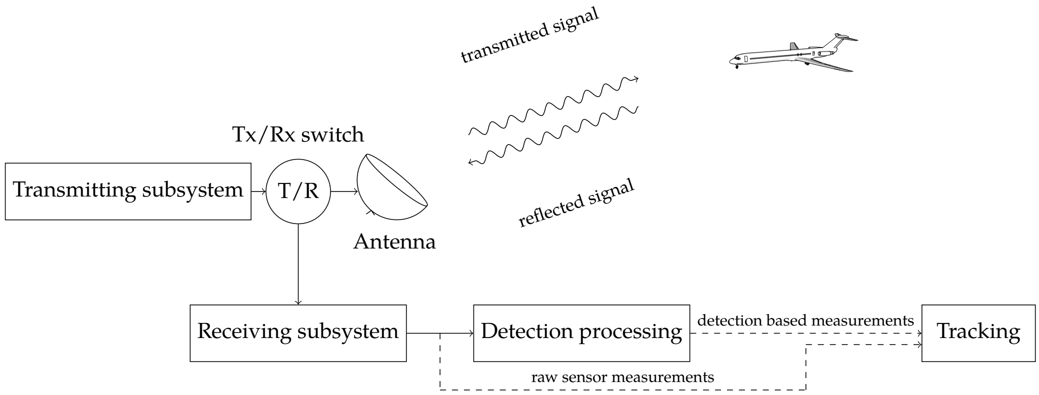

Figure 2.1: Components of a typical monostatic radar system

In addition to returns form the target of interest, backscatter signals are reflected from surrounding environment and other disturbances. These unwanted returned signals are known as clutter and can be categorised as either surface (such as the ground or sea) or volume (rain and chaff). In addition to clutter, interference or jamming signals, both intentional and unintentional can degrade the received signal quality. The performance of the radar or its ability distinguish a target from the background is largely determined by the signal-to-interference ratio (SIR)

$$SIR = \frac{P_{target}}{P_n + P_c + P_j} \tag{2.3}$$

where P_n is the receiver power from the radar thermal noise, P_c the clutter power and P_j received power from a jamming source. Thermal noise $P_n = kTFB$ where

Boltzmann's constant $k \approx 1.38 \times 10^{-23}\,\mathrm{J\,K^{-1}}$, T the temperature of the receiver system, F and B the receiver noise factor and bandwidth. For a point-source target (or clutter) of known range, the peak received power for a monostatic radar is

$$P_r = \frac{P_t G_t G_r \lambda^2 \sigma}{(4\pi)^3 R^4 L_s} \tag{2.4}$$

where G_t, G_r represents the antenna transmit and receive antenna gains, P_t the transmitted power, σ the radar cross section (RCS) of the target and L_s system losses such as those from the transmitter, receiver, atmosphere and signal processing losses. Assuming a interference free, homogeneous environment the maximal range performance of a radar system can be described by the classic (free space) radar range equation:

$$R_{\max} = \left(\frac{P_t G_t G_r \lambda^2 \sigma}{(4\pi)^3 L_s S_{\min}(P_n + P_c)} \right)^{\frac{1}{4}} \tag{2.5}$$

where $S_{\min}$ is the SIR detection threshold. The radar range equation (2.5) highlights the significant $1/r^4$ losses for point-source targets associated with increases in target range, and the extreme returns from nearby objects particularly those of large RCS. The difficulty of distinguishing genuine and generally uncooperative targets from a dense clutter environment within the time scales that radar operates is an outstanding problem. For homogenous clutter environments, this loss relationship is exacerbated, changing to $1/r^3$ for surface clutter and $1/r^2$ for volume clutter due to the beam divergence or cross-section increasing with range.

Whilst previously performance increases drove the development of more powerful radar systems, today the focus has transitioned towards the increased effective utilisation of available resources to improve capability.

2.1.1 Target radar cross section fluctuation

The radar response from real targets (and clutter) means that the radar cross section of a complex target is non-static in nature and may vary between measurement epochs. As a result, it is best characterised by a statistical instead of a static model. These were introduced by Swerling (1960) as a distribution in the location-scale family of chi-squared distributions where Swerling divided RCS responses into classes known as Swerling targets (I - V). For a Swerling I target, the probability density function (PDF) of the target RCS is given by the Rayleigh function

$$p(\sigma) = \frac{1}{\sigma_{av}} \mathrm{e}^{-\frac{\sigma}{\sigma_{av}}} \tag{2.6}$$

where σ_{av} is the mean target RCS and the RCS is considered constant from scan-to-scan. For a Swerling II target, the PDF of the target RCS is also (2.6) but the RCS varies from pulse to pulse. These models can be applied to targets that comprise of many individual scatterers of similar size, such as airplanes. Targets that consist of one large scatterer and many smaller scatterers such as ships can be represented by Swerling III and IV targets. The PDF of the scan-to scan fluctuation of a Swerling III target is

$$p(\sigma) = \frac{4\sigma}{\sigma_{av}^2} \mathrm{e}^{-\frac{2\sigma}{\sigma_{av}}} \tag{2.7}$$

where for the Swerling IV, the PDF of the RCS is also (2.7) but varies from pulse to pulse. The Swerling IV (also Swerling 0) target is an idealised model without any fluctuation. The performance of a binary classifier can be illustrated using a receiver operating characteristic (ROC) curve. The variation in RCS results in fluctuation loss to achieve a desired target probability of detection P_d for a specified probability of false alarm P_{fa}. Figure 2.2 shows the detection performance for various target Swerling models at specified SIRs.

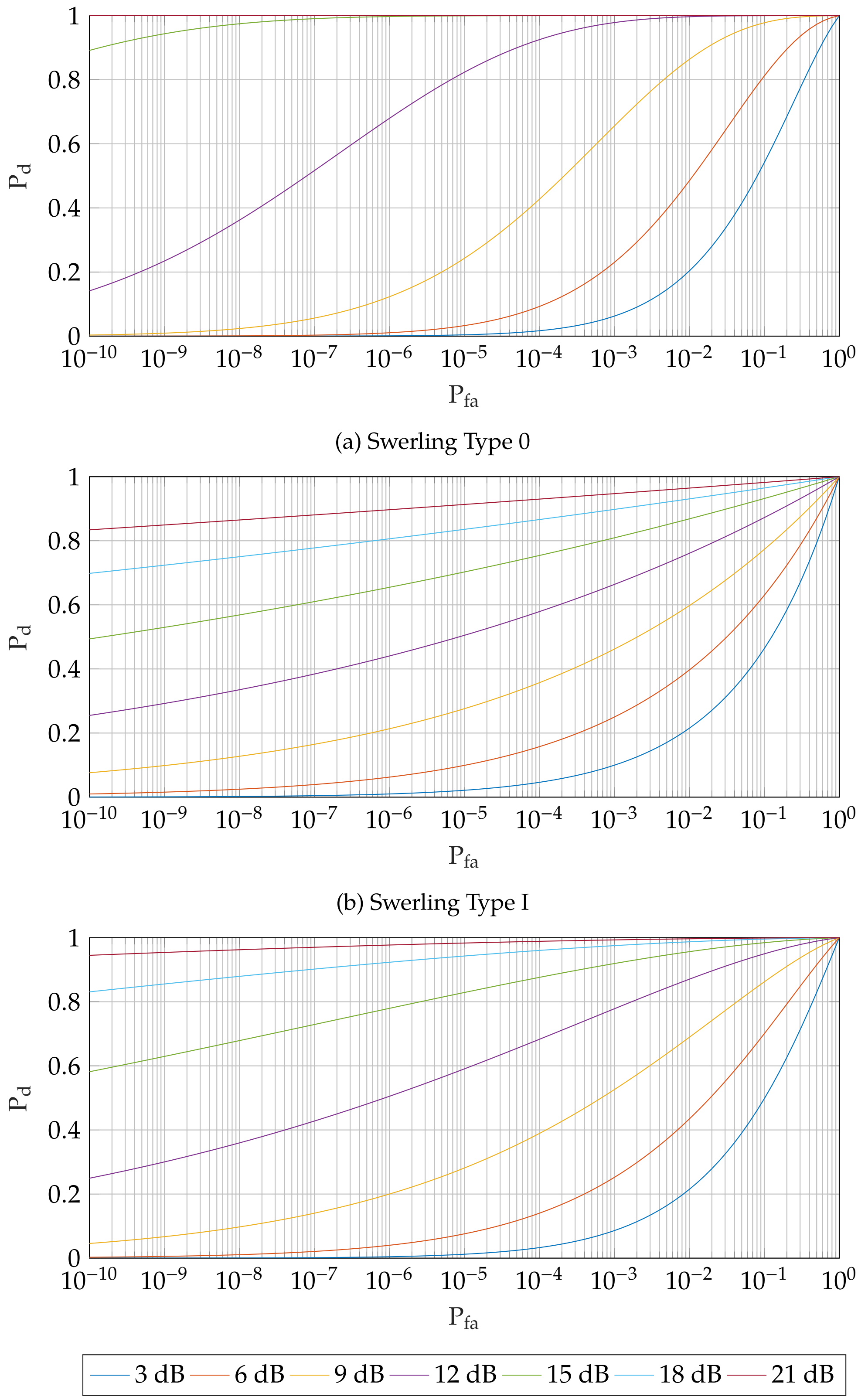

(a) Swerling Type 0

(b) Swerling Type I

(c) Swerling Type III

Figure 2.2: Receiver operating characteristic curves using binary classifier for various target signal-to-interference ratios

2.2 Optimal radar receiver processing

For a typical pulsed active radar, the illumination is a narrowband signal for reasons of practicality (Levanon and Mozeson 2004). This can described as an amplitude waveform signal $a(t)$ or *envelope* modulated onto a higher frequency sinusoidal carrier of frequency f_0,

$$x(t) = a(t) \cos\left(2\pi\left(\phi\left(t\right) + f_0 t\right)\right), \quad -\frac{T}{2} \leq t \leq \frac{T}{2} \tag{2.8}$$

where $\phi(t)$ is the instantaneous phase or frequency modulation and typically $a(t)$ occupies less than 1/10 the bandwidth of f_0. Equivalently, (2.8) can also be represented in analytic form as

$$x(t) = x_I(t) \cos\left(2\pi f_0 t\right) - x_Q(t) \sin\left(2\pi f_0 t\right) \tag{2.9}$$

where the in-phase x_I and quadrature x_Q signals are

$$x_I(t) = a(t) \sin\left(\phi(t)\right) \tag{2.10a}$$

$$x_Q(t) = a(t) \cos\left(\phi(t)\right) \tag{2.10b}$$

and the *complex envelope* or *baseband* signal:

$$\tilde{x}(t) = x_I(t) + j x_Q(t) \tag{2.11}$$

When the signal is reflected from a moving target, the relative velocity difference between it and the radar results in the Doppler effect that increases (redshift) or decreases (blueshift) the wavelength of the transmitted signal. For a narrowband signal, the reflected signal from a point source target is well approximated by an attenuated, delayed and frequency shifted version of the original signal,

$$s(t) = \alpha \tilde{x}(t - \tau)\, \mathrm{e}^{j2\pi f_d t}\, \mathrm{e}^{-j2\pi(f_0 + f_d)\tau}, \quad v \ll c \tag{2.12}$$

where α is the attenuation coefficient and f_d is the equivalent frequency shift from the Doppler effect. The return from a complex scene consisting of multiple scatterers such as that from an extended target can be formed using the principle of superposition by the summation of the return from all of the individual targets.

The matched filter receiver is the optimal linear filter for maximising the signal-to-noise ratio (SNR) in the presence of additive stochastic noise (Turin 1960). It can be expressed by the convolution integral between the filters impulse response and the received signal

$$y(t) = \int_{\infty}^{\infty} s_r(u)h(t-u)\,.\mathrm{d}u \tag{2.13}$$

where $h(t)$ is the filter's impulse response and noisy received signal

$$s_r(t) = s(t) + n(t) \tag{2.14}$$

for noise process $n(t)$. Maximisation of the receiver SNR can be achieved by selecting the matched filter impulse response

$$h(t) = x^*(\tau - t) \tag{2.15}$$

where * indicates the complex conjugate. The matched filter response is related to the waveform ambiguity function (Section 3.3.2) and can be found by the cross-correlation of the received signal with a delayed replica of the transmitted signal,

$$y(t) = \int_{-\infty}^{\infty} s_r(u)s^*(\tau - t + u)\,.\mathrm{d}u \coloneqq \overline{R}_{s_r s}(t-\tau) \tag{2.16}$$

where $\overline{R}_{s_r s}$ is the cross-correlation function between the $s_r(t)$ and $s(\tau - t)$. By considering (2.12), we can rewrite the matched filter response as,

$$y(t) = \int_{-\infty}^{\infty} \tilde{x}(u-\tau_0)\,\mathrm{e}^{j2\pi f_d \tau_0}\,\mathrm{e}^{-j2\pi(f_0+f_d)\tau_0}\,\tilde{x}^*(t-\tau_0+u)\,.\mathrm{d}u \tag{2.17}$$

to include the Doppler shift from moving targets. Letting $z = u - \tau_0$ and with a change of variables the matched filter response in both delay and Doppler is

$$y(t, f_d) = \mathrm{e}^{-j2\pi f_0 \tau_0} \int_{-\infty}^{\infty} \tilde{x}(z)\,\tilde{x}^*(t-z)\,\mathrm{e}^{-j2\pi f_d z}\,.\mathrm{d}z \tag{2.18}$$

2.2.1 Doppler processing

Doppler processing utilises the Doppler shift information in the received signal for the purpose of measuring target radial velocity and improved contrast of targets from background clutter such as ground and vegetation. Pulse-Doppler radar utilises the time delay to measure target range and the Doppler effect of the reflected signal to determine the targets radial velocity. This can considerably improve the detectability of targets in some operational uses by separating moving targets from stationary clutter. A pulse train of coherent transmitted pulses is used to interrogate the scene,

$$s(t) = \sum_{k=0}^{K-1} x(t + kT) \tag{2.19}$$

where T is the pulse train pulse repetition interval (PRI). The phase shift of the k-th pulse is proportional to the target range. The received downconverted baseband signal from the pulse train is

$$\begin{aligned} y(k) &= \alpha\, \mathrm{e}^{-j\left(\phi - \frac{4\pi}{\lambda}(R_0 - vkT)\right)} && (2.20) \\ &= \alpha\, \mathrm{e}^{-j2\pi f_d kT}\, \mathrm{e}^{-j\left(\phi - \frac{4\pi R_0}{\lambda}\right)}, \quad k = 0, \ldots, K-1 && (2.21) \end{aligned}$$

As a result, the phase shift between successive pulses is a function of its Doppler frequency. This allows the target Doppler frequency and resultant radial velocity along each range bin to be estimated from the phase shift between the successive pulses in the train using spectral analysis techniques such as fast Fourier transform (FFT) (Cooley and Tukey 1965).

2.3 Electronically scanned array multi-function radar

The introduction of phased array radar and particularly active electronically scanned array has led to the development of multi-function radar. Phased array radar (PAR) technology allows the radar beam to be controlled and applied instantaneously so that the radar may be directed to perform multiple tasks in sequence or even simultaneously. The flexibility of modern electronically scanned array (ESA) hardware allows the radar to alter diversity parameters, such as polarisation, antenna beamshape, transmit power, and search patterns. Being almost instantaneously configurable over a diverse range of operational parameters permits the tailoring of resources to specific mission profiles on a pulse-to-pulse basis. A survey conducted by Ding (2008; 2009) showed that current advanced naval multi-function radar (MFR) systems were already capable of performing the tasks formerly completed by a series of individual dedicated radars. In a naval defence context, tasks have included those such as in Figure 2.3. In general these radars are operated in a conventional manner, using pre-programmed waveforms and receiver processing deliberately selected for each tasks, targets and clutter.

2.3.1 Active electronically scanned array radar architecture

In this subsection, we provide a brief description of the system level architecture of active electronically scanned array (AESA) MFR. The design of MFR is a detailed sub-

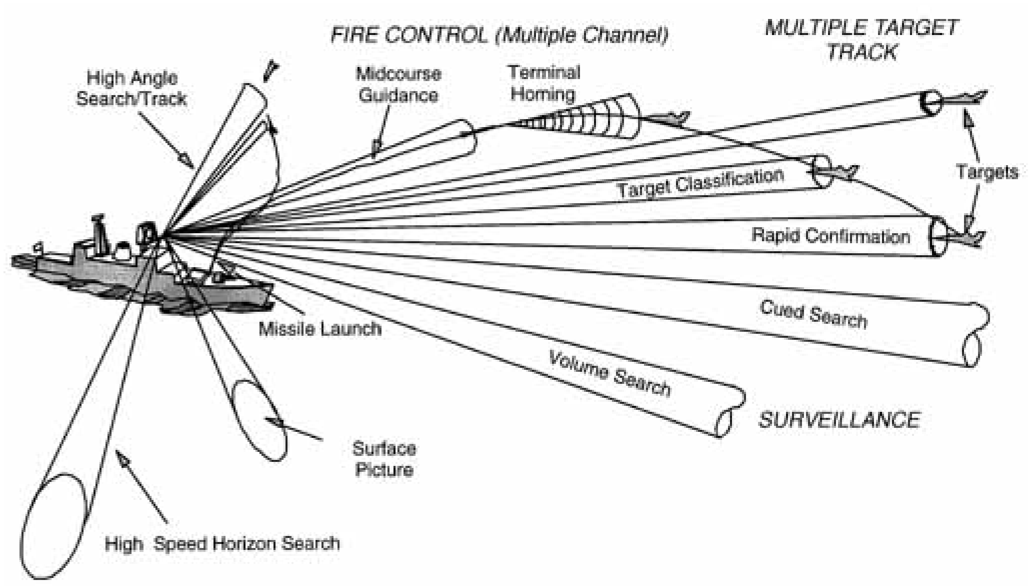

Figure 2.3: Typical functions of a MFR for naval defence operations, Butler (1998)

ject and has been published in dedicated texts and chapters (Belcher 2013, Billetter 1989, Sabatini and Tarantino 1994). A radar consists of three major components; a transmitter, receiver and signal processor (Figure 2.1). A key feature of AESA is the use of a phased array antenna. This antenna allows for beam-steering and/or beamforming through control of either phase, frequency or time delay between each of the individual antenna elements. Whilst not necessarily unique to AESA, a radar management system or radar resource manager (RRM) is typically employed for the control of the radar operation such as that shown in Figure 2.4. This allows the radar operation to dynamically alter its resource utilisation, processing algorithms and task prioritisation according to some demand process or resourcing schedule to maximise its utility (Ding and Moo 2017, Schikorr *et al.* 2016).

The adoption of scalable radar architectures (Nalecz *et al.* 1997) and single chip designs (Li *et al.* 2010) has seen a separation of the radio frequency (RF) hardware and computational aspects in modern radar. Highly configurable computation and signal processing with customised RF hardware is beginning to support the use of common subassemblies in multiple applications with minimal modifications (Evans *et al.* 2013; 2014). Another scenario is the use of modern radar systems that operate across multiple tasks or objectives simultaneously in a dynamic environment (Barbaresco *et al.* 2009, Cabrera 2013). In the following section, we explore RRM, with particular emphasis on its use in an adaptive radar setting.

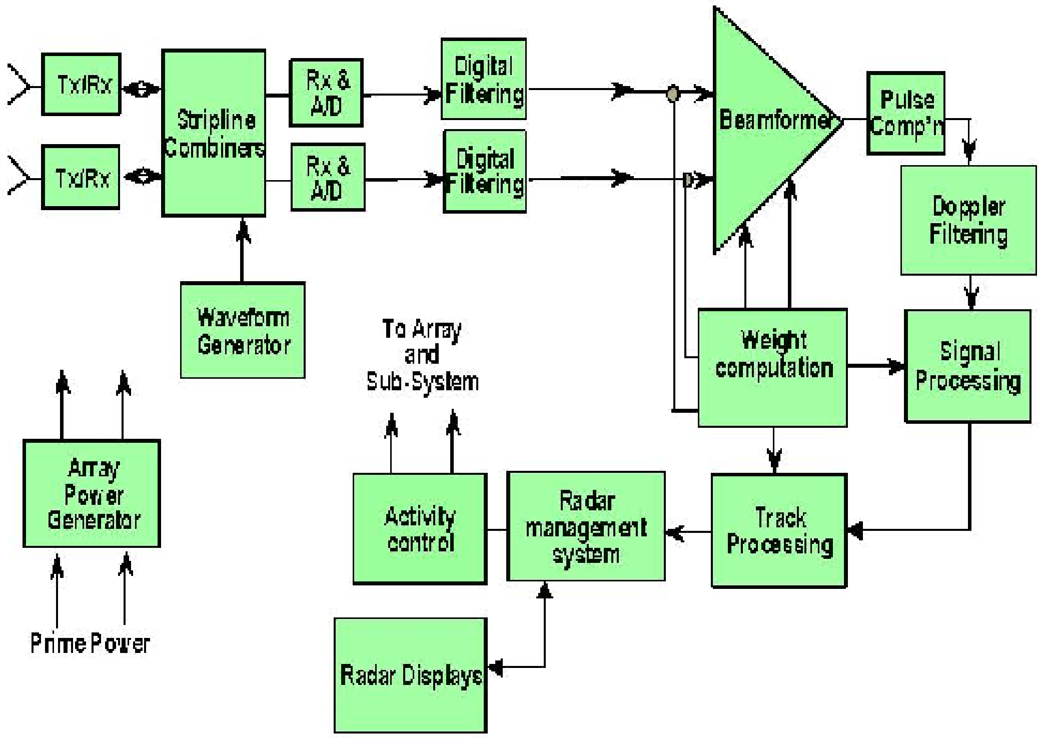

Figure 2.4: Simplified block diagram of the BAE Systems Integrated System Technologies (Insyte) Multi-function Electronically Scanned Adaptive Radar (MESAR), Stafford (2007)

2.4 Radar resource management

Sensor management is the control of the degrees of freedom in an agile sensing system given a knowledge state to satisfy operational constraints and achieve operational goals. This is an area of continued research from a need to manage, coordinate and integrate the sensor usage to accomplish specific and often dynamic mission objectives (Ng and Ng 2000). Such mission objectives can include target detection, classification and tracking, surveillance or even imaging, discussed in greater detail in Section 3.4. Sensor management for radar is coordinated by a central function known as the radar resource management system or radar resource manager (RRM). The major resource budgets the RRM must manage are time, energy and processing power, with all three being somewhat interlinked. Although it does not define the hardware or theoretical capabilities of the radar, the objective of the RRM is it to maximise the overall utility of the radar through the careful management of the radar's finite resources. Optimal performance is defined according to a suitable cost function within the budgetary confines that the radar must operate, such as those later discussed in Section 3.5 for target tracking. The challenges imposed on the RRM exist when one or more of the radar resources are insufficient to meet the demands of the system or the operational environment. In this situation, the radar will be forced to prioritise and degrade the performance or one or more allocated tasks or potentially cease the completion of others.

RRMs can be categorised as either non-adaptive or adaptive. In a non-adaptive setting, tasks priorities are predetermined and scheduled according to some defined decision logic, rules or heuristic measures Wintenby and Krishnamurthy (2006). Although heuristic rules may be employed to act in real time, they do not operate according to some cost objective and are not considered as being optimal (Strömberg 1996, Strömberg and Grahn 1996). In adaptive RRM, the scheduling process is more complex and tasks are dynamically selected according to the scenario and available resources. Resource can then allocated according to some objective through some optimisation process. Ding (2009) provides an excellent survey of adaptive RRM methods with a comparison between adaptive with non-adaptive methods in Moo and Ding (2015). The general requirements of the adaptive RRM are to:

- Accept the radar mission;
- Select the radar tasks to fulfil the mission;
- Prioritise the radar tasks according to the objective function; and
- Execute the radar tasks using the radar resources from the within the available budget.

To realise the available utility of the MFR, the RRM must be able to select the radars tasks in a way that maximises the radar performance according to its mission objective through the scheduling of its available resources. In this context, we define the tasks being the 'jobs' the radar needs to complete to achieve the operative mission and the resources or 'tools' to be the operational parameters such as beamshapes, frequency, waveforms, polarisation and signal processing. In the following sections, we briefly summarise the different adaptive RRM categories according to those defined in Ding (2008; 2009).

2.4.1 Artificial intelligence algorithms

Artificial intelligence algorithms for RRM are best suited to task prioritisation and scheduling within the constraints of the radar resource budget. Example techniques include the use of neural networks (Izquierdo-Fuente and Casar-Corredera 1994,

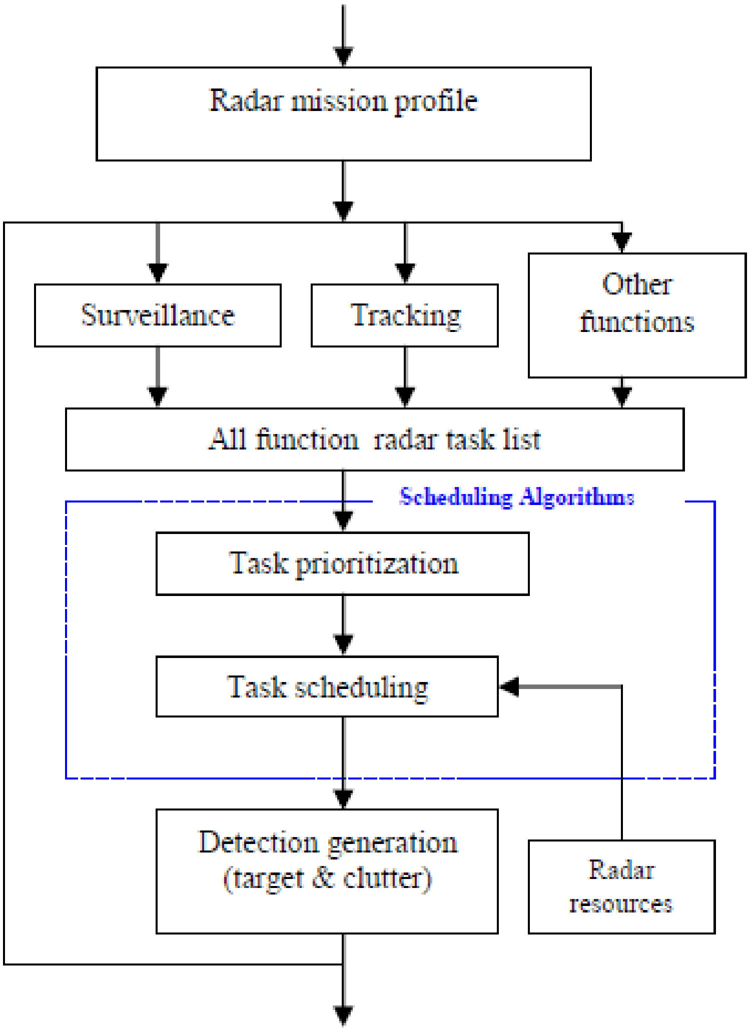

Figure 2.5: Example MRF resource management model, Ding (2009)

Komorniczak and Pietrasinski 2000), expert systems (Vannicola 1990) and fuzzy logic (Miranda *et al.* 2004b; 2006, Vine 2001). The general approach of these systems is to categorise and then prioritise targets based on distinguishing features. For these systems to operate successfully, a prior knowledge base such as a learning dataset or fuzzy rules must be established which can greatly effect the efficiency and effectiveness of the system.

To illustrate, in the fuzzy logic approach of Miranda *et al.* (2006), an example architecture is provided for a radar within a military operational environment. This is based upon providing intelligent prioritisation by evaluating the linguistic variables of *threat*, *hostility*, *weapons systems capabilities of the platform*, *quality of tracking* and *relative position of the target*. Priority is then assigned at one of seven levels, ranging from *very low* to *very high*. The processing speed of fuzzy logic controllers are a key factor which makes them a desirable candidate for implementation within a real-time systems when compared with neural networks.

2.4.2 Stochastic dynamic programming algorithms

Stochastic dynamic programming methods for RRM attempt to deal with the dual problem of task prioritisation and resource scheduling. A multi-stage cost function in which multiple tasks are developed to accomplish the radar mission objectives. Costs and rewards may be assigned to each radar task to be scheduled and the associated resources required to complete the task. The RRM then optimises the combination of tasks based on the overall cost and reward of the proposals. Although it is possible to adopt a brute force approach to evaluate these cost functions such as exhaustive search, efficient evaluation of has proven to be challenging given its expanse of the solution space and the typical operational time scale of radar, especially for multi-step ahead or non-myopic problems (La Scala *et al.* 2003, Williams 2011). Approaches to overcome the computation problem have included formulating the beam scheduling problem for PAR under a track scenario using the multi-arm bandit problem formulation (Krishnamurthy *et al.* 1999, La Scala and Moran 2006). In this solution, the target state was modelled according to a Markov chain, with the conditional estimated target state computed by a tracker. For a multiple target tracking problem, the optimal target to interrogate at each epoch was computed using the Gittens index (Gittins 1979, Whittle 1980).

More established dynamic programming RRM algorithms include Orman and Butler scheduling (Miranda *et al.* 2006). Orman scheduling utilises a coupled-task scheme where two distinct tasks such as transmitting a radar waveform and receiving a reflected pulse are coupled under the constraint that the radar cannot complete both tasks simultaneously (Orman and Potts 1997, Orman *et al.* 1996). By recognising that these tasks must be completed in a pre-determined order with a specified separation time interval, the RRM is able to utilise the separation period by queuing tasks up so they do not overlap in time. Given that some jobs are cyclic and others are dynamic, the RRM performs on-line scheduling to separate these tasks out both spatially and temporally. Heuristics may be employed to deal with prioritisation management in time constrained systems. The Butler type scheduler uses a timebalance concept to manage the scheduling of tasks requested by the RRM (Butler 1998). Tasks are grouped into jobs the radar must complete, such as tracking a target. A timebalance cost is associated with each task and increases as time elapses as a means to prioritise tasks. When tasks are completed late, a positive time balance is allocated, if the task is completed early the timebalance becomes negative and jobs completed on time achieve a timebalance of zero. The scheduler prioritises scheduled jobs by first selecting uncommenced jobs with the greatest timebalance . Whilst the Orman scheduler will attempt to maintain some level of performance for lower priority tasks by better utilisation of unused schedule occupancy the Butler scheduler can attain greater overall time utilisation by rescheduling of tasks Miranda *et al.* (2004a). However, both of these methods manage the issue of task scheduling and prioritisation, without directly addressing the resource scheduling problem.

2.4.3 Q-resource allocation model algorithms

Q-resource allocation model (Q-RAM) algorithms evolved from those developed for the communications industry where quality of service (QoS) is used as a metric of performance (Lee *et al.* 1999, Rajkumar *et al.* 1997). The Q-RAM algorithm seeks to maximise a system utility (such as minimisation of global system error) under the resource constraints given a set of tasks by finding a operating point to a multi-variate system utility function (Ghosh 2004, Ghosh *et al.* 2004a, Hansen *et al.* 2006, Hansen and Lehoczky 2004). However, this utility function can be nondeterministic polynomial time (NP) hard so a concave majorant operation is employed to reduce the number of setpoints that need to be evaluated with heuristics and non-linear programming. Ghosh *et al.* (2004b) considers the hardware system resources of the radar to be scarce in comparison with the computing resources. A two-layer approach is adopted where the QoS optimisation is performed to determine task resource allocation followed by scheduling of the tasks *ensuring schedulability*, by making sure that the radar resource budget constraints are met. These two layers are tightly integrated as the Q-RAM scheduler adjusts the scheduling bounds within the radar operational constraints to determine the optimal operating point. Off-line storage of the operating points or 'service classes' allow a discrete set of task configurations to be developed across an operating range from a template. Whilst this form of scheduling has limited scope for resource diversity, it is well suited to systems with defined operating points and can be considered to be efficient to implement with predictable performance.

Katsilieris *et al.* (2012) considers the problem of surveillance control for MFR using a method based on the continuous double auction parameter selection (CDAPS) algorithm (Charlish *et al.* 2011). The CDAPS algorithm is an agent based approach to multi-objective optimisation defined in terms of a utility given a global resource constraint that settles upon a market equilibrium that satisfies the

Karush–Kuhn–Tucker (KKT) conditions. A particle filter is used to estimate the density of undetected target locations and the CDAPS algorithm applied to optimise the utility of the radar system. The utility function is defined to map each task onto a utility, such as the value of detecting a new target. In the double auction, agents are able to both buy or sell resources, given the performance of the represented tasks that included target tracking and surveillance. Charlish *et al.* (2015) also considered the application of CDAPS for AESA RRM, in a multiple target tracking scenario.

2.4.4 Waveform-aided algorithms

The transition from analogue compression waveform synthesis techniques such as surface acoustic wave (SAW) filters towards programmable digital waveform generation has lead to the capability to easily create diverse radar waveforms with differing characteristics. Waveform-aided algorithms were introduced in Kershaw and Evans (1994) as a method of optimal tracking for sonar with closed loop solution available for certain waveform library types. This class of RRM algorithm assumes that task prioritisation and scheduling is implemented by a task scheduler and focuses on resource management by way of waveform selection. By optimisation of the waveform resource, the time, energy and processing budgets can be reduced, improving the utility of the radar. This is a dynamic process, using information about the scene to design the waveforms to use at the next interrogation from epoch to epoch. This class of RRM is best suited to target tracking problems as they do not address the issue of task prioritisation. An excellent review of waveform-agile algorithms is provided by Sira *et al.* (2006).

Advances in sensor technology have opened up the application of waveform design for specific objectives, such as reduced target track error, improved target detection or target identification. The application of Woodward's ambiguity function Woodward (1967) has been fundamental to the development of waveform aided algorithms. Waveforms are selected according to some cost that is a function of the target track characteristics (Cochran *et al.* 2009, Howard *et al.* 2004) and these algorithms have been used to improve tracking in the presence of clutter (Kershaw and Evans 1997). Multiple approaches to the waveform-aided algorithm have been proposed, incurring control theoretic (Hong *et al.* 2005, Kershaw and Evans 1994; 1997, Sira *et al.* 2007c) and information theoretic methods (Bell 1993, Howard *et al.* 2004) with similar results. In both of these methods, the resource optimisation process forms a part of a feedback loop that seeks to select or design the optimal waveform at the next measurement epoch based on the information contained within the previous set of measurements and the dynamics of the target of interest. However, these algorithms are generally considered to be NP-hard and are barely tractable within the timescales involved in radar. Compact waveform libraries were proposed by Suvorova *et al.* (2009) to reduce the number of iterations required to evaluate the solution space by the use of a utility function that describes the value of the library.

For beamform scheduling in AESA radar, Berry and Fogg (2003) investigated a multiple target tracking problem using an information theoretic based scheduling methods that sought to maximise the entropy of the joint system of independent targets. Intuitively, the authors found this scheduler selected targets that exhibited the largest predicted covariance, the smaller measurement covariance and the greatest probability of being detected to interrogate.

2.4.5 Adaptive update rate algorithms

Adaptive update rate algorithms are an extension of target trackers that utilise a uniform update period. The target update rates or epochs are selected to match the scene, such as the surrounding clutter and target dynamics as well as the desired target track performance whereby increasing the update period, the radar usage can be minimised. These algorithms are based on the use of decoupled Kalman filters developed for use with PAR to deal with ill-conditioning of other non-linearities (Daum and Fitzgerald 1983).

Keuk and Blackman (1993) proposed the implementation of adaptive update rate algorithm that sought to minimise the energy required to maintain a (threshold) target track for a PAR. Using the predicted target position, the algorithm was shown to work for steady state conditions as well as non-stationary target scenarios (Hong and Jung 1998). Adaptive update rate algorithm trackers have been extended to include manoeuvring targets using an interacting multiple model (IMM) based tracker (Benoudnine *et al.* 2006, Sarunic and Evans 1997, Shin *et al.* 1995) as well operating in the presence of clutter (Jung and Hong 1999). Coetzee *et al.* (2003) investigated this problem with regard to MFR and how the radar may be liberated to perform other non-tracking related tasks. For this class of RRM, the use of non-uniform update rates can be challenging for task scheduling in MFR due to the increased complexity in computing non-linear components of target dynamic models. (Zhang *et al.* 2006) found that the specific implementation of the tracker and the scenario itself can have significant bearing on the track quality compared with a uniformly sampled tracker.

2.5 Adaptive radar

The concept of adaptive radar emerged from Sowelam and Tewfik (1994) who proposed a waveform selection strategy for a target classification problem using imaging radar . Independently, an adaptive method for optimal waveform selection was developed by Kershaw and Evans (1994) for a target tracking scenario using sonar. Since then, there have been numerous publication in the field of adaptive radar which try to address the resource allocation problem within a modern radar operating environment. Later, Haykin (2006) introduced the term *cognitive radar* as a way to describe a way to use knowledge to control an adaptive radar in a cognitive manner. Recently, Horne *et al.* (2018) proposed an ontology for taxonomy surrounding this class of technologies to clarify the disarray of terms used to describe similar concepts. Horne *et al.* (2018) suggested that radars be separated into two categories, adaptive and non-adaptive as shown in Figure 2.6. An adaptive radar is then defined as a system that 'adapts its processing and control to improve achievement of a desired function' (Inggs 2010). Horne *et al.* (2018) categorised cognitive radar (CR) as a class of intelligent radar that belongs to the wider adaptive radar class, adapting its operation and processing in response to the dynamics of the target scene and operating environment and may do so over an extended period, a definition we adopt for this thesis.

Whilst modern MFR are already capable of online scheduling, the RRM methods and particularly those discussed in Sections 2.4.1 to 2.4.3 are task prioritisation centric, deploying already specified resources for planned tasks such as surveillance, target identification and tracking. Fully adaptive or cognitive radar on the other hand, has the potential to to further improve radar utility by incorporating the information the radar may have learnt about the scene. The development of modern radar hardware and advances in computing power and algorithms are beginning to pull together to provide the necessary ingredients of CR. In the following subsections, we review the perception-action cycle with a emphasis to its use in sensor scheduling, cognitive radar itself, its potential applications and the ensuing challenges with its implementation.

2.5.1 The perception-action cycle

During adaptive sensor management, the sensor is used to obtain information about the state of a scene or dynamical system(s). Acting upon the information received about the interrogated scene, the sensor can learn about the target (or environment) and control its future actions through selection or scheduling of

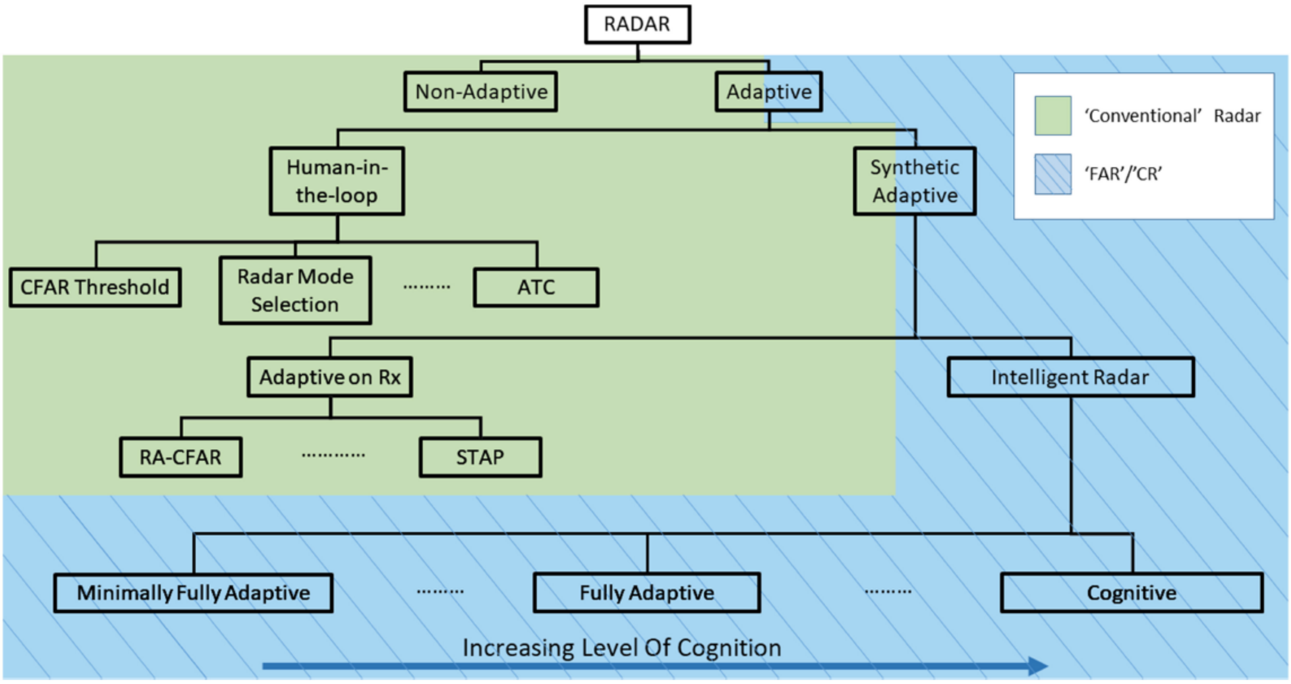

Figure 2.6: Taxonomy for adaptive and non-adaptive radar, Horne *et al.* (2018)

resources from a library in accordance with the objective of the sensor. Cognitive radar systems that featured a dynamic closed feedback loop encompassing the transmitter, environment and the receiver were heralded by Haykin as the 'way of the future' (Haykin 2006). Within this system, he described there being three critical components:

1. Intelligent signal processing that building on learning through interactions of the radar from the surrounding environment;

2. Feedback from the receiver to the transmitter, or the facilitation of the transfer of intelligence; and

3. The preservation of information contained by the radar returns.

Whilst some of these components are already commonplace in radar, the application of the three processes within the perception-action cycle allows the available information to be processed and interpreted in the context of the perceived situation. This form of intelligent feedback process is synonymous to the neurobiological echolocation systems of species of dolphins, bats and whales, who possess the ability to adjust the pitch, frequency and repetition of the signals emitted from their bio-sonars in accordance to the environment as a means of sensing (Leighton *et al.* 2004, Vespe *et al.* 2009).

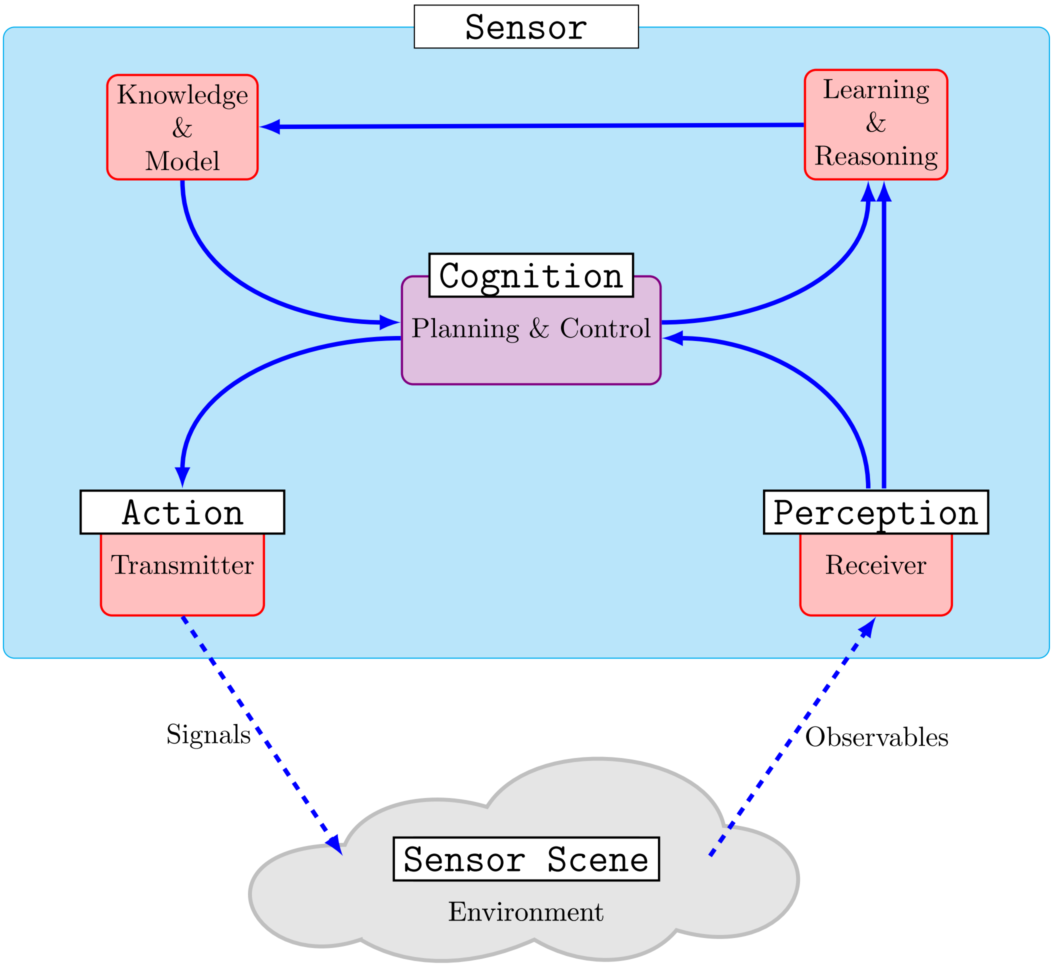

Figure 2.7: Cognitive perception-action system architecture in an active sensing application

A dynamic closed-loop feedback system as shown in Figure 2.7 can be used to represent the perception-action cycle. The CR would possess the ability to continuously learn about its environment through interactions and continually update its processor with relevant information about the environment. Building upon this information, the transmitter would then alter the way it interrogated the scene by adjusting the transmitted signal parameters. An example of this radar might comprise of an adaptive front-end such as an AESA (Section 2.3) coupled with a knowledge-aided perceptive receiver to provide feedback. This becomes an informed decision making process, by allowing the establishment of a solution space and the selection of a subset according to a desired objective. In this case, a scheduler selects the operational parameters to achieve a specific performance objective, such as target tracking.

The perception-action cycle ties together the perception and estimation process with the action through some form of control mechanism. Haykin *et al.* (2012) considers the concept of CR to mimic that of the *visual brain*. Establishing a causal cyclic relationship between the radar and its operating environment, the CR controls aspects of the sensing process by scheduling of resources. Resources to be scheduled by the radar would include those of both the transmitter and the receiver. With the receiver providing feedback information about the radar environment, the radar is able to select a transmitter action appropriate for the environment. For an active CR, the transmitter indirectly also controls the receiver action through the selected means of illuminating the scene. For a target tracking scenario, optimal perception in the receiver can be achieved by treating it as a state-estimation problem under a Bayesian framework and an approximate Bayesian filter for a nonlinear target state-space model (Haykin 2006).

2.5.2 Cognitive radar

Cognition refers to the high level brain function of receiving and information, processing it and retaining memory. From a neurological standpoint, can be stated as the behaviour of an organism when subject to the continuous flow of information between itself and the environment. The environmental stimuli are received and processed by sensors, resulting in actions which in return provide new sensory inputs. Fuster (2003; 2006) described the existence of five cognitive functions that dealt with logical or analytical aspects: perception, memory, attention, language and intelligence. Perception relates to one's understanding of the world or environment around them. It extends beyond sensory inputs to include the functions of memory and attention. Fuster surmised that cognits were hierarchical and Krishnan *et al.* (2016) considered that high level reasoning and low level responses can be adopted to radar when combined with appropriate signal processing and engineering mathematics. From a radar operation perspective, the function of memory is to store interpreted information, reinforced through repeated experiences, and to recall when needed. Attention refers to the efficient application of resources when fulfilling a task.

Haykin's definition for cognitive radar 'constituents a dynamic closed feedback loop encompassing the transmitter, environment, and receiver' (Haykin 2006; 2012). Through the perception-action cycle, the CR senses the non-stationary environment, learning about the scene including the target and background, then adapts the transmit action to optimise its knowledge state about the scene according to the mission objective of the radar. A generalised framework that supports the implementation of CR is shown in Figure 2.8. In addition to the general features of a MFR (Section 2.3), the framework comprises of a number of key features to fulfil the aspects of the perception-action cycle (Martone 2014). These include:

1. *Environmental and radar sensors* for target detection and awareness of the environment to provide the CR with supplemental information to enhance the radar performance;

2. *Receiver to transmitter feedback* to maximise target detection performance through resource selection and mitigation of effects from interference and clutter;

3. *Resource library* to select radar operational parameters such as transmit waveforms and signal processing algorithms;

4. *Learning algorithms* to continuously improve performance and adapt to changes in the environment;

5. *Knowledge database* to maintain target, environmental, operational, clutter and other a-priori information; and

6. *Informed decision making* via a decision-theoretic approach that makes use of a-priori and a-posteriori information about the state of the environment.

The decision making process forms a key part of the receiver to transmitter feedback process, using current, past and even predicted information to select future actions. This can include actions such as target assessment based on detection and classification processes and the perceived threat level. The target behavioural assessment process may be performed over a period of time using memory and a set of criteria defined in the database with classification accuracy assessed as part of the learning process. Typical decision outcomes would include the selection of appropriate radar resources to interrogate the scene, such as target priority, illumination waveforms and accompanying receiver signal processing.

As part of the implementation of the decision making phase, two main concepts exist, a Bayesian approach that builds upon prior distributions that describe the target state used in conjunction with models of the environment (Haykin 2006, Kershaw and Evans 1994, Sira *et al.* 2009a) and a machine learning approach. The latter has been proposed for the adaptive determination of the optimal detection thresholds in non-Gaussian clutter within a low sample support regime (Metcalf *et al.* 2015). Further application has been suggested in Shaghaghi and Adve (2018) who proposed a machine learning based RRM to reduce the complexity of NP-hard

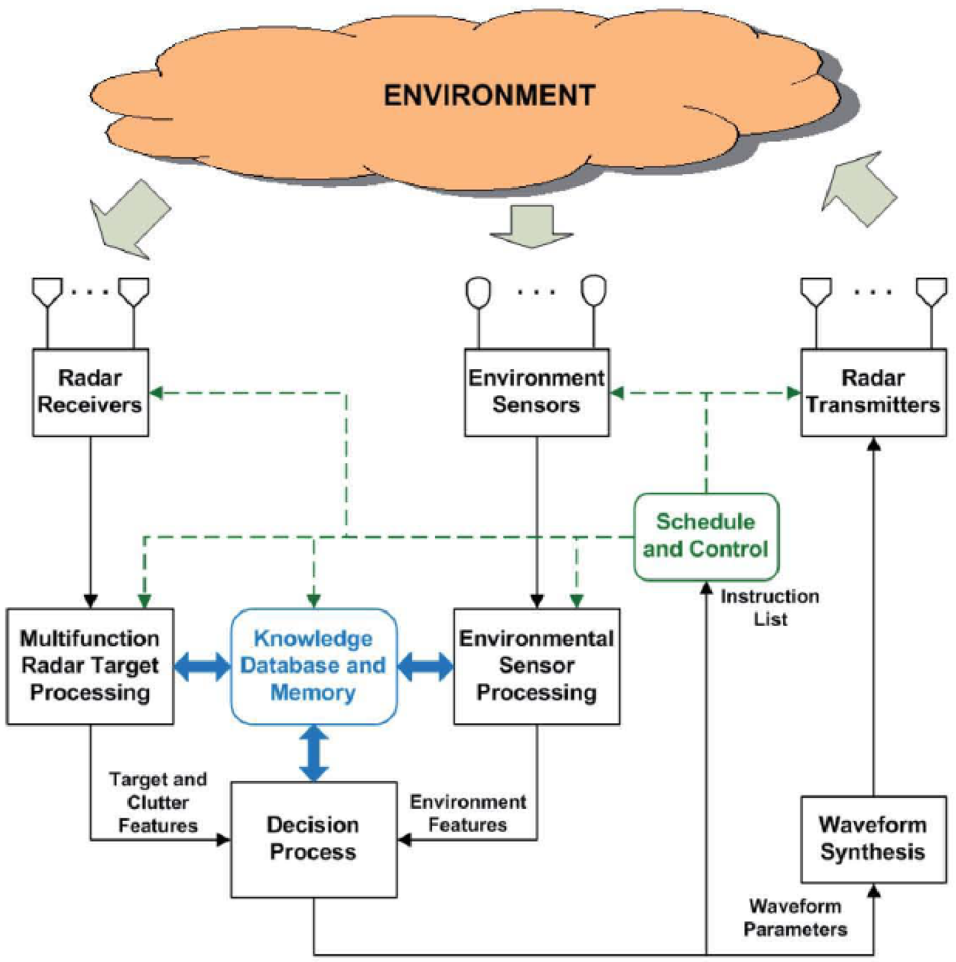

Figure 2.8: A generalised cognitive radar framework (Martone 2014)

scheduling problem for a multi-channel radar. This methods relies on branch-and-bound (B&B) methods to train the scheduler for a more efficient search within the resource scheduling space with the aide of a neural network. In the following subsections, we provide a brief summary of proposed implementations for CR.

Cognitive radar has been proposed for a range of applications spanning from spectral management to target tracking for both passive and active radars (Greco *et al.* 2016; 2018) through the control of radar operational parameters such as illumination transmit power, polarisation, waveform characteristics such as pulse compression, duration and pulse repetition to optimise system performance. Many of the hardware technologies required to implement key features of CR already exist as part of modern AESA radar. Indeed, a unscheduled radar design may pay attention to the selection of these optimal operational parameters. However, they must be chosen a-prioiri and are therefore only optimal for the anticipated scenario. With little or no parametric feedback, variations will undoubtedly result in shortfalls and periods of suboptimal radar performance. In the following subsections, we provide a brief summary of proposed implementations for CR.

2.5.2.1 Networked and passive cognitive radar

The ideas of cognitive radar can be extended to cover non-monostatic forms, such as a network of multiple radars that operate cooperatively to achieve an objective (Griffiths 2010, Haykin 2005). By utilising a cooperative network, the system objective grows to attain a sensing capability in excess of what any individual radar in the network might have otherwise achieved. Haykin (2005) describes two forms of cognitive network; *centralised cognition* where cognition is restrained to central base or hub and a *distributed cognition* where each radar in the network as well any central base includes cognitive abilities. An application of such a network could be the use of multiple radar nodes to track targets. Each track from the individual radars would provide the basis for a sensor fusion mechanism by the central node to compute a composite track of greater quality than would otherwise have been possible from any single radar. Smits *et al.* (2008) proposed a cognitive radar network architecture to allow information to be exchanged at various abstraction levels for an artificial cognition system based on reinforcement learning techniques. Borrowing from the communications sector, a hierarchical model was founded on the revised Joint Directors of Laboratories (JDL) model by Steinberg and Bowman (2004) where two or more cognitive radars can exchange information at various levels. Depending on the abstraction level, differing communications technologies can be used to establish the information sharing. Smits *et al.* (2008) provide an example of a cognitive network of air surveillance radars operating in a littoral environment that operate cooperatively to develop a policy of radar modes for each MFR sector as a function of the radar position throughout a complex trajectory.

The concept of networked CR is extended by Inggs (2009; 2010) who proposed an implementation that exploits illuminators of opportunity for passive coherent location (PCL) (Baker *et al.* 2005, Griffiths and Baker 2005), otherwise termed passive bistatic radar (PBR) (Willis and Griffiths 2007). The proposed cognitive PCL would combine the estimates from multiple illumination sources and receiver nodes to overcome processing limitations from waveform categories such as frequency modulation (FM) radio and analogue television (TV). Griffiths (2010) describe an 'adaptive intelligent radar network' that utilises electronically-steered transmit and receive beams at at each node with the control of the network and tracking of the targets sharing similarities to a monostatic MFR such as task prioritisation and dynamic scheduling. This form of MFR would contain many of the operational benefits that bistatic or multistatic radar operation such as clutter diversity, spatial diversity in the target detection through effects like forward scatter and 'graceful degradation' in the case of multi-node network. Should one or more nodes in the network fail, this is type performance degradation is much like that observed in PAR when elements in the array fail (Griffiths and Baker 2013).

2.5.2.2 Spectral sensing

Another application of CR is in spectral management within an increasingly crowded radio spectrum. By recognising the frequencies used by adjacent transmitters in real time, the objective the radar is to design the transmit waveform to limit interference between itself and neighbouring services such as communications systems. Whilst a typical mitigation approach might have included limiting transmit power and beamshape to minimise interference, in this approach, CR is used. In this case, the perception-action process of cognition is fulfilled by spectral sensing and spectrum sharing (Stinco *et al.* 2016). The transmitters other than the radar are considered to be primary users of the spectrum and the radar itself a lower priority secondary user. Assuming that the frequency band of a communications systems can be broken up into several channels, the primary user does not occupy all channels simultaneously, all of them time. Therefore, some of the channels are opportunistically available provided the radar avoid interference to the primary user as shown in Figure 2.9. By using a separate receiver channel the usage of the spectrum can be observed and fed into a channel characterisation function.

By dynamically controlling typical radar transmitter characteristics including bandwidth, frequency and PRI, increased spectrum utilisation can be achieved whilst avoiding interference with primary users by the statistical characterisation of these opportunities. The role of the channel characteriser is to observe spectral utilisation and estimate parameters of the model used to describe the spectral occupancy of the channel. Most communications channels are quite specific in their usage depending on the location and time. A simple model used to describe channel occupation is a Poisson arrival process where the number of spectrum occupancies over a fixed period follow a Poisson distribution of a given arrival rate. However, as the mean duration of a blank space is inconsistent and can vary according to numerous factors, a Markov modulated Poisson process is instead used to represent the real-traffic with time varying arrival and death rates (Adas 1997, Barnes and Maharaj 2011). This allows the dynamics between the actual primary user states and the sensed states by the radar to be modelled using a Hidden Markov model (HMM). In this process, parameters are estimated for the HMM using a training sequence to account for errors arising from the noisy channel (LaManna 2015, Stinco *et al.* 2014a). The ensuing spectrum occupancy model is then used to inform the spectrum sharing scheduler by anticipating the primary user behaviour and reacting to avoid interference. Spectral sensing has also been proposed for use with compressed sensing (Stinco *et al.* 2014b). In this application, spectral sensing is used to estimate spectral occupancy, with the wideband transmit signal suitably notched to avoid interference with primary users.

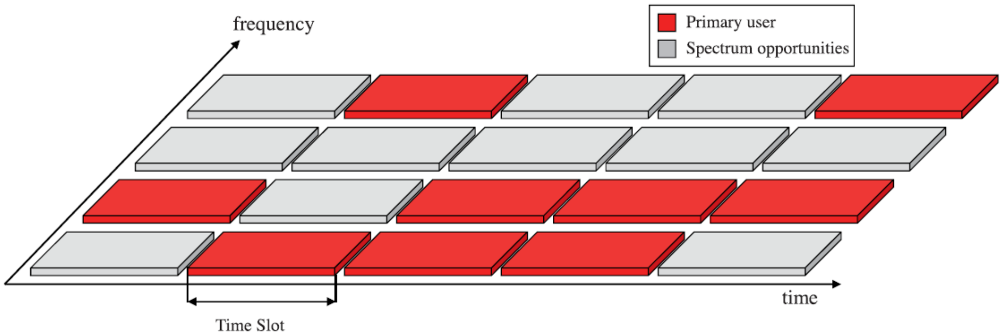

Figure 2.9: Spectral occupancy in the time-frequency channel (Stinco *et al.* 2016)

2.5.2.3 Target detection, identification and tracking

The application of CR for target detection, identification, classification and tracking has received a lot of attention. Tracing back to the application of CR in Haykin (2006), it is closely related to adaptive waveform tracking problem (Cochran 2005, Kershaw and Evans 1994, Patini and Vigilante 2008, Sira *et al.* 2006) and knowledge-aided waveform radar detection and tracking (Gini and Rangaswamy 2008, Guerci 2010). In many of these problems, target tracking is performed using some form of Bayesian recursive estimator such as a Kalman filter. Resources to be scheduled can include waveforms and bandwidths, beam shapes and direction, power and pulse repetition frequency (PRF), carrier frequency and polarisation. In multiple or mobile sensor systems, this may expanded to also include sensor position.

The use of information as a surrogate for waveform scheduling was suggested by Bell (1993) as a cost for optimal waveform selection (Howard *et al.* 2004). Proposed adaptive waveform schemes have also used similar posterior Cramér-Rao bound (PCRB) based criterion to improve target track uncertainty and radar processing error under with various optimisation schemes (Calderbank *et al.* 2009, Haykin *et al.*

2010, Hong *et al.* 2005, Howard *et al.* 2004, Kershaw and Evans 1997, La Scala *et al.* 2005, Niu *et al.* 2002, Sira *et al.* 2009a, Suvorova *et al.* 2006b). Within a dense urban environment, target tracking can become difficult due to multipath channel effects and other reflectors in the scene. Chavali and Nehorai (2010) propose a way to exploit the spatial diversity from multipath propagation effects using a CR network for a single target tracking problem, jointly estimate the target and channel and target states based on a PCRB based optimisation criterion.

Considering a unified framework applicable to MFR technology and the mission profile of the radar, the scheduler may be required to allocate resources to accomplish alternate objectives such as target identification. Goodman *et al.* (2007) described a CR target identification problem where the scheduler selected waveforms as part of a sequential hypothesis testing (SHT) framework to estimate the properties of the transmission channel, customising them until the target could be identified. For extended target recognition, Wei *et al.* (2010) considered a problem for a centralised CR network where radar echoes can be received from multiple aspect angle simultaneously. The inclusion of additional information as part of the estimation process providing the potential to improve robustness of detection performance and target position and aspect angle estimation. Meng *et al.* (2012) investigated the design of phase-coded waveforms for extended target identification in the presence of coloured Gaussian noise using CR.

Task scheduling can be considered a compromise between competing actions such as surveillance (search) and target track (revisit) functions. In these multitasking problems, the spatial and temporal requirements can result in the radar prioritising the track tasks at expense of other tasks such as searching for emergent targets. Kreucher *et al.* (2005b) considered both target track and search functions within the same system, scheduling tasks using a threat based criterion. Suvorova *et al.* (2006a) attempted to unify the problem of resource scheduling utilising permanent virtual targets to overcome the issue of a declining belief in the existence of new undetected targets. A performance bound was applied to set the number of epoch allowed before the radar must revisit any known target, minimise the amount of time the radar spent tracking known targets and freeing up the radar to perform alternate tasks. White *et al.* (2008) proposed a user defined search-to-track ratio to partition the problem into distinct track and search sub-problems. By estimating the spatial density of undetected targets, a search task is initiated and the radar action selected to maximise the number of newly detected targets. Chavali and Nehorai (2012) described a CR network for the challenging problem of multi-target tracking using adaptive sensor scheduling and power allocation. System performance is improved applying several radars in parallel compared with what might otherwise achieved using a single radar. As the computational cost processing measurements increases with number of radars and communications between the network nodes, only a subset of the sensors and power allocation are scheduled at each epoch. Selvi *et al.* (2018) considered the problem of target tracking in the presence of an interferer in the form of a communications source that shared the radar bandwidth. Reinforcement learning methods are applied to solve the optimisation problem of minimising the interference between the radar and the communications system by modelling the communications system as a Markov decision process (MDP) and optimising transmission bands and power levels. Zhang *et al.* (2019) devised a joint beam, power and waveform selection strategy for a multiple-input multiple-output (MIMO) radar for a multiple target tracking problem. Scheduling was based on a PCRB criterion with the difficult multi-objective optimisation problem is broken into a simpler objective function based on the Zoutendijk feasible direction method (Zoutendijk 1970). More recently, Xiang *et al.* (2019) proposed a target tracking framework for simultaneous sensor selection, waveform design and path planning for radars on moving platforms, such as unmanned aerial vehicles (UAVs) within a centralised CR network. The scheduling problem was formulated as a combinatorial optimisation problem to select the optimal subset of sensors to interrogate the target as well as the optimal waveforms using a PCRB based metric.

A more general fully adaptive radar (FAR) framework was proposed by Bell *et al.* (2014a), initially for a target tracking problem. This model utilised a low level radar processor for received signals and a high level task processor for higher level tasks such as tracking and target classification. In Bell *et al.* (2014b), the authors specialise the framework for a target detection and track initiation scenario. Bell *et al.* (2015a) described a generalised CR framework for all of the target tracking phases, including track initiation, update and termination. These frameworks are combined in Bell *et al.* (2015a) with cost functions selected to minimise the time required to detect the presence or absence of a target and minimise the predicted conditional mean square error of the target state. The framework is applied to select the optimal sensor to observe a target within a multiple sensor example. Smith *et al.* (2016) later reports on experimental results from a CR prototype concept applied in a single target tracking scenario based on the work of Bell *et al.* (2015a). In this experiment, the radar PRF was optimised, affecting the resolved target Doppler response. Using both fixed and varying pulse train lengths, the authors varied the radar PRF to optimise the target placement in the radar range-Doppler response for the selected Doppler filter resolution, ambiguous velocity and clutter line given the predicted target state. Mitchell *et al.* (2017) extends these experiments by using the same cognitive processing framework, optimising the radar PRF for a single target in track but instead using radar network. Bell *et al.* (2018) extends this framework to include multiple tasks priorities, involving a scenario with multiple targets. Employing multiple perception-action cycles, the CR is tasked with the identification, classification and tracking of each target.

2.5.3 Challenges with implementation of adaptive radar

Despite the significant advances in radar and signal processing technology, it is acknowledged that whilst conceptually possible there are still a number of hurdles to overcome in the implementation of a cognitive system (Guerci *et al.* 2014). A central issue that remains is the computational tractability of CR processing — how to schedule the radar resources and prioritise tasks economically within the operational time scales the radar operates within, particularly for a rich resource library with a vast combinatorial solution space.

Cochran (2005) foresaw many of the implementation challenges associated with the adaptive and particularly cognitive radar. The author speculated whether the use of cost functions that rely upon theoretical measures as a performance criteria would prove a reliable means of quantifying predicted waveform performance for real targets and considered the difficulty of computing a solution to the complex multi-stage optimisation process of resource scheduling. Cochran posited that the use of scheduling for waveform blocks or alternate signal processing techniques such as analogue or optical processing may overcome some of the optimisation hurdles (Casasent 1980, Casasent *et al.* 1980, Vannicola 1980). Various optimisation methods such as convex relaxation have been proposed as a way deal with the computational complexity associated with waveform selection to attain a sparse solution (Joshi and Boyd 2009, Rangarajan *et al.* 2006). Kreucher and Hero (2005) investigate the use of dynamic programming approximations and reinforcement learning as approaches that could be used to deal with the complexities of a non-myopic scheduler. Acknowledging that a dynamic programming solution does not permit their direct application to the dimensionality problem with a tractable solution within any real time frame, (Wintenby and Krishnamurthy 2006) consider a hierarchical method for AESA surveillance radar resource management by solving the slowtime scheduling dynamic programming problem using approximate Lagrangian relaxation.

Other issues issues include the potential of competing performance criteria, the design of robust cost functions or operating 'figures of merit' (Greenspan 2014), and the implementation of the dynamic reconfiguration of the radar waveform within the constraints of a library, a property known as *waveform diversity* (Wicks *et al.* 2011).

Ender and Bruggenwirth (2015) summarised the CR implementation approaches described by Haykin (2012) and Guerci (2010) and emphasised the requirement for real-time processing of sophisticated algorithms. The authors considered the implementation problem by proposing a three layered abstraction model that can be used achieve the perception-action cycle (Section 2.5.1).

Working towards developing a prototype in collaboration with Defense Advanced Research Projects Agency (DARPA), Guerci and Baranoski (2006) proposed the development of a knowledge-aided adaptive radar architecture based on an adaptive space-time beamforming front-end. In their implementation, the authors recognised that memory quantities such as environmental knowledge are inherently difficult to access at the rates necessary to meet radar front-end throughput. Guerci *et al.* (2014) later devised the Cognitive Fully Adaptive Radar (CoFAR) architecture to address many of the performance demands and operational constraints. This design adopted four dedicated processors to deal with the high computational load associated with CR processing namely, transmit and receive signal processing, setting radar mission objectives, resource scheduling and channel estimation. Beyond computational complexity, distinct practical challenges exist with the implementation of multistatic CR network. These include geolocation, synchronisation and data sharing across the radar network (Griffiths and Baker 2013). While some technologies such as Global Navigation Satellite System (GNSS) can be used as part of the synchronisation solution, such services may be potentially denied, especially in a military operational environment.

Stochastic optimisation methods are a strong candidate for the MFR resource allocation and scheduling problem because of the stochastic nature of the radar scene and target dynamics. This approach can be formulated in feedback based control scheme that adapts to changes in the environment or operational requirements by leveraging the virtually instantaneous diversity of the radar hardware operating parameters. In the subsequent chapter, we provide some background on radar waveform accuracy and consider the problem of adaptive radar resource scheduling and the impact of update rates in the context of a radar target tracking application.

Chapter 3

Scheduling for adaptive radar

The intent of this chapter is to provide a summary of the key concepts related to the sensor and particularly radar resource scheduling. A brief primer on target tracking based on a Bayesian framework is included before describing the problem of resource scheduling for adaptive radar. This is followed by an outline of resource diversity for radar with a focus on radar waveforms and the use of the ambiguity function to describe the waveform accuracy. We then look more specifically at the use of waveform scheduling in radar and its briefly its application in target detection and classification. A more detailed review is provided for waveform scheduling for target tracking, including control theoretic and information theoretic approaches. The conclude, we provide an example that considers the value of scheduling and associated cost of delaying updates for a linear system that is estimated by a Bayesian filter to help motivate the use of resource scheduling under time constraints.

3.1 Bayesian framework for tracking radar

The primary objective of target tracking is to estimate the trajectory or state of a target. If we assume that the target dynamics can be represented by a Markovian process, the trajectory of an target can generally be described by a stochastic differentiable continuous time equation with an additive noise process

$$\mathbf{x}'(t) = f\left(\mathbf{x}(t), \mathbf{u}(t), t\right) + \mathbf{w}(t) \tag{3.1a}$$

$$\mathbf{z}(t) = h\left(\mathbf{x}(t), t\right) + \mathbf{v}(t) \tag{3.1b}$$

where $\mathbf{x}(t)$, $\mathbf{u}(t)$ and $\mathbf{z}(t)$ are the target state, control input and observation vectors at time t and $\mathbf{w}(t)$ and $\mathbf{v}(t)$ are the process and measurement noise processes. Function $f(\cdot)$ is used to describe the state transition model and $h(\cdot)$ the observation model. For convenience, it can be easier to represent this continuous state representation in discrete time as a stochastic difference equation

$$\mathbf{x}_{k+1} = f\left(\mathbf{x}_k, \mathbf{u}_k\right) + \mathbf{w}_k \tag{3.2a}$$

$$\mathbf{z}_k = h\left(\mathbf{x}_k\right) + \mathbf{v}_k \tag{3.2b}$$

where discrete time index $k = 0, 1, 2, \ldots$ and noise processes $\mathbf{w}_k, \mathbf{v}_k$ are temporally uncorrelated. The transition and observation model functions are assumed to be known and deterministic with the measurements or observations received sequentially over time. When we consider the problem of target tracking or state estimation often it is more appropriate to use mixed-time models, combining (3.1) and (3.2) where convenient (Li and Jilkov 2003). This form of description is commonly referred to as a state-space model or representation and can be used to describe both linear and non-linear stochastic dynamical models of moving targets.

3.1.1 General recursive Bayesian estimation for target tracking

The Bayesian approach is a well-developed probabilistic and statistical theory that is widely used in engineering and statistical community and may be readily applied to the problems encountered in object tracking. The premise of this approach is Bayes' theorem, which describes the probability of an event given some observed condition. This leads us to Bayesian inference, a statistical method where Bayes' theorem is applied to update the probability of a hypothesis as more evidence or information becomes accessible.

In this approach, the posterior distribution about an event is proportional to the likelihood of the event multiplied by the prior distribution, normalised by the evidence or marginal probability. Mathematically, this can be written elegantly as

$$p\left(\theta|y\right) = \frac{p\left(y|\theta\right) p\left(\theta\right)}{p(y)} \tag{3.3}$$

where the posterior probability $p\left(\theta|y\right)$ is the parameter we wish to estimate after evidence y given our prior probability $p\left(\theta\right)$. Likelihood $p\left(y|\theta\right)$ indicates the probability that the evidence is y given θ. The marginal probability or evidence that normalises the result is $p\left(y\right)$.

Bayesian inference is particularly useful for the dynamic analysis of data sequences, often incurred in target tracking problems. We denote the target state at discrete time k as $\mathbf{x}_k$ and the sequence of states up to k as

$$\mathbf{x}^k = \begin{bmatrix} \mathbf{x}_1^\top & \mathbf{x}_2^\top & \mathbf{x}_3^\top & \cdots & \mathbf{x}_k^\top \end{bmatrix}^\top \tag{3.4}$$

where the state $\mathbf{x}$ is vector that contains information such as position and velocity. The sequence of measurements to $\mathbf{z}_k$ can be written as

$$\mathbf{z}^k = \begin{bmatrix} \mathbf{z}_1^\top & \mathbf{z}_2^\top & \mathbf{z}_3^\top & \cdots & \mathbf{z}_k^\top \end{bmatrix}^\top \tag{3.5}$$

where for radar, $\mathbf{z}$ typically includes range, radial velocity and pointing angles. From Bayes' inference, we can write the posterior distribution as

$$p(\mathbf{x}_k|\mathbf{z}^k) = \frac{p(\mathbf{z}_k|\mathbf{x}_k, \mathbf{z}^{k-1})p(\mathbf{x}_k|\mathbf{z}^{k-1})}{p(\mathbf{z}_k|\mathbf{z}^{k-1})} \tag{3.6}$$

by assuming that the state transitions are Markovian in sense that

$$p(\mathbf{x}_k|\mathbf{x}^{k-1}) = p(\mathbf{x}_k|\mathbf{x}_{k-1}) \tag{3.7}$$

where the probability of the k-th index given the previous step is conditionally independent of all the other states. Using this, we can write (3.6) in a recursive form between the posterior distributions at time index k and $k-1$ comprising of two distinct steps; a prediction followed by an update.

3.1.1.1 Prediction step

The predicted or prior density predicts the state estimate at time index k given the knowledge about the state at $k-1$ and observations up to and including $\mathbf{z}_{k-1}$. Assuming the posterior $p(\mathbf{x}_{k-1}|\mathbf{z}^{k-1})$ is known, the transitional density can be calculated using marginalisation by the Chapman–Kolmogorov equation:

$$\begin{aligned} p(\mathbf{x}_k|\mathbf{z}^{k-1}) &= \int p\left(\mathbf{x}_k, \mathbf{x}_{k-1}|\mathbf{z}^{k-1}\right) \mathrm{d}\mathbf{x}_{k-1} \\ &= \int p\left(\mathbf{x}_k|\mathbf{x}_{k-1}\right) p\left(\mathbf{x}_{k-1}|\mathbf{z}^{k-1}\right) \mathrm{d}\mathbf{x}_{k-1} \end{aligned} \tag{3.8}$$

For the Markov system described by (3.2a), we can use a transformation of random variables and write the prediction density (3.8) as

$$p(\mathbf{x}_k|\mathbf{z}^{k-1}) = \int p_w\left(\mathbf{x}_k - f_k(\mathbf{x}_{k-1})\right) p\left(\mathbf{x}_{k-1}|\mathbf{z}^{k-1}\right) \mathrm{d}\mathbf{x}_{k-1} \tag{3.9}$$

where f_k is the state transition function at the k-th index and process noise $\mathbf{w}_k \sim p_w(\cdot)$ is assumed to be temporally uncorrelated.

3.1.1.2 Update step

Using the measurement likelihood $p(\mathbf{z}_k, |\mathbf{x}_k)$, the prior is informed by this new information and updated as

$$p(\mathbf{x}_k|\mathbf{z}^k) \propto p(\mathbf{z}_k|\mathbf{x}_k)p(\mathbf{x}_k|\mathbf{z}^{k-1}) \tag{3.10}$$

Again by applying a transformation of variables, from (3.2b), this can be written as

$$p(\mathbf{x}_k|\mathbf{z}^k) \propto p_v\left(\mathbf{z}_k - h_k(\mathbf{x}_k)\right) p(\mathbf{x}_k|\mathbf{z}^{k-1}) \tag{3.11}$$

where h_k is observation function at the k-th index and measurement noise $\mathbf{v}_k \sim p_v(\cdot)$ is also assumed to be temporally uncorrelated. To complete the application of Bayes' theorem, the normalising constant must be computed. As this is a marginal distribution, it can be found by integrating (3.10) and then applying the transformation of variables,

$$\begin{aligned} p\left(\mathbf{z}_k|\mathbf{z}^{k-1}\right) &= \int p\left(\mathbf{z}_k|\mathbf{x}_k\right) p\left(\mathbf{x}_k|\mathbf{z}^{k-1}\right) \mathrm{d}\mathbf{x}_k \\ &= \int p_v\left(\mathbf{z}_k - h_k\left(\mathbf{x}_k\right)\right) p\left(\mathbf{x}_k|\mathbf{z}^{k-1}\right) \mathrm{d}\mathbf{x}_k \end{aligned} \tag{3.12}$$

Substituting into (3.6), the update can be completed as,

$$p(\mathbf{x}_k|\mathbf{z}^k) = \frac{p_v\left(\mathbf{z}_k - h_k(\mathbf{x}_k)\right) p(\mathbf{x}_k|\mathbf{z}^{k-1})}{\int p_v\left(\mathbf{z}_k - h_k\left(\mathbf{x}_k\right)\right) p\left(\mathbf{x}_k|\mathbf{z}^{k-1}\right) \mathrm{d}\mathbf{x}_k} \tag{3.13}$$

$$= \frac{p_v\left(\mathbf{z}_k - h_k(\mathbf{x}_k)\right) \int p_w\left(\mathbf{x}_k - f_k(\mathbf{x}_{k-1})\right) p\left(\mathbf{x}_{k-1}|\mathbf{z}^{k-1}\right) \mathrm{d}\mathbf{x}_{k-1}}{\int p_v\left(\mathbf{z}_k - h_k\left(\mathbf{x}_k\right)\right) \left[\int p_w\left(\mathbf{x}_k - f_k(\mathbf{x}_{k-1})\right) p\left(\mathbf{x}_{k-1}|\mathbf{z}^{k-1}\right) \mathrm{d}\mathbf{x}_{k-1}\right] \mathrm{d}\mathbf{x}_k} \tag{3.14}$$

This is known as the general Bayesian recursion and is the basis for Bayesian filtering algorithms such as the Kalman filter. It is often depicted as four discrete steps for computational convenience as illustrated in Figure 3.1.

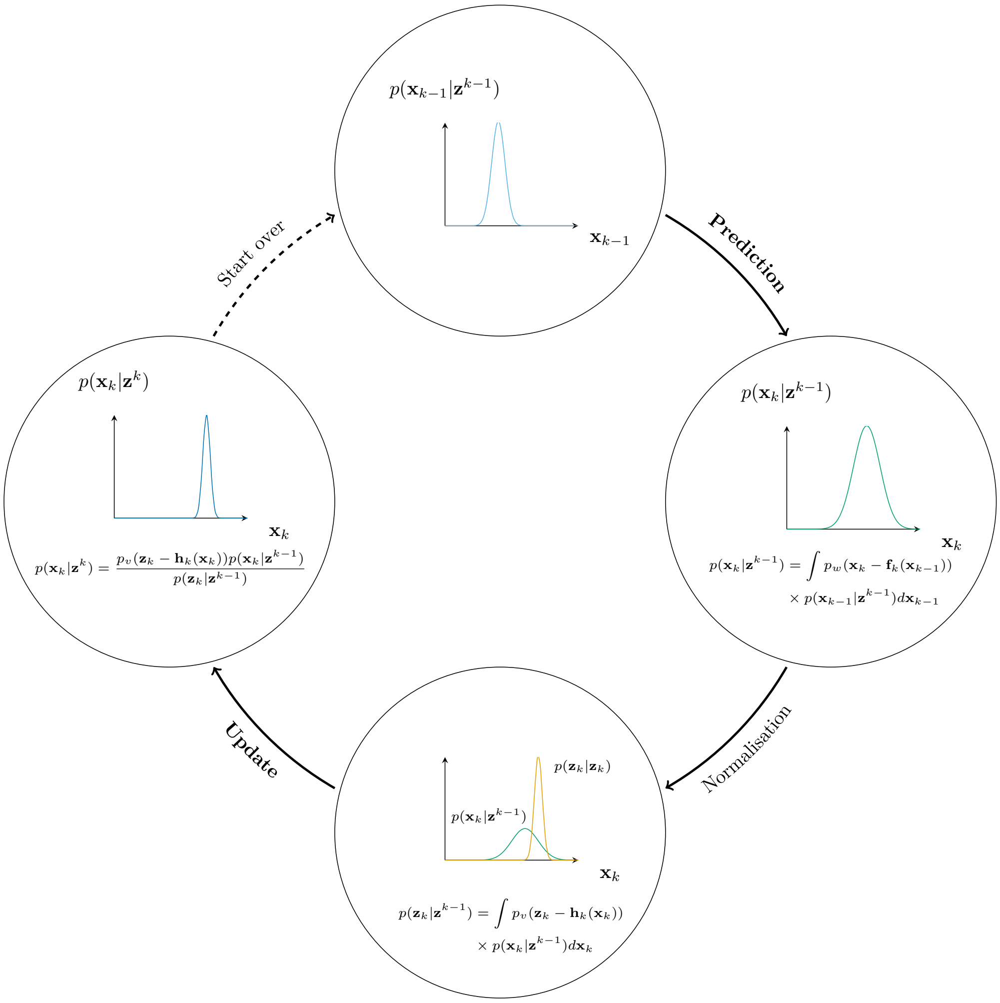

Figure 3.1: General Bayesian recursion as a continuous loop

3.2 Resource scheduling for adaptive radar

Conventional radar scheduling can be performed using task oriented methods that consider time as the cost (Ng and Ng 2000). Tasks are categorised into levels of time criticality before being ordered using task or bin packing algorithms, interleaving the tasks within the radar budget constraints. The ordered tasks are drawn from the queue and executed in sequence using the chosen sensor. In this definition, we refer to a sensor as being the radar system operated and its action (Hero and Cochran 2011). For example, selecting different waveforms for a single radar or switching transmitter sites would both be considered different sensors. Sensor management requires the dynamic selection of a sensor amongst a set of available sensors to use at each epoch that achieves the system objective or optimises some form of performance metric. We consider the closed loop solution to this problem; selection of the physical sensor system, accompanying choice of operating mode and configuration parameters or action based on information from prior knowledge, previous measurements and intrinsic information about state of the radar itself, such as position and orientation as shown in Figure 3.2.

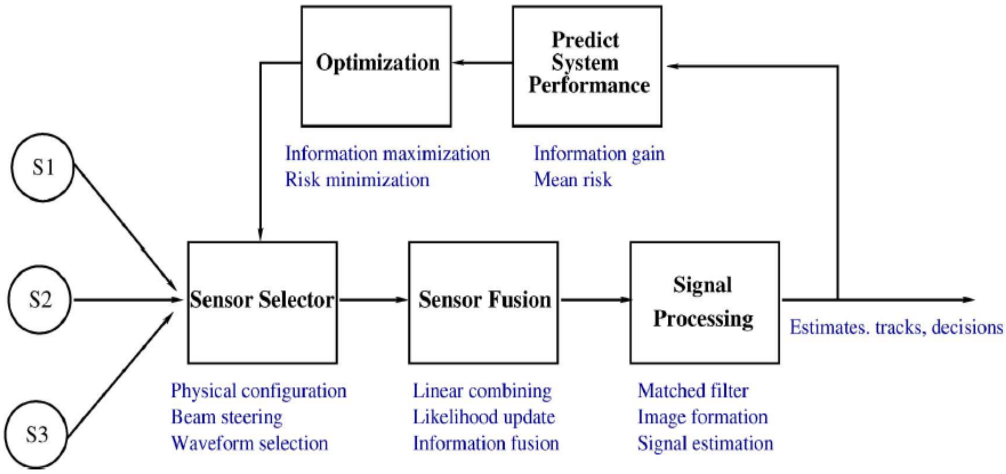

Figure 3.2: Conceptual diagram of a sensor management system showing the choice of three possible actions, (Hero and Cochran 2011)

Sensor management is often be perceived to be a control problem, governed by some feedback control process. However, an important distinction is that in traditional feedback control, sensors are used to measure the dynamic state of the plant. The control action is selected based upon this information through the control policy. In sensor management, the control policy involves selecting control action based on the information received about a scene, which happens to be the sensor action itself. Once a measurement is acquired, the data is combined with past measurements to form information used in the optimisation decision process based on some merit. This process can range from statistical to completely heuristic.

The sensor management system must select the optimal sensing action before it receives the measurement using prior information and learning. Adaptive radar is amongst the numerous applications of sensor management, led by the embrace of AESA MFR (Section 2.3). This technology has provided an unprecedented number of controllable degrees of freedom within the radar. This includes the ability to alter both transmit and received antenna patterns through beamforming despite sharing an antenna, as seen in simultaneous transmit and receive (STAR) systems with full-duplex capabilities (Fitz *et al.* 2014, Kolodziej *et al.* 2015). The use of digital waveform synthesis permits the generation of arbitrary waveforms as seen in waveform-agile radar (Sira *et al.* 2006), within the constraints of the system resources budget (Section 2.4). An attribute which makes radar, particularly for pulsed systems an attractive candidate for sensor scheduling is that time can be segmented into a sequence of distinct epochs. Using this paradigm, a different sensor can be selected at each epochs, creating a discrete-time problem. Within target detection, identification and tracking problems (Section 2.5.2.3) performance metrics have already been identified along with established target dynamical models (Section 3.1).

3.2.1 Resource diversity

Traditionally, radars operational parameters were preconfigured by the designer and combined into groups or sets according to specific operational modes to provide radar function. State of the art technology allows the radar to operate deftly across space, time and frequency with a extensive set of diverse operational conditions. Resource diversity can be categorised as being either physical or waveform related. Physical diversity involves control of the direction and polarisation of the transmitted radar signal during the illumination of the radar scene, and the subsequent positioning of the associated receiver(s). Scatterer RCS is dependant upon multiple parameters including the physical positioning of the transmitter, receiver and orientation of incident EM wave. The RCS (Section 2.1.1) can be described as $\sigma(\boldsymbol{k}, \boldsymbol{e}|\boldsymbol{\kappa}, \boldsymbol{\epsilon})$ where $\boldsymbol{\kappa}, \boldsymbol{\epsilon}$ are the direction of arrival and complex polarisation vector of the illuminating wave and $\boldsymbol{k}, \boldsymbol{e}$ are the propagation direction and polarisation of the reflected wave (Calderbank *et al.* 2009, Skolnik 2001).

Waveform diversity refers to the ability of the radar to illuminate the scene with different waveforms, even simultaneously through multiple antennas, at up to an interpulse basis. Waveforms are chosen according to the radar scene the selected task (Gini *et al.* 2012, Wicks *et al.* 2011). The waveforms can be synthesised by varying parameters such as power, frequency, modulation, duration and PRI to achieve desirable properties, affecting target detectability, range and accuracy when used the applicable signal processing methods as described in the following section.

3.3 Radar waveforms

We consider the case of radar signals that are defined as being narrow bandpass signals where the angular frequency of the waveform is bounded by $\pm\Delta W$ about a carrier frequency ω_c due to the practicality of their generation (Levanon and Mozeson 2004). The transmitted radar signal comprises of a baseband signal or complex envelope $\tilde{s}(t)$ that is modulated onto a sinusoidal carrier frequency (2.8)

$$\tilde{s}(t) = a(t) \exp\left(j\phi(t)\right) \tag{3.15}$$

where $a(t)$ is the *natural* envelope of $x(t)$ and $\phi(t)$ is the instantaneous phase. For a train of $2N + 1$ pulses with constant pulse repetition interval T_r, the duration of the pulse train is

$$T_d \triangleq 2NT_r + T_p$$

where T_p is the interpulse spacing. The complex envelope of the pulse train is

$$\tilde{s}(t) = \frac{1}{(2N+1)^{\frac{1}{2}}} \sum_{n=-N}^{N} \tilde{u}_n(t - nT_r) \tag{3.16}$$

and $\tilde{u}_n(t)$ is envelope of the n-th pulse in the train (Levanon and Mozeson 2004). For a coherent transmitter, the pulse phase can be made invariant from pulse to pulse. When using a matched filter receiver, the accuracy of the radar pulse can be represented by its ambiguity function (Section 3.3.2).

3.3.1 Pulse compression

Pulse compression is utilised as a technique to address the challenge of improving target SNR. This is achieved by increasing incident energy without adversely affecting range resolution from the short pulses, despite transmitter peak power limitations (Klauder *et al.* 1960). Through modulation of a longer pulse, the range resolution is commensurate with that of an unmodulated pulse of short duration when used in conjunction with appropriate receiver processing (Section 2.2) and is inversely proportionate to the bandwidth of the pulse. Much of the work regarding the design of waveform modulation schemes is to control or suppress the formation of the ensuing sidelobe structure of the processed signals (Levanon and Mozeson 2004). This is important given that most target detection techniques rely on identification of contrasting features in the received signal. In a complex scene comprising of multiple scatterers, targets are superpositioned with each other and the background clutter, making discrimination of target mainlobe responses from sidelobes and clutter challenging.

A frequently used form of pulse compression is linear frequency modulation (LFM), commonly referred to as a chirp. The normalised complex baseband representation of a LFM chirp of pulsewidth T is

$$\tilde{s}_{LFM} = \frac{1}{\sqrt{T}} e^{j\theta(t)} \tag{3.17}$$

where phase function

$$\theta_{LFM}(t) = \pm \frac{\pi B t^2}{T}, \quad -\frac{T}{2} \leq t \leq \frac{T}{2} \tag{3.18}$$

and $\pm$ indicates either an upchirp (increasing frequency) or downchirp (decreasing frequency) and BT the time-bandwidth product the chirp or its compression ratio. This is also known as the coherent gain, the relative gain in SNR compared with an equivalent uncompressed pulse.

3.3.2 Radar ambiguity

The time-frequency auto correlation function or radar ambiguity function (AF) was introduced by Ville (1948) and later studied in detail by Woodward (1967) and hence, is sometimes referred to as Woodward's ambiguity function. It can be used to represent the time and frequency response of a matched filter for a nominal target with range and Doppler given a finite energy signal. The radar AF is normally used as a tool to investigate the range and Doppler resolution and distortion properties of different waveforms and their suitability through the ambiguity diagram (Figure 3.3). Neglecting the ambiguity function sidelobes, the accuracy of a pulse can be characterised by the AF. Given an associated narrowband waveform, for a monostatic radar the AF is

$$|\chi(\tau', \nu')| \triangleq \left| \int u\left(t - \frac{\tau'}{2}\right) u^*\left(t + \frac{\tau'}{2}\right) e^{-j\nu' t}\, dt \right| \tag{3.19}$$

for normalised complex waveform envelope $u(t)$ where received signal delay $\tau' = \tau - \tau_0$ and Doppler shift $\nu' = \nu - \nu_0$ are relative to the nominal values expected by the filter (Van Trees 2001, Woodward 1967). Ambiguity function $\chi(\tau', \nu')$ is maximised at the target true position (τ_0, ν_0) with a increasing τ implying that the target that is further away from the radar and a positive ν, a target with a closing radial velocity.

3.3.2.1 Properties of the ambiguity function

The are five main properties of the AF, assuming that the energy of $u(t)$ is normalised to unity (Levanon and Mozeson 2004, Mahafza 2013).

Property 1 (Maximum at the origin)**.**

$$|\chi(\tau,\nu)| \leq |\chi(0,0)| = 1 \tag{3.20}$$

The AF cannot be higher anywhere other that at the origin, where it is normalised to unity from Schwartz inequality.

Property 2 (Volume invariance)**.**

$$\int_{-\infty}^{\infty}\int_{-\infty}^{\infty} |\chi(\tau,\nu)|^2 \, d\tau d\nu = 1 \tag{3.21}$$

The total volume under the ambiguity function squared is unity, regardless of the waveform.

Property 3 (Symmetry with respect to the origin)**.**

$$|\chi(\tau,\nu)| = |\chi(-\tau,-\nu)| \tag{3.22}$$

The AF is symmetric about both the delay and Doppler planes.

Property 4 (Modulation by linear frequency modulation signal)**.**

$$x(t)\exp(j\pi\kappa t^2) \Leftrightarrow |\chi(\tau,\nu-\kappa\tau)| \tag{3.23}$$

Given an complex envelope $u(t)$ and it corresponding ambiguity function $\chi(\tau,\nu)$, then by adding linear frequency modulation of chirp rate κ results in the shearing of the ambiguity function along the Doppler axis, resulting in an improvement in the delay resolution as a function of the chirp bandwidth.

Property 5 (Frequency energy spectrum)**.**

$$|\chi(\tau,\nu)|^2 = \left|\frac{1}{2\pi}\int_{-\infty}^{\infty} U^*\left(\nu-\frac{\nu'}{2}\right) U\left(\nu+\frac{\nu'}{2}\right) e^{-j\nu\tau'} \, d\nu\right|^2 \tag{3.24}$$

If $\frac{1}{2\pi}U(\nu)$ is the Fourier transform of $u(t)$, then by Parseval's theorem the volume is unitary.

Whilst the ideal AF can be represented by a thumbtack response, Property 1 and Property 2 imply that any attempt to squeeze the AF into a narrow peak, results in the peak not exceeding 1, and the volume squeezed out of the peak reappearing elsewhere. This is an important attribute, as techniques such as pulse compression can improve range resolution, they come with the expense such as a loss in Doppler resolution or increased sidelobes. For a single rectangular (unmodulated) pulse, the AF can be shown in Figure 3.3a and shearing evident for a LFM pulse (Property 4) in Figure 3.3b.

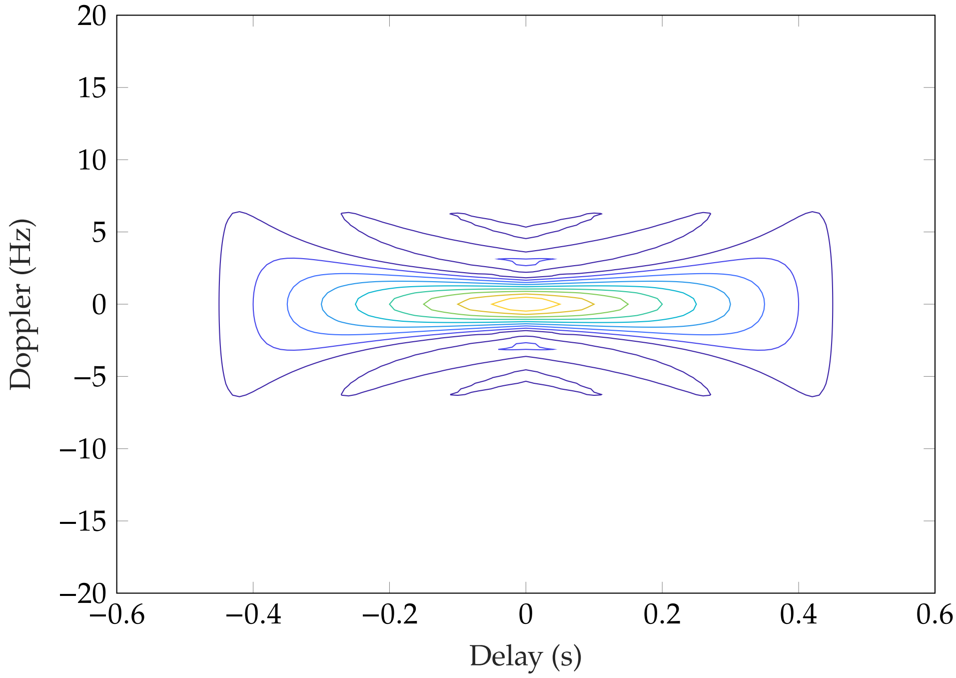

(a) 1 s uncompressed pulse

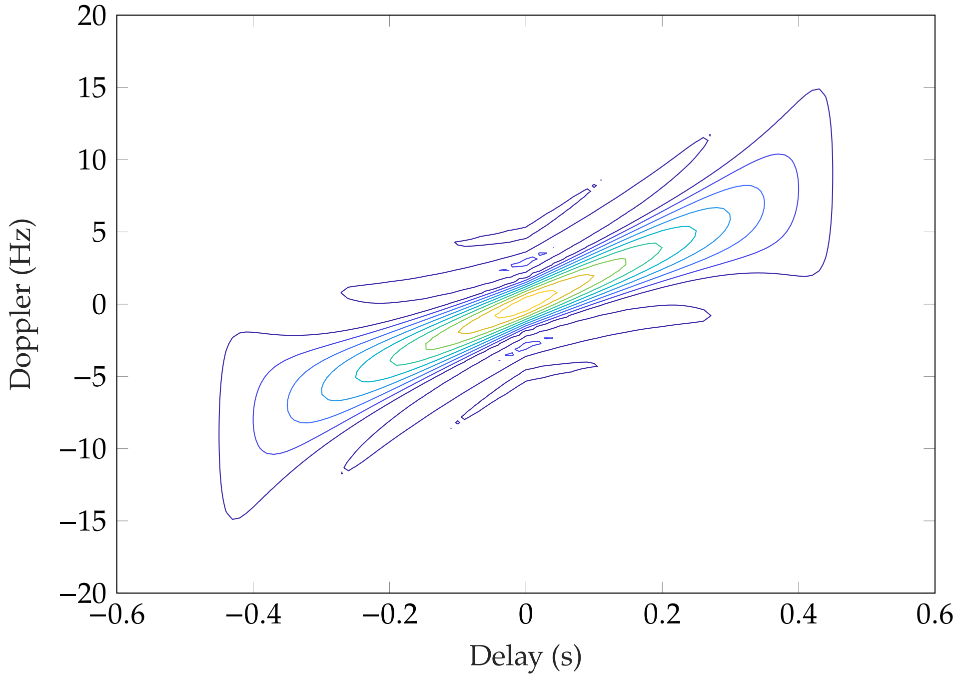

(b) 100 kHz LFM chirp (3.17)

Figure 3.3: Ambiguity function for unmodulated (above) and linear frequency modulation (below) pulses of unit duration

3.3.3 Local accuracy for radar pulses

The ambiguity function (Section 3.3.2) describes the global pulse accuracy of the system. In this subsection, we consider the accuracy of estimates in delay and Doppler (τ, ν) for a received signal of target of high SNR and low error, a problem of *local accuracy*. For an unbiased estimator, the bound for the error covariance of the received pulse approaches that described by the Cramér-Rao lower bound (CRLB) (Van Trees 2001)

$$\mathbf{J} = \frac{2E_r}{N_0}\begin{bmatrix} \overline{\omega^2} - (\bar{\omega})^2 & \overline{\omega t} - \bar{\omega}\bar{t} \\ \overline{\omega t} - \bar{\omega}\bar{t} & \overline{t^2} - (\bar{t})^2 \end{bmatrix} = \eta \mathbf{U} \tag{3.25}$$

whose elements are the second derivatives of the ambiguity function (3.19) evaluated at the target true position (τ_0, ν_0) and η is the measurement SNR. Separating the signal-to-noise ratio, the elements of matrix $\mathbf{U}$ are computed by inverting the Hessian of the ambiguity function evaluated at the true target delay and Doppler (Van Trees 2001) as

$$\overline{\omega^2} - (\bar{\omega})^2 = -\left.\frac{\partial^2 \chi(\tau,\nu)}{\partial \tau^2}\right|_{\substack{\tau=\tau_0,\\ \nu=\nu_0}} \tag{3.26}$$

$$\overline{\omega t} - \bar{\omega}\bar{t} = -\left.\frac{\partial^2 \chi(\tau,\nu)}{\partial \tau \nu}\right|_{\substack{\tau=\tau_0,\\ \nu=\nu_0}} \tag{3.27}$$

$$\overline{t^2} - (\bar{t})^2 = -\left.\frac{\partial^2 \chi(\tau,\nu)}{\partial \nu^2}\right|_{\substack{\tau=\tau_0,\\ \nu=\nu_0}} \tag{3.28}$$

The elements of symmetric matrix $\mathbf{U}$ are a function of the pulse parameters and can be computed as (Kershaw and Evans 1994, Van Trees 2001)

$$u_{11} = \overline{\omega^2} - (\bar{\omega})^2 = \frac{1}{2\pi}\int_{-\infty}^{\infty} \omega |\tilde{S}(\omega)|^2 \,\mathrm{d}\omega \tag{3.29a}$$

$$u_{12} = u_{21} = \overline{\omega t} - \bar{\omega}\bar{t} = \int_{-\infty}^{\infty} t\varphi'(t)|\tilde{s}(t)|^2 \,\mathrm{d}t \tag{3.29b}$$

$$u_{22} = \overline{t^2} - (\bar{t})^2 = \int_{-\infty}^{\infty} t|\tilde{s}(t)|^2 \,\mathrm{d}t \tag{3.29c}$$

where the waveform envelope and its Fourier transform can be expressed as

$$\tilde{s}(t) = |\tilde{s}(t)| \exp\big(j\varphi(t)\big) \tag{3.30a}$$

$$\tilde{S}(\omega) = \int_{-\infty}^{\infty} \tilde{s}(t)\mathrm{e}^{j\omega t}\,\mathrm{d}t \tag{3.30b}$$

Assuming mean time $\bar{t}$ and frequency $\bar{\omega}$ to be zero (Van Trees 2001), the pulse CRLB can then be simply expressed as

$$\begin{aligned}\mathbf{U}^{-1} &= \frac{1}{(\overline{\omega^2})(\overline{t^2}) - \overline{\omega t}^2}\begin{bmatrix}\overline{t^2} & -\overline{\omega t}\\ -\overline{\omega t} & \overline{\omega^2}\end{bmatrix}\\ &= \begin{bmatrix}\sigma_\tau^2 & \rho_{\tau\nu}\\ \rho_{\tau\nu} & \sigma_\nu^2\end{bmatrix}\end{aligned} \tag{3.31}$$

where $\sigma_\tau^2, \sigma_\nu^2$ represent the delay and Doppler resolution properties of the pulse.

3.4 Waveform scheduling

In general when constrained in pulse length and bandwidth, a waveform can possess good range or good Doppler resolution but not both (Property 1 and Property 2). Waveform scheduling is motivated by the sense that an improvement in radar performance or utility can be achieved by the optimal selection of variations or parameters under control of the radar waveform (Section 3.2.1). Waveform scheduling was proposed for a target classification problem in a radar imaging in Sowelam and Tewfik (1994) and a target tracking problem in Kershaw and Evans (1994). Since then, many authors have built upon the concept of scene interrogate using adaptive waveform selection, particularly for tracking applications including sonar (Hong *et al.* 2005) and in particular radar (Calderbank *et al.* 2009, Cochran *et al.* 2009).

Sensor scheduling may be represented by a closed-loop process such as that shown in Figure 3.5. After each measurement epoch, the radar updates its knowledge state of the scene. Using this information to update the knowledge state, actions such as waveforms are selected from a resource library according to some criterion to optimise the acquisition of new information about the scene. This new action is placed into a queue to be executed at a future epoch according to the scheduling policy of the radar. In the target tracking example of Figure 3.5, the predicted target state(s) for the scene are used to inform the waveform selection process. The scheduling process can involve multiple dynamic models and other scene models such as clutter to evaluate the effectiveness of the candidate waveform solutions. An optimal waveform is then selected according to a criterion or cost function is then use to illuminate the scene. Received signals are processed, detected targets identified and associated with candidate target tracks for update before the cycle repeats.

A summary of the challenges associated with waveform agile sensing is included

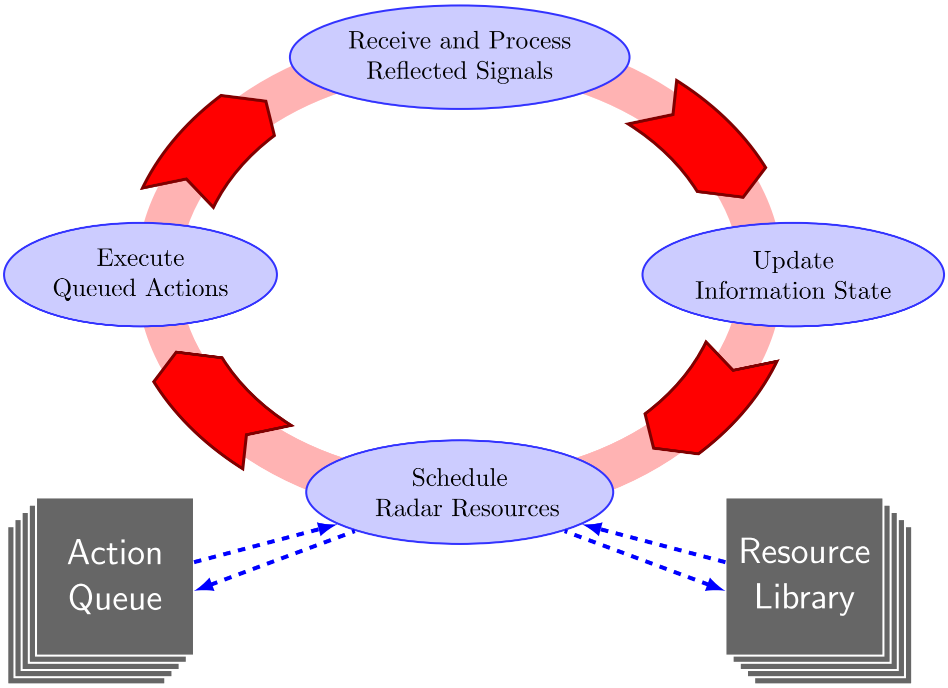

Figure 3.4: Sensor scheduling as a dynamic closed-loop process

in Cochran (2005). Many of these are related to the time cost of signal processing and optimisation within the scheduling loop. Epoch intervals (typically less than 100 ms) can make it challenging to design waveforms online interpulse on a real time basis. With tracking scenarios often involving multiple targets, clutter with non-linear models (3.2), and closed form solutions not always available, the use of waveform libraries designed offline (Howard *et al.* 2004) can reduce the size of selection problem. In a single step ahead, or myopic scheduling problem, the computational complexity of evaluating the library can be expected to be proportional to the size of the library (Cochran *et al.* 2009). Unfortunately, with multi-step or non-myopic problems the 'curse of dimensionality' means the complexity grows exponentially. However, the opportunity to divide up a waveform library into a subset of smaller libraries characterised by a utility function presents as a means to more efficiently downselect to a waveform subset (Howard *et al.* 2004). In the following subsections, we briefly summarise the application of waveform scheduling for tasks normally associated with MFR, namely target detection, classification and tracking.

3.4.1 Target detection

The detection of targets or surveillance is concerned with the identification of any or known targets by the radar sensor in the presence of noise and clutter. The

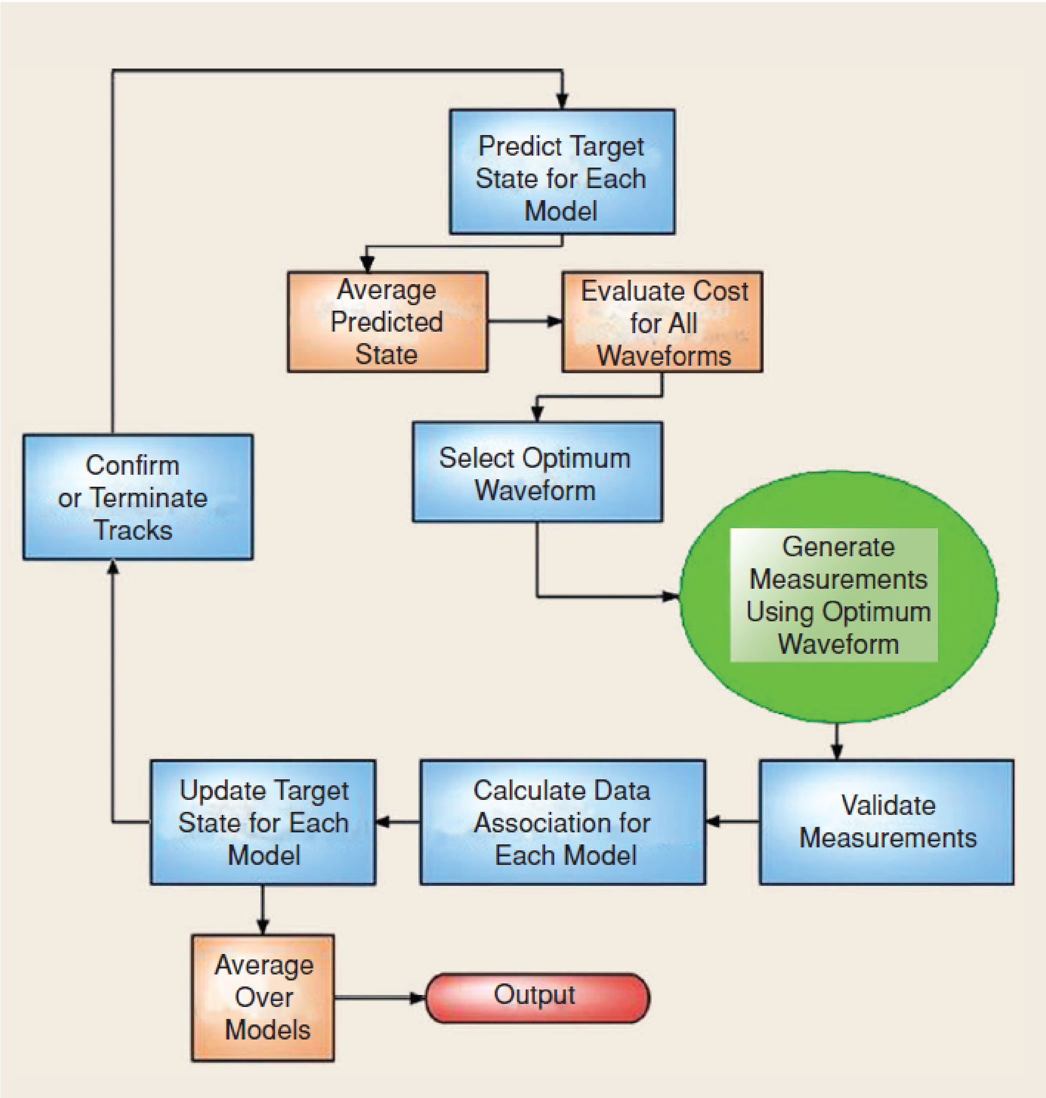

Figure 3.5: Components of a typical radar waveform scheduler in a target tracking application, (Cochran *et al.* 2009)

goal of sensor scheduling is to select the sensor action that minimises the time or cost associated with detecting the presence or absence of a target. Most adaptive detection schemes focus on the design and scheduling of optimal waveforms to interrogate the scene and receiver processing to maximise the likelihood of target detection within a specific operational scenario. Waveform diversity for target detection was considered in Rago *et al.* (1998) who investigated probability of detection contours associated with various detection thresholds and the use of combinations of diverse waveforms for target detection for radar and sonar. A review of recent developments in waveform design specific to target detection is included in Beun (2017).

In the context of MFR, La Scala *et al.* (2003) considered waveform scheduling for target detection by formulating it as a stochastic dynamic programming problem in the framework of a partially observable Markov decision process (POMDP). This allowed the solution to drawn out as an optimal control policy that selected the waveform sequence to maximise a target detection reward, such as timeliness or target priority over a finite horizon under the assumption that the radar scene does not change appreciable within the interrogation period. The stochastic control problem is formed by dividing the processed return range-Doppler space from the radar beam into a grid of cells or bins and the radar action or waveform sequence selected to maximise the expected reward as a function of the a-priori density of the scene. An example provided by the authors is the measurement probability of the target scene under a multiple hypothesis test with the optimal waveform sequence solution found using dynamic programming algorithm.

For the detection of low RCS targets on the ocean surface in a low signal-to-clutter ratio (SCR) environment, an adaptive waveform design method was proposed by Sira *et al.* (2007b). Following this method of estimating the sea clutter statistics, Li *et al.* (2009a) also investigated waveform selection to improve target detectability by maximisation of the received SCR. Waveforms were designed to suppress the sea clutter in areas of interest to improve target detection using a compound Gaussian sea clutter model and an online estimation method of the sea clutter statistics based on the expectation-maximisation algorithm (Dempster *et al.* 1977). A phase modulation (PM) waveform was synthesised by selecting chirp rates that corresponded to waveform autocorrelation functions that were minimised at ranges where the sea clutter was greatest. This resulted in minimising the spread of out-of-bin energy from clutter into the range cell under test for the target. Similarly, Wang *et al.* (2013a) also considered the application of adaptive waveform selection for the detection of targets in a maritime environment, but assumed that the sea clutter is time varying and utilised recursive Bayesian methods to estimate the statistics for each radar dwell.

Nieh and Romero (2014) investigated the problem of extended target detection using an eigenwaveform (Bell 1993, Nieh and Romero 2013, Romero *et al.* 2011) based on the probability weighted eigenwaveform (PWE) technique for target identification (Romero and Goodman 2009a). For a given a target profile, the authors found that maximisation of the matched filter response for the extended target occupying multiple range bins was achieved by illuminating the scene using a signal that convolved the eigenwaveform with the target response itself. A closed-loop scheme using a technique known as match-filtered probability weighted eigenwaveform (MF-PWE) based on maximum a posteriori probability weighted eigenwaveform (MAP-PWE) (Romero and Goodman 2009a) was proposed for the integrated target detection and identification of moving targets when using range-Doppler processing. For a known set of candidate targets, transmit waveforms were designed in the closed-loop scheme using MF-PWE for sets of coherent pulses to interrogate the scene until target detection and identification was confirmed by a multiple hypothesis test. Tang and Tang (2016) also investigated the waveform design problem for extended target detection in the presence of interference under the assumption an inaccurate target prior was available. Using the target impulse response prior, maximisation of the target SIR over an uncertainty region was performed using an inflated interference to increase the robustness of the interrogation signal.

For target detection in the presence of varying clutter, Metcalf *et al.* (2015) proposed a machine learning approach. The clutter statistics were assumed to be a spherically invariant random vector (SIRV), a multi-dimensional example of a spherically invariant random processes (SIRPs). A target detector was formulated as a binary hypothesis test based on the Neyman-Pearson lemma. Both weighted sum of order statistics and the extended Ozturk algorithm were used to suggest optimal detection threshold levels that can be paired with a library of SIRV distributions for clutter (Metcalf *et al.* 2014). For moving targets, Zhu *et al.* (2016) assumed that the scene clutter was be divided into two parts, moving and static which were summed together for each range bin in the processed received signal. The target spectral response was placed to minimise the clutter return, by estimating the power spectral density of the clutter and selecting the interrogation waveform centre frequency.

By empirically characterising the frequency response of a number of candidate targets and clutter, Kirk *et al.* (2016) proposed atarget-to-clutter ratio (TCR) waveform for a targets of known spectral response. The waveform was designed by simply dividing the spectral response of the target with that of the clutter, emphasising frequencies where the target has a greater response than the clutter. Simulations showed that interrogating the scene with the TCR waveform improved the target SCR by suppressing the clutter response and increasing target contrast when compared with waveforms of a flat spectral response. Kirk *et al.* (2017) extended this work by utilising an environmental dynamic database (EDDB) with pre-calculated clutter characteristics to generate the waveform dynamically in the presence of radio frequency interference (RFI). The TCR waveform was designed in conjunction with frequency notching to avoid adjacent emitters.

Target detection in the presence of heavy inhomogeneous clutter is challenging as target Doppler may not always be sufficient to discriminate it from the surrounding clutter in the scene. Ioannidis and Hammers (1979) proposed a method to select optimal antenna polarisations for target detection in the presence of clutter. Hurtado *et al.* (2012) built upon this applying polarisation diversity within a closed-loop scheduling that sequentially estimated the target and clutter polarimetric scattering parameters with the radar transmitter and receiver polarisation scattering matrices formulated as part of the generalised likelihood ratio test (GLRT) based detector. The polarisation of transmitted waveforms were adaptively selected to maximise a non-centrality parameter that defined the test statistic under the alternate hypothesis based on the system response.

When considering MFR, the problem of target detection expands beyond waveform selection to also include task allocation. Suvorova *et al.* (2006a) investigated this more complete problem using both beamform and waveform agility. Instead of the entropy based method of La Scala *et al.* (2003), the authors proposed the placement of virtual targets equidistant apart around the perimeter of the radar field of view. Over time, as information about each of the targets stagnanted, the radar was forced to schedule re-visits towards the virtual targets over actual targets in track as a form of surveillance task. A linear multitarget integrated probabilistic data association (LMIPDA) tracker (Mušicki *et al.* 2004) combined with an IMM approach was used to estimate the states of the manoeuvring targets whilst minimising track error. Waveform and revisit times for each target, both real and virtual were selected to maximise the time between revisits, subject to a track quality constraint based on the target a-posteriori covariance.

3.4.2 Target classification

Target classification can be described as the broad categorisation of a detected target into a disjoint known set of target classes, such as ships, ground vehicles or air vehicles. Typical methods for target classification include imaging the target at an appropriately high resolution and comparing the target signature with a established template library, using distinguishing features such as range profiles, silhouettes or micro-Doppler signatures. More recently, technologies such as machine learning have been applied to efficiently classify targets based on these features (Kim and Ling 2009, Zhao and Principe 2001).

Waveform diversity for the identification of targets entails the selection of methods that enhance characteristics of the candidate target to aid in its discrimination from alternate target categories. The reflected signal from an interrogated scene contains information about the target profile and its motion, combined with that of the environment. Radar waveforms can be selected to maximise the dissimilarity between the interrogated target and alternate targets, or minimise the probability of confusion or misclassification, in the presence of clutter, noise and potentially jamming.

The use of information theoretic measures for target classification were proposed by Sowelam and Tewfik (1997) to minimise the average decision time or number of interrogation pulses required to classify a target. Successive waveforms to illuminate the target were selected to maximise the Kullback-Leibler distance between them under the assumption that the radar scene is stationary during the interrogation period. Later in Sowelam and Tewfik (2000), the authors represented targets using a reflectivity function with the interrogation waveform sequence selected offline. A target classifier was implemented using a sequential binary hypothesis test which was continued until a hypothesis could be confirmed.

Formulating the target classification problem as a POMDP, Castañón (1997) used a large state space for management of multiple sensors with multiple modes. Under this process, the multiple sensors and their modes were viewed as resources and their measurements of different objects as tasks to be completed using the resources. An algorithm was developed that combined stochastic dynamic programming with non-differential optimisation to control the multiple sensor modes and the classification of multiple categories of objects over a finite horizon under the assumption that the scene was stationary over the interrogation period. Classification was based on a sequential multiple hypothesis test and the expected reward computed for the library of interrogation waveforms using the Witness algorithm given an a-priori distribution Littman *et al.* (1995).

A method of designing illumination waveforms was proposed in Pillai *et al.* (2000) to achieve a finite energy transmit-receive signal pair that maximised the SNR of the receiver matched filter for a known target impulse response in the presence of both noise and clutter. Garren *et al.* (2001) extended this, investigating the effectiveness of Pillai's waveform synthesis method for target detection and classification using the waveforms designed to maximise the Mahalanobis distance between the returns of the various target classes.

Under a CR framework, Goodman *et al.* (2007) utilised a hypothesis test in the form of a sequential probability ratio test (SPRT) that assumed that each target was characterised by a known impulse response. Illumination waveforms were designed to maximise either the SNR between the hypotheses in the presence the whitened receiver noise based the eigenvector solution of Garren *et al.* (2001), Pillai *et al.* (2000) or an information theoretic metric (Bell 1993) using the water-filling solution (Cover and Thomas 2006). Later, Goodman (2012) extended this result to include targets that do not fit the stationarity assumptions of (Goodman *et al.* 2007) by considering target impulses that were of finite duration. Also considering an information theoretic waveform approach based on spectral variance, Kim *et al.* (2017) used the mutual information based on energy spectral variance (MIESV) waveform algorithm Romero and Goodman (2009b) to optimise waveforms.

More recently, Wang *et al.* (2013c) considered the selection of radar waveform range and Doppler resolution parameters for target classification. Targets are described in the range-Doppler space by a practical resolution cell related to the waveform, target state and measurement model (Cheng *et al.* 2012). Under a binary hypothesis test between two targets, a Kullback-Leibler divergence based metric was maximised to optimise the separation between the hypotheses. In Wang *et al.* (2013d), the authors extended this work by considering the use of Chernoff information as a metric between the two PDFs for each hypothesis. In the context of CR, Wang *et al.* (2014) investigated adaptive waveform design for target classification in the presence of noise and clutter. A multiple hypothesis test in the form of a SPRT was used to classify targets with waveforms selected to maximise the signal-to-interference-plus-noise ratio (SINR) given the frequency response of the targets. Separately, Zhang *et al.* (2017) investigated waveform spectrum optimisation for estimating the impulse response of unknown extended targets using Bayesian methods.

3.4.3 Target tracking

Waveform scheduling for target tracking involves the adaptive selection or design of transmit waveforms to illuminate a scene in order to optimise some cost function associated with the target state as estimated by a tracker. In the majority of target tracking scenarios, we assume that the target state dynamic model can be represented by under a Markovian process with some Brownian noise. For convenience, this can be characterised using a discrete time state space model such as that in Section 3.1. Selected cost functions typically include metrics based on predicted target track error or information theoretic approaches.

The application of waveform design and selection for target tracking was introduced by Kershaw and Evans (1994) who considered waveform optimisation scheduling for a linear target. The authors later extended this work to consider the problem of target tracking in the presence of clutter (Kershaw and Evans 1997), replacing the Kalman filter with a waveform dependant probabilistic data association (PDA) filter that utilised a cost function based on either the track mean square error (MSE) or PDA filter validation gate volume. A comprehensive review of waveform agile tracking is included in Sira *et al.* (2009a) and Sira *et al.* (2009b) which also investigates the application of non-linear frequency modulation waveforms in these applications. An extensive study that investigated the impact of waveform diversity on the target track quality by exploring waveform shape or its 'resolution cell' as defined by the waveform ambiguity function was also performed in Niu *et al.* (1999; 2002). The authors noted that when using LFM waveforms, the optimal chirp rate was a function of the expected manoeuvring index

$$\lambda_{man} = \frac{\sigma_v (\Delta t)^2}{\sigma_w} \tag{3.32}$$

where σ_v^2 is the process noise variance, σ_w the measurement noise standard deviation and Δt the interval between updates (Bar-Shalom *et al.* 2001). This manoeuvring index could be used in some sense to provide a level of intuition about the target's elusiveness to tracking with sensitivity to waveform selection reducing as the target becomes more agile. As higher sweep rates confer with greater range accuracy, these are of benefit when tracking slower moving targets by improving posterior accuracy. Heuristics of the effect of various ambiguity rotations in Figure 3.6 illustrate that the measurement that orients the waveform uncertainty or ambiguity ellipse orthogonal to the track error covariance or prior minimises the expected posterior. A more recent survey on waveform selection schemes for target tracking is included in Cabrera (2014), which categorised work by target models, tracker types, waveform parameters and selection cost functions. This work was extended in Cabrera (2015) to include close form solutions to waveform selection cost functions for a linear multiple target tracking scenario that minimised confusion by maximising the Bhattacharyya distance between the predicted target observations.

For the tracking of multiple manoeuvring targets in the presence of clutter Suvorova *et al.* (2005) proposed a non-myopic waveform scheduler that sought to interrogate individual targets in an order that preserves the track uncertainty upper bound. La Scala *et al.* (2005) considered non-myopic waveform selection as a stochastic dynamic programming problem over an infinite horizon. The authors

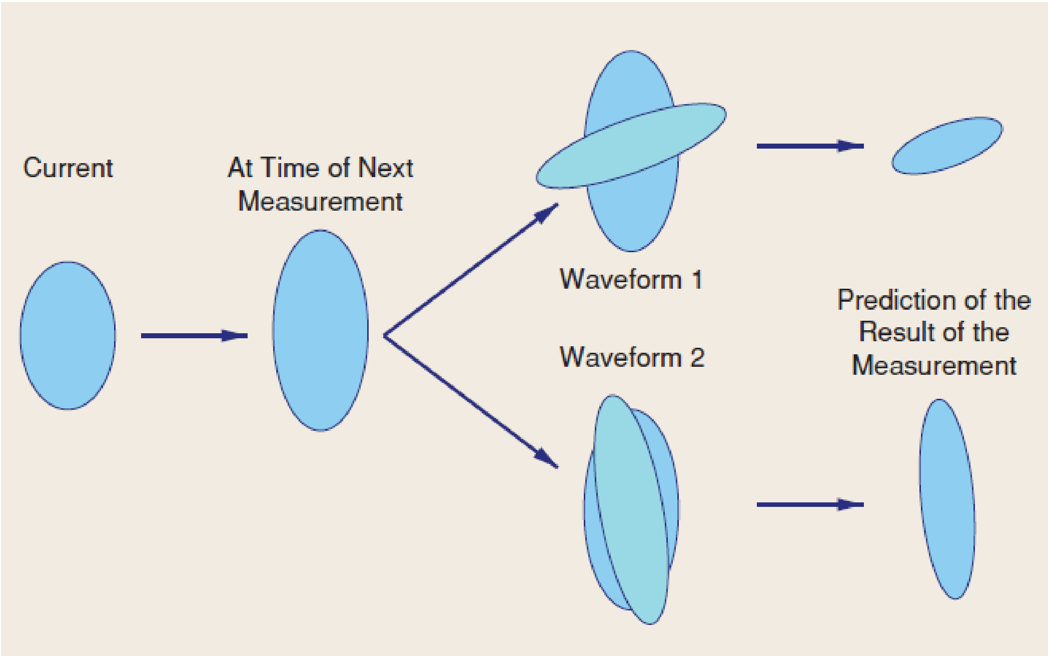

Figure 3.6: Candidate waveform evaluation for a myopic scheduler, (Cochran *et al.* 2009)

solved this using a solution known as Incremental Pruning (Cassandra *et al.* 1997) but found that the implementation of this scheduling algorithm for any more than a trivial example too computationally intensive to be feasible for an online scheduling system. To include the long-term impact of sensor scheduling decisions, in Li *et al.* (2006; 2009b) the authors considered the problem of sensor scheduling as a POMDP. The sensor decision making process was based on the resultant measurement history and sensor scheduling actions with the recursive computation of the posterior distribution of the underlying state conditioned on the target state approximated by a particle filter. A non-myopic scheduling scheme was developed for a multiple target and sensor tracking scenario that applied a simulation based Q-value approximation to trade tracking performance and sensor cost in the sensing policy.

The design of diverse waveforms for target tracking was investigated in Howard *et al.* (2004) who studied the use of LFM and rotational waveform libraries. The fractional Fourier transform (FrFT) was proposed by Savage and Moran (2007) as a method to design these waveforms by rotating the ambiguity function of a base waveform about the range-Doppler axis. This work was extended in Feng *et al.* (2018) who used eigenvalue decomposition an efficient means to compute the optimal rotation angle for the FrFT. The use of complementary pairs of phased coded waveforms was studied in Suvorova *et al.* (2013). who selected the waveform sequences in the order of Reed-Müller codes in order to minimise or suppress Doppler sidelobes in the autocorrelation function of the resultant waveform sequence for a target in track (Suvorova *et al.* 2007; 2006c).

More recently, Ghosh and Ertin (2010) considered a waveform scheduling problem for multiple collaborative tracking radars of arbitrary geometry by fusing their independent measurements together as part of a joint update and Zhang *et al.* (2017) investigated the use of waveform design for target tracking and the Bayesian estimation of the impulse responses unknown extended targets.

3.5 Measures of effectiveness for target tracking

The design of measures of effectiveness (MOE) for radar scheduling specifies a method of quantifying the payoff for a given radar action as a function between the controllable degrees of freedom and predicted target state. The adaptive radar scheduler evaluates the MOE to determine future states of operation and actions, whether it be waveform selection or even triggering some other scheduling process. Target tracking is a problem well suited to the waveform diversity as the use of a Bayesian target tracker (Section 3.1) helps preserves information accumulated from previous observations. When suitably applied, waveform diversity has shown the potential to yield significant performance improvements over traditional fixed waveforms by carefully matching transmit waveforms to the sensing objectives of the scene. Two main approaches to waveform scheduling for target tracking have been considered, a control theoretic approach that seeks to tune the sensor within a control loop to meet a specific objective, such as minimisation of track loss or improving probability of target detection and an information theoretic approach that seeks to optimise some information metric such as the expected information gain (Kreucher *et al.* 2005a, Sira *et al.* 2009a).

3.5.1 Control theoretic approaches

Optimal waveform modulation design using a control theoretic approach was considered by Athans and Schweppe (1967) for a system under power, energy and bandwidth constraints based on the modulation optimisation work of Schweppe and Gray (1966). Dynamic waveform selection for target tracking based on a control theoretic approach was later visited by (Kershaw and Evans 1994) where the authors selected waveform θ to minimise the predicted target track error within a Bayesian track framework,

$$\theta^*_{k+1} = \arg\min_{\theta \in \Theta} f\left(\mathbf{P}_{k+1|k+1}(\theta_{k+1})\right) \tag{3.33}$$

where $\mathbf{P}_{k+1|k+1}$ is the predicted target track covariance and cost function $f(\cdot)$ typically seeking to minimise the track MSE (matrix trace) or validation gate volume (determinant). For linear target tracking in a single dimension, the authors derived closed form solutions for optimal waveform selection from a library of triangular and Gaussian weighted waveforms. The authors expanded this work in Kershaw and Evans (1996) replacing the Kalman filter with a PDA filter for tracking targets in the presence of clutter.

Using a similar cost function to Kershaw and Evans (1994), Sira *et al.* (2007c) investigated waveform selection for wideband signals and classes of non-linear modulated pulses, such as the generalised frequency modulation and hyperbolic frequency modulation chirps in a non-linear target tracking scenario. Describing a performance index that included the probability of track loss, Hong *et al.* (2005) proposed both waveform selection and detection threshold optimisation for a target tracking problem. Savage and Moran (2007) used an IMM framework for tracking accelerating objects with waveform selection based on a minimax criterion to select the best track covariance angle to discriminate the predicted estimated states between the different state models of the IMM. O'Connor (2009) used the Pontryagin maximum principle to trade between present and future costs whilst investigating various myopic and non-myopic scheduling policies under a control theoretic approach. More recently, Wang *et al.* (2013b) proposed a waveform optimisation function based on predicted track covariance for a tracking problem formulated around a particle filter based tracker.

An alternate control theoretic MOE for target tracking is to use information from the estimated target state and the predicted clutter distribution. The integrated clutter measure (ICM) calculates the waveform sidelobe energy from the clutter in the vicinity of the predicted target position using the clutter power and the AF of the candidate waveform,

$$F_k(\theta) = \left| \int\int_{V_k} \left(\int\int_{\mathbb{R}_2} \chi_\theta(t - t', \omega - \omega') \gamma_k(t', \omega') \, \mathrm{d}t' \, \mathrm{d}\omega' \right) \mathrm{d}t \, \mathrm{d}\omega \right| \tag{3.34}$$

where $\gamma_k(t', \omega')$ is the estimated clutter power at range and Doppler (t, ω) and $V_k = \pi g^2 |\mathbf{S}_k|^{1/2}$ is the track validation gate where measurement residual $y \sim \mathcal{N}(\mathbf{y}_k, \mathbf{S}_k)$ and g is a specified threshold (Moran *et al.* 2008). Clutter statistics can be estimated using methods such as those described in Mušicki and Evans (2004), Mušicki *et al.* (2005) and waveforms are selected to minimise the estimated 'spillage' of the sidelobe response of the clutter into the predicted target track validation window,

$$\theta^* = \arg\min_{\theta \in \Theta} F_k(\theta) \tag{3.35}$$

Calculation of (3.34) can be simplified by approximating ambiguity function and its sidelobes at the target $\chi_\theta(\mathbf{z})$ as a Gaussian mixture and summing the resultant power across the clutter points (Moran *et al.* 2008).

3.5.2 Information theoretic approaches

Information gain is considered a more fundamental quantity than a task specific reward function. The emergence of this method can be traced back to Bell (1993; 1999) which described the use of information theory to the design waveforms for extracting extended target information. Its invariance to transformations of the data makes it robust to the challenges of sensor scheduling (Hintz and McVey 1991) and its associated real scenarios complications such as model mismatches, accommodation of changing priorities as well as increased versatility to different tasks, such as classification and tracking (Hero and Cochran 2011, Hero *et al.* 2008). This is achieved by separation of the sensor operation into two independent processes, information collection and optimisation.

The expected information that can be obtained from a measurement action can be given as the mutual information between the target state and processed received signals can also be defined as the expected reduction in entropy given by the measurement as Cover and Thomas (2006)

$$I(X; Z) = H(X) - H(X|Z) \tag{3.36}$$

$$= H(Z) - H(Z|X) \tag{3.37}$$

where $H(X)$ is the Shannon entropy of probability function $P(X)$. This was demonstrated by Logothetis and Isaksson (1999) who investigated a sensor scheduling problem similar that described in Kershaw and Evans (1994) but selected the waveform sequence or sensor order from a known library in an open-loop scheduler that maximised the mutual information between final state and the entire sequence. In a closed-loop scheduler, increases in mutual information result in an improvement in the expected accuracy in the estimated target state information, commensurate to minimising the uncertainty in X given the conditional entropy $H(X|Z)$ The expected information obtained from a measurement given the current knowledge state of the target can be computed as,

$$I(X;Z(\theta_k)) = \log\det(\mathbf{I} + \mathbf{R}_k^{-1}(\theta_k)(\mathbf{P}_k) \tag{3.38}$$

where $\mathbf{I}$ is the identity matrix , measurement $z \sim \mathcal{N}(\mathbf{z}_k, \mathbf{R}_k)$ and $\mathbf{P}_k$ contains the knowledge of the state covariance of target (Howard *et al.* 2004). The Kullback-Leibler (KL) divergence or relative entropy, denoted $D_{KL}(P \parallel Q)$ is a measure of distance between two distributions P and Q,

$$D_{KL}(P \parallel Q) = \int_{-\infty}^{\infty} p(x) \log \frac{p(x)}{q(x)} \, dx \tag{3.39}$$

where $p(x)$ and $q(x)$ are the distributions of random variable x. The divergence can be viewed as the information gained if the knowledge about the state is updated from a prior Q to the posterior distribution P. The use of the KL divergence as a metric for adaptive scheduling when tracking has been shown to be equivalent in performance with mutual information. In this case, we are concerned with the determining the divergence associated with prior state $p(X^k|Y^{k-1})$ and the posterior $p(X^k|Y^k)$, defined as:

$$\begin{aligned} D(y_K) &= D(p(X^k|Y^k) \parallel p(X^k|Y^{k-1})) \\ &= \int p(X^K|z_k) \log \frac{p(X^K|z_k)}{p(X^k)} \, dx \end{aligned} \tag{3.40}$$

Under a linear Gauss-Markov system (3.2) estimated by a Kalman filter, this can be computed as

$$D(\mathbf{y}_K) = \frac{1}{2}\left[\log\det(\mathbf{S}_k {\mathbf{R}_k}^{-1}) + \mathrm{Tr}(\mathbf{R}_k {\mathbf{S}_k}^{-1}) + (\mathbf{K}_k\mathbf{y}_k)^\top \mathbf{P}_k^{-1}(\mathbf{K}_k\mathbf{y}_k)) - d\right] \tag{3.41}$$

where measurement residual $\mathbf{y}_k = \mathbf{z}_k - \mathbf{H}\hat{x}_k$, $y \sim \mathcal{N}(\mathbf{y}_k, \mathbf{S}_k)$, d is the dimension of measurement $\mathbf{z}_k$ and $\mathbf{K}_k$ is the gain of the filter (Charlish *et al.* 2010). Although this metric can be applied in waveform selection for target classification problems (Sowelam and Tewfik 1997; 2000, Wang *et al.* 2013c;d), it requires the measurement to already be processed by the estimator, given use of the measurement residual. Although it is possible to estimate this quantity for a well behaved process, such as when the estimator approaches stationary conditions, $\mathbf{K}_{k+1} \to \mathbf{K}_k$, it desirable to know a-priori the level of performance gain that is expected to be obtained before the measurement is made, such as in our adaptive scheduling scenario. Performance of both mutual information and KL divergence metrics were shown to be similar in Charlish *et al.* (2010), particularly as the first term of (3.41) is also (3.38) if $\mathbf{HH}^\top = \mathbf{I}$, making mutual information a more favourable inference criterion particularly due to its ease of computation and suitability for processes that are not approaching stationarity.

In general, a radar's waveform libraries are developed with a specific application in mind. Given the cost of evaluating a large set of candidate waveforms in an online scheduler when using the expected information (3.38) is an effectiveness measure, Howard *et al.* (2004) defined a utility of a family or waveform library $\mathcal{L} \subset \mathrm{L}^2(\mathbf{R})$ with respect to a distribution F of all the possible state covariance matrices as,

$$G_F(\mathcal{L}) = \int_{\mathbf{P}>0} \max_{\theta \in \mathcal{L}} \log \det(\mathbf{I} + \mathbf{R}_\theta^{-1}\mathbf{P})\, dF(\mathbf{P}) \tag{3.42}$$

allowing the waveforms libraries to be formed offline into a compact mapping or set of actions for the scheduler to select from. Applying the results of Howard *et al.* (2004), Suvorova *et al.* (2006b) investigated a manoeuvring target tracking problem using an IMM filter to estimate target states for a compact LFM rotation waveform library.

By extending the work of Bell (1993), the authors of Leshem and Nehorai (2006) and Leshem *et al.* (2007) proposed an information theoretic approach to waveform design for the simultaneous tracking of multiple targets using the linear combination of mutual informations between the targets and the illuminating waveform. For both MIMO and more conventional single input single output (SISO) radar, Yang and Blum (2006; 2007) studied waveform design by both the maximisation of mutual information as well as a control theoretic approach of under power constraints. A water-filling approach was used to optimise under power constraints and interestingly, the authors found that the information theoretic approach to be equivalent the control theoretic approach of minimising track mean square error.

3.5.2.1 Information theoretic measures under greedy policies

Assuming a finite sensor scheduling solution map, the curse of dimensionality can result in a non-myopic scheduling solution quickly becoming intractable to solve, even for a modest horizon. To illustrate, consider the complexity of evaluating the performance across a set of candidate actions $u \in \mathcal{U}$ where $M = |\mathcal{U}|$ is the total number of possible actions that the radar can take and K the number of time intervals we wish to optimise for into the horizon. The time complexity of evaluating the possible actions a radar can take under an optimal non-myopic scheme is upper bound by an exponential cost $T(K) \leq f(M^K) \in \mathcal{O}(c^K)$ and reduces to a linear cost $T(K) \leq K f(M) \in \mathcal{O}(K)$ under a greedy scheduling scheme.

To embody the effect of order in a non-myopic scheduler, Setlur and Devroye (2012), Setlur *et al.* (2012) proposed the use of directed instead of mutual information as a cost function. Williams *et al.* (2007a;b) investigated the loss in performance associated with greedy sequential scheduling policy from the optimal horizon which can be realised by the performance guarantee

$$I(X; y_1^{o_1}, y_2^{o_2}) \leq 2I(X; y_1^{g_1}, y_2^{g_2}) \tag{3.43}$$

where $\{o_1, o_2\}$ represents the measurements made under a two stage horizon optimal selection scheme $\{o_1, o_2\} = \arg\max_{u_1,u_2} I(X; y_1^{u_1}, y_2^{u_2})$ and $\{g_1, g_2\}$ those selected under a greedy scheme where $g_1 = \arg\max_{u_1} I(X, y_1^{u_1})$ and $g_2 = \arg\max_{u_2} I(X, y_2^{u_2}|y_1^{u_1})$.

Assuming all other things equal, the authors found that the expected performance of a greedy scheme is lower bound by half that of the optimal scheme and that the tightness of the bound is dependant upon the model characteristics. For small measurement covariance $\mathbf{R}$, the greedy heuristic was found to be perform close to that of the optimal result whereas for large $\mathbf{R}$, the performance guarantee is much closer to that of the bound. This was termed *diffusiveness*, where the correlation between states at different time intervals reduces as the time between these intervals increases. By intuition, one would expect that the greedy heuristic would closer to the optimal selection for smaller process noise.

Exploiting this allows us to rewrite (3.43) with a strengthened bound as

$$I(X; y_1^{o_1}, \ldots, y_K^{o_K}) \leq (1 + \alpha)I(X; y_1^{g_1}, \ldots, y_K^{g_K}) \tag{3.44}$$

where diffusion parameter $\alpha < 1$ (Williams 2007). Although non-optimal, the performance of such a scheduling scheme is still good in practice and given the performance bound (3.43), the reduction in evaluation complexity may allow the radar to obtain additional or more frequent but suboptimal measurements under a greedy scheme given the smaller computation expense.

3.6 Optimal measurement scheduling for linear Gaussian systems

In this section we wish to motivate the value of resource scheduling with an example that illustrates the trade off between measurement duration and quality for a noisy sensor. Consider the following linear system where x_k denotes the target state and

z_k the discrete measurement state:

$$x_k = x_{k-1} + w_k \tag{3.45a}$$

$$z_k = x_k + v_k \tag{3.45b}$$

where for simplicity, we assume that the state is scalar $x \in \mathbb{R}^1$, prior distribution $x_{k-1} \sim \mathcal{N}\left(\hat{x}_{k-1}, \rho_{k-1}\right)$ and disturbance $w_k \sim \mathcal{N}\left(0, qT\right)$. The time between k-th measurement epoch $T = t_k - t_{k-1}$ and ρ_{k-1}, q, $T > 0$ are independent variables. The measurement noise, v_k as a function of the measurement period such that $v_k \sim \mathcal{N}\left(0, r\left(T\right)\right)$. It is assumed that the measurement noise variance $r\left(T\right)$ models a situation in which an expected improvement obtained by scheduling, as reflected in the measurement noise variance, improves with the increased time T spent selecting better or performing a longer improved observations of the system. An analogy to this is pulse integration, where under the appropriate circumstances, the integration of an increased number of pulses results in improved resolution. This is represented by the assumption that $r(T) > 0$ and $r'(T) \leq 0 \; \forall \; T$. As such, we find as $|r'(T)| \longrightarrow 0$ as $T \longrightarrow \infty$ so that $r(T) \longrightarrow \bar{r}$, a limit we may define. Such a limit may be found given a circumstance where increasing T yields no better measurement over a closed resource library or a resolution limit has been reached. We can also deduce that with greater T comes greater variance in w_k, as a linear function of process noise q. A trade-off arises here as the uncertainty in the state x_t increases with T as the variance of the measurement decreases.

From this we seek to find the optimal measurement epoch T^* for this particular system. As we have a linear system, we can use an optimal Kalman filter, to track the target. The posterior of $x_t \sim \mathcal{N}(\hat{x}_t, \rho)$ can be computed as

$$\hat{x}_k = \hat{x}_{k-1} + g_k(z_k - \hat{x}_{k-1}) \tag{3.46a}$$

$$\rho_k = (1 - g_k)(\rho_{k-1} + qT) \tag{3.46b}$$

where filter gain

$$g_k = \frac{\rho_{k-1} + qT}{\rho_{k-1} + qT + r(T)}$$

From (3.46b), it follows that

$$\rho_k(T) = \frac{r(T)(\rho_{k-1} + qT)}{r(T) + \rho_{k-1} + qT} \tag{3.47}$$

As $T \longrightarrow \infty$, the posterior variance will converge toward the measurement noise variance $\rho_k(T) \longrightarrow \bar{r}$. This limit can be reached from either above or below. If there exists an optimal update period $T^* > 0$ such that $\rho_k'(T^*) = 0$ then the limit is approached from below and an optimal scheduling epoch T^* can exist for $\rho_k'(T) = 0$. Differentiation of (3.47) yields,

$$\rho_k'(T) = \frac{\left(r(T) + qT + \rho_{k-1}\right)\left(r'(T)(qT + \rho_{k-1}) + qr(T)\right) - \left(r(T)\left(qT + \rho_{k-1}\right)\left(r'(T) + q\right)\right)}{\left(r(T) + qT + \rho_{k-1}\right)^2} \tag{3.48}$$

which can be simplified to

$$\rho_k'(T) = \frac{r'(T)\left(qT + \rho_{k-1}\right)^2 + qr\left(T\right)^2}{\left(r(T) + qT + \rho_{k-1}\right)^2} \tag{3.49}$$

We can then find T^* by equating (3.49) to 0 accordingly,

$$r'(T^*)\left(qT^* + \rho_{k-1}\right)^2 + q\left(r\left(T^*\right)\right)^2 = 0 \tag{3.50}$$

From here, the possibility of finding a non-negative T^* depends on the form of $r(T)$. If we assume a hyperbolically decreasing $r(T) = a + b/T$,then we can solve for T^* as,

$$T^* = \frac{b\left(\rho_{k-1} - a\right) \pm \sqrt{b/q}\left(bq - a\rho_{k-1}\right)^2}{a^2 - bq}, \quad a^2 \neq bq \tag{3.51}$$

As quantities $a, b, \rho, q > 0$, we can simplify (3.51)

$$T^* = \max\left\{0, \frac{b(\rho_{k-1} - a) \pm \sqrt{b/q}|a\rho_{k-1} - bq|}{a^2 - bq}\right\} \tag{3.52}$$

For this rather trivial example, provided $q < a^2/b$, an optimal T^* can be found where $\rho_k'(T^*) = 0$. Here, the limit $\bar{r}$ is approached from above suggesting that T^* should be selected to be as large as possible. This means that it is better to spend more time selecting improved observations, at least if our goal is to minimise posterior variance.

For real systems the actual form of $r(T)$ is not always known, nor does the measurement noise variance necessarily decrease hyperbolically with time. A more configurable measurement noise variance model that could be considered is a decay in the form of $r(T) = a + be^{-cT}$. Given a numerical solution to $r(T)$, it would be conceivable to manage the complexity of a resource library and allow the scheduler to select the optimal resources within some defined constraint or bound informed by qT.

Chapter 4

Joint estimation of range and Doppler using LFM chirp diversity

The issue of linear frequency modulation (LFM) range-Doppler coupling in radar has resulted in various compensation techniques for its associated range bias (Fitzgerald 1974). Joint estimation provides an efficient means of simultaneously estimating multiple parameters of interest about a target. In Bello (1960), the author derives a maximum likelihood estimation (MLE) based method of jointly estimating target delay, Doppler and Doppler rate using long pulse trains by assuming independent target scintillation from pulse to pulse. This is further extended in Kelly (1961) where the accuracy of coherent radar is derived for both amplitude and frequency modulated waveforms. More recently, MLE methods have been applied for estimation of target parameters from non-linear multi-dimensional likelihood functions particularly when the target occupies multiple range-Doppler resolution cells when using wideband LFM pulse trains in synthetic radar aperture (SAR) applications (Abatzoglou and Gheen 1998).

In this chapter, we re-consider the issue of LFM range-Doppler coupling and its effect on range-only measurement systems. In Section 4.2, we review the shearing effect of the LFM ambiguity function. We assume a non-coherent system that obtains range only measurements from known LFM pulses using a matched filter receiver. By exploitation of the range-Doppler coupling bias from moving targets, we establish a MLE based method in Section 4.3 to jointly estimate the target range and range-rate from a known train of diverse LFM pulses. In Sections 4.4 & 4.5 we formulate online methods of optimal pulse train design for target acquisition as well as tracking that are linear in computational cost as pulse train length is increased. In Section 5.4 we compare the performance of our joint estimator with established methods such as range-averaging and pulse-Doppler processing with some simulation results with a steady state tracking problem under a limited LFM waveform library.

4.1 Background

The impact of waveform choice on the accuracy of tracking systems has been of concern to those involved in radar and sonar design (Calderbank *et al.* 2009, Cochran 2005, Cochran *et al.* 2009, Hong *et al.* 2005, Niu *et al.* 2002, Sira *et al.* 2007c). Recent developments in waveform diversity include adaptive sequential design for the purpose of target angle estimation using multiple-input multiple-output (MIMO) radar (Huleihel *et al.* 2012; 2013). Other waveform diversity schemes have varied pulse duration and modulation in response to tracker outputs to improve target range and range-rate estimate accuracy in under a range of tracking scenarios for both sonar (Cabrera 2014, Kershaw and Evans 1994) and radar (O'Connor 2009, Suvorova *et al.* 2006b). As part of this, pulse compression has been universally adopted as a means of significantly improving the range resolution of radar under power constraints without compromise to target signal-to-noise ratio (SNR). The LFM waveform is a commonly selected form of pulse compression because of ease of accurate waveform generation using both analog hardware means and digital synthesis, providing improved range and range-rate information over uncompressed waveforms (Cook and Bernfeld 1967, Rihaczek 1996). One of the issues emanating from the use of LFM waveforms is the range-Doppler coupling effect (Fitzgerald 1974) where the measured target range is biased by a function of the target range-rate and pulse parameters and this cannot be distinguished from a true shift in target range. For slow moving targets, range-Doppler coupling results in small displacements. However, for faster targets or waveforms without large bandwidths, this can be result is large displacements. For example, high frequency (HF) surface wave radar operates with bandwidths of ~100 kHz. Even for comparatively slow targets observed with such systems such as ships, experimental results in Bruno *et al.* (2013) demonstrate errors of hundreds of meters. In conventional pulsed non-coherent radar systems that obtain only range measurements, strategies to mitigate coupling error include simply ignoring the bias and estimating the target state using a tracking filter or to transmit a series of alternating up and down chirps that aggregate to nullify the effects of the range bias (Fitzgerald 1974). Additional methods include use of non-optimal steady state filters such as $\alpha\beta$ and $\alpha\beta\gamma$ and approximating filter gains to try and account for the bias (Wong and Blair 2000). Others have acknowledged the correlation between the range and range-rate measurements for a LFM chirp and incorporated this into the measurement covariance matrix to improve track process, particularly for manoeuvring targets Bar-Shalom (2001), Niu *et al.* (2002).

4.2 LFM waveforms

The use of LFM waveforms has been popularised as a method of pulse compression because it decouples the pulse duration and range resolution relationship allowing increased energy on target whilst retaining range resolution. In pulsed radar, a matched filter receiver is commonly used to maximise the return energy of the reflected pulse from the target with the ensuing return delay used to estimate the target range. Additionally in coherent systems, the phase differential between consecutive identical pulses can be used to measure Doppler and estimate the target range-rate.

4.2.1 Local accuracy of LFM pulses in range

The local accuracy of a pulse can be characterised by the complex ambiguity function associated with a received waveform (Van Trees 2001, Woodward 1967), as detailed in Section 3.3.3. For an arbitrary unmodulated base pulse ϕ, LFM results in the ambiguity function being sheared parallel to the Doppler axis (Levanon and Mozeson 2004, Papoulis 1977). Using this property, we can write it as the coordinate transformation of the ambiguity function of an unmodulated base pulse $\chi_\phi(\tau, \nu)$ accordingly,

$$|\chi_\kappa(\tau, \nu)^\top| = |\chi_\phi\left(\mathbf{S}(\kappa)(\tau, \nu)^\top\right)| \tag{4.1}$$

Linear transformation of delay and Doppler (τ, ν) into range and range-rate can be performed from the receiver parameter estimation vector as $\mathbf{y} = \mathbf{T}\begin{bmatrix}\tau & \nu\end{bmatrix}^\top$ where Doppler $\nu = 2\pi f_d$. Transformation matrix $\mathbf{T}$ and unimodular shear matrix $\mathbf{S}(\kappa)$ are

$$\mathbf{T} = \begin{bmatrix} c/2 & 0 \\ 0 & c/2\omega_0 \end{bmatrix}, \quad \mathbf{S}(\kappa) = \begin{bmatrix} 1 & 0 \\ -\kappa & 1 \end{bmatrix}$$

for chirp rate $\kappa = \frac{f_2 - f_1}{2\lambda}$ and carrier frequency $\omega_0 = 2\pi f_0$ where the chirp bandwidth is $(f_2 - f_1)$ and pulse duration is 2λ. Similarly, the measurement noise covariance matrix can be approximated by the inverse of the Fisher information matrix (FIM) of the LFM pulse. This can be obtained by

$$\mathbf{\Sigma}(\kappa) = \frac{1}{\eta}\mathbf{T}\mathbf{S}(\kappa)\mathbf{U}_\phi^{-1}\mathbf{S}^\top(\kappa)\mathbf{T} = \begin{bmatrix} \sigma^2_{rr} & \sigma^2_{r\dot{r}} \\ \sigma^2_{r\dot{r}} & \sigma^2_{\dot{r}\dot{r}} \end{bmatrix} \tag{4.2}$$

where $\eta\mathbf{U}_\phi$ is the FIM of the base pulse (Dogandzic and Nehorai 2001, Kershaw and Evans 1994) and η is the SNR. Given a range only measurement, our biased estimate (4.8) arises from calculation of delay measurement $\arg\max_\tau |\chi_\kappa(\tau, \nu)|$ along the line $\nu = 0$.

We find that

$$\frac{1}{\sigma^2(\kappa)} \leq \begin{bmatrix} 1 & 0 \end{bmatrix} \mathbf{\Sigma}^{-1}(\kappa) \begin{bmatrix} 1 \\ 0 \end{bmatrix}$$

and the variance of the range estimate for a LFM pulse using a matched filter receiver is bound by

$$\sigma^2(\kappa) \leq \frac{|\mathbf{\Sigma}(\kappa)|}{\Sigma_{22}(\kappa)} = \Sigma_{11} - \frac{{\Sigma_{12}}^2}{\Sigma_{22}} \tag{4.3}$$

where $|\cdot|$ denotes the matrix determinant.

4.2.2 Range-Doppler coupling in LFM waveforms

Processing of the LFM waveform by the matched filter results in the delay measurement being a combination of the target's true range r and range-rate $\dot{r}$ (Fitzgerald 1974) as a result of coupling from the LFM shearing. The measured round trip time delay τ is given by

$$\tau = \tau_0 + \Delta\tau \tag{4.4}$$

where τ_0 is the delay associated with the true target range and incremental delay $\Delta\tau$ is a linear function of the target Doppler response.

$$\Delta\tau = -\frac{2\lambda}{f_2 - f_1}\Delta f \tag{4.5}$$

where the Doppler shift of the return is

$$\Delta f = f_r - f_0 = -\dot{r}\left[\frac{2f_0}{c}\right] \tag{4.6}$$

where f_r and f_0 are center frequencies of the received and transmitted pulses. Substituting (4.5) & (4.6) into (4.4) the delay can be represented as a function of the target radial velocity.

$$\tau = \tau_0 + \left(\frac{4\lambda f_0}{c(f_2 - f_1)}\right)\dot{r} \tag{4.7}$$

Through transformation of the time delay, we obtain the biased range measurement.

$$r_b = r + \Delta t\dot{r} \tag{4.8}$$

where quantity $\Delta t = \frac{2\lambda f_0}{f_2 - f_1}$ is a function of the transmit waveform and is positive for an upsweep chirp $f_2 > f_1$ and negative for a downsweep chirp.

4.3 Joint estimation using diverse LFM pulse train

Assuming that our radar system uses a matched filter receiver, by measuring the peak of the time autocorrelation function a single range measurement is acquired from each LFM pulse (4.8). Defining $\boldsymbol{\theta} = \begin{bmatrix} r & \dot{r} \end{bmatrix}^\top$ we can form a linear observation model as:

$$\mathbf{m} = \mathbf{H}\boldsymbol{\theta} + \mathbf{w} \tag{4.9}$$

where $\mathbf{m} = \begin{bmatrix} m_1, & \cdots, & m_{2N+1} \end{bmatrix}^\top$ is the vector of biased range measurements and observation matrix $\mathbf{H}$

$$\mathbf{H}(\boldsymbol{\kappa}) = \begin{bmatrix} 1 & \Delta t(\kappa_1) \\ 1 & \Delta t(\kappa_2) \\ \vdots & \vdots \\ 1 & \Delta t(\kappa_{2N+1}) \end{bmatrix} \tag{4.10}$$

Vector $\boldsymbol{\kappa} = \begin{bmatrix} \kappa_1, & \cdots, & \kappa_{2N+1} \end{bmatrix}$ is the chirp rates of the successive pulses within train and noise $\mathbf{w} \sim \mathcal{N}(\mathbf{0}, \mathbf{C})$. Note that $2N + 1$ here does not necessarily denote an odd number of pulses but is instead selected for convenience. Assume that in a pulse train of pulse repetition interval (PRI) T, $2\lambda << T$ and each of the measurements are uncorrelated. The covariance $\mathbf{C}$ can be written as a $(2N+1) \times (2N+1)$ diagonal matrix of range variance terms (4.3). The likelihood of the measurement vector can be expressed as $p(\mathbf{m}; \boldsymbol{\theta}) \sim \mathcal{N}(\mathbf{H}\boldsymbol{\theta}, \mathbf{C})$. It is straightforward to shown that the MLE for $\boldsymbol{\theta}$ can be expressed as

$$\hat{\boldsymbol{\theta}}_{\text{MLE}} \sim \mathcal{N}\left(\left(\mathbf{H}^\top\mathbf{C}^{-1}\mathbf{H}\right)^{-1}\mathbf{H}^\top\mathbf{C}^{-1}\mathbf{m}, \left(\mathbf{H}^\top\mathbf{C}^{-1}\mathbf{H}\right)^{-1}\right) \tag{4.11}$$

for pulse train of length $2N + 1 \geq 2$ (Kay 1993, Scharf and Demeure 1991).

4.3.1 Range migration mitigation

The estimator (4.11) assumes that target range and range rate are stationary during the measurement interval. For radar in general, this is not always the case particularly for high velocity targets where significant range shifts can occur during the measurement interval, a problem known as range migration. For coherent radar such as range-Doppler, range migration can result in smearing or spread in the estimate and can be corrected using methods such as Keystone transformation (Perry *et al.* 1999). However, for incoherent radar systems, each pulse is considered independently and range migration results in its bias. To manage these effects, we incorporate the expected difference in target position between pulses into the measurement model using information about its dynamics. Assuming a constant velocity, the range captured at the i-th pulse in the train is shifted as a linear function of the target velocity. Adopting the mid-point of the pulse train as a reference, the compensated range from the i-th pulse in the train can be expressed as

$$\tilde{r}(i) = r(i) + T\alpha(i,N)\mathbb{E}[\dot{r}], \quad -N \leq i \leq N \tag{4.12}$$

where correction factor $\alpha = N + 1 - i$ and $\mathbb{E}[\dot{r}]$ is the expected or average target velocity during the pulse train. Combining the set of shifted range measurements from (4.12) we can use the compensated biased measurement vector $\tilde{\mathbf{m}}$ in (4.11). We refer to this as the motion compensated estimator as it requires knowledge of the target velocity which can be estimated if the target is already under track.

Using the linear motion model of (4.9), we incorporate this shift in range into the observation matrix (4.10) as a temporal shift

$$\overline{\mathbf{H}} = \begin{bmatrix} 1 & \Delta t(\kappa_1) - \alpha_1 T \\ 1 & \Delta t(\kappa_2) - \alpha_2 T \\ \vdots & \vdots \\ 1 & \Delta t(\kappa_{2N+1}) - \alpha_{2N+1} T \end{bmatrix} \tag{4.13}$$

for vector $\bar{\boldsymbol{\theta}} = \begin{bmatrix} \bar{r} & \dot{r} \end{bmatrix}^\top$. We refer to this as the temporally aligned estimator, where $\bar{r}$ is the temporally aligned range estimate and compare its performance with (4.11) in Section 4.7.1. This estimator has the inherent advantage of making the second column of $\bar{\mathbf{H}}$ diverse even for a pulse train of identical pulses. As a result, matrix $\bar{\mathbf{H}}^\top(\boldsymbol{\kappa})\mathbf{C}^{-1}(\boldsymbol{\kappa})\bar{\mathbf{H}}(\boldsymbol{\kappa})$ is typically non-singular and its inverse can be calculated even for systems where the chirp rate is invariant within a pulse train. This makes it a more versatile processing method than motion compensation which requires a chirp diversity within the pulse train to meet requirement that $\text{rank}(\mathbf{H}) = 2$.

4.4 Pulse train design

In the following section, we present an iterative online method of designing pulse train for targets that are in track. By taking into account prior information about the track estimate quality and range bias from the pulse itself selection methods can be used to design a pulse train seeks to minimise target track uncertainty (Niu *et al.* 2002). Although, global optimisation of the pulse train can be performed by exhaustively evaluating the set of chirp rates the LFM waveform library holds, as the pulse train and matrices $\mathbf{H}$, $\mathbf{C}$ grow in size, computing $\boldsymbol{\Sigma}_{\hat{\theta}}(\boldsymbol{\kappa})$ can become increasing difficult. Therefore, we present a more tractable method of defining an objective function that maintains a fixed level of complexity regardless of the pulse train length. The estimator covariance (4.11) can be defined as

$$\boldsymbol{\Sigma}_{\hat{\theta}}(\boldsymbol{\kappa}) = \left(\mathbf{H}^{\top}(\boldsymbol{\kappa})\mathbf{C}^{-1}(\boldsymbol{\kappa})\mathbf{H}(\boldsymbol{\kappa})\right)^{-1} \tag{4.14}$$

Using (4.10), we can rewrite (4.14) as

$$\boldsymbol{\Sigma}_{\hat{\theta}}(\boldsymbol{\kappa}) = \left(\sum_{i=-N}^{N} \frac{1}{\sigma^2(\kappa_i)} \begin{bmatrix} 1 & \Delta t(\kappa_i) \\ \Delta t(\kappa_i) & \Delta t^2(\kappa_i) \end{bmatrix}\right)^{-1} \tag{4.15}$$

As this is simply the inverse of the sum of covariances of each pulse in the train, the order is unimportant. We propose a simple greedy iterative method of pulse train selection. Whilst this does not guarantee optimality for the pulse train, simulations have found that a greedy implementation results in a solution equivalent or close to the optimal solution. To implement, we express (4.15) for a pulse train up to the n-th pulse as

$$\boldsymbol{\Sigma}_{\hat{\theta}}^{-1}(\boldsymbol{\kappa}^{n}) = \mathbf{A}(\boldsymbol{\kappa}^{n-1}) + \mathbf{B}_{\hat{\theta}}(\kappa_n) \tag{4.16}$$

where inverse covariance or precision matrix for the already selected pulse train $\boldsymbol{\kappa}^{n-1}$ is

$$\mathbf{A}(\boldsymbol{\kappa}^{n-1}) = \sum_{i=-N}^{n-1} \frac{1}{\sigma^2(\kappa_i)} \begin{bmatrix} 1 & \Delta t(\kappa_i) \\ \Delta t(\kappa_i) & \Delta t^2(\kappa_i) \end{bmatrix} \tag{4.17}$$

and precision matrix for the pulse under consideration is simply

$$\mathbf{B}_{\hat{\theta}}(\kappa) = \frac{1}{\sigma^2(\kappa)} \begin{bmatrix} 1 & \Delta t(\kappa) \\ \Delta t(\kappa) & \Delta t^2(\kappa) \end{bmatrix} \tag{4.18}$$

Next, we present two methods of selecting $\boldsymbol{\kappa}$, the vector of chirp rates from $\mathbf{K}$, the waveform library of permissible chirp rates.

4.4.1 Minimisation of measurement covariance volume

Minimisation of the covariance volume of (4.11) can be achieved by minimisation of the determinant of (4.14).

$$\begin{aligned} \boldsymbol{\kappa}^{*} &= \arg\min_{\boldsymbol{\kappa}\subseteq\mathbf{K}} |\boldsymbol{\Sigma}_{\hat{\theta}}(\boldsymbol{\kappa})| \\ &= \arg\max_{\boldsymbol{\kappa}\subseteq\mathbf{K}} |\mathbf{B}_{\hat{\theta}}(\boldsymbol{\kappa})| \end{aligned} \tag{4.19}$$

Adopting our greedy approach (4.16) we select the n-th pulse in the train according to:

$$\kappa_n^* = \arg\max_{\kappa \in \mathbf{K}} |\mathbf{A}_n + \mathbf{B}_{\hat{\theta}}(\kappa)| \tag{4.20}$$

Given that $\mathbf{A}_n$ is constant, using (4.18) with some rearranging the n-th pulse in the train can be selected according to:

$$\kappa_n^* = \arg\max_{\kappa \in \mathbf{K}} \frac{1}{\sigma^2(\kappa)} \left(A_{11}\Delta t^2(\kappa) + A_{22} - 2A_{12}\Delta t(\kappa) \right) \tag{4.21}$$

4.4.2 Minimisation of measurement mean square error

The minimisation of the estimator mean square error (MSE) can attained through minimisation of the trace of (4.14).

$$\boldsymbol{\kappa}^* = \arg\min_{\boldsymbol{\kappa} \subseteq \mathbf{K}} \operatorname{Tr}\left(\boldsymbol{\Sigma}_{\hat{\theta}}(\boldsymbol{\kappa}) \right) \tag{4.22}$$

Following, (4.16) select the next pulse in the train according to

$$\kappa_n^* = \arg\min_{\kappa \in \mathbf{K}} \operatorname{Tr}\left(\left(\mathbf{A}_n + \mathbf{B}_{\hat{\theta}}(\kappa) \right)^{-1} \right) \tag{4.23}$$

By expanding, we can apply the solution from (4.21)

$$\kappa_n^* = \arg\min_{\kappa \in \mathbf{K}} \frac{\operatorname{Tr}(\mathbf{A}_n) + \operatorname{Tr}\left(\mathbf{B}_{\hat{\theta}}(\kappa)\right)}{|\mathbf{A}_n + \mathbf{B}_{\hat{\theta}}(\kappa)|} \tag{4.24a}$$

$$= \arg\min_{\kappa \in \mathbf{K}} \frac{\operatorname{Tr}(\mathbf{A}_n) + \operatorname{Tr}\left(\mathbf{B}_{\hat{\theta}}(\kappa)\right)}{|\mathbf{A}_n| + \frac{1}{\sigma^2(\kappa)}\left(A_{11}\Delta t^2(\kappa) + A_{22} - 2A_{12}\Delta t(\kappa)\right)} \tag{4.24b}$$

As (4.21) & (4.24) require a solution to $\mathbf{A}_n$ to commence the iteration, the initial pulses of the train must be selected according to some criteria such that $\mathbf{A}_n$ is non-singular. One option would be to select alternating up/down chirp pulses of the greatest rate from the library. As (4.3) is negative quadratic in κ, this coincidentally provides the maximum amount of information about the target Howard *et al.* (2004). However, for targets already in track we already have some information about the target state that may be better used to initiate the pulse train selection process.

4.5 Pulse train design for target tracking

In this section, we consider optimal LFM pulse train design under a target tracking scenario. These schemes for designing diverse pulse trains are intended to be computed in linear time as a function the pulse train length. The following subsection is provided as a brief primer to the Kalman filter as a background to the methodology in the development of these schemes. Assuming a linear constant velocity target model with Markov dynamics, the state space model can be expressed as

$$\mathbf{x}_k = \mathbf{F}_\mu \mathbf{x}_{k-1} + \mathbf{w}_\mu \tag{4.25}$$

where $\mathbf{F}_\mu$ is a known transition matrix and independent and identically distributed (i.i.d.) noise process $\mathbf{w}_\mu \sim \mathcal{N}(\mathbf{0}, \mathbf{Q}_\mu)$ where $\mu = 2$ corresponds to the filter update rate. Target state estimation is assumed to be performed using a Kalman filter (Kalman 1960) in slow time after the subsequent processing of the received pulse train at processing interval T_2 with the mid-point of the pulse train selected as the time reference. From the standard Kalman filter equations, the a-priori state and covariance can be predicted as

$$\hat{\mathbf{x}}_{k|k-1} = \mathbf{F}_2 \hat{\mathbf{x}}_{k-1|k-1} \tag{4.26a}$$

$$\mathbf{P}_{k|k-1} = \mathbf{F}_2 \mathbf{P}_{k-1|k-1} \mathbf{F}_2^\top + \mathbf{Q}_2 \tag{4.26b}$$

and the a-posteriori state estimate and covariance are

$$\hat{\mathbf{x}}_{k|k} = \mathbf{x}_{k|k-1} + \mathbf{K}_k \mathbf{e}_k \tag{4.27a}$$

$$\mathbf{P}_{k|k} = (\mathbf{I} - \mathbf{K}_k \mathbf{H})\, \mathbf{P}_{k|k-1} \tag{4.27b}$$

where $\mathbf{I}$ is the identity matrix. For a target under track, the predicted covariance of the posterior are described by

$$\mathbf{P}_{k+1|k+1} = \mathbf{P} - \mathbf{P}\mathbf{H}^\top \mathbf{S}_{k+1|k+1}^{-1}(\boldsymbol{\kappa})\mathbf{H}\mathbf{P} \tag{4.28}$$

where for brevity $\mathbf{P} = \mathbf{P}_{k+1|k}$. The predicted innovation covariance can be given by

$$\mathbf{S}_{k+1|k+1} = \mathbf{H}\mathbf{P}\mathbf{H}^\top + \mathbf{R}_{k+1|k+1} \tag{4.29}$$

The measurement innovation, its covariance and Kalman filter gain are computed according to the following equations

$$\mathbf{e}_k = \mathbf{z}_k - \mathbf{H}\hat{\mathbf{x}}_{k|k-1} \tag{4.30a}$$

$$\mathbf{S}_k = \mathbf{H}\mathbf{P}_{k|k-1}\mathbf{H}^\top + \mathbf{R}_k \tag{4.30b}$$

$$\mathbf{K}_k = \mathbf{P}_{k|k-1}\mathbf{H}^\top \mathbf{S}_k^{-1} \tag{4.30c}$$

where measurement $\mathbf{z}_k$ and its covariance $\mathbf{R}_k$ are functions of the estimation process from the radar pulse train. For the diverse LFM pulse train, these are computed according to (4.11).

4.5.1 Minimisation of track mean square error

Minimisation of track MSE translates to the minimisation of the trace of (4.28).

$$\boldsymbol{\kappa}^*_{k+1} = \arg\min_{\boldsymbol{\kappa}\subseteq\mathbf{K}} \left[\mathrm{Tr}\left(\mathbf{P}\right) - \mathrm{Tr}\left(\mathbf{P}\mathbf{H}^\top\mathbf{S}^{-1}(\boldsymbol{\kappa})\mathbf{H}\mathbf{P}\right)\right] \tag{4.31}$$

As $\mathbf{P}$ is constant, we maximise the second term. From (4.29),

$$\boldsymbol{\kappa}^*_{k+1} = \arg\max_{\boldsymbol{\kappa}\subseteq\mathbf{K}} \mathrm{Tr}\left(\mathbf{P}\mathbf{H}^\top\left(\mathbf{H}\mathbf{P}\mathbf{H}^\top + \mathbf{R}(\boldsymbol{\kappa})\right)^{-1}\mathbf{H}\mathbf{P}\right) \tag{4.32}$$

Applying Woodbury's Identity (Henderson and Searle 1981, Woodbury 1950), we obtain

$$\boldsymbol{\kappa}^*_{k+1} = \arg\max_{\boldsymbol{\kappa}\subseteq\mathbf{K}} \mathrm{Tr}\left(\mathbf{P}\mathbf{H}^\top\mathbf{R}^{-1}(\boldsymbol{\kappa})\mathbf{H}\left(\mathbf{P}^{-1} + \mathbf{H}^\top\mathbf{R}^{-1}(\boldsymbol{\kappa})\mathbf{H}\right)^{-1}\right) \tag{4.33}$$

As $\mathbf{H}, \mathbf{P}$ are independent of $\boldsymbol{\kappa}$ and known a-priori, we can implement our greedy selection process (4.16), sequentially selecting the n-th pulse in the train

$$\kappa^*_{k+1,n} = \arg\max_{\kappa\in\mathbf{K}} \mathrm{Tr}\left(\mathbf{P}\mathbf{H}^\top\left(\mathbf{A}_n + \mathbf{B}_{\hat{\theta}}(\kappa)\right)\mathbf{H}\left(\mathbf{P}^{-1} + \mathbf{H}^\top\left(\mathbf{A}_n + \mathbf{B}_{\hat{\theta}}(\kappa)\right)\mathbf{H}\right)^{-1}\right) \tag{4.34}$$

4.5.2 Minimisation of validation gate volume

The minimisation of the validation gate volume corresponds to the minimisation of the determinant of (4.28). From (4.29),

$$\boldsymbol{\kappa}^*_{k+1} = \arg\min_{\boldsymbol{\kappa}\subseteq\mathbf{K}} \left|\mathbf{P} - \left(\mathbf{P}\mathbf{H}^\top\left(\mathbf{H}\mathbf{P}\mathbf{H}^\top + \mathbf{R}(\boldsymbol{\kappa})\right)^{-1}\mathbf{H}\mathbf{P}\right)\right| \tag{4.35}$$

Applying Woodbury's identity again and implementing our greedy selection strategy (4.16) we can sequentially select the n-th pulse in the train

$$\kappa^*_{k+1,n} = \arg\min_{\kappa\in\mathbf{K}} \left|\mathbf{P} - \mathbf{P}\mathbf{H}^\top\left(\mathbf{A}_n + \mathbf{B}_{\hat{\theta}}(\kappa)\right)\mathbf{H}\left(\mathbf{P}^{-1} + \mathbf{H}^\top\left(\mathbf{A}_n + \mathbf{B}_{\hat{\theta}}(\kappa)\right)\mathbf{H}\right)^{-1}\right| \tag{4.36}$$

4.5.3 Maximisation of mutual information

An accepted surrogate to optimal pulse train selection is to maximise the mutual information between the knowledge state represented by the a-priori target state covariance $\mathbf{P}$ and the resulting estimate from the pulse train (Howard *et al.* 2004, Suvorova *et al.* 2006b). The resultant optimisation problem can then be written as

$$\boldsymbol{\kappa}^*_{k+1} = \arg\max_{\boldsymbol{\kappa}\subseteq\mathbf{K}} I(X;Y) = \log\left|\mathbf{I} + \mathbf{R}^{-1}(\boldsymbol{\kappa})\mathbf{H}\mathbf{P}\mathbf{H}^\top\right| \tag{4.37}$$

Letting $\mathbf{D} = \mathbf{H}\mathbf{P}\mathbf{H}^\top$ and $\mathbf{R}$ being 2×2 matrices,

$$\boldsymbol{\kappa}^*_{k+1} = \arg\max_{\boldsymbol{\kappa}\subseteq\mathbf{K}} \left(\left|\mathbf{R}^{-1}(\boldsymbol{\kappa})\mathbf{D}\right| + \operatorname{Tr}\left(\mathbf{R}^{-1}(\boldsymbol{\kappa})\mathbf{D}\right)\right) \tag{4.38}$$

By adopting our greedy strategy (4.16) we find,

$$\kappa^*_{k+1,n} = \arg\max_{\kappa\in\mathbf{K}} \left(\left|\mathbf{A}_n + \mathbf{B}_{\hat{\theta}}(\kappa)\right|\left|\mathbf{D}\right| + \operatorname{Tr}\left(\left(\mathbf{A}_n + \mathbf{B}_{\hat{\theta}}(\kappa)\right)\mathbf{D}\right)\right) \tag{4.39}$$

and with some further simplification and the use of (4.21) we find

$$\begin{aligned}\kappa^*_{k+1,n} = \arg\max_{\kappa\in\mathbf{K}} \Bigg(& \frac{|\mathbf{D}|}{\sigma^2(\kappa)}\left(A_{11}\Delta t^2(\kappa) - 2A_{12}\Delta t(\kappa)\right. \\ & \left. + A_{22}\right) + \frac{1}{\sigma^2(\kappa)}\left(D_{22}\Delta t^2(\kappa) + 2D_{12}\Delta t(\kappa) + D_{11}\right)\Bigg)\end{aligned} \tag{4.40}$$

To commence the iteration, precision matrix $\mathbf{A}$ is initialised as $\mathbf{A}_1 = \mathbf{0}_{2,2}$. The optimisation functions presented in this section are designed to be computed in linear time as a function the pulse train length. The use of a greedy selection process means that as long as the pulse order is retained, in the event that the pulse train be truncated, the resultant estimate will still be optimal.

4.6 Alternate estimators

In this section, we describe a radar setup to evaluate the effectiveness of the joint MLE processing method described in Section 4.3 within a target tracking scenario. This is compared with two alternate non-MLE based processing methods including range averaging for trains of alternating (up/down chirp) LFM pulses and range-Doppler processing. The selected non-MLE methods for processing pulse trains are described in the following two subsections.

4.6.1 Alternating chirp range averaging

In non-coherent radar processing, the target range-rate is not observed and the range bias cannot be easily estimated. One strategy is to mitigate range bias is to select a pulse train comprising of alternating upchirp and downchirp pulses of equivalent chirp ratesFitzgerald (1974). This strategy also has the benefit of reducing posterior uncertainty over multiple pulses by minimising the overlap of the uncertainty intersection between successive pulses Niu *et al.* (2002). By averaging the biased measurements across the pulse train, the range biases can be nullified as

$$z = \frac{1}{2\alpha} \sum_{i=-N, i\in\kappa^+}^{N} m_i + \frac{1}{2\beta} \sum_{j=-N, j\in\kappa^-}^{N} m_j \tag{4.41}$$

where $\mathbf{m}$ is a vector of biased range measurements, α, β are the number of upchirps and downchirps in the train and $\alpha + \beta = 2N + 1$.

4.6.2 Pulse-Doppler processing

By comparing the phase shift between successive coherent pulses in a train, a pulse-Doppler radar is able to estimate both target range and range-rate simultaneously. For comparison purposes, we model both a pulse-Doppler radar using LFM biased range measurements as well one that provides range compensation based on the known chirp rate and the estimated range-rate from the pulse train. For the uncorrected estimate, the measurement is modelled as the weighted average of the biased range (4.8) and range-rate.

$$\mathbf{z}_b = \frac{\sum_{-N}^{N} \eta(n)\mathbf{x}_b(n)}{\sum_{-N}^{N} \eta(n)} + \mathbf{v}_2 = \begin{bmatrix} \hat{r}_b & \hat{\dot{r}} \end{bmatrix}^\top \tag{4.42}$$

where $\mathbf{x}_b(n) = \begin{bmatrix} r_b(n) & \dot{r}(n) \end{bmatrix}^\top$ is the range-biased truth state at the n-th pulse and $\mathbf{v}_2 \sim \mathcal{N}(\mathbf{0}, \mathbf{R}(\boldsymbol{\kappa}))$. The measurement covariance $\mathbf{R}$ is computed according to (4.2) using the pulse train characteristics in (4.47). For the compensated range-Doppler radar, we can correct the biased range estimate as a linear combination of the estimated range and range-rate:

$$\mathbf{z}_c = \begin{bmatrix} \hat{r}_c & \hat{\dot{r}} \end{bmatrix}^\top, \quad \hat{r}_c = \hat{r}_b - \Delta t \hat{\dot{r}} \tag{4.43}$$

Using bilinearity, the new elements of the bias corrected estimator covariance $\mathbf{R}_c$ can be computed from (4.2) as

$$\sigma^2_{r_c r_c} = \sigma^2_{rr} + \Delta t^2 \sigma^2_{\dot{r}\dot{r}} - 2\Delta t \sigma^2_{r\dot{r}} \tag{4.44a}$$

$$\sigma^2_{r_c \dot{r}} = \sigma^2_{r\dot{r}} - \Delta t \sigma^2_{\dot{r}\dot{r}} \tag{4.44b}$$

4.7 Simulation results

In the following section, we present some simulation results for the estimation processes described in Section 4.3 where we explore two separate target tracking scenarios. The first scenario investigates the effectiveness of the joint estimators in Section 4.3 using an alternating pulse train in a simple scenario featuring a target travelling in a straight line. As this linear trajectory does not provide the challenging environment to evaluate the chirp rate scheduling pulse train design methods of Section 4.4, a more complex scenario involving a manoeuvring target that completes a series of coordinated turns is used. The LFM pulses are modelled assuming a Gaussian weighting function. Define a Gaussian weighted continuous wave (CW) pulse with envelope

$$\tilde{s}(t) = \left(\frac{1}{\pi\lambda^2}\right)^{\frac{1}{4}} \exp\left(\frac{-t^2}{2\lambda^2}\right) \tag{4.45}$$

where λ is the pulse duration parameter. The measurement noise covariance (4.2) can be found through solving the normalised FIM in Appendix 4.A.1. We find the elements of $\mathbf{U}_{\phi}^{-1}$ for a single pulse to be

$$\sigma_\tau^2 = 2\lambda^2,\ \sigma_\nu^2 = \frac{2}{\lambda^2},\ \rho_{\tau\nu} = 0 \tag{4.46}$$

To model a coherent (pulse-Doppler) transmitter, the pulse phase can be made invariant from pulse to pulse. For a train of $2N+1$ identical Gaussian pulses with constant pulse repetition interval T and assuming that $2\lambda \ll T$, then from (3.16) the envelope can be written as,

$$\tilde{s}(t) = \frac{1}{(2N+1)^{\frac{1}{2}}} \left(\frac{1}{\pi\lambda^2}\right)^{\frac{1}{4}} \sum_{k=-N}^{N} \mathrm{e}^{-\frac{(t-kT)^2}{2\lambda^2}} \tag{4.47}$$

By solving the normalised FIM for (4.47) in Appendix 4.A.2, we approximate the delay and Doppler variances of for the coherent pulse train (4.A.17) as

$$\sigma_\nu^2 \approx \frac{6}{2NT^2(N+1)+3\lambda^2} \tag{4.48a}$$

$$\sigma_\tau^2 \approx \frac{2(2N+1)\lambda^2}{2\lceil N\rceil+1} \tag{4.48b}$$

where $\lceil\cdot\rceil$ is the ceil function. The signal-to-noise ratio $\eta = \frac{2E_r}{N_0}$, is modelled as an energy loss in an isotropic environment where N_0 is the noise density. The received

SNR is calculated in reference to the target SNR at a range of 1000 m as

$$\eta(r) = \left(\frac{1000}{r}\right)^4 \eta_{1000}$$

4.7.1 Linear target tracking using alternating pulse trains

Consider a target with nearly constant acceleration dynamics travelling along a straight line (4.25) with matrices

$$\mathbf{F}_\mu = \begin{bmatrix} 1 & T_\mu & T_\mu^2/2 \\ 0 & 1 & T_\mu \\ 0 & 0 & 1 \end{bmatrix}, \quad \mathbf{Q}_\mu = q \begin{bmatrix} \frac{T_\mu{}^5}{20} & \frac{T_\mu{}^4}{8} & \frac{T_\mu{}^3}{6} \\ \frac{T_\mu{}^4}{8} & \frac{T_\mu{}^3}{3} & \frac{T_\mu{}^2}{2} \\ \frac{T_\mu{}^3}{6} & \frac{T_\mu{}^2}{2} & T_\mu \end{bmatrix} \tag{4.49}$$

where T_1 is inter pulse period and $q = 0.001$. A radar is modelled operating at 3 GHz with LFM bandwidth of 10 MHz, pulse duration of 10 µs, PRI of 500 µs and pulse train length of 512. It is assumed that the radar has a task allocation of 1/25 for tracking the target with a resultant scan-to-scan or track update period of $T_2 = 6.4$ s. The target state is initialised as $\mathbf{x}(0) \sim \mathcal{N}(\mathbf{x}_\mu, \mathbf{P}_0)$ where $\mathbb{E}[\mathbf{x}(0)] = \begin{bmatrix} 10 & 250 & 0 \end{bmatrix}^\top$ (km, m s^{-1}, m/s^2) and $\mathbf{P}_0 = \mathrm{diag}(100, 25, 0.01)$ with reference SNR $\eta_{1000} = 80$ dB. For comparison, this is roughly equivalent to a radar operating with a peak power of 10 kW, antenna gain of 28 dBi and a target radar cross section (RCS) of 2-3 m^2. The observation matrix for the tracker in Section 4.5 is $\mathbf{H} = \begin{bmatrix} 1 & 0 & 0 \\ 0 & 1 & 0 \end{bmatrix}$ and for the range averaging estimator of Section 4.6.1, $\mathbf{H}$ reduces to $\begin{bmatrix} 1 & 0 & 0 \\ 0 & 0 & 0 \end{bmatrix}$. Results are averaged over 10000 Monte Carlo trials. The evaluation of the joint estimation methods described in Section 4.3 and alternate baseline estimators of Section 4.6 utilise a fixed pulse train comprising of alternating upchirp and downchirp pulses to form the initial (biased) range measurements. The evaluated measurement processing methods include:

1. *Range averaging* as described in Section 4.6.1. The biased ranges are averaged using (4.41) to form a range only measurement;

2. *Joint estimation* of both range and range-rate as described in Section 4.3. This uses the observation matrix of (4.10), $\mathbf{H}(\boldsymbol{\kappa})$;

3. *Time compensated joint estimation* as described in Section 4.3.1 using corrected range measurements $\tilde{\mathbf{m}}$. The range measurements are corrected according to

(4.12) using the predicted target radial velocity and the position of the pulse in the train; and the

4. *Temporally aligned joint estimator* which incorporates the temporal shift in (4.13) to form observation matrix $\bar{\mathbf{H}}(\boldsymbol{\kappa})$ as part of the measurement processing.

For baseline comparison, an upchirp only pulse train was also used, with the measurements formed by the coherent processing methods described in Section 4.6.2 including:

5. *Range-Doppler processing* with LFM range-Doppler coupling bias according to (4.42); and

6. *Range-Doppler LFM coupling compensated* where the biased range measurement is corrected using the estimated range-rate according to (4.43).

From Figure 4.1a, the effect of range bias is evident with significant range error evident for the upchirp pulse train even for the compensated range-Doppler processing. On the other hand, the average range error was found to be very similar for all of the methods that utilised the alternating chirp pulse trains. In Figure 4.1b, the velocity estimate of the temporally aligned estimator outperforms the other joint estimators. Both the range-Doppler estimators perform equitably with their similar Doppler processing methods.

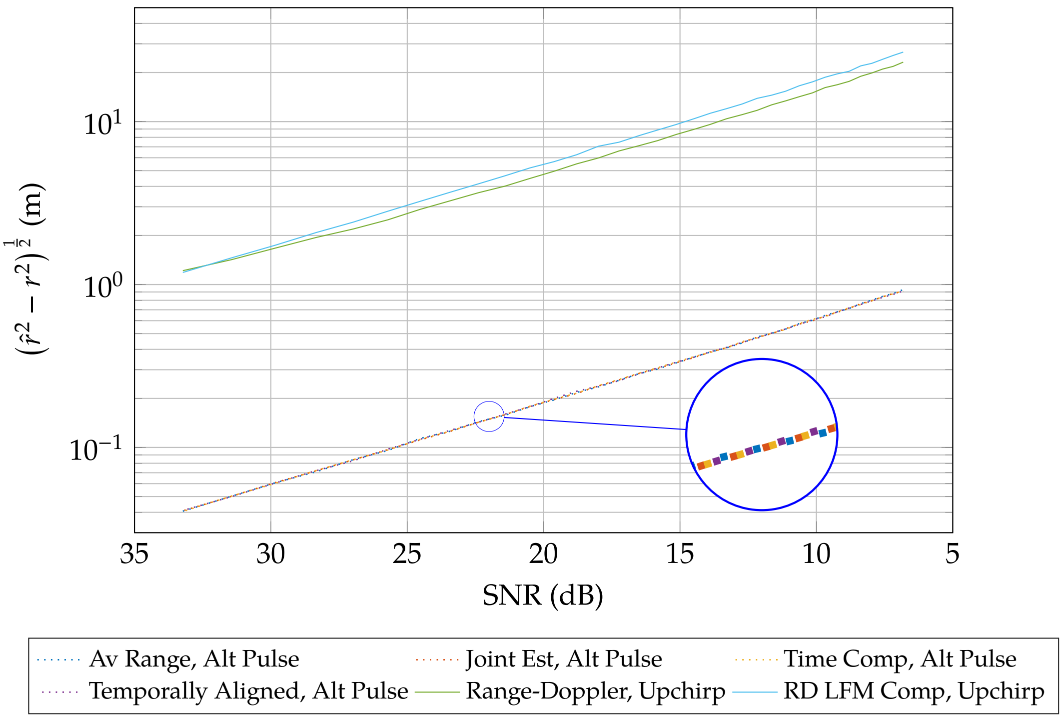

(a) Range error

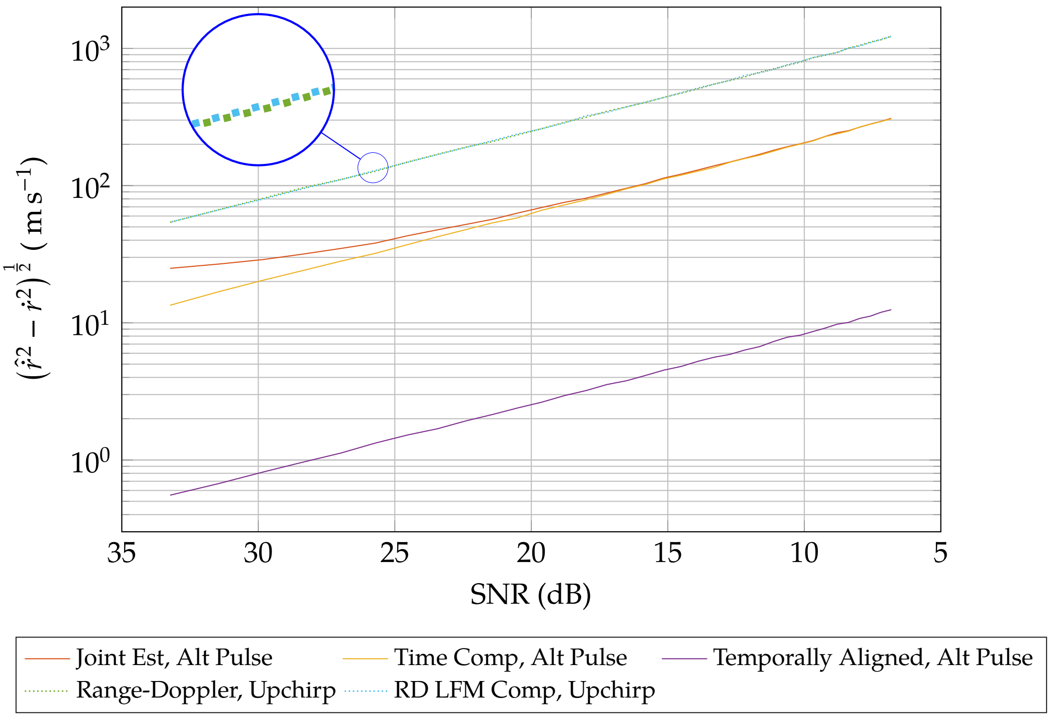

(b) Velocity error

Figure 4.1: Average measurement RMSE for joint estimation methods with an alternating chirp train and upchirp only for range-Doppler

A performance bound of the variance of unbiased estimator $\hat{\boldsymbol{\theta}}(\mathbf{y})$ of parameter $\boldsymbol{\theta} = [\theta_1, \ldots, \theta_M]^\top$ from observations $\mathbf{y} = \left[y_1, \ldots, y_N\right]^\top$ can be represented by the Cramér-Rao lower bound (CRLB) (Section 3.3.3) whereby the estimator MSE satisfies

$$\mathrm{MSE}\left(\hat{\boldsymbol{\theta}}(\mathbf{y})\right) = \mathbb{E}\left[\hat{\boldsymbol{\theta}}(\mathbf{y}) - \boldsymbol{\theta}\right]\left[\hat{\boldsymbol{\theta}}(\mathbf{y}) - \boldsymbol{\theta}\right]^\top \geq \mathbf{J}^{-1} \tag{4.50}$$

where $\mathbb{E}$ is the expectation operator, the FIM (3.25) is

$$\mathbf{J} = -\mathbb{E}\left[\nabla_{\boldsymbol{\theta}} \nabla_{\boldsymbol{\theta}}^\top \log p(\mathbf{y}, \boldsymbol{\theta})\right] \tag{4.51}$$

and $\nabla_{\boldsymbol{\theta}} = [\partial/\partial\theta_1, \ldots, \partial/\partial\theta_M]^\top$. As the CRLB only applies to deterministic parameters, the posterior Cramér-Rao bound (PCRB) can be used instead as a performance bound for a Bayesian filter (Van Trees 1968) and can be computed recursively (Challa *et al.* 2011, Tichavsky *et al.* 1998) for the Gaussian system in this example as:

$$\mathbf{J}_k(\mathbf{x}_k) = \mathbf{H}^\top \mathbf{R}_k^{-1} \mathbf{H} + \mathbf{Q}_k^{-1} - \mathbf{Q}_k^{-1} \mathbf{F}_k \left(\mathbf{J}_{k-1}(\mathbf{x}_{k-1}) + \mathbf{F}_k^\top \mathbf{Q}_k^{-1} \mathbf{F}_k\right)^{-1} \mathbf{F}_k^\top \mathbf{Q}_k^{-1} \tag{4.52}$$

In Figure 4.2, we compare the track error for the various estimators presented in Sections 4.2, 4.3 and 4.6 using the same alternating and upchirp pulse trains as those in Figure 4.1. For comparison purposes, the PCRB (4.52) has been calculated for the alternating pulse joint estimator (Section 4.3) and pulse-Doppler processing (Section 4.6.2). The impact of the range bias from the upchirp pulse trains is reflected in range error for the range-Doppler processing measurements, but significantly improved when using the compensated range-Doppler processing as seen in Figure 4.1. It also shows that whilst the bias can be compensated by averaging the measurements from the alternating pulse train, joint estimation can provide superior track performance for this pulse train, with similar track error for all of the joint estimation methods.

4.7.2 Manoeuvring target tracking using scheduled pulse trains

In this scenario, we compare the tracking performance of the optimal pulse train selection strategies of Section 4.5 using the temporally aligned joint estimator (4.13) for a narrow bandwidth radar. We model a manoeuvring target that travels in a straight line before performing a 360° clockwise coordinated turn followed by a 200° counter-clockwise coordinated turn of turn rates $\omega = \pm\pi/120\ \mathrm{rad\,s^{-1}}$ as shown in Figure 4.3. The target trajectories are generated using (4.25) with coordinated

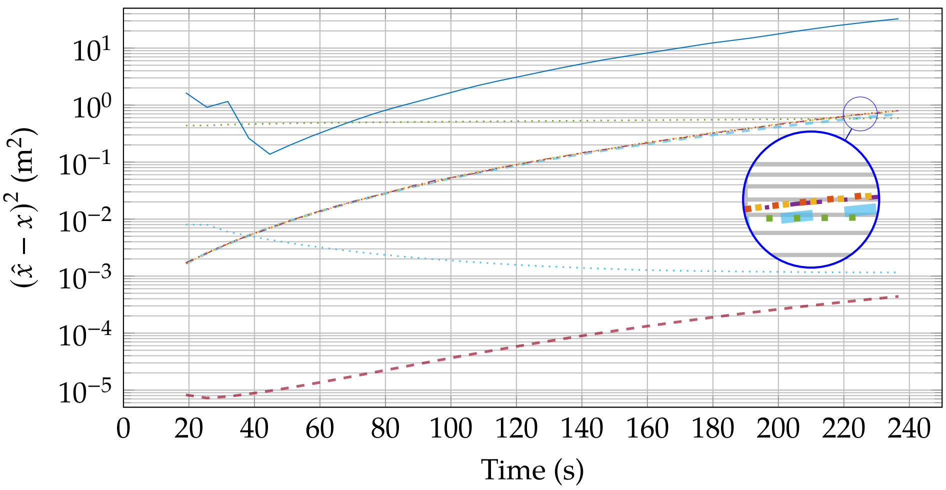

(a) Range error

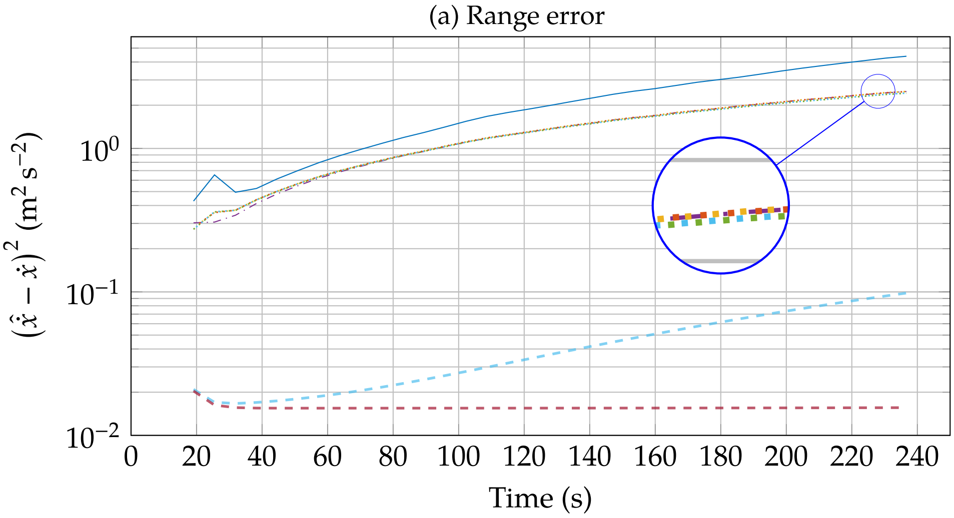

(b) Velocity error

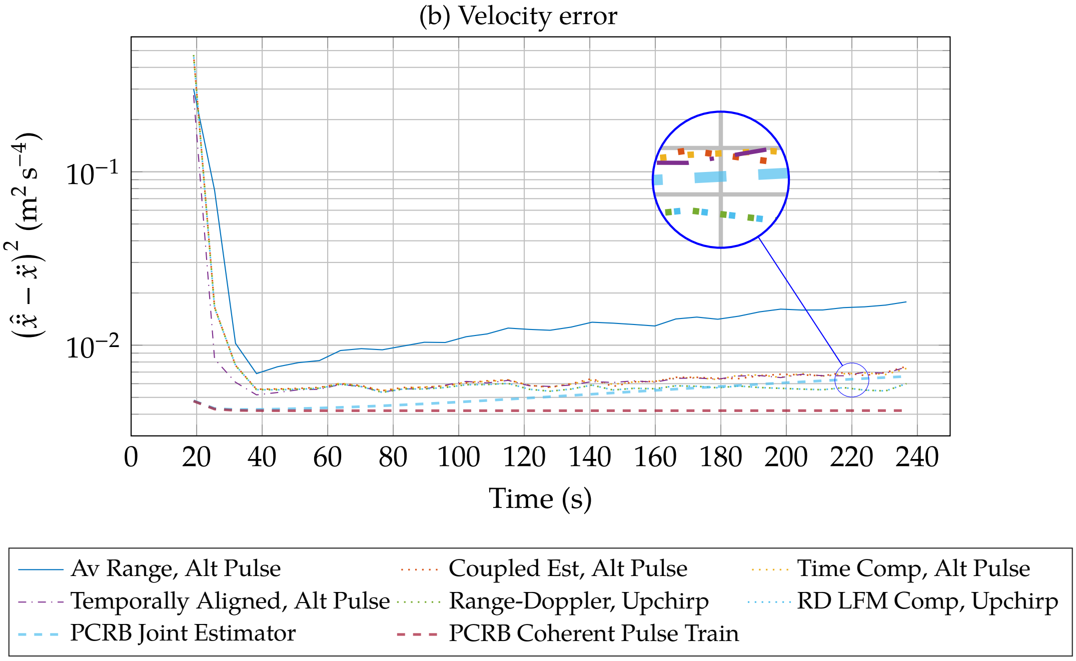

(c) Acceleration error

Figure 4.2: Average track MSE for joint estimation methods with an alternating chirp train and upchirp only train for range-Doppler

turn transition matrices

$$\mathbf{F}_\mu(\omega) = \begin{bmatrix} 1 & \sin(\omega T_\mu)/\omega & 0 & 0 & (\cos(\omega T_\mu) - 1)/\omega & 0 \\ 0 & \cos(\omega T_\mu) & 0 & 0 & -\sin \omega T_\mu & 0 \\ 0 & 0 & 1 & 0 & 0 & 0 \\ 1 & (1 - \cos(\omega T_\mu))/\omega & 0 & 1 & \sin(\omega T_\mu)/\omega & 0 \\ 0 & \sin(\omega T_\mu) & 0 & 0 & \cos(\omega T_\mu) & 0 \\ 0 & 0 & 0 & 0 & 0 & 1 \end{bmatrix}$$

$$\mathbf{Q}_\mu(\omega) = q \begin{bmatrix} \mathbf{Q}_\mu & \mathbf{0} \\ \mathbf{0} & \mathbf{Q}_\mu \end{bmatrix} \tag{4.53}$$

Whilst both the down and cross range trajectory are modelled, the radar only observes and tracks $\mathbf{x}(k)$ in the downrange direction. The target state is initialised as $\mathbb{E}[\mathbf{x}(0)] = \begin{bmatrix} 10 & 300 & 0, & 0 & 0 & 0 \end{bmatrix}^\top$ (km, m s^{-1}, m s^{-2}) and $\mathbf{P}_0 = \mathrm{diag}(100, 25, 0.01, 100, 25, 0.01)$ with reference SNR $\eta_{1000} = 85\,\mathrm{dB}$. As bearing information is unmeasured in this scenario, the observation matrix $\mathbf{H}$ is the same as used in the linear target example of Section 4.7.1. To compensate, the tracker (Section 4.5) uses an inflated target process noise of $q = 5$. This radar is modelled to be operating at 3 GHz with a pulse of duration 75 µs, a PRI of 750 µs and a train length of 512 pulses. Again, we assume a track task allocation of 1/25 for this target with a resultant track update period $T_2 = 9.6\,\mathrm{s}$. This is equivalent to the 10 kW radar example in Section 4.7.1 but a reduced target RCS of approximately 1 m^2. The average target SNR is shown in Figure 4.4.

Waveforms are selected from a library comprising of LFM chirps from ± 20 kHz to 140 kHz in 20 kHz steps is used. The scheduler maintains a frequency overlap of at least 90% between the transmitted and received pulses to limit energy loss from filter mismatch. This is achieved by pruning low bandwidth waveforms from the library using the predicted target velocity with a margin of 50 m s^{-1}. Evaluation of the pulse selection strategies utilises the temporally aligned joint estimator (4.13) for the measurement processing. The three optimal pulse train algorithms of Section 4.5 are compared with a series of fixed pulse trains as follows:

1. *Alternating pulses* where the pulse train comprises of interchanging maximal rate upchirp and downchirp pulses;

2. *Diverse pulse train* consisting of the entire library of permissible waveforms in succession. The succession is repeated until the pulse train is filled;

3. *Upchirp only* pulse train using maximal rate upchirps solely; and

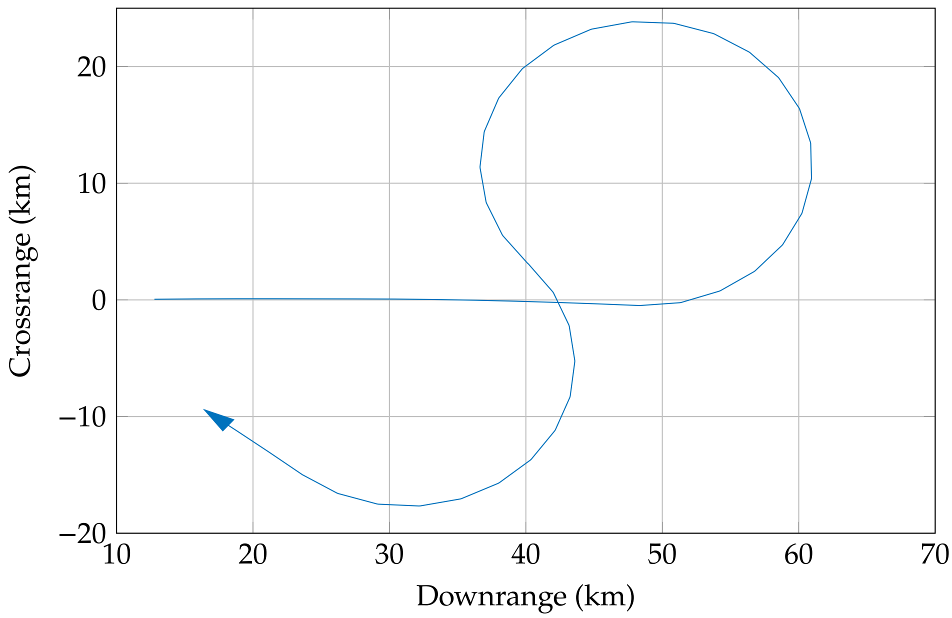

Figure 4.3: Coordinated turn target trajectory

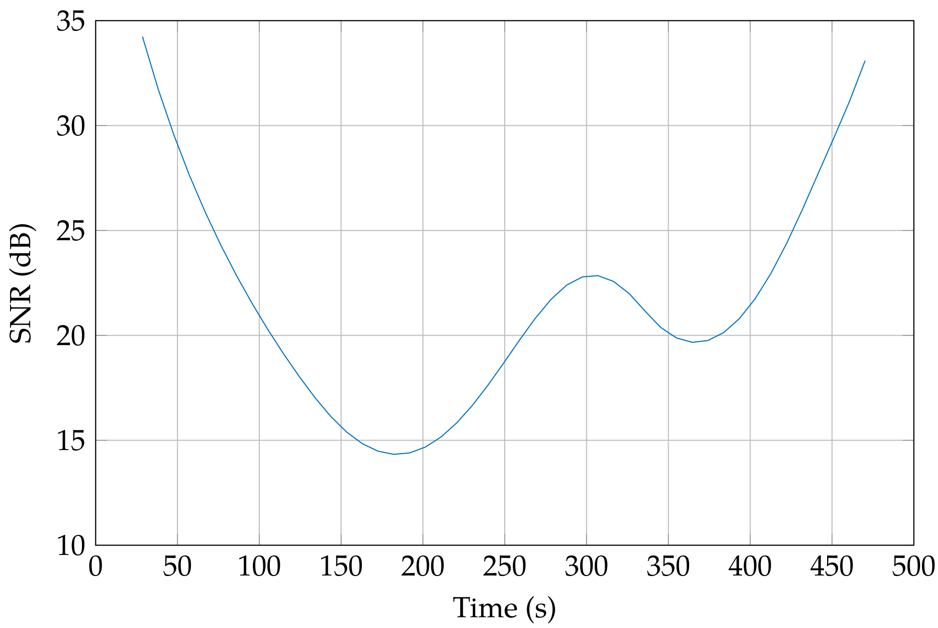

Figure 4.4: Target single pulse average SNR

4. *Alternating trains* using only maximal rate upchirp pulses followed by a train of only downchirp pulses.

For the manoeuvring target, the composite track error in Figure 4.5a shows improved track performance for both the alternating pulse train and the minimisation of track MSE (Section 4.5.1) pulse train when compared with the other optimal pulse train selection strategies at low target radial velocities and comparable performance at higher velocities with minimal total track error as expected for this particular metric. The periods of low target radial velocity occur as the target motion crosses around the radar during the coordinated turns. This is evident in the average SNR gradient of Figure 4.4 with the inflections indicating the target downrange direction swaps. The optimal strategies and the alternating pulse train all show superior performance to the diverse pulse train and particularly the trains of upchirps and downchirps which both appear to still suffer from bias error. Closer examination of Figure 4.6 and in particular Figures 4.6a & 4.6b show that during periods of low target velocity, the tracker is able to access low bandwidth waveforms and trade range accuracy for improved Doppler accuracy according to the selected cost function. Similarly, the track posterior covariance determinant in Figure 4.5b shows improvement for the optimal pulse trains over the alternating train during the periods of low target velocity. Interestingly, the minimisation of the track covariance determinant and the maximisation of the mutual information cost functions show virtually indistinguishable performance.

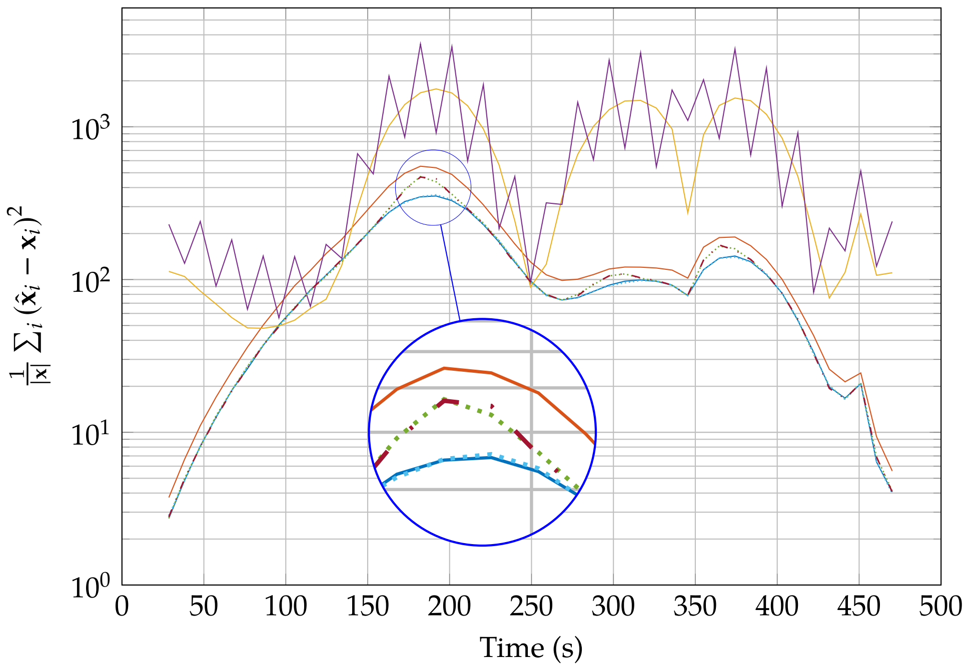

(a) Track sum mean square error

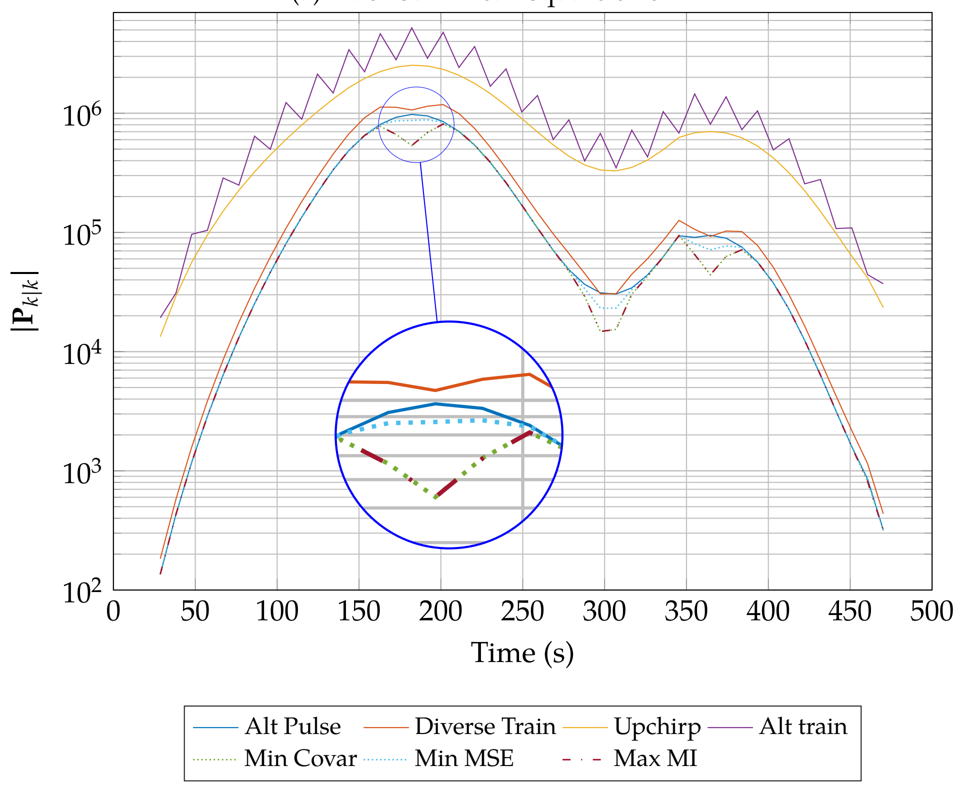

(b) Track posterior covariance determinant

Figure 4.5: Average temporally aligned joint estimator state error and posterior covariance for fixed and adaptive pulse trains

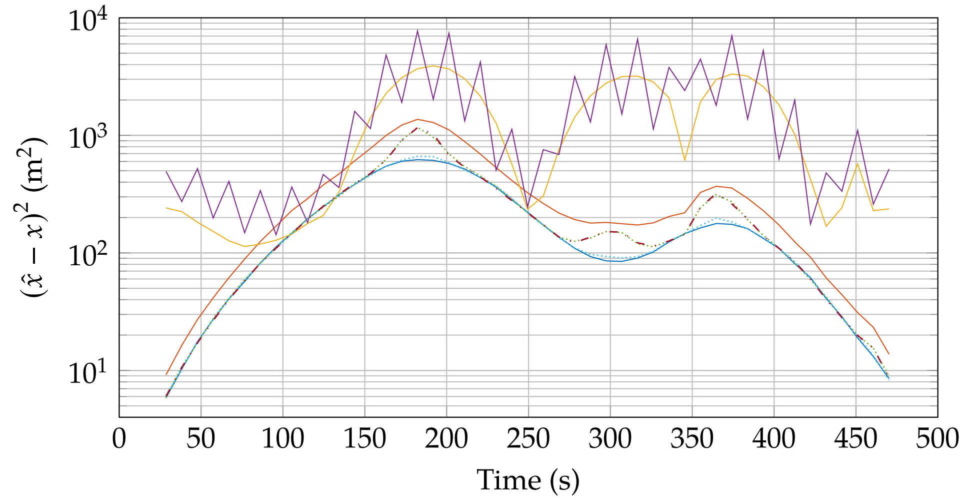

(a) Range error

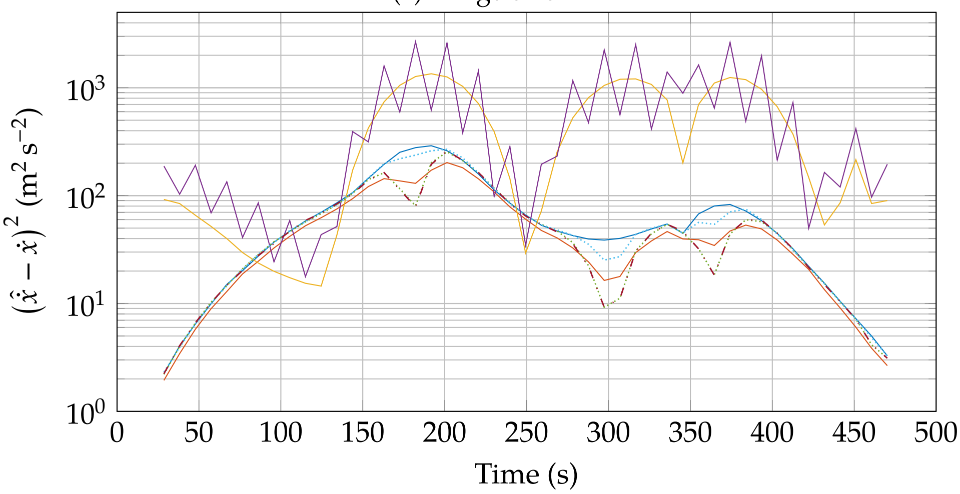

(b) Velocity error

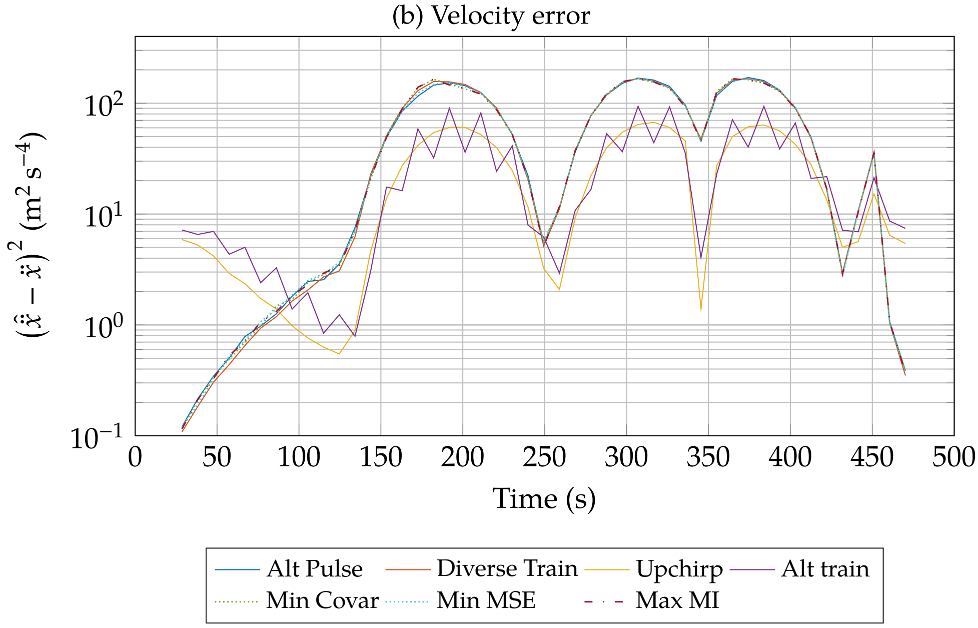

(c) Acceleration error

Figure 4.6: Average temporally aligned joint estimator track MSE for fixed and adaptive pulse trains

4.8 Conclusion

In this chapter, we presented a method of jointly estimating a detected target's range and range-rate using a series of biased range measurements from LFM pulses of known chirp rates. Using a diverse LFM pulse train, we show that our joint estimator significantly improve the measurement and track performance of non-coherent radar systems when compared with range averaging and even range-Doppler processing for moving targets. As the method we demonstrate only relies on the range measurements obtained from a matched filter receiver, it is suitable for potential implementation on existing coherent and non-coherent pulsed radar and sonar systems with minimal hardware modification. The application of the temporally-aligned joint estimator (Section 4.3.1) provides an advantage of not requiring the pulse train to comprise of diverse waveforms, making it possible to implement without alteration to existing radar RF front end hardware.

We derived joint estimation methods that are not fixed to any pulse train length and present greedy methods of waveform selection from a defined library. Being sequential, the MLE based estimator is suitable for both mechanically steered and electronically scanned array radar systems. It circumvents constricting properties such as fixed dwell times as a result of scan rates and beamshapes that might limit opportunities to complete planned long pulse train sequences as well systems that re-schedule mid-train. For the example target dynamics presented here, a pulse train that comprises solely maximal rate up and down chirps provides close to optimal performance and processor savings can be gained by restricting the waveform library to these pulse types for high bandwidth systems.

The use of a bandwidth limited waveform library accentuates the range-Doppler coupling bias error and is particularly evident in the pulse trains that lack inter pulse waveform diversity. In such situations, the use of adaptive pulse train strategies can offer improved track performance through the controlled exploitation of range-Doppler bias for an appropriate library of pulses. Range bias may also be used to intentionally shift a moving targets range response although, in multiple target or low signal-to-clutter ratio (SCR) situations, care should be taken to avoid placing legitimate targets within range bins that may be otherwise occupied by other genuine targets or clutter. The lack of Doppler tolerance in low bandwidth LFM pulses means that some waveforms can be unsuitable for targets that have large range-rates because of excessive coupling although this can be accounted for through use of mismatched receiver filters (McAulay and Johnson 1969, Niu *et al.* 2002, Xue *et al.* 2014).

Appendices

4.A Cramér-Rao lower bound for range and range-rate estimates

The local accuracy of a pulse can be described by the complex ambiguity function associated with a received waveform Van Trees (2001), Woodward (1967) as

$$\chi(\tau', \nu') \triangleq \int u\left(t - \frac{\tau'}{2}\right) u^*\left(t + \frac{\tau'}{2}\right) \mathrm{e}^{-j\nu' t}\,\mathrm{d}t \tag{4.A.1}$$

for normalised waveform envelope $u(t)$ where $\tau' = \tau - \tau_0$ and $\nu' = \nu - \nu_0$. The ambiguity function $\chi(\tau', \nu')$ is maximised at the target true position (τ_0, ν_0). We utilise the Cramér-Rao lower bound as an estimate for the error variance of the received pulse which can be computed from the inverse of the Fisher information matrix $\mathbf{J}$ whose elements are the second derivatives of the ambiguity function evaluated at the target true range (delay) and Doppler (Van Trees 2001) and as outlined in Section 3.3.3.

4.A.1 Gaussian weighted continuous wave pulse

For a Gaussian weighted CW pulse with envelope

$$\tilde{s}(t) = \left(\frac{1}{\pi\lambda^2}\right)^{\frac{1}{4}} \exp\left(\frac{-t^2}{2\lambda^2}\right) \tag{4.A.2a}$$

$$\tilde{S}(\omega) = (4\pi\lambda)^{\frac{1}{4}} \exp\left(\frac{-\omega^2\lambda^2}{2}\right) \tag{4.A.2b}$$

where pulse duration is 2λ for a rectangular pulse. The effective pulse length for the pulse is considered to be when

$$\tilde{s}(t) \leq \frac{1}{1000} \max \tilde{s}(t)$$

and is $\lambda_{eff} \approx 7.4338\lambda$ for a Gaussian pulse Kershaw and Evans (1994). Solving (3.29),

$$\overline{t^2} = \left(\frac{1}{\pi\lambda^2}\right)^{\frac{1}{2}} \int_{-\infty}^{\infty} t^2 \left|\exp\left(-\frac{t^2}{2\lambda^2}\right)\right|^2 \mathrm{d}t = \frac{\lambda^2}{2} \tag{4.A.3a}$$

$$\overline{\omega^2} = \frac{(4\pi\lambda)^{\frac{1}{2}}}{2\pi} \int_{-\infty}^{\infty} \omega^2 \left|\exp\left(-\frac{\omega^2\lambda^2}{2}\right)\right|^2 \mathrm{d}\omega = \frac{1}{2\lambda^2} \tag{4.A.3b}$$

As $\overline{\omega t} = 0$, substituting into (3.31), we obtain

$$\sigma_\tau^2 = 2\lambda^2,\ \sigma_\nu^2 = \frac{2}{\lambda^2},\ \rho_{\tau\nu} = 0 \tag{4.A.4}$$

4.A.2 Gaussian weighted continuous wave pulse train

Assuming that $2\lambda \ll T$ for a train of $2N+1$ identical Gaussian weighted CW pulses with PRI T, the envelope (4.A.2a) and its associated Fourier transform (3.30b) can be described as

$$\tilde{s}(t) = \frac{1}{(2N+1)^{\frac{1}{2}}}\left(\frac{1}{\pi\lambda^2}\right)^{\frac{1}{4}} \sum_{n=-N}^{N} \mathrm{e}^{-\frac{(t-nT)^2}{2\lambda^2}} \tag{4.A.5a}$$

$$\begin{aligned}\tilde{S}(\omega) &= \frac{1}{(2N+1)^{\frac{1}{2}}}\left(\frac{1}{\pi\lambda^2}\right)^{\frac{1}{4}} \sum_{k=-N}^{N} \int_{-\infty}^{\infty} \mathrm{e}^{-\frac{(t-kT)^2}{2\lambda^2}} \mathrm{e}^{j\omega t}\,\mathrm{d}t \\ &= \left(\frac{2\lambda\sqrt{\pi}}{2N+1}\right)^{\frac{1}{2}} \mathrm{e}^{-\frac{\lambda^2\omega^2}{2}} \sum_{k=-N}^{N} \mathrm{e}^{jkT\omega}\end{aligned} \tag{4.A.5b}$$

We obtain the entries of the FIM by solving (3.29). Commence by solving (3.29c) as

$$\overline{t^2} = \frac{1}{2N+1}\left(\frac{1}{\pi\lambda^2}\right)^{\frac{1}{2}} \int_{-\infty}^{\infty} t^2 \left|\sum_{k=-N}^{N} \mathrm{e}^{-\frac{(t-kT)^2}{2\lambda^2}}\right|^2 \mathrm{d}t \tag{4.A.6}$$

Expanding the summation,

$$\begin{aligned}\overline{t^2} = \overline{t^2}_a + \overline{t^2}_b &= \frac{1}{2N+1}\left(\frac{1}{\pi\lambda^2}\right)^{\frac{1}{2}} \sum_{k=-N}^{N} \int_{-\infty}^{\infty} t^2 \mathrm{e}^{-\frac{(t-kT)^2}{\lambda^2}}\,\mathrm{d}t \\ &+ \frac{2}{2N+1}\left(\frac{1}{\pi\lambda^2}\right)^{\frac{1}{2}} \sum_{n=-N+1}^{N} \sum_{m=-N}^{n-1} \int_{-\infty}^{\infty} t^2 \mathrm{e}^{-\frac{(t-mT)^2}{2\lambda^2}} \mathrm{e}^{-\frac{(t-nT)^2}{2\lambda^2}}\,\mathrm{d}t\end{aligned} \tag{4.A.7}$$

Solving the first part of (4.A.7),

$$\begin{aligned}\overline{t^2}_a &= \frac{1}{2N+1}\left(\frac{1}{\pi\lambda^2}\right)^{\frac{1}{2}} \sum_{k=-N}^{N} \frac{(\lambda^2\pi)^{\frac{1}{2}}}{2}\left(2k^2T^2 + \lambda^2\right) \\ &= \frac{T^2 N(N+1)}{3} + \frac{\lambda^2}{2}\end{aligned} \tag{4.A.8}$$

Next, by expanding and rearrange, the second part of (4.A.7) is:

$$\overline{t^2}_b = \frac{2}{2N+1}\left(\frac{1}{\pi\lambda^2}\right)^{\frac{1}{2}} \sum_{n=-N+1}^{N}\sum_{m=-N}^{n-1} \mathrm{e}^{-\frac{T^2(m^2+n^2)}{2\lambda^2}} \int_{-\infty}^{\infty} t^2 \mathrm{e}^{-\frac{t^2-tT(m+n)}{\lambda^2}}\,\mathrm{d}t \tag{4.A.9}$$

Solving the integral:

$$\begin{aligned}\overline{t^2}_b =& \frac{2}{2N+1}\left(\frac{1}{\pi\lambda^2}\right)^{\frac{1}{2}} \sum_{n=-N+1}^{N}\sum_{m=-N}^{n-1} \mathrm{e}^{-\frac{T^2(m^2+n^2)}{2\lambda^2}} \frac{1}{4}\mathrm{e}^{\frac{T^2(m+n)^2}{(2\lambda)^2}} \left(\sqrt{\pi}\lambda T^2(m+n)^2 + 2\lambda^3\sqrt{\pi}\right)\\ =& \frac{1}{2(2N+1)} \sum_{n=-N+1}^{N}\sum_{m=-N}^{n-1} \mathrm{e}^{-\frac{T^2(m-n)^2}{4\lambda^2}} \left(T^2(m+n)^2 + 2\lambda^2\right)\end{aligned} \tag{4.A.10}$$

Substituting (4.A.8) & (4.A.10) back into (4.A.7),

$$\overline{t^2} = \frac{T^2N(N+1)}{3} + \frac{\lambda^2}{2} + \frac{1}{2(2N+1)} f(\lambda,T,N) \tag{4.A.11}$$

where

$$f(\lambda,T,N) = \sum_{n=-N+1}^{N}\sum_{m=-N}^{n-1} \mathrm{e}^{-\frac{T^2(m-n)^2}{4\lambda^2}} \left(T^2(m+n)^2 + 2\lambda^2\right)$$

Assuming that $T \gg \lambda$, as a result when ratio $T^2/\lambda^2 \to \infty$, also $f(\lambda,T,N) \to 0$. Therefore;

$$\overline{t^2} > \frac{T^2N(N+1)}{3} + \frac{\lambda^2}{2} \tag{4.A.12}$$

Next, to find entry (3.29a)

$$\begin{aligned}\overline{\omega^2} &= \frac{\lambda}{\sqrt{\pi}(2N+1)} \int_{-\infty}^{\infty} \omega^2 \mathrm{e}^{-\lambda^2\omega^2} \left|\sum_{k=-N}^{N} \mathrm{e}^{jkT\omega}\right|^2 \mathrm{d}\omega\\ &= \frac{\lambda}{\sqrt{\pi}(2N+1)}\left[\sum_{k=-N}^{N}\int_{-\infty}^{\infty} \omega^2 \mathrm{e}^{-\lambda^2\omega^2}\mathrm{e}^{2jkT\omega}\,\mathrm{d}\omega + 2\sum_{\substack{m,n=-N\\ m<n}}^{N}\int_{-\infty}^{\infty} \omega^2 \mathrm{e}^{-\lambda^2\omega^2}\mathrm{e}^{j(m+n)T\omega}\,\mathrm{d}\omega\right]\end{aligned} \tag{4.A.13}$$

By solving the integrals, we find

$$\overline{\omega^2} = \frac{\lambda}{\sqrt{\pi}(2N+1)}\left[g(\lambda,T,N) + 2h(\lambda,T,N)\right] \tag{4.A.14a}$$

where

$$g(\lambda, T, N) = \frac{\sqrt{\pi}}{2\lambda^3} \sum_{k=-N}^{N} \mathrm{e}^{\frac{-k^2T^2}{\lambda^2}} \left(1 - \frac{2k^2T^2}{\lambda^2}\right) \tag{4.A.14b}$$

$$h(\lambda, T, N) = \frac{\sqrt{\pi}}{2\lambda^3} \sum_{\substack{m,n=-N \\ m<n}}^{N} \mathrm{e}^{\frac{-(m+n)^2T^2}{\lambda^2}} \left(1 - \frac{(m+n)^2T^2}{2\lambda^2}\right) \tag{4.A.14c}$$

Again, assuming that $T \gg \lambda$, then as $T^2/\lambda^2 \to \infty$ also $\mathrm{e}^{\alpha\frac{T^2}{\lambda^2}} \to 0$ if $\alpha \neq 0$ since $\alpha \leq 0$. This means we only need to consider the cases of $k = 0$ and $m = -n$. The bounds for (4.A.14b) & (4.A.14c) can be found as

$$g(\lambda, T, N) = \frac{\sqrt{\pi}}{2\lambda^3} \left[1 + \sum_{\substack{k=-N \\ k\neq 0}}^{N} \mathrm{e}^{\frac{-k^2T^2}{\lambda^2}} \left(1 - \frac{2k^2T^2}{\lambda^2}\right)\right] > \frac{\sqrt{\pi}}{2\lambda^3} \tag{4.A.15a}$$

$$h(\lambda, T, N) = \frac{\sqrt{\pi}}{2\lambda^3} \left[\lceil N \rceil + \sum_{\substack{m,n=-N \\ m<n, m\neq -n}}^{N} \mathrm{e}^{\frac{-(m+n)^2T^2}{\lambda^2}} \left(1 - \frac{(m+n)^2T^2}{2\lambda^2}\right)\right] > \frac{\sqrt{\pi}\lceil N \rceil}{2\lambda^3} \tag{4.A.15b}$$

where $\lceil \cdot \rceil$ is the ceil function. Substituting (4.A.15a) & (4.A.15b) back into (4.A.14a) we obtain

$$\begin{aligned} \overline{\omega^2} &> \frac{\lambda}{\sqrt{\pi}(2N+1)} \left(\frac{\sqrt{\pi}}{2\lambda^3} + \frac{2\sqrt{\pi}\lceil N \rceil}{2\lambda^3}\right) \\ &= \frac{2\lceil N \rceil + 1}{2(2N+1)\lambda^2} \end{aligned} \tag{4.A.16}$$

From (3.31), for (4.A.12) & (4.A.16) we find the delay and Doppler properties of the pulse train to be

$$\sigma_\nu^2 < \frac{6}{2NT^2(N+1) + 3\lambda^2} \tag{4.A.17a}$$

$$\sigma_\tau^2 < \frac{2(2N+1)\lambda^2}{2\lceil N \rceil + 1} \tag{4.A.17b}$$

Chapter 5

Concurrent processing for adaptive radar

Pipeline processing for radar has been proposed for computationally intensive real time application such as space-time adaptive processing (STAP) Choudhary *et al.* (1998; 2000), Liao *et al.* (2005). Through offering a high bandwidth solution with multiple parallel processors, a pipeline architecture is suited to complex independent processing applications Forsberg *et al.* (2001), Hyun *et al.* (2015). In this chapter, we consider the time costs associated with radar processing activities essential for the successful implementation of a knowledge based diversity or 'cognitive' scheme (Section 2.5.2). In Section 5.1, we review the adaptive sensor scheduling problem with an emphasis on target tracking for radar. We then look at the modelling the time cost of the associated radar processing tasks in Sections 5.1.1 to 5.1.2. These include tasks associated with scene interrogation, received signal processing, subsequent state estimation as well as the scheduling activities, such as selecting the next target to interrogate, the radar resources to utilise and activating the selected resources. By recognising the time cost and subsequent repercussion it can have on the feedback cycle, varying processor capabilities, architectures and consideration for performance compromises for a specific radar objective such as target tracking can be given. In Section 5.2 we consider the application of pipeline processing for the adaptive radar resource scheduling problem. To illustrate, in Section 5.3 we model an example of a sensor scheduling strategy with different scheduling costs for the computing aspects of the radar feedback loop cycle as applied to a multi-target tracking problem and compare the target tracking performance for both serial and parallel radar processors in Section 5.4.

5.1 Background

The introduction of technologies such as software defined radar has placed the emphasis of signal processing aspects of radar operations being performed using flexible processing hardware and arbitrary waveform generation Bell *et al.* (2015b). However, impact of the time associated with radar signal processing related tasks is rarely considered, particularly with regard to resource scheduling. In this chapter, we consider the problem of the overlying perception-action cycle (Section 2.5.1) requiring the performance of 'advanced near-real-time analytical techniques' Zasada *et al.* (2014). Whilst, the implementation of a rich resource library might allow to scheduler the improve the utility of the radar, the cost of evaluating a expansive library can prove prohibitive with the time required to perform this task potentially long in comparison to the frequency that measurements are acquired. Conversely, the scheduler may choose to select resources that result in the radar becoming front-end bound, providing more time for the deployment of intensive processing activities or scheduling to complement the increased time now available for processing activities.

To maximise throughput and total utility of the radar, a scheduler could choose to dynamically allocate available capacity, including processing based on some form of criteria or cost function to balances its objectives. This might include governing the rate at which the radar acquires new measurements or the assignment of multiple (parallel) processors or central processing units (CPUs) to manage the completion time of the cycle so that the following task in the sequence may commence. In a myopic scheduling scheme, this could be achieved by scheduling the radar resources as a utility of the current target state estimate for a defined resource library, $\mathbf{\Theta}$. This can be formulated as a optimisation problem where the role of the scheduler is to select the best resources from an admissible subset of resources $\boldsymbol{\theta}^* \in \mathbf{\Theta}$ according to a scheduling policy:

$$\boldsymbol{\theta}^*_{k+1} = J\left(\hat{\mathbf{x}}_k\right) \tag{5.1.1}$$

where $\hat{\mathbf{x}}_k$ is the state estimate at the k-th time step. Unfortunately, there is rarely any guarantee of convexity in the solution as the resource sets combinations are evaluated separately making this form of optimisation problem to be generally considered as NP-hard. As a results, the computational resources required to implement such schemes can be quite considerable even if closed form solutions exist. Compounding this challenge, the curse of dimensionality can make non-myopic scheduling schemes even more prohibitive to implement. Even through Moore's Law (Moore 1998), significant processor gains from today's computer developments are no longer achieved through faster processor clock cycles, but rather the shift to parallel processing architectures and enlarged data busses between parallel CPU cores. As the increase of computation throughput through a parallel processing scheme may not necessarily increase the speed by which the scheduling activity can occur particularly given its sequential nature, we consider different processing arrangements that might take advantage of the increased available bandwidth.

To maximise utility, a system would need to avoid bottlenecking from throughput constraints in both the radar front-end and its processor. For example, a front-end may be capable of obtaining a large set of measurements rapidly in time Δt about a set of targets $\tau \in \boldsymbol{\tau}$. However, should the period required to update the knowledge state about the targets using its processing algorithm exceeds Δt then the radar must either buffer the next set of measurements, resulting in lag between the new measurements and the knowledge state, forcing it to become stale or discard measurements to catch up, wasting information it has just obtained.

A common metric that can be applied to the separated operations of the radar transmitter and receiver is the processing between successive updates, which is directly related to the cumulative coherent processing interval (CCPI) Butterfield *et al.* (2016) which is given by,

$$ccpi(t) = \sum_{i}^{N} cpi\big(\boldsymbol{\theta}\,(t_i)\big), \quad 0 \leq t_0, \leq t_1 \leq, \ldots, \leq t_N \tag{5.1.2}$$

where $cpi\big(\boldsymbol{\theta}\,(t_i)\big)$ is coherent processing interval (CPI) of the i-th pulse of the chosen action $\boldsymbol{\theta} \in \boldsymbol{\Theta}$. Given the time scales that radar typically operates on, the complexity of tasks that can be completed within this time frame are somewhat limited. Ultimately, some compromise between the size of the library resourcefulness, scheduling decision time/ effort and update rates must be found with the possibility requiring scheduling of more time expensive, albeit richer measurements to lower the measurement frequency to the processor and vice-versa.

5.1.1 Formulation of time costs associated with cognitive radar operations

In this subsection, we consider the time costs associated with radar sub-tasks with an emphasis on those associated a cognitive perception-action cycle within a Bayesian target tracking context. These include,

1. Illumination of the radar scene with a selected action(s),
2. Acquisition of reflected signals during the current epoch,
3. Processing of the received signals to form a measurement,
4. Prediction of the estimated target state,
5. Updating the new estimate of the target state, and

6. Selecting (scheduling) the radar resources to interrogate the scene at the future epoch.

Steps 3 - 6 are normally identified with the signal processing aspects of cognitive radar. Through radar signal processing techniques, multiple sequential pulses that are closely spaced in time can be processed together to obtain an improved measurement by means such as non-coherent integration or pulse-Doppler processing. Assuming that the time associated with storing and retrieving a signal is negligible, the time cost associated with the interrogation or measurement interval is a linear function of the transmit, wait and receive intervals or pulse repetition interval (PRI). The total time is then simply the number of pulses in the processing interval n multiplied by the PRI:

$$\Delta t_{burst} = n \Delta t_{pri}, \quad n \in \mathbb{Z} \tag{5.1.3}$$

5.1.2 Modelling time costs associated with radar processing and scheduling activities

To represent the time associated with the radar processing activities, including selecting a radar action $\theta(k) \in \mathbf{\Theta}(k)$ at potentially every epoch, we use a concept termed '*decision time*'. With radar pulse repetition frequencys (PRFs) in the order of kHz, not a significant amount of time exists between measurements to perform the necessary processing tasks. In previous adaptive radar sensor tracking work Haykin *et al.* (2010), Kershaw and Evans (1994; 1997), Nguyen *et al.* (2015; 2014), Sira *et al.* (2006), Suvorova *et al.* (2006b), Zhang *et al.* (2017), it often assumed that decision time is (almost) instantaneous on a pulse to pulse basis or at least between bursts for every epoch. For such an assumption to be valid, the decision time would need to abide by the upper bound, $d(k) \ll \Delta t_{pri}$. For an adaptive radar operating on a single (serial) radar processing architecture using the update cycle described in Section 3.4 , a decision time $d(k) \geq \Delta t_{pri}$ can result in a delay within the radar operation timeline. This delay, or 'dead time' appears sandwiched between the successive pulse bursts as the radar completes its signal processing tasks. The update period for such a system then can be described simply as

$$\Delta t(k) = \Delta t_{burst}(k) + d(k) \tag{5.1.4}$$

where Δt_{burst} is the duration of the pulse burst, normally associated with the radar CCPI and $d(k)$ the decision time or dead time in this case. As the complexity of the scheduling process and associated time cost increase, we expect that $d(k)$ increases accordingly. Conversely, a reduction in the decision time and delay for an identical scheduling cost can be attained by increasing the computation rate (and potential hardware cost). To evaluate the cost of these radar processing activities, we utilise decision time as a proxy to associate the cost of an agent performing the processing activity (including scheduling) within an arbitrary decision period. In doing so, the temporal impact can be readily included as part of the signal processing steps in addition to the interrogation process. For simplicity here, we limit scope to a scenario where a pulse-Doppler radar is concerned with tracking of multiple spatially separated targets $\tau \in \boldsymbol{\tau}$.

5.2 Concurrent adaptive radar signal processing

As the trend to achieve processor performance improvements move away from faster clock speeds and toward multi threaded architectures due to breakdown of Dennard scaling DeBenedictis (2017), Dennard *et al.* (1999), the practicability of reducing or eliminating dead time between epoch becomes more challenging for a serial processor architecture. To exploit the processing capability gains afforded by multiprocessor architectures, we propose the use of a parallelised pipeline radar processing design. The use of pipeline computing model for radar signal processing application is not new, particularly for extremely computationally intensive operations such as STAP Choudhary *et al.* (1998; 2000), Liao *et al.* (2005) and other high bandwidth applications Forsberg *et al.* (2001), Hyun *et al.* (2015). In the context of adaptive radar, separating the tasks associated with the decision period into multiple streams (Figure 5.2.1) allows the processor to complete them simultaneously. In the following section, we describe two methods to divide the processing streams up into multiple threads that attempt to maximise the utility of the radar front-end by minimisation or elimination of dead time. Using this strategy, the radar front-end is able to continuously transmit and receive pulse trains as the processor processes the received signals and selects the radars future actions.

Instruction \ Cycle	0	1	2	3	4	5	7	8	9
Process Signals		k	$k+1$	$k+2$	$k+3$				
Detect Target			k	$k+1$	$k+2$	$k+3$			
Update Track				k	$k+1$	$k+2$	$k+3$		
Schedule Resources					k	$k+1$	$k+2$	$k+3$	

Figure 5.2.1: Processing for an adaptive sensor in a target tracking application performed as a four stage pipelined process across bursts $k, \ldots, k+3$

5.2.1 Delayed pipeline radar processing

The requirement to complete the processing tasks in a sequential loop means that an adaptive process does not lend naturally towards parallelisation. One method to achieve parallelisation is to implement a *delayed pipeline* architecture, where a scheduled queue of radar actions is formed based on the delayed state update. Unlike the sequential process where the most recent update is used to selecting future actions, we rely on information from a previous update and the expected outcome from future actions to select the next action. Being parallel, whilst scheduling the an action the radar can simultaneously interrogate the scene according to the action queue. By matching the action queue length with the decision time, we can pipeline the radar processes accordingly, as shown in Figure 5.2.2. We assume that once the action selection process has commenced, the target state information or *prior* cannot be updated. This results in the action selection process occurring with a *delay time* — an associated 'staleness' of the information rather. Action selection then occurs using knowledge from the last updated a-posteriori state estimate $\hat{\boldsymbol{x}}_{k-n}$ and the selected but yet to be processed action queue $\theta_{k,\ldots,k-n+1}$;

$$\theta^*_{k+1} = f\left(\hat{\boldsymbol{x}}_{k-n}, \theta_{k,\ldots,k-n+1}\right)$$

As the decision time increases, the number of parallel processes can increase accordingly along with the associated decision delay and queue depth according to

$$n = \left\lceil \frac{d(k)}{\Delta t_{burst}} \right\rceil \tag{5.2.1}$$

By doing this, whilst one thread is occupied with processing the returns from the target currently being interrogated, another thread can be potentially scheduling the next set of actions based on the state estimate from the previous update in a alternating 'hopping' cycle.

5.2.2 Concurrent pipeline radar processing

In the concurrent pipeline model, a partial update of the state estimate is used to inform the scheduling process through exploitation of the pulse integration process. As the coherent pulse integration process of pulse-Doppler radar requires the transmission and reception of a burst of identical pulses, part way through the processing interval an incomplete train can be used to create a somewhat less informed 'partial measurement'. Whilst the partial measurements are not used to update the state estimate, they can be applied to augment the delayed prior

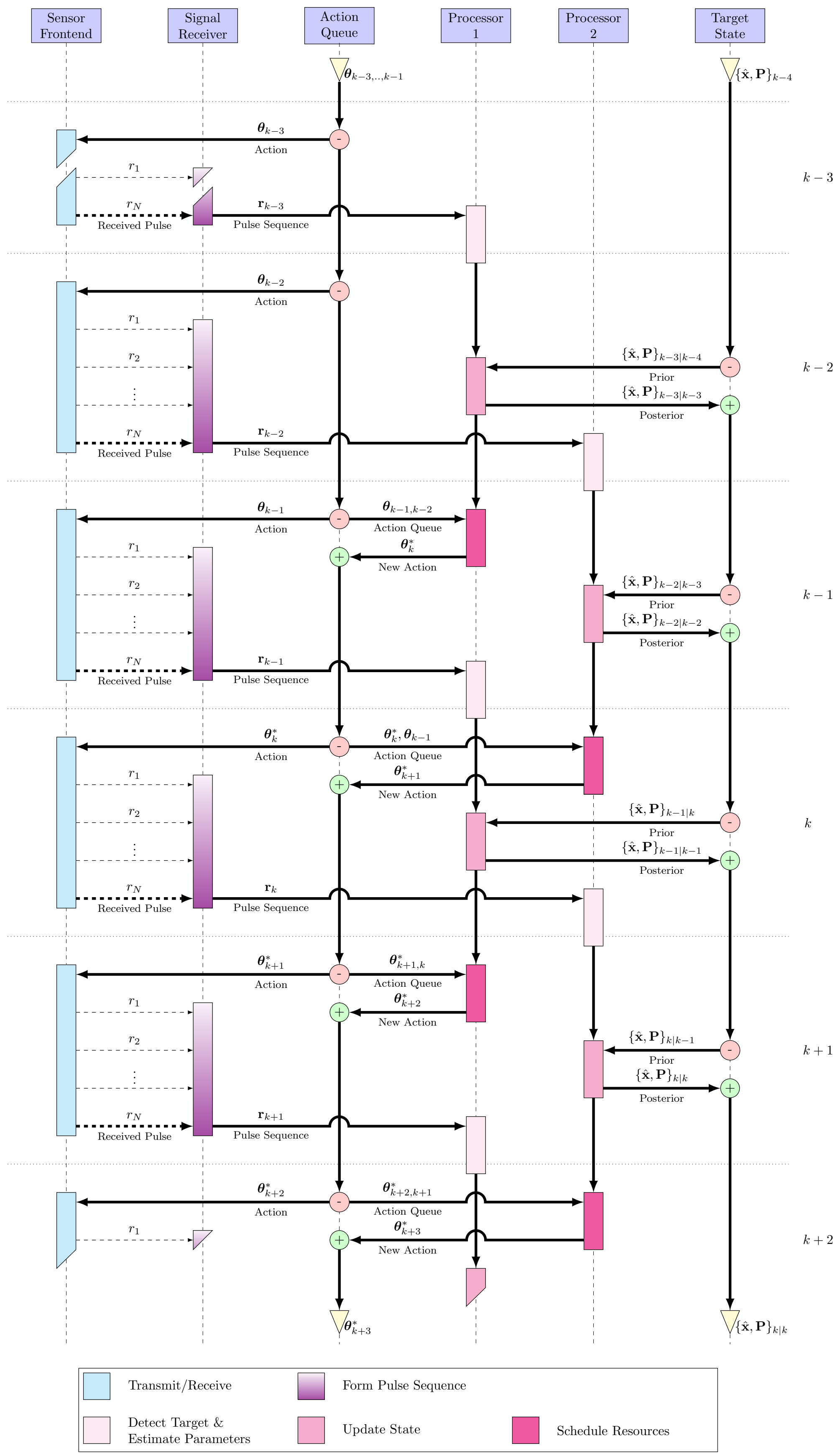

Figure 5.2.2: Sequence diagram of a delayed pipelined radar using two processors and a two CCPI delay

state in a 'refreshment' of the prior in what we term a *pseudo-update*. The refreshed pseudo-update is used to inform the action selection process as

$$\theta^*_{k+1} = f\left(\hat{\boldsymbol{x}}_{k-n'}, \theta_{k,\dots,k-n+1}\right)$$

where $n' < n$ is the delay. Once the entire burst has been received, the pseudo-update can be discarded and a complete measurement and state update performed in a similar manner to that of the delayed pipeline process (Section 5.2.1) as depicted in Figure 5.2.3.

The concurrent pipeline process differs from the delayed pipeline process which commences inter-train, with a decision period that is a integer number of pulse trains. The concurrent pipeline process commences intra-train within the coherent processing interval resulting in a decision period that is a integer number of pulse trains plus a partial pulse train and requiring additional processing to form the partial measurements for the scheduling process.

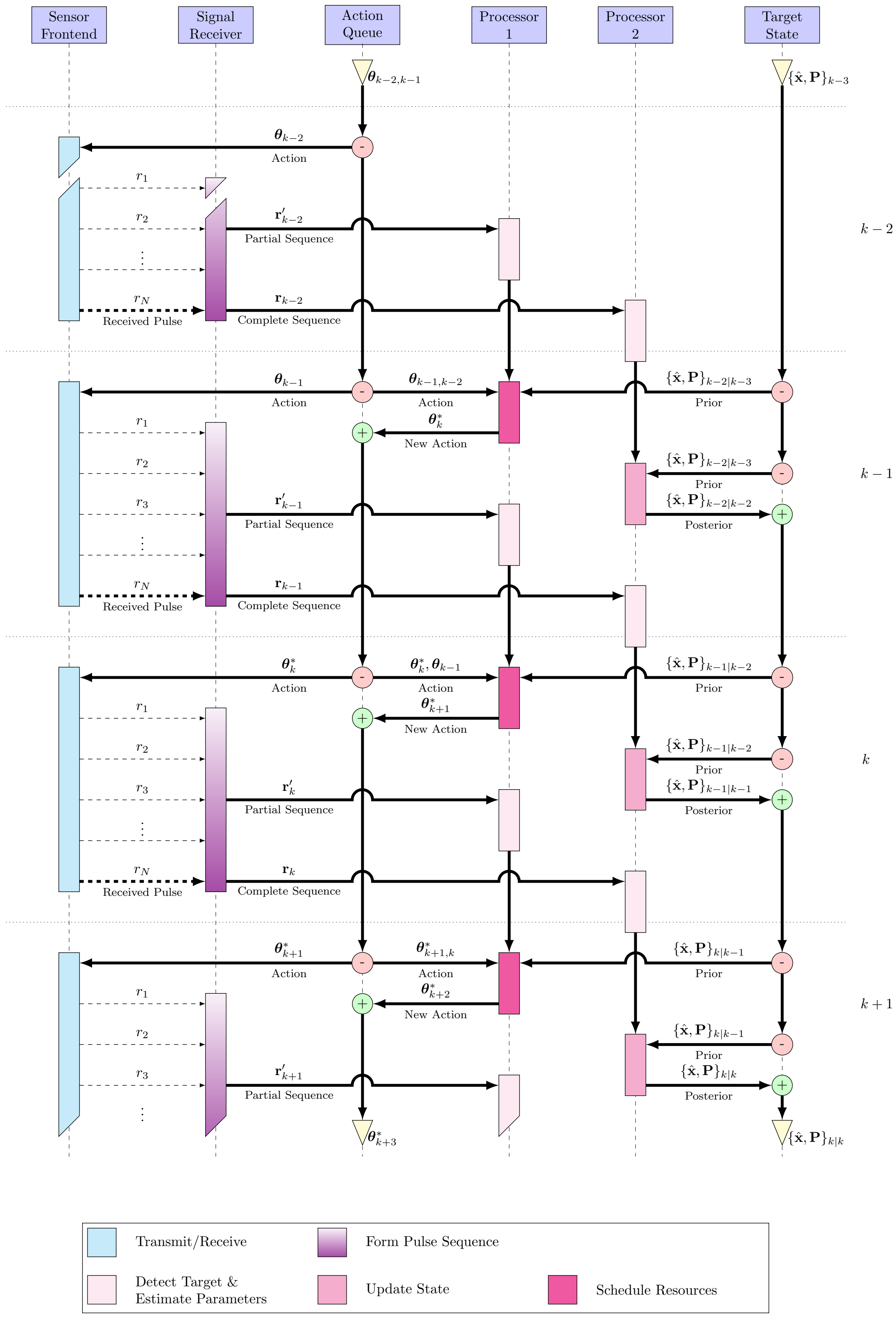

Figure 5.2.3: Sequence diagram of a concurrent pipelined radar using two processors with a single CCPI delay

5.3 A multiple manoeuvring target example

To illustrate effectiveness and associated cost of resource scheduling under the described scheduling architectures, we consider an example involving a multi-function radar (MFR) system in a multi-target tracking scenario. We consider the radar RF front-end (transmitter and receiver combination) to be a single input single output (SISO) system with a multipurpose processor tasked to perform the radar signal processing and scheduling operations of the system. Measurement are made at fixed intervals using a known waveform and it is assumed that the radar observes one target at time but is permitted to interrogate the spatially separated targets in any order. The scheduler employs a finite-horizon, myopic scheduling scheme where action set simply comprises of which target the radar shall interrogate at each measurement epoch. Selected is performed using a Bayesian approach that builds upon prior distributions using a knowledge aided methodology. Serial (sequential) and parallel (pipeline) processor architectures are modelled with the processor decision time is used as a surrogate to quantify the costs associated with radar processing and resource scheduling within the adaptive radar system. This is exhibited in the form of dead time for the serial scheduler model and delay time (Section 5.1.1) for the concurrent adaptive schedulers. To consider the impact of varying processor capacity assigned to the processing solution, we vary the dead (serial) or delay (parallel) time. For simplicity, we assume that decision time is an integer multiple of the (fixed) radar PRI and CCPI,

$$d(k) = m\text{PRI} + n\text{CCPI}, \quad m, n \in \mathbb{Z} \tag{5.3.1}$$

The scheduler uses a waveform aided type cost function to select the target to interrogate according to minimax selection criterion (Section 5.3.3). Evaluation of the impact of decision time for the processor architectures, is based on average estimator root mean square error (RMSE) over a number of Monte Carlo trials as a metric for track quality.

5.3.1 Target tracking

To track each of the individual targets, an interacting multiple model (IMM) Blom and Bar-Shalom (1988), Blom (1984) extended Kalman filter (EKF) Kalman (1960) is used due to its natural ability to follow manoeuvring vehicles Mazor *et al.* (1998). For simplicity, it is assumed that targets cannot be confused with each other and measurements occur with a 100 % probability of detection. As targets are not observed according to a consistent schedule, a variable rate tracker is utilised for each target that uses the mid-point of the pulse train as the time reference. A brief description of the IMM algorithm Genovese (2001) is provided here as context for the minimax target selection described further in Section 5.3.3. Model-conditioned initialisation for the target under observation, $\tau \in \boldsymbol{\tau}$, the mixing estimate and covariance are computed for each IMM model $m_i \in \mathbb{M}$. The i-th mixed filter state $\bar{\mathbf{x}}^{(i)}_{k-1|k-1}$ is computed by summing the over the j-th model filtered states $\hat{\mathbf{x}}^{(j)}_{k-1|k-1}$ as;

$$\bar{\mathbf{x}}^{(i)}_{k-1|k-1} = \sum_j \hat{\mathbf{x}}^{(j)}_{k-1|k-1} \mu^{j|i}_{k-1} \tag{5.3.2a}$$

$$\bar{\mathbf{P}}^{(i)}_{(k-1|k-1)} = \sum_j \left[\bar{\mathbf{P}}^{(j)}_{(k-1|k-1)} + \left(\bar{\mathbf{x}}^{(i)}_{(k-1|k-1)} - \hat{\mathbf{x}}^{(j)}_{(k-1|k-1)} \right) \left(\bar{\mathbf{x}}^{(i)}_{(k-1|k-1)} - \hat{\mathbf{x}}^{(j)}_{(k-1|k-1)} \right)^{\top} \right] \mu^{j|i}_{(k-1)} \tag{5.3.2b}$$

The predicted model probability and mixing probabilities can be found as:

$$\mu^{(i)}_{k|k-1} = \sum_j \pi_{ji} \mu^{(j)}_{k-1} \tag{5.3.3a}$$

$$\mu^{j|i}_{k-1} = \frac{\pi_{ji} \mu^{(j)}_{k-1}}{\mu^{(i)}_{k|k-1}} \tag{5.3.3b}$$

where $\mu^{(j)}_{k-1}$ is a-priori j-th model probability at time $k-1$ and π_{ji} is (j, i) -th element of the transition probability matrix $\boldsymbol{\pi}_{ji}(k)$, i.e., the probability of switching from model j to model i. In the model-conditioned filtering stage, the a-priori state estimate and covariance is predicted for each IMM as;

$$\hat{\mathbf{x}}^{(i)}_{k|k-1} = \mathbf{F}^{(i)}_k \bar{\mathbf{x}}^{(i)}_{k-1|k-1} \tag{5.3.4a}$$

$$\mathbf{P}^{(i)}_{k|k-1} = \mathbf{F}^{(i)}_k \bar{\mathbf{P}}^{(i)}_{k-1|k-1} \mathbf{F}^{(i)\top}_k + \mathbf{Q}^{(i)}_k \tag{5.3.4b}$$

The measurement residual and associated covariance are computed as;

$$\tilde{\mathbf{z}}^{(i)}_k = \mathbf{z}_k - \mathbf{H}^{(i)}_k \bar{\mathbf{x}}^{(i)}_{k|k-1} \tag{5.3.5a}$$

$$\mathbf{S}^{(i)}_k = \mathbf{H}^{(i)}_k \mathbf{P}^{(i)}_{k|k-1} \mathbf{H}^{(i)\top}_k + \mathbf{R}_k \tag{5.3.5b}$$

The IMM filter gain and updated states can be found using the Kalman filter equations for each IMM.

$$\mathbf{K}^{(i)}_k = \mathbf{P}^{(i)}_{k|k-1} \mathbf{H}^{(i)\top}_k \mathbf{S}^{(i)-1}_k \tag{5.3.6a}$$

$$\hat{\mathbf{x}}_{k|k}^{(i)} = \hat{\mathbf{x}}_{k|k-1}^{(i)} + \mathbf{K}_k^{(i)} \tilde{\mathbf{z}}_k^{(i)} \tag{5.3.6b}$$

$$\mathbf{P}_{k|k}^{(i)} = \mathbf{P}_{k|k-1}^{(i)} - \mathbf{K}_k^{(i)} \mathbf{S}_k^{(i)} \mathbf{K}^{(i)}{}_k^{\top} \tag{5.3.6c}$$

Final IMM fusion is then performed for the target in track.

$$\hat{\mathbf{x}}_{k|k} = \sum_i \hat{\mathbf{x}}_{k|k}^{(i)} \mu_k^{(i)} \tag{5.3.7a}$$

$$\mathbf{P}_{k|k} = \sum_i \left[\mathbf{P}_{k|k}^{(i)} + \left(\hat{\mathbf{x}}_{k|k} - \hat{\mathbf{x}}_{k|k}^{(i)} \right) \left(\hat{\mathbf{x}}_{k|k} - \hat{\mathbf{x}}_{k|k}^{(i)} \right)^{\top} \right] \mu_k^{(i)} \tag{5.3.7b}$$

where model probability is updated as

$$\mu_k^{(i)} = \frac{\mu_{k|k-1}^{(i)} \mathcal{L}_k^{(i)}}{\sum_j \mu_{k|k-1}^{(j)} \mathcal{L}_k^{(j)}} \tag{5.3.8}$$

and $\mathcal{L}_k^{(i)} \sim \boldsymbol{\mathcal{N}} \left(\tilde{\mathbf{z}}_k^{(i)}; \mathbf{0}, \mathbf{S}_k^{(i)} \right)$ is the likelihood function for the innovations of the i-th model.

5.3.2 Variable-rate track update

As the scheduler is only able to select a single target for the radar to interrogate at each measurement epoch or pulse integration interval, a separate variable rate tracker is utilised for each target. The IMM for the targets comprise of a constant velocity (CV) and multiple coordinated turn (CT) models of varying turn rates in both clockwise and counter-clockwise directions. The probability transition matrix is formed as a function of the update period as;

$$\boldsymbol{\pi}_{ji}(k) = \begin{bmatrix} 1-\gamma & \gamma & 0 & 0 & \dots & 0 \\ \gamma & 1-2\gamma & \gamma & 0 & \dots & 0 \\ 0 & \gamma & 1-2\gamma & \ddots & \dots & 0 \\ 0 & 0 & \ddots & \ddots & \gamma & 0 \\ \vdots & \vdots & \vdots & \gamma & 1-2\gamma & \gamma \\ 0 & 0 & 0 & 0 & \gamma & 1-\gamma \end{bmatrix}^{n(k)} \tag{5.3.9}$$

where $n \geq 1, n \in \mathbb{Z}$ is the number of measurement epochs since the last update of the target under track and γ is a probability transition parameter as described in Section 5.3.7.

It is assumed that the radar observation $\mathbf{z}$ include both target bearing and elevation angle of arrivals. The observation matrix $\mathbf{H}$ is computed by the Jacobian of the observation function $h(\mathbf{x})$ evaluated at the predicted state for the IMM, $\mathbf{H}^{(i)} = \frac{\partial h}{\partial \mathbf{x}}\big|_{\mathbf{x}=\hat{\mathbf{x}}^{i}_{k|k-1}}$ where

$$h(\mathbf{x}) = \begin{bmatrix} r & = \left(x^2+y^2+z^2\right)^{1/2} \\ \alpha_{az} & = \tan^{-1}\frac{y}{x} \\ \alpha_{el} & = \tan^{-1}\frac{z}{\left(x^2+y^2\right)^{1/2}} \\ \dot{r} & = \frac{x\dot{x}+y\dot{y}+z\dot{z}}{\left(x^2+y^2+z^2\right)^{1/2}} \end{bmatrix} \tag{5.3.10}$$

5.3.3 Minimax criterion target selection

Resource scheduling to optimise the utilisation of the radar front-end is performed at every radar epoch after processing the most recently received measurements. The scheduling process utilises the information available from the current epoch k as encapsulated in the series IMM mixed posteriors $\hat{\mathbf{x}}^{(\tau)} \underset{\text{assume}}{\sim} \boldsymbol{\mathcal{N}}\left(\hat{\mathbf{x}}^{(\tau)}_{k|k}, \mathbf{P}^{(\tau)}_{k|k}\right), \tau \in \boldsymbol{\tau}$ (5.3.7), one for each target τ being tracked. In our example, the agent (scheduler) employs a minimax criterion that seeks minimise the worst target uncertainty of all the targets if only one can be observed at each epoch. This is achieved by selecting action $\boldsymbol{\theta}(k) \in \boldsymbol{\Theta}(k)$ to act upon target $\tau \in \boldsymbol{\tau}$ at future measurement epoch $k+n$ as described by the following cost function:

$$\boldsymbol{\theta}(\tau)^{*}_{k+n} = \arg\inf_{\tau\in\boldsymbol{\tau}} \sup_{\boldsymbol{\theta}\in\boldsymbol{\Theta}} J\left(\hat{\mathbf{x}}(\tau)_{k+n}, \boldsymbol{\theta}(\tau)\right), \quad , \forall\boldsymbol{\theta}\in\boldsymbol{\Theta}, \forall\tau\in\boldsymbol{\tau} \tag{5.3.11}$$

To illustrate, consider a simple example where the action set is to simply select which target to interrogate at the next epoch in order to maximise the quality of the worst target track at the end of the scheduled measurement epoch. This is akin to minimising the risk of the worst-case scenario given the (predicted) state of all the targets, otherwise known as regret minimisation. We adopt an control theoretic approach to the cost function (Kershaw and Evans 1994) that operates on the predicted track uncertainty or track covariances for each of the targets , if only one of them is observed at the future $k+n$-th epoch (Nguyen *et al.* 2015).

$$J\left(\hat{\mathbf{x}}_{k+n}, \tau = i\right) = f\left(\mathbf{P}^{(\tau=i)}_{k+n|k+n}, \mathbf{P}^{(\tau=j)}_{k+n|k}\right), \quad i,j = 1,\ldots,|\boldsymbol{\tau}|, \quad j = \boldsymbol{\tau}\setminus i \tag{5.3.12}$$

where $|\boldsymbol{\tau}|$ is the number of targets being tracked. In this particular example, we select cost function J to be the volume spanned by the parallelotope represented by the state estimate covariance after the measurement is incorporated into the track.

This can be found by the matrix determinate and (5.3.11) can be stated as,

$$\boldsymbol{\theta}^*(\tau)_{k+n} = \arg\inf_{\tau\in\boldsymbol{\tau}} \sup_{\boldsymbol{\theta}\in\boldsymbol{\Theta}} \left\{ \left| \mathbf{P}^{(\tau=i)}_{k+n|k+n,\boldsymbol{\theta}(\tau)} \right|, \left| \mathbf{P}^{(\tau=j)}_{k+n|k} \right| \right\}, \quad \forall \boldsymbol{\theta} \in \boldsymbol{\Theta}, \forall \tau \in \boldsymbol{\tau}, \quad i,j = 1,\ldots,T, \quad j = \boldsymbol{\tau}\backslash i \tag{5.3.13}$$

where k is the iteration of the filter for the τ-th target and n is the duration of the delay time measured in epochs for pipeline processor and $n = 1$ for the sequential processor.

5.3.4 Calculation of the predicted target track

To predict the posterior of the target track from a candidate action, we commence by computing the fused predicted estimate from (5.3.7a) for the target under consideration.

$$\hat{\mathbf{x}}_{k+1|k} = \sum_i \hat{\mathbf{x}}^{(i)}_{k+1|k} \mu^{(i)}_{k+1|k} \tag{5.3.14}$$

where $\hat{\mathbf{x}}^{(i)}_{k+1|k}$ is updated according to (5.3.4a) and $\mu^{(i)}_{k+1|k}$ to (5.3.3a). The candidate action or 'virtual' measurement and its associated covariance $\hat{\mathbf{R}}_{k+1}\left(\boldsymbol{\theta}(k+1)|\hat{\mathbf{x}}_{k+1|k+1}\right)$ can be found given the future predicted target position from (5.3.18) and used to form the IMM predicted track covariance matrix.

$$\mathbf{P}_{k+1|k+1} = \sum_i \left[\mathbf{P}^{(i)}_{k+1|k+1} + \left(\hat{\mathbf{x}}_{k+1|k} - \hat{\mathbf{x}}^{(i)}_{k+1|k} \right) \left(\hat{\mathbf{x}}_{k+1|k} - \hat{\mathbf{x}}^{(i)}_{k+1|k} \right)^\top \right] \mu^{(i)}_{k+1|k} \tag{5.3.15}$$

where

$$\mathbf{P}^{(i)}_{k+1|k+1} = \left(\mathbf{I} - \mathbf{P}^{(i)}_{k+1|k} \mathbf{H}^{(i)\top}_{k+1} \mathbf{S}^{(i)^{-1}}_{k+1} \mathbf{H}^{(i)}_{k+1} \right) \mathbf{P}^{(i)}_{k+1|k} \tag{5.3.16a}$$

$$\mathbf{P}_{k+1|k} = \sum_i \left[\mathbf{P}^{(i)}_{k+1|k} + \left(\hat{\mathbf{x}}_{k+1|k} - \hat{\mathbf{x}}^{(i)}_{k+1|k} \right) \left(\hat{\mathbf{x}}_{k+1|k} - \hat{\mathbf{x}}^{(i)}_{k+1|k} \right)^\top \right] \mu^{(i)}_{k+1|k} \tag{5.3.16b}$$

Jacobian $\mathbf{H}^{(i)}_{k+1} = \frac{\partial h}{\partial \mathbf{x}}\Big|_{\mathbf{x}=\hat{\mathbf{x}}^i_{k+1|k}}$ can be calculated from (5.3.10) and $\mathbf{P}^{(i)}_{k+1|k}$ according to (5.3.4b). The cycle is repeated for until the all the action in the queue have been processed. For the concurrent pipeline processor, the underlying posterior is initially updated using the pseudo-update, denoted k' before calculation of the predicted target track. The predicted state covariance is propagated without update using the standard EKF equations for the remaining unobserved targets.

5.3.5 Radar measurement modelling

Radar observations are modelling for a coherent radar capable of both bearing and elevation angle of arrival measurements as

$$\mathbf{z}_k = h(\mathbf{x}_k) + \mathbf{v}_k \tag{5.3.17}$$

where measurement vector $\mathbf{z} = \begin{bmatrix} r, & \alpha_{az}, & \alpha_{el}, & \dot{r} \end{bmatrix}^\top$, $\mathbf{v}_k \sim \mathcal{N}(\mathbf{0}, \mathbf{R}_k)$ and covariance matrix

$$\mathbf{R} = \begin{bmatrix} \sigma_r^2 & 0 & \dots & \rho_{r\dot{r}}\sigma_r\sigma_{\dot{r}} \\ 0 & \sigma_{\alpha_{az}}^2 & \dots & 0 \\ \vdots & \vdots & \sigma_{\alpha_{el}}^2 & 0 \\ \rho_{r\dot{r}}\sigma_r\sigma_{\dot{r}} & 0 & \dots & \sigma_{\dot{r}}^2 \end{bmatrix} \tag{5.3.18}$$

A pulse-Doppler signal processing system is modelled under the assumption that the target is only detected within a single range and Doppler bin (Blackman and Popoli 1999).

$$\sigma_r^2 = \frac{\Delta r^2}{12}, \quad \sigma_{\dot{r}}^2 = \frac{\Delta \dot{r}^2}{12} \tag{5.3.19}$$

where $\Delta r, \Delta \dot{r}$ are the range and range-rate resolutions of the radar waveform and associated Doppler processing. For simplicity, we assume the range and Doppler processing are uncorrelated such that $\rho_{r\dot{r}} = 0$. The target is considered to have some range extent, with the arrival beam accuracy is modelled as

$$\sigma_\alpha^2 = \left(\tilde{\sigma}_\alpha + \tilde{\sigma}_g\right)^2 \tag{5.3.20}$$

The monopulse angle of arrival with respect to antenna boresight accuracy is (Blackman and Popoli 1999, Blair *et al.* 2010)

$$\tilde{\sigma}_\alpha = \frac{\theta_\beta^2}{2\eta k_m^2} \tag{5.3.21}$$

where θ_β is the 3 dB beamwidth of the antenna and monopulse slope parameter k_m (Barton and Ward 1969) is assumed to be 1.57 (Blackman and Popoli 1999). The effect of angular glint is modelled assuming a *dumbbell* target model radar cross section (RCS) model (Barton 1988, De Martino 2012).

$$\tilde{\sigma}_g = \frac{3 l_{\text{eff}}}{r} \tag{5.3.22}$$

where l_{eff} is the effective length of the target and r the range to the target. Whilst this model is simplistic, its intent is to prevent the collapse of the arrival beam accuracy as (5.3.21) shrinks when the target nears the sensor from short range theory (Delano 1953). The integrated signal-to-noise ratio η is modelled according to a free space path loss for a target RCS distribution of a type 1 Swerling model (Swerling 1960).

5.3.6 Track generation process

The target tracks are is formed in discrete time according to the following linear state space model,

$$\mathbf{x}_{k+1} = \mathbf{F}_k \mathbf{x}_k + \mathbf{w}_k \tag{5.3.23}$$

where independent and identically distributed (i.i.d.) noise process $\mathbf{w}_k \sim \mathcal{N}(\mathbf{0}, \mathbf{Q}_k)$ and state vector $\mathbf{x} = \begin{bmatrix} x, & \dot{x}, & y, & \dot{y}, & z, & \dot{z} \end{bmatrix}^\top$. The target trajectories comprise of coordinated turns inter-spaced with constant velocity sections facilitated by state transition matrices defined using horizontal coordinated turn models of known radii (Li and Jilkov 2003):

$$\mathbf{F}_{CT}(t) = \begin{bmatrix} 1 & \frac{\sin\omega\Delta t}{\omega} & 0 & -\frac{1-\cos\omega\Delta t}{\omega} & 0 & 0 \\ 0 & \cos\omega\Delta t & 0 & -\sin\omega\Delta t & 0 & 0 \\ 0 & \frac{1-\cos\omega\Delta t}{\omega} & 0 & -\sin\omega\Delta t & 0 & 0 \\ 0 & \sin\omega\Delta t & 0 & \cos\omega\Delta t & 0 & 0 \\ 0 & 0 & 0 & 0 & 1 & \Delta t \\ 0 & 0 & 0 & 0 & 0 & 1 \end{bmatrix} \tag{5.3.24a}$$

$$\mathbf{Q}_{CT}(t) = q \begin{bmatrix} \frac{2(\omega\Delta t-\sin\omega\Delta t)}{\omega^3} & \frac{1-\cos\omega\Delta t}{\omega^2} & 0 & \frac{\omega\Delta t-\sin\omega\Delta t}{\omega^2} & 0 & 0 \\ \frac{1-\cos\omega\Delta t}{\omega^2} & \Delta t & -\frac{\omega\Delta t-\sin\omega\Delta t}{\omega^2} & 0 & 0 & 0 \\ 0 & -\frac{\omega\Delta t-\sin\omega\Delta t}{\omega^2} & \frac{2(\omega\Delta t-\sin\omega\Delta t)}{\omega^3} & \frac{1-\cos\omega\Delta t}{\omega^2} & 0 & 0 \\ \frac{\omega\Delta t-\sin\omega\Delta t}{\omega^2} & 0 & \frac{1-\cos\omega\Delta t}{\omega^2} & \Delta t & 0 & 0 \\ 0 & 0 & 0 & 0 & \frac{\Delta t^3}{3} & \frac{\Delta t^3}{3} \\ 0 & 0 & 0 & 0 & \frac{\Delta t^3}{3} & \Delta t \end{bmatrix} \tag{5.3.24b}$$

where ω is the turn rate and Δt is time difference. For the constant velocity model,

$$\mathbf{F}_{CV}(t) = \begin{bmatrix} 1 & \Delta t \\ 0 & 1 \end{bmatrix} \otimes \mathbf{I}_3, \quad \mathbf{Q}_{CV}(t) = q \begin{bmatrix} \frac{\Delta t^3}{3} & \frac{\Delta t^3}{3} \\ \frac{\Delta t^3}{3} & \Delta t \end{bmatrix} \otimes \mathbf{I}_3 \tag{5.3.25}$$

where $\otimes$ is the Kronecker product and $\mathbf{I}$ the identity matrix.

5.3.7 Scenario description parameters

To model the sensor, we assume a coherent S-band radar system operating at a centre frequency of 3.2 GHz. The transmitted pulses are assumed to be 10 µs in duration, of bandwidth 10 MHz with a PRI of 150 µs in a burst of 32 pulses. This results in a CPI of 4.8 ms and range and range-rate resolutions of 15 m and 9.8 m s^{-1} respectively. Antenna 3 dB beamwidths are 5° in both azimuth and elevation directions. For comparison, this is approximately equivalent to a radar operating with a peak power of 10 kW, antenna gains of 28 dBi and system losses of 10 dB. Four distinct targets are modelled each with a RCS distribution of a type 1 Swerling model and equivalent length l_{eff} of 10 m. The targets range in RCS from −6 to 12 dBm^2 in 6 dB increments, with single pulse reference signal-to-noise ratio (SNR) of $\eta_{1000} = \{40.4, 46.4, 52.4, 58.4\}$ dB at a distance of 1 km. Target tracking is performed using a 17 state IMM, comprising of CV and CT models with turns rates of $\omega^{(i)} \in \{-0.22, \ldots, 0.22\}$ rad s^{-1} and probability transition parameter $\gamma = 1 \times 10^{-5} \Delta t_{epoch}/\Delta t_{CPI}$.

Target tracks are initialised at $\mathbf{x}_0 \sim \mathcal{N}(\mathbf{x}_\mu, \mathbf{P}_0)$ where $\mathbf{P}_0 = \mathbf{I}_3 \otimes \text{diag}(100, 25)$ (m^2 ,m^2/s^2). Mean initial range and range-rates are 2 km and 275 m s^{-1} relative to the radar in any bearing with an initial azimuth angle of $\alpha_{az0} \sim \mathcal{U}(0°, 20°)$. The target trajectories consist of a manoeuvre made of two successive coordinated turns in the shape of an 'S' in the horizontal plane sandwiched between CV flight sections. The manoeuvre commences after an initial $\mathcal{U}(3, 7)$ seconds of CV flight. The successive coordinated turns in the manoeuvre are performed in opposite directions at maximal turn rates of $\pm\omega$ and durations $\frac{11\pi}{8\omega_1}$ and $\frac{3\pi}{2\omega_1}$ where $\omega \sim \mathcal{U}\left(\frac{2\pi}{80}, \frac{2\pi}{40}\right)$. The turn rate increases and decreases linearly to its peak over a period of $|\frac{11\pi}{40\omega_1}|$. Process noise parameter q is selected to be 0.1. A typical target track shown in Figure 5.3.1.

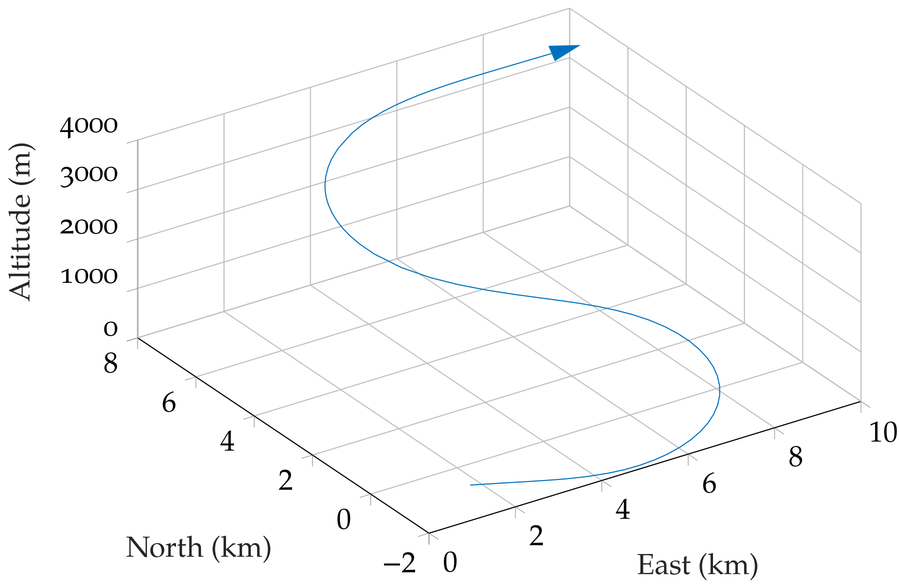

Figure 5.3.1: Example target track illustrating consecutive horizontal coordinated turn manoeuvres

5.4 Simulation results

To evaluate the effectiveness of each of the scheduling schemes, we compare the position and velocity (ensemble) averaged RMSE of the target tracks. Target tracks are considered to be dropped if the position RMSE exceeds 100 m and results are averaged over 1200 Monte Carlo trials for the targets that remain in track. In addition to track error, we also consider the radar utilisation or duty for each target which is related to the CCPI (Butterfield *et al.* 2016) or the cumulative number of revisits for the target. To assess the apparent value of resource scheduling on target track quality, a non-pipelined sequential scheduler is modelled where the decision period (Section 5.1.1) used to perform associated processing tasks requires the radar to 'pause' interrogating the scene, resulting in front-end downtime and reduced duty. The performance of the sensor is measured using the RMSE of worst target track at each epoch averaged over the duration of the trial which we term the peak track error. This metric is consistent with the minimax target selection criterion (5.3.13) implemented and for comparison purposes, a conventional selection process that chooses each target in sequence is also modelled.

Figure 5.4.1 shows the peak track error for the conventional target selection increases proportionally with the processing cost or decision (dead) time. This is as expected as track update frequency falls as a result of the increased front-end down-time between pulse bursts when $d(k)$ is increased. Peak track error (Figure 5.4.1a) for the minimax target selection criterion shows a significant improvement in peak position error with a decision period almost as long as a pulse train is necessary before peak track position error degrades to that of the conventional target selection process with no processing cost. This equivalent to almost requiring half the front-end duty for the minimax target selection criterion to achieve the same peak track position error for the conventional scheduler. Similar peak velocity errors are achieved for both the minimax and conventional target selection criterion (Figure 5.4.1b). This typifies the objective of the minimax criterion cost function, prioritising target position error as it represents the greatest contribution to the parallelotope volume of the predicted prior (5.3.13).

Both target selection criterion show similar median target track errors under equivalent processing costs for the sequential processing architecture (Figure 5.4.1). However, the use of the minimax criterion for target selection exemplifies the reduction in the spread of the mean track error for each of the targets (Figures 5.4.2a & 5.4.2b) compared with the conventional scheduler (Figures 5.4.2c & 5.4.2d). This is achieved by the minimax criterion scheduler being able to adaptively prioritise radar resources accordingly as displayed in Figure 5.4.3.

5.4.1 Pipeline processing

In the implementation of the pipeline processors, the decision period no longer represents the delay between epochs with the elimination of front-end dead time, but rather the delay between the current epoch and the future epoch that the scheduler must choose an action for. For the delayed pipeline processor, the decision period is measured in CCPI or number of epochs. A decision period of $d(k) = 0$ is equivalent to a serial processor also of $d(k) = 0$, with increasing decision periods requiring more parallel processes to maintain the same epoch throughput (5.2.1).

For the modelled concurrent pipeline processor as illustrated in Figure 5.2.3, the processor is required to schedule the optimal resources not for the next but the following epoch within a fixed update lag, a form of deadline constraint. This enforces a bound on the decision period such that $1 \leq d(k) \leq 2$ CCPI, with increasing decision period requiring the processing commence to earlier to achieve the deadline. By minimising the time required to perform the processing activities, we can increase the quantity of pulses (or information) available to the scheduler for the pseudo-update of the posterior in the resource scheduling process as $\mathbf{z}(k') \longrightarrow \mathbf{z}(k)$ and $\mathbf{R}(k') \geq \mathbf{R}(k)$ in a positive semi-definite sense. For the lower bound case of $d(k) = 1$ CCPI, the concurrent pipeline processor is akin the scheduler having access to the entire pulse train to generate the pseudo-update and is equivalent to the delayed

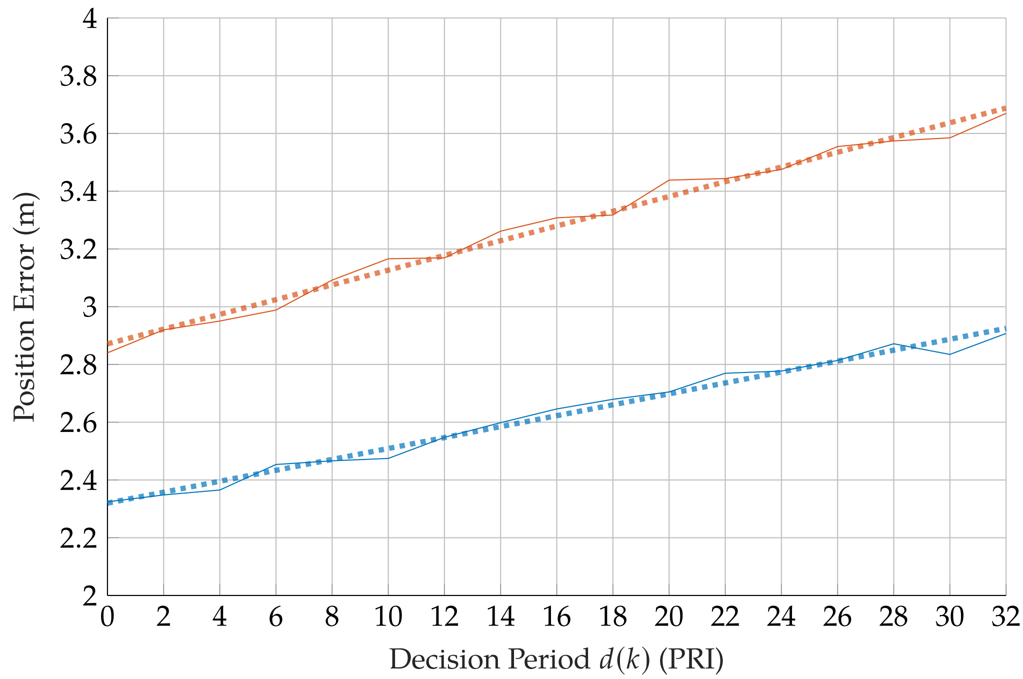

(a) Position error

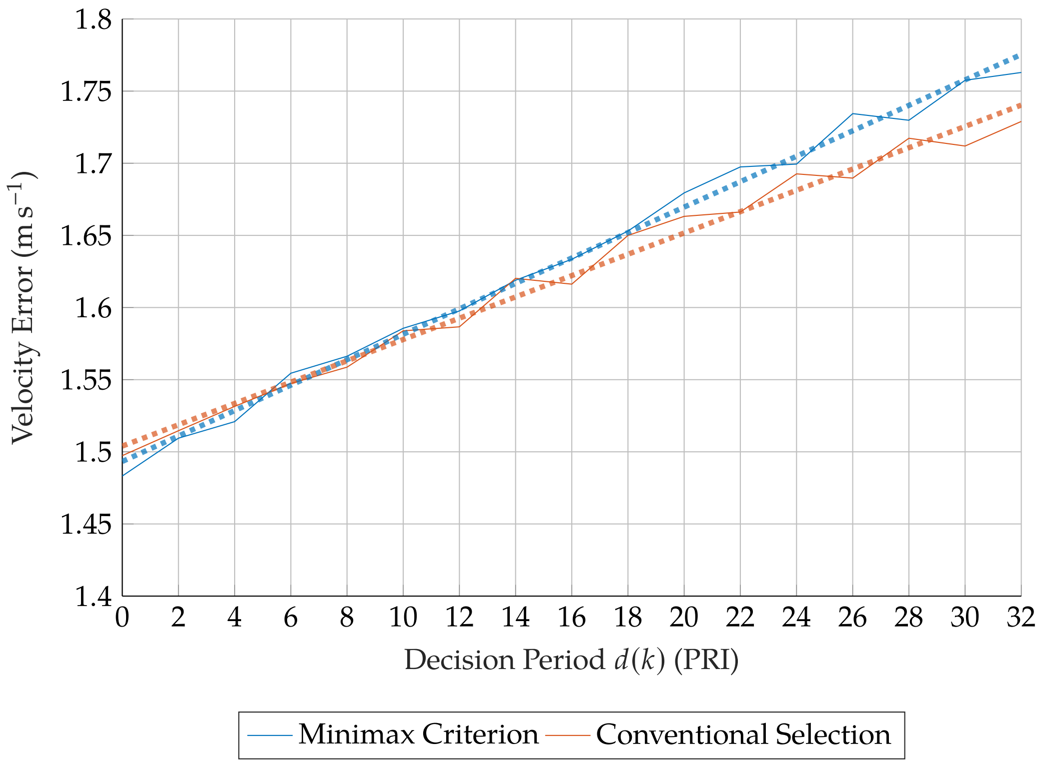

(b) Velocity error

Figure 5.4.1: Average peak target track RMSE for a sequential (non-pipeline) processing architecture using a minimax criterion and conventional target selection processes. Broken line represents least squares line of best fit.

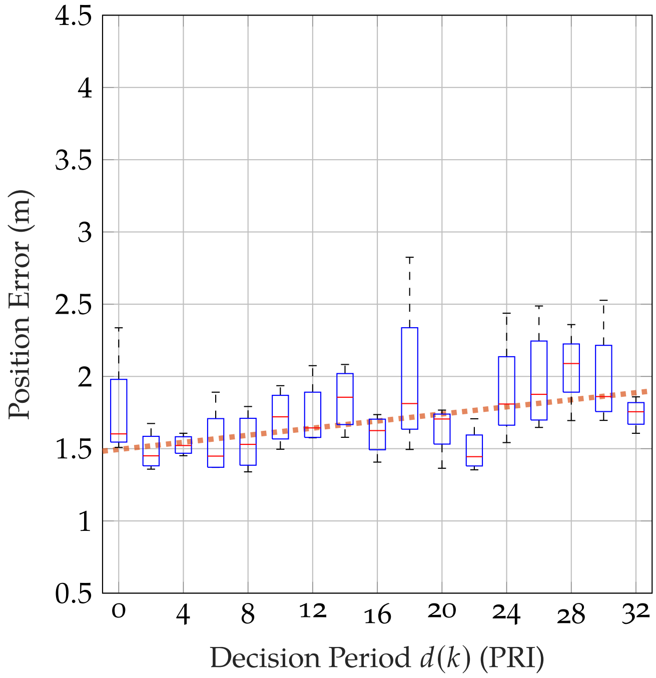

(a) Minimax scheduler target position RMSE

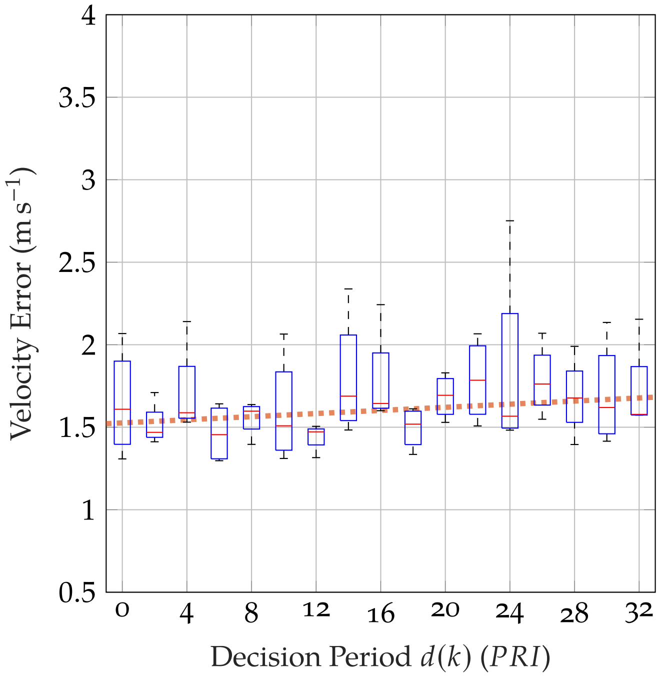

(b) Minimax scheduler target velocity RMSE

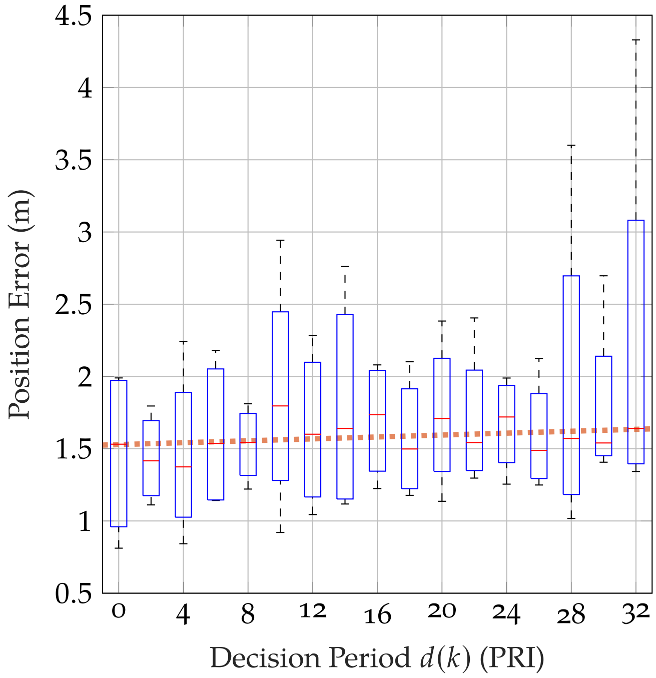

(c) Conventional scheduler target position RMSE

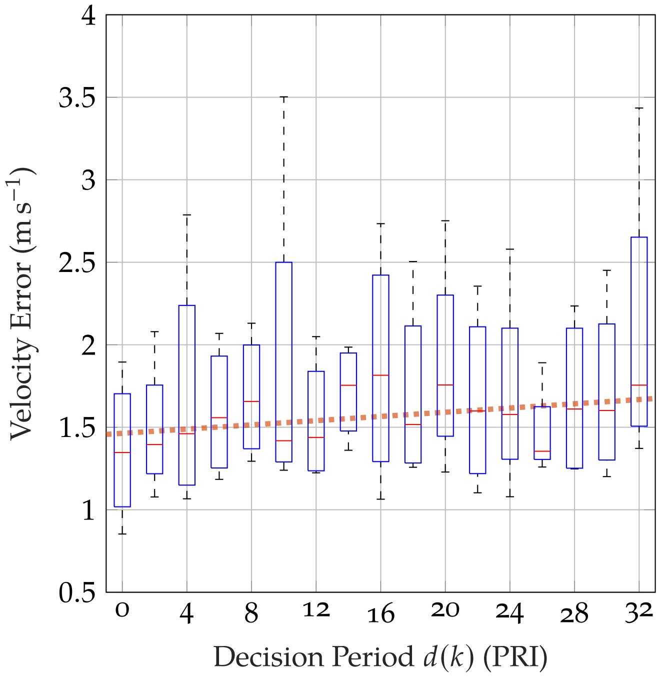

(d) Conventional scheduler target velocity RMSE

Figure 5.4.2: Average target track RMS error for RCS of $-6, 0, 6, 12$ dBm^2 using serial processing for minimax (above) and conventional (below) target selection criterion. Box top and bottom edges indicate the 25-th and 75-th percentiles whilst central mark indicates median. Broken line represents median least squares line of best fit.

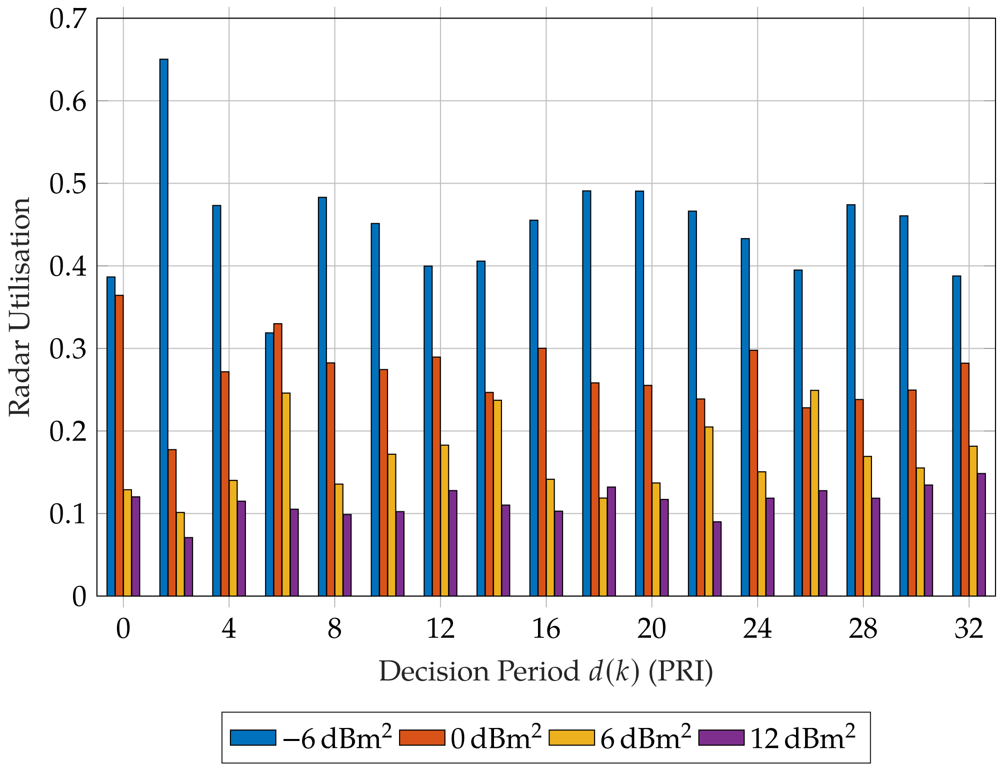

Figure 5.4.3: Radar allocation for sequential resource scheduler using minimax target selection criterion

pipeline processor with a decision period of $d(k) = 1$ CCPI.

The average peak target error for the pipeline schedulers (Figure 5.4.4) shows that increasing $d(k)$ results in a linear performance degradation for both delayed and concurrent pipeline processing.. Use of the delayed pipeline processing (Figure 5.4.4a) with a decision period of 9 CCPI demonstrates a peak track error performance degradation similar to a decision period of only 6 PRI for the sequential processor (Figure 5.4.1). This is equivalent to a duty reduction of approximately 10% despite the massive increase in the decision time, or available processing time. For the concurrent processor (Figure 5.4.4b), increasing the decision period also resulted in a peak track error performance degradation, albeit a much smaller one given the narrower time range.

Use of the minimax target selection criterion for the pipelined processing results in a reduction in the spread in the track RMSE for the disparate targets (Figure 5.4.5) similar to that of the sequential processor (Figure 5.4.2). The peak track error degradation is echoed in the median target error for the delayed pipeline processor (Figures 5.4.5a & 5.4.5b) but not reflected in that of the concurrent pipeline (Figures 5.4.5c & 5.4.5d) which shows a small decrease in the median track error trend

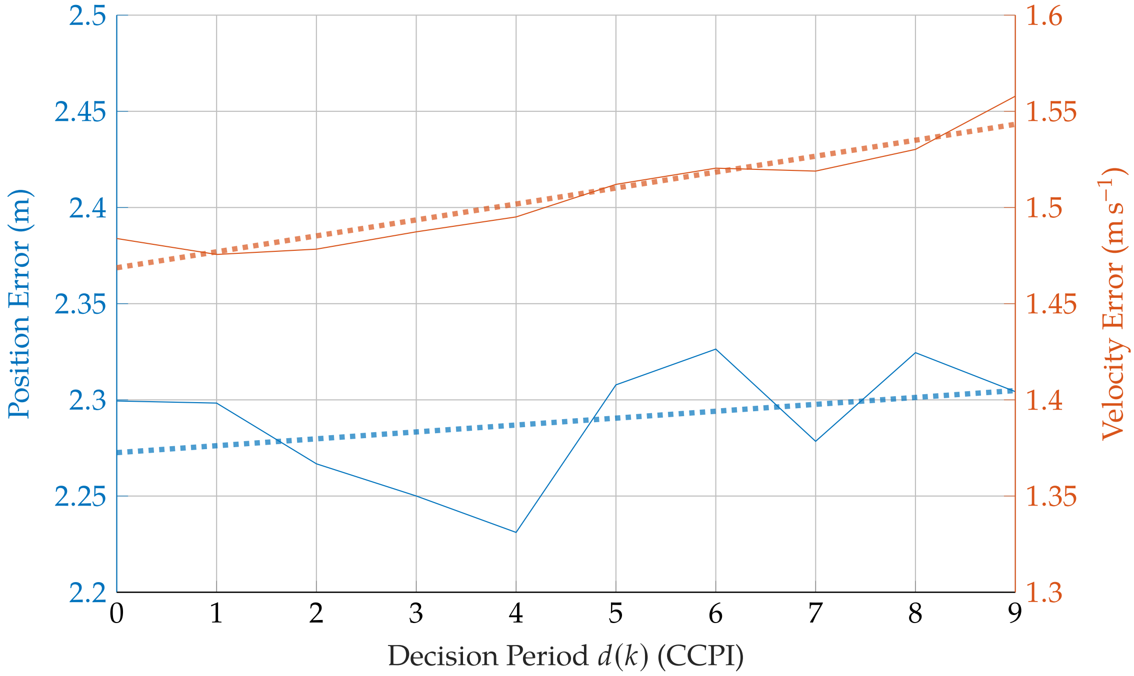

(a) Delayed pipeline processor

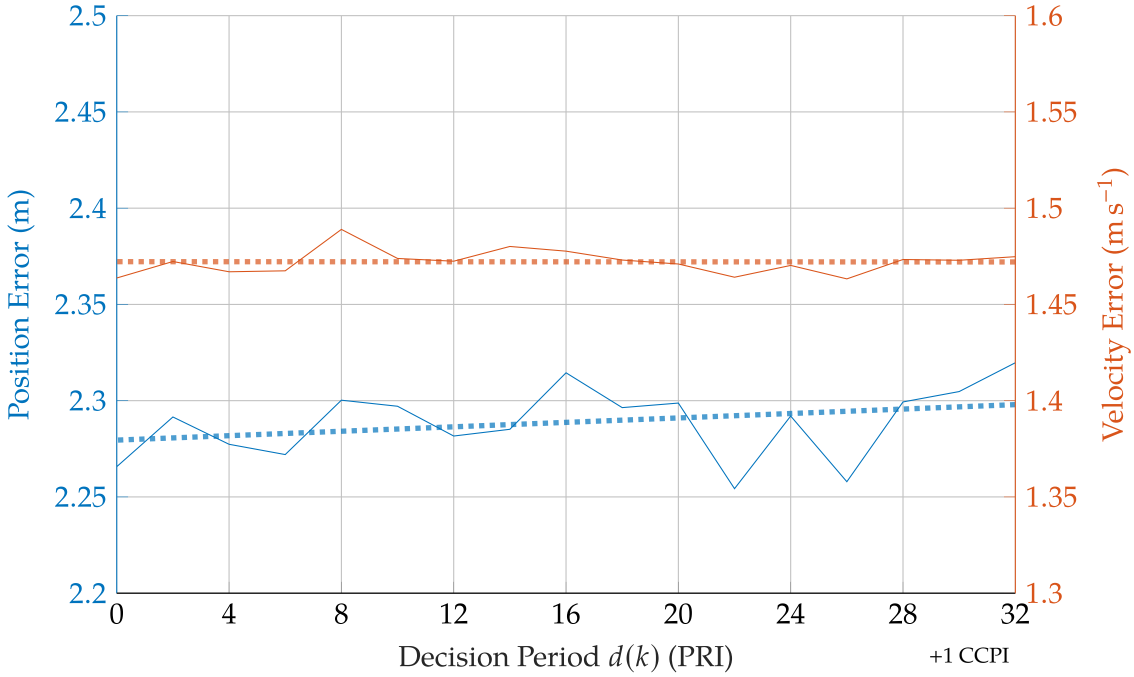

(b) Concurrent pipeline processor

Figure 5.4.4: Average peak track RMSE for pipeline processors using minimax target selection criterion. Broken line represents least squares line of best fit.

as the decision period is increased. Radar allocation for both pipeline processors (Figure 5.4.6) shows that minimax target selection criterion is able to dynamically allocate resources regardless of the decision period.

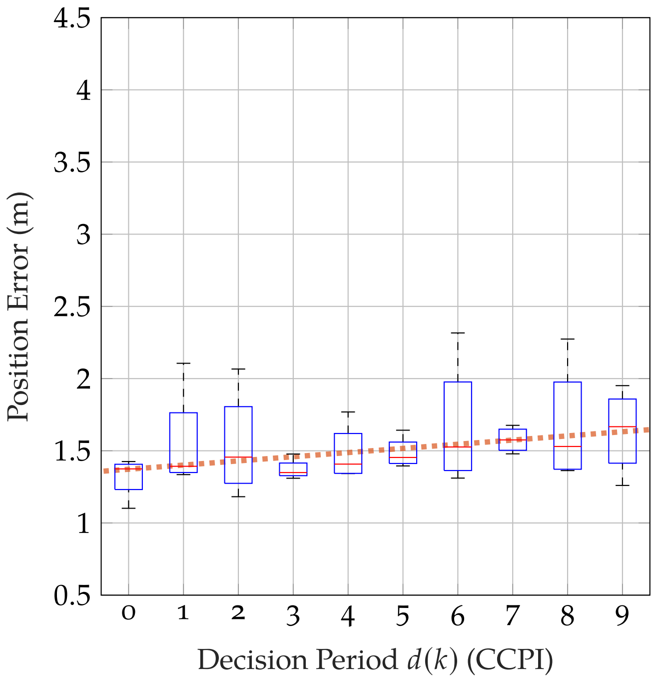

(a) Delayed pipeline processor RMS position error

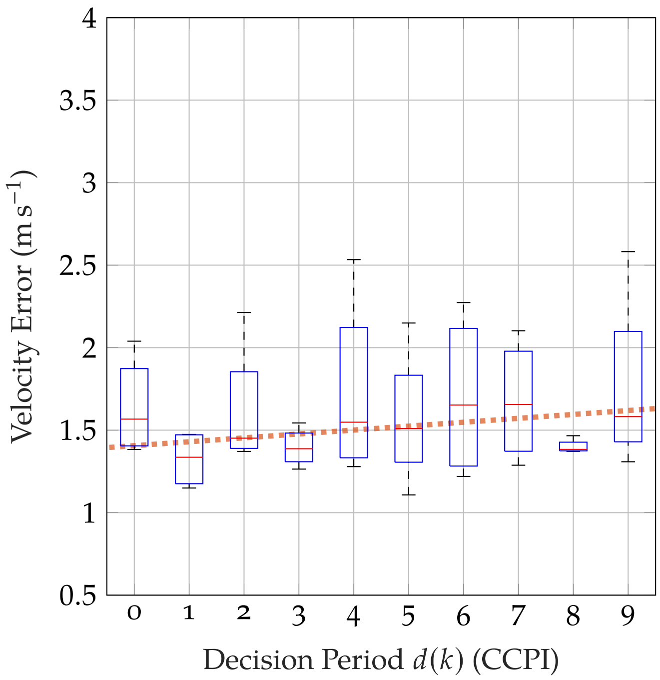

(b) Delayed pipeline processor RMS velocity error

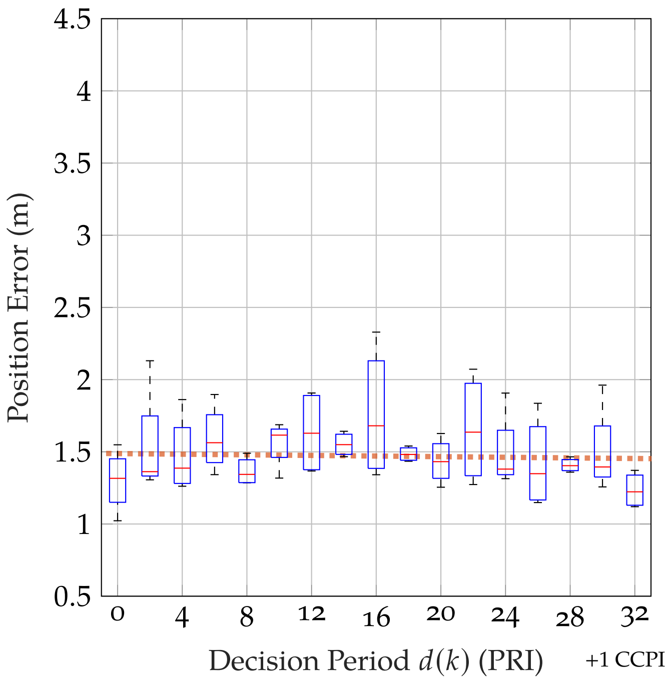

(c) Concurrent pipeline processor RMS position error

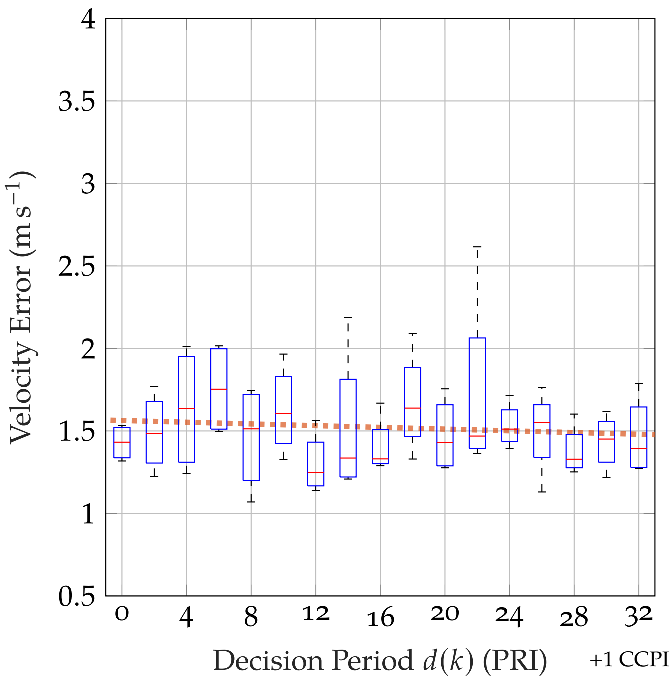

(d) Concurrent pipeline processor RMS velocity error

Figure 5.4.5: Average target track RMSE for RCS of $-6, 0, 6, 12$ dBm^2 using a minimax target selection criterion for a delayed pipeline (above) and concurrent pipeline (below) resource scheduler architectures

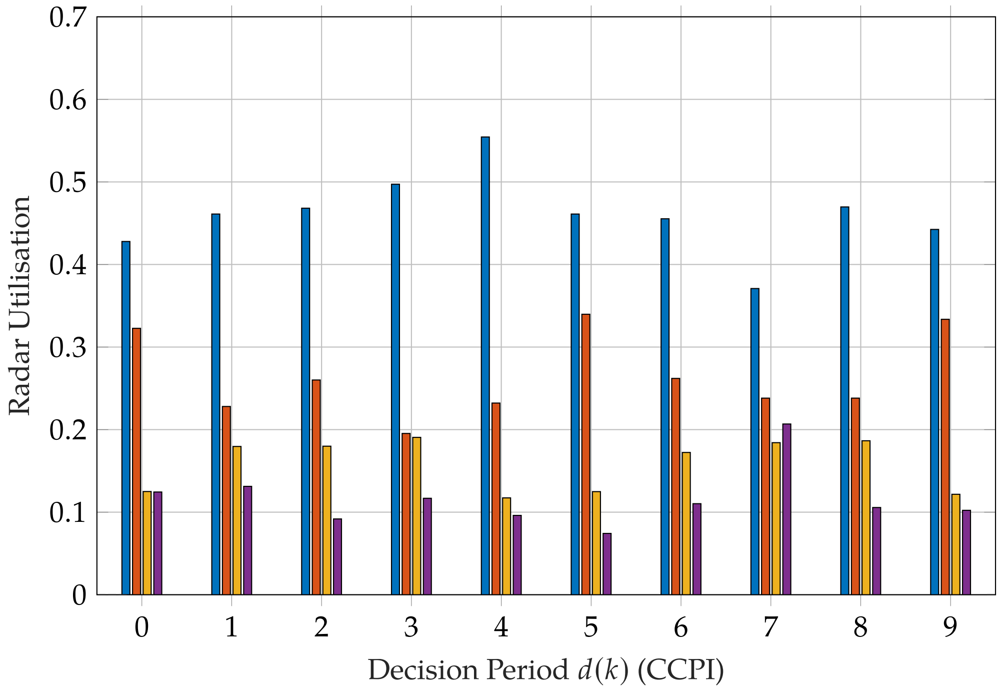

(a) Delayed pipeline processor

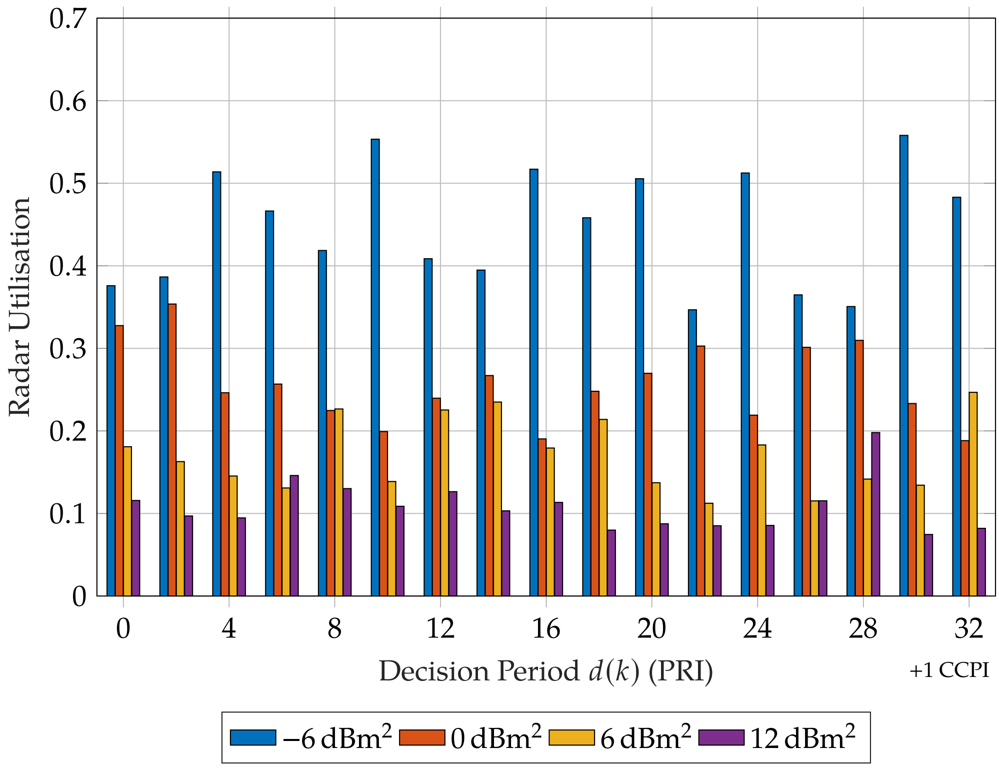

(b) Concurrent pipeline processor

Figure 5.4.6: Radar target allocation for pipeline processors using minimax target selection criterion

5.5 Conclusion

In this chapter, we have considered the requisite tasks required to implement an adaptive or cognitive sensor system, particularly for a target tracking scenario. We presented the use of decision time as a measure of the processing cost associated with the operation of a such system and described the use of parallel or pipeline processing as a means to obtain an increase in available decision time whilst minimising the impact on system duty cycle. Two alternate pipeline processing solution were proposed. One that introduced a lag in the issue of the radar action solution termed delayed pipeline processing. The other utilised the received partial pulse trains to inform the resource scheduling processing which were separated from the general target tracking process termed concurrent pipeline processing.

A scenario involving a radar tracking four manoeuvring targets of varying RCS simultaneously was simulated to evaluate the effectiveness of the pipelined processing architectures. Target tracking is performed using a variable rate IMM EKF with constant velocity and coordinated turn models of varying turn rates. A minimax target selection criterion is employed to choose the order in which the radar interrogates the targets with an objective to minimise the track uncertainty of the worst possible target at the end of the epoch.

Track performance is assessed using the peak target track RMSE - the error for the worst target track for the set targets in track. Compared with a conventional scheduling strategy that simply selects each target in turn, the minimax target selection criterion was able to significantly improve the peak target error, almost halving the front-end duty required to attain the same position RMSE. By prioritising the radar resources, the spread in target track errors was greatly reduced.

To eliminate front-end downtime, pipeline processing was used to parallelise the sensor processing with an action queue established to manage the associated delay. The simulation was used to investigate the relationship between the number of parallel processes and computation speed through modelling the associated processing update lag or necessary depth of the action queue. Both of the pipeline processors showed a significant improvement in the peak target track error compared with the conventional scheduling strategy, despite the long lag between measurement epochs and the future scheduled action being executed.

For the delayed pipeline processor, a decision period of 9 CCPI was found to be achieve equivalent track performance to the sequential processor with a decision period of only 6 PRI. This is equivalent a sensor front-end dead time of less than 20% of a CPI between epochs. The concurrent processor was also found to improve target track RMSE similar to the delayed pipeline. However, the inclusion of additional pulses in the pseudo-update as part of the scheduling process was found to provide make minimal difference to track RMSE and may possibly be attributed to the particular scenario modelled in this example.

Chapter 6

Parametric sea clutter texture estimation and prediction

In this chapter we present a deterministic parametric sea clutter texture model for high-resolution radar backscatter at low grazing angles in the open ocean. The clutter texture forms a component of the compound-Gaussian sea clutter model and we exploit the spatio-temporal relationships in the clutter by relating it to its physical source: sea swell. We present an efficient algorithm for the estimation of the spectral components for the parametric texture model through the estimation of two-dimensional 'tones' across contiguous range-bins instead of a series of one-dimensional estimates as is used elsewhere. Validation is performed by comparing the predictive fit for our estimator with a series of temporal estimators and a non-parametric estimator using measured sea clutter data. Implementation of the spatio-temporal estimator results in a more parsimonious estimate with improved reliability due to the increased separation of the tones in two-dimensional space. In Section 6.2.1 we briefly review the compound-Gaussian clutter model, considering the clutter as a cyclostationary process. We derive a parametric spatio-temporal relationship for sea clutter based on the physical attributes of the sea surface in Section 6.2.2 and represent the texture as the planar summation of real cosinusoid terms. In Section 6.3 we review methods of temporal texture estimation, introducing an efficient version of the CM-RELAX algorithm (Gini and Greco 2002) for estimation of harmonics in the presence of multiplicative noise in Section 6.3.2. Then in Section 6.5, using data collected by the McMaster University IPIX radar, we estimate the texture and demonstrate the spatial relationship between frequency components of the texture estimate. Model accuracy is investigated by comparing predicted texture with a non-parametric estimate.

6.1 Background

Sea clutter is the unwanted echoes resulting from radar returns reflected off the ocean surface when operating a radar in a maritime environment. The prevalence of this physical phenomena presents a challenge for the radar designer, frequently presenting itself as the dominant component of interference particularly at low-grazing angles. It has the potential to place limitations on the detectability of targets that may be obscured because of the physical structure of the sea. Historically, the amplitude distribution of the sea clutter has been modelled as a Gaussian stochastic process with Rayleigh amplitude statistics because of the apparent random nature of the clutter return (Ward *et al.* 2006). This assumption has validity for low resolution radar systems where the macroscopic structure of the sea surface cannot be resolved by the radar. The application of modern high resolution radar systems combined with low grazing angles has shown that the statistics of the sea clutter can deviate greatly from this Gaussian assumption (Farina *et al.* 1997).

The statistical approach has been further developed into a set of more complex stochastic models based on various long-tailed distributions. These included the Log-Normal, Weibull and more frequently, the compound K-distribution (Baker 1991, Ward *et al.* 1990, Watts 1987, Watts and Ward 1987) given its ability to incorporate the effects of spatial and temporal correlations of the clutter (Watts 1989). Experimental analyses, using data collected at numerous sites has shown that the clutter distribution approaches that of the compound K-distribution for X-band radar systems (Antipov 1998a, Farina *et al.* 1997, Gini 2000, Ward *et al.* 1990). Heavier tailed distributions been considered to deal with the additional spikiness of HH polarised sea clutter at low grazing angles such as the Pareto distribution (Farshchian and Posner 2010), KA and more tractable KK models at higher grazing angles (Dong 2006, Dong and Haywood 2007). More recently, Pareto plus noise and K plus noise distributions accounting for the thermal noise present in the signal have been shown to provide an improved fit to clutter data at these high grazing angles and increased range resolutions (Bocquet 2015, Ritchie *et al.* 2014, Rosenberg and Bocquet 2013).

An efficient, parsimonious and deterministic clutter model would allow for quick radar performance estimation, prediction and optimisation of radar scheduling algorithms and detectors in a challenging operational environment. In a radar tracking scenario, knowledge, albeit partial, of the clutter, enables waveforms to be scheduled to minimise the spread of clutter into the target range zone such as that described in (Sira *et al.* 2007a). Accumulated clutter data and estimation is obtainable via a parallel system that provides predicted texture information to such an adaptive tracking system.

Attempts to create deterministic clutter models based on chaotic processes have utilised a series of radial bias functions (RBFs) neural networks to attempt to reconstruct the sea clutter dynamic (Haykin and Puthusserypady 1997, Hennessey *et al.* 2001, Leung 1995, Leung *et al.* 2002, Leung and Lo 1993). Analysis using measured data has shown that the algorithms used to estimate the invariants of the chaotic process lack the necessary discriminative power to distinguish between a deterministic chaotic process and a stochastic one (Haykin *et al.* 2002, Unsworth *et al.* 2002).

Our model is based on the compound Gaussian clutter model of which the compound-K distribution is a special form (Raj and Bovik 2012). This is the most commonly applied sea clutter model used for high resolution radar measurements at low grazing angles (Gini *et al.* 2001, Wang *et al.* 2006). When the sea is considered to be fully developed, sea clutter over a reasonable observation period ($> 30\,\mathrm{s}$) can be observed to possess a quasi-periodic structure for a given patch of ocean. This phenomenon is consistent with the observed waves present at the ocean surface, with a characteristic periodic structure clearly visible in a radar range-time plot. Assuming that the sea clutter is a cyclostationary process, we estimate a set of deterministic components that form the *texture* or macrostructure component of the sea clutter. This has been shown to be a valid model for long observation periods (Conte and Longo 1987).

In this chapter, we create a physically grounded model for the representation of radar clutter signals in a blue water or open ocean environment. Previous statistical estimators of these deterministic components (Gini and Greco 2001; 2002) did not include the spatial relationship of adjacent range bins in the measurement set instead, independently estimating the texture for each range bin. We exploit the factors that contribute to the creation of the sea clutter itself to derive the joint spatio-temporal relationship of the estimated texture components. We present an algorithm for the two-dimensional estimation of these components resulting in a parsimonious sea clutter model. Our work builds on the earlier work of Gini *et al.* (2001) and Gini and Greco (2001; 2002).

6.2 Parametric texture modelling

A radar measurement for a monostatic system is the received backscatter of the incident electromagnetic beam of the scene being interrogated. In the case of the ocean, this makes the sea clutter a function of the dielectric properties of the sea for the given RF operating conditions: the geometry of the sea surface and the angle of incidence of the radar. If we assume the angle of incidence to be fixed and the radar operating condition to be constant, the model of the sea clutter can be simplified to be a function of backscattered return from the ocean surface.

We define a fully developed or arisen sea as one where a wind of some velocity has been blowing over a fetch that we can consider to be infinitely large. We adopt a two scale model where the sea surface is composed of waves of both short and long wavelengths to describe the small and large scale roughness factors (Wright 1968). Assume the depth of blue water permits us to ignore the effects of the underlying topography of the seabed. Given that sea water is homogeneous, it is primarily the nature of the sea surface roughness that determines the properties of the radar return, the result of changes in the surface geometry via wave actions. Ocean waves may generally be characterised by two fundamental types. The first type is capillary waves or ripples, the outcome of turbulent gusts of wind at the sea surface, restored by the surface tension of the water. These waves typically have a wavelength in the order of centimetres. The second, longer gravity waves have wavelengths of less than a metre up to hundreds of metres; the restoring force being gravity (Greco *et al.* 2004, Haykin *et al.* 2002). At any point of the ocean surface the observed waves are the result of the locally generated wind (capillary) waves (short waves) modulated onto the longer (gravity) waves that may last several days and propagate long distances. This permits the representation of the sea clutter using two different surface roughness scales: one that describes the small scale roughness or *speckle* often associated with whitecaps and foam, and large scale roughness or *texture*, associated with the swell. This forms the physical basis for the compound-Gaussian model described in the following section.

6.2.1 The compound-Gaussian sea clutter model and cyclostationarity

The compound-Gaussian model is frequently used to characterise heavy-tailed clutter distributions in radar, especially sea clutter (Greco *et al.* 2004, Haykin *et al.* 2002). For compound-Gaussian distributed clutter, the complex envelope z may be described in discrete time as a multiplicative noise process, the product of texture τ and speckle x components:

$$z(n) = \sqrt{\tau(n)}\, x(n) \tag{6.2.1}$$

for $n = 1, \ldots, N$ time indices which are used here to delineate different radar processing intervals. This model describes the texture or slow-moving component of the sea clutter as a non-negative real random process. For a given patch of the sea surface, it is a function of the local mean sea height and is responsible for the mean power level of the backscatter. The speckle on the other hand is the result of localised backscattering from capillary waves or ripples often from gusts of near-surface wind, restored by the surface tension of the water as discussed in Section 6.2. The localised nature of these waves means that they are only spatially correlated locally. The speckle can be considered to be a complex Gaussian stationary process with zero mean and unit power such that

$$x(n) = x_I(n) + jx_Q(n) \text{ and } x(n) \sim \mathbb{C}\mathcal{N}(0,1) \tag{6.2.2}$$

where $x_I(n)$ and $x_Q(n)$ are the in-phase and quadrature components of the speckle. The texture and speckle are considered to be independent processes with the sea clutter the result of the texture amplitude modulating the speckle. In this paper, we consider the texture to be a cyclostationary process and briefly outline the cyclostationarity characteristics of sea clutter relevant to this paper as it is covered more thoroughly in (Conte and Longo 1987). Because of the periodic structure of the sea swell, we represent the texture parametrically using a cyclic mean texture model $\tau_{cm}(n)$ comprising of sum of K cosinusoids at some given range:

$$\tau_{CM}(n) = A_0 + \sum_{k=1}^{K} A_k \cos\left(2\pi f_k n + \phi_k\right) \tag{6.2.3}$$

where we assume that A_k, $k = 0, \ldots, K$ are deterministic positive constants, $f_k = \omega_k/2\pi$, $\omega_k \in (0,\pi]$ and $\phi_k \in (-\pi,\pi]$ for $k = 1,\ldots,K$.

A process is considered to be first-order cyclostationary if the time varying mean is (almost) periodic. Define the cyclic mean of the intensity data with removal of the DC component A_0 as follows (Gardner *et al.* 2006);

$$\begin{aligned} m_{1Y}(n) &\triangleq \mathbb{E}\left[Y(n)\right] && (6.2.4a)\\ &= \tau(n)\mathbb{E}\left[|x(n)|^2\right] - \frac{1}{N}\sum_{i=1}^{N}\mathbb{E}\left[|x(i)|^2\right] && (6.2.4b)\\ &\cong \tau_{CM}(n)\sigma_x^2 - A_0 = \sigma_x^2 \sum_{k=1}^{K} A_k \cos(2\pi f_k n + \phi_k) && (6.2.4c) \end{aligned}$$

where $Y(n) = I(n) - A_0$, the intensity or amplitude of the clutter sample is defined as

$$I(n) = |z(n)|^2 = \tau(n)|x(n)|^2 \tag{6.2.5}$$

and A_0 is the DC component of the texture such that $A_0 \triangleq M_{1Y}(0)$. Applying (6.2.2) and (6.2.3) allows the harmonic components of the texture to be estimated from the Fourier transform of the cyclic mean of the intensity scaled by the normalised amplitude A_k

$$M_{1Y}(\omega) \triangleq \lim_{N\to\infty} \frac{1}{N} \sum_{n=1}^{N} m_{1Y}(n) \mathrm{e}^{-j\omega n} \tag{6.2.6}$$

$$= \sum_{k=1}^{K} \left(\frac{A_k}{2} \mathrm{e}^{j\phi_k} \delta(\omega - 2\pi f_k) + \frac{A_k}{2} \mathrm{e}^{-j\phi_k} \delta(\omega + 2\pi f_k) \right) \tag{6.2.7}$$

where ω is the cycle frequency.

6.2.2 A parametric spatio-temporal texture model

The texture component of the sea clutter is a function of the sea swell. This is a series of surface gravity waves often generated far from where they break. The phase velocity c of a surface gravity wave may be approximated by

$$c = \sqrt{\frac{g\lambda}{2\pi} \tanh\left(\frac{2\pi h}{\lambda}\right)} \tag{6.2.8}$$

where λ is the wavelength of the wave, h is the water depth and g is the acceleration as a result of gravity (Lamb 1932). In deep water (6.2.8) may be simplified to:

$$c_{deep} = \sqrt{\frac{g\lambda}{2\pi}}, \ \forall h \geq \frac{\lambda}{2} \tag{6.2.9}$$

Intuitively, we see that the longer the wavelength, the faster it travels through the water. The time it takes for the wave to travel a distance – the propagation time of the ocean swell can be given by:

$$t = \frac{4\pi d}{gT}$$

where T is the wave period and d is distance the wave travels. Under the gravity wave assumption, identification of the individual harmonics comprising the texture allows the derivation of its associated phase as a function of both its wavelength and range. We expect for a fully developed sea, the wavelengths of the harmonics to be close together, each travelling at its respective velocity giving the swell its characteristic 'rolling wave' profile. Using this physical relationship, we describe the sea clutter as a function of both range and time:

$$z(n,r) = \sqrt{\tau_{CM}(n,r)}\, x(n,r) \tag{6.2.10}$$

where $\tau_{CM}(n,r)$ and $x(n,r)$ are the discretised texture and speckle functions in delay and range. This leads us to consider the speckle distributed as $x(n,r) \sim \mathbb{C}\mathcal{N}(0,\Sigma)$

where Σ is non-zero around the diagonal terms and zero elsewhere, i.e. the speckle is correlated only in short time (< 10 ms) and short range (millimetres) due to the wavelength of the capillary waves within the defined ocean patch (Greco *et al.* 2004). The relatively short wavelength of these capillary waves in comparison with the measurement range bin width allows us to consider the speckle to be spatially decorrelated between range cells in subsequent sections (Antipov 1998b).

By estimating the texture component for adjacent range bins and identifying common frequency components, we show the texture is the result of the wave travelling across the sea surface in R range bins. This approach differs from existing methods which fail to exploit this spatial property. In these methods, the texture of the surveillance region is considered to be a series of independent texture vectors in range. At the r-th range cell the texture is described as:

$$\tau_{CM}\left(n, r; \boldsymbol{\theta}_{0:K}(r)\right) = A_0(r) + \sum_{k=1}^{K} A_k(r) \cos\left(2\pi f_k(r) n + \phi_k(r)\right) \tag{6.2.11}$$

where $\boldsymbol{\theta}_{0:K}(r) = \left[\theta_0(r), \boldsymbol{\theta}_1^T(r), \ldots, \boldsymbol{\theta}_K^T(r)\right]^T$ is the concatenated vector of frequency components parameters at the r-th range bin, $\theta_0(r) = A_0(r)$ and $\boldsymbol{\theta}_k(r) = \left[A_k(r), f_k(r), \phi_k(r)\right]^T$.

The spatio-temporal sea clutter model suggests that the sea clutter parameters can be estimated across range bins instead of separately in each range bin. We therefore formulate the texture as a stationary process comprised of a series of scaled frequency components that exist in adjacent range bins shifted in phase. We further assume in this spatial relationship the frequency components are in fact identical in each of the range bins and that the phase shift is a linear function in range we term the '*phase rate*' as a result of the gravity waves travelling across the ocean surface. Next, consider a texture model that is the planar sum of a set of K harmonics across of a series of R contiguous, evenly spaced and sized range bins:

$$\tau_{CM}\left(n, r; \boldsymbol{\theta}_{0:K}\right) = A_0 + \sum_{k=1}^{K} A_k \cos\left(2\pi f_k n + \phi_k + \psi_k r\right) \tag{6.2.12}$$

where $\boldsymbol{\theta}_{0:K} = \left[\theta_0, \boldsymbol{\theta}_1^T, \ldots, \boldsymbol{\theta}_K^T\right]^T$, $\boldsymbol{\theta}_k = \left[A_k, f_k, \phi_k, \psi_k\right]^T$ are the common harmonic components of the texture across all of the range cells and $\psi_k \in (-\pi, \pi]$ is used to describe the phase rate of the k-th harmonic of the texture in range.

6.3 Temporal methods for texture estimation

In this section we consider the methods proposed for estimation of the clutter in a particular range bin. These approaches do not exploit the spatial properties of the clutter across range bins. We omit index r for notational brevity.

6.3.1 Moving weighted filter for non-parametric estimation

Because of the physically different origins of the speckle and texture they exhibit different correlation lengths. The speckle is actually a wideband noise and is considered to be spatially uncorrelated between range bins but temporally correlated over a short period. This does not affect the texture component of the clutter as it only varies slowly with time. It also allows the use of the mean over the expected correlation period to be used as an estimator of the texture as this modulates the power level relative to the underlying sea swell. The difference in the correlation period between the texture and the speckle allows them to be separated using low-pass filtering.

We can estimate the texture from the clutter intensity (6.2.5) non-parametrically using a moving window (MW) filter of length $L+1$ (Gini *et al.* 2001) as:

$$\begin{aligned}\hat{\tau}_{MW}(n) &= \frac{1}{L+1}\sum_{m=n-\frac{L}{2}}^{n+\frac{L}{2}} I(m) \\ &\cong \tau(n)\frac{1}{L+1}\sum_{m=n-\frac{L}{2}}^{n+\frac{L}{2}} |x(m)|^2 = \tau(n)\hat{\sigma}_X^2 \end{aligned} \tag{6.3.1}$$

assuming the radar pulse repetition interval (PRI) ΔT is fixed during the interrogation period and the thermal noise is negligible in comparison to the clutter. In order for the approximation of (6.3.1) to be valid, we select L such that

$$\Delta T L_x \ll \Delta T L \ll \Delta T L_\tau$$

where $\Delta T L_x$ and $\Delta T L_\tau$ are the respective speckle and texture correlation periods. For X-band sea clutter, coherence analysis shows a decorrelation period of about 5 ms to 15 ms for the speckle, whereas the texture decorrelation times are in the order of several seconds (Antipov 1998a, Farina *et al.* 1997). Whilst the MW filter is not useful for texture prediction, it is presented as a benchmark of assessing the performance of our parametric model.

6.3.2 Parametric texture estimation using CM-RELAX Newton

Texture estimation from the measured intensity requires the retrieval of closely spaced harmonic components in the presence of the speckle, a complex multiplicative noise. The closeness of these components prevents us from using traditional spectral analysis methods to estimate the harmonics, as illustrated in Figure 6.3.1.

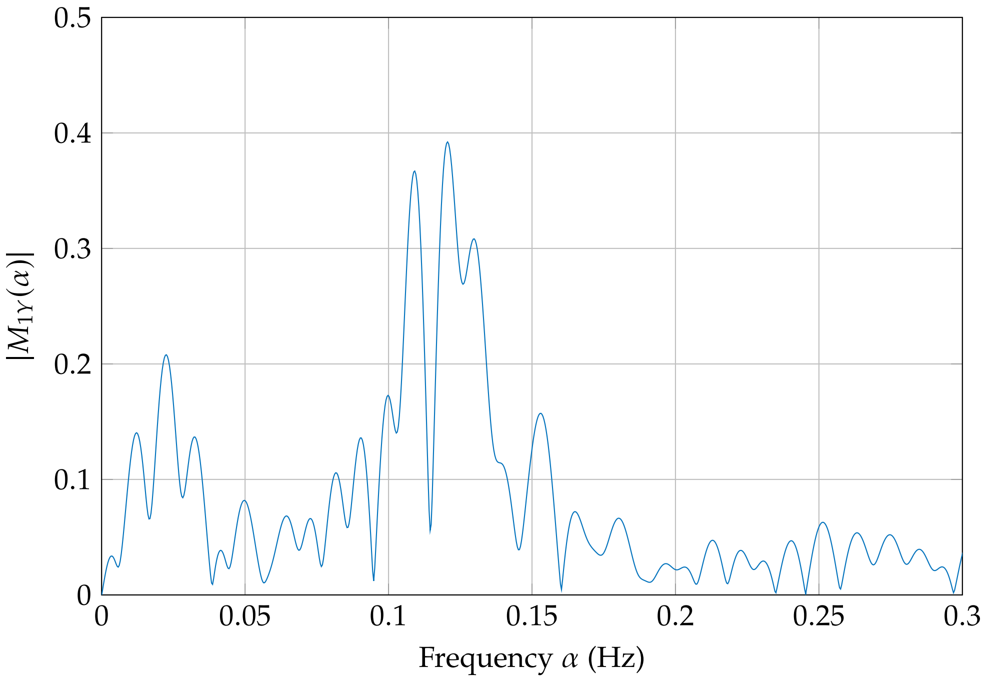

Figure 6.3.1: The cyclic spectrum for r = 2604 m

We introduce an estimation technique using a modified version of the CM-RELAX algorithm (Gini and Greco 2001) that recursively estimates harmonics of the cyclic mean from the texture intensity. This RELAXation algorithm was originally introduced as an optimisation approach for estimating harmonic parameters in data sequences corrupted by autoregressive (AR) noise (Li and Stoica 1996, Li *et al.* 1995; 1997). We present two sub-variants of Algorithm 1 that we call CM-RELAX Newton: one that independently estimates the frequency components of each range bin as described in this section, the other estimates the frequency components for R adjacent range bins simultaneously by the exploiting the spatio-temporal relationship of the sea clutter as detailed in Section 6.4.2.

The method we introduce here differs from CM-RELAX in a number of ways. Firstly, we exploit the symmetry of the intensity periodogram when estimating its frequency components through maximisation. This replaces the need to estimate both sides of the periodogram separately to achieve convergence, reducing the time complexity required for the algorithm to run. Secondly, we use the Newton-Raphson method to find the maximum of the periodogram of the k-th order of the cyclic mean. This numerical method provides a practical means of finding closely spaced frequency components without needing to perform extremely long fast Fourier transforms (FFTs). By doing this, we found that it was unnecessary to continually re-estimate already estimated tones until the texture estimate settled as in CM-RELAX (Gini and Greco 2001). With i^* iterations, the time complexity of the algorithm is:

$$T(K) = 1 + i^* \left[\frac{K(K+1)}{2} - 1 \right], \ \forall K > 1 \tag{6.3.2}$$

Therefore by setting $i^* = 1$, we reduce the expense to $\frac{K(K+1)}{2}$. Using Big-Θ notation, although the complexity order $T(K) \in \Theta(K^2)$ is unchanged and is indeed the same for CM-RELAX, the reduction in i^* does linearly reduce the algorithm runtime and is noticeable particularly for large K.

Based on the model from existing work (Gini *et al.* 2001, Gini and Greco 2002), we apply Algorithm 1 using the clutter measurements from the r-th range bin, $\mathbf{z} = [z(1,r), \ldots, z(N,r)]$ to form the parametric estimate $\hat{\boldsymbol{\theta}}_{0:K}$ for the particular range. The function $\mathbf{g}(\cdot)$ appearing on lines 9, 15 and 20 of Algorithm 1 estimates clutter parameters $\hat{\boldsymbol{\theta}}_k$ from data $\mathbf{Y}_{k-1} = [Y_{k-1}(1), \ldots, Y_{k-1}(N)]$ is defined as:

$$\mathbf{g}(\mathbf{Y}_{k-1}) = \left[\hat{A}_k, \hat{f}_k, \hat{\phi}_k\right]^T \tag{6.3.3}$$

where $\hat{A}_k = 2\left|\hat{M}_{1Y_{k-1}}(\hat{\omega}_k)\right|$, $\hat{\phi}_k = \angle \hat{M}_{1Y_{k-1}}(\hat{\omega}_k)$ and

$$\hat{M}_{1Y_{k-1}}(\hat{\omega}_k) = \frac{1}{N} \sum_{n=1}^{N} Y_{k-1}(n) \mathrm{e}^{-j\hat{\omega}_k n} \tag{6.3.4}$$

The frequency estimate $\hat{\omega}_k$ is obtained as follows. Using the texture model of (6.2.3), we form the intensity $I(n)$ using (6.2.5). The clutter power is estimated from the intensity as:

$$\hat{A}_0 = \frac{1}{N} \sum_{n=1}^{N} I(n) \tag{6.3.5}$$

By removal of the previously estimated lower k-th order frequency components from the intensity data:

$$Y_{k-1}(n) = I(n) - \tau_{CM}(n; \hat{\boldsymbol{\theta}}_{0:k-1}) \tag{6.3.6}$$

Algorithm 1: CM-RELAX NEWTON

Input: A R dimensional time series data array: $\mathbf{z}$
Output: $\hat{\boldsymbol{\theta}}_{0:K}$, the K-th order spectral estimate parameters of the $\mathbf{z}$

```
// Form the Intensity of the input
```
$\mathbf{I}(n_1, \ldots, n_R) \leftarrow \mathbf{z}(n_1, \ldots, n_R)\mathbf{z}^*(n_1, \ldots, n_R)$
```
// Estimate the 0-th harmonic component
```
$\hat{A}_0 \leftarrow \mathrm{mean}(\mathbf{I})$
$\hat{\theta}_0 \leftarrow \{\hat{A}_0\}$
```
// Remove the 0-th frequency texture estimate from the
   Intensity data
```
$\mathbf{Y}_0 \leftarrow \mathbf{I} - \boldsymbol{\tau}_{CM}(\hat{\theta}_0)$
```
// Use 1-D maximisation or 2-D if multiple range bins
```
if $R > 1$ **then** $\boldsymbol{\lambda} \leftarrow (\omega, \psi)$
else $\lambda \leftarrow \omega$
```
// Estimate the 1-st harmonic by maximising the log-periodogram
```
$\hat{\mathbf{M}}_{1Y_0} \leftarrow \mathrm{FFT}(\mathbf{Y}_0)$
$\hat{\boldsymbol{\lambda}}_1 \leftarrow \arg\max_{\boldsymbol{\lambda}} \log|\hat{M}_{1Y_0}(\boldsymbol{\lambda})|^2$
$\hat{\boldsymbol{\theta}}_1 \leftarrow \mathbf{g}(\mathbf{Y}_0)$
```
// Estimate remaining harmonics up to K
```
for $k \leftarrow 2$ ***to*** K **do**
    `// Iterate the process` i^* `times`
    for $i \leftarrow 1$ ***to*** i^* **do**
        $\mathbf{Y}_{k-1} \leftarrow \mathbf{I} - \boldsymbol{\tau}_{CM}(\hat{\boldsymbol{\theta}}_{0:k-1})$
        $\hat{\mathbf{M}}_{1Y_{k-1}} \leftarrow \mathrm{FFT}(\mathbf{Y}_{k-1})$
        $\hat{\boldsymbol{\lambda}}_k \leftarrow \arg\max_{\boldsymbol{\lambda}} \log|\hat{M}_{1Y_{k-1}}(\boldsymbol{\lambda})|^2$
        $\hat{\boldsymbol{\theta}}_k \leftarrow \mathbf{g}(\mathbf{Y}_{k-1})$
        `// Re-estimate the` j`-th frequency`
        for $j \leftarrow 1$ **to** $k-1$ **do**
            $\mathbf{Y}'_{k-1} \leftarrow \mathbf{I} - \boldsymbol{\tau}_{CM}(\hat{\boldsymbol{\theta}}_{0:k,\notin j})$
            $\hat{\mathbf{M}}_{1Y'_{k-1}} \leftarrow \mathrm{FFT}(\mathbf{Y}'_{k-1})$
            $\hat{\boldsymbol{\lambda}}_j \leftarrow \arg\max_{\boldsymbol{\lambda}} \log|\hat{M}_{1Y'_{k-1}}(\boldsymbol{\lambda})|^2$
            $\hat{\boldsymbol{\theta}}_j \leftarrow \mathbf{g}(\mathbf{Y}'_{k-1})$
            $j \leftarrow j + 1$
        $i \leftarrow i + 1$

return $\hat{\boldsymbol{\theta}}_{0:K}$

we can form the first order spectral estimate from the zero-padded data as

$$\hat{M}_{1Y_{k-1}}(\alpha) = \frac{1}{P}\sum_{n=1}^{P} Y_{k-1}(n)\mathrm{e}^{-j\alpha n} \tag{6.3.7}$$

where P is the padded length and $Y_{k-1}(n) = 0$ for $n = N+1,\ldots,P$. $\hat{M}_{1_{Y_{k-1}}}(\alpha)$ can be efficiently computed using an algorithm such the FFT. Unfortunately this method only computes the spectrum at so called *discrete* Fourier frequencies, limiting the achievable resolution of the estimate:

$$\hat{\omega}_{k,0} = \arg\max_{\alpha\in\mathcal{A}} \left|\hat{M}_{1Y_{k-1}}(\alpha)\right| \tag{6.3.8}$$

where $\mathcal{A} = \{2\pi p/P : p = 0,\ldots,(P-1)/2\}$. To overcome this, after we form an initial estimate of the peak harmonic $\hat{\omega}_{k,0}$ from $\hat{M}_{1Y_{k-1}}(\alpha)$ we continue to refine the estimate numerically using the Newton-Raphson method to maximise the log-periodogram (Quinn *et al.* 2008). Define the periodogram as:

$$I_{Y_{k-1}}(\omega) = \left|\hat{M}_{1Y_{k-1}}(\omega)\right|^2 \tag{6.3.9}$$

Maximisation of the log-periodogram is performed until convergence according to, for $m = 0,1,\ldots,$

$$\hat{\omega}_{k,m+1} = \hat{\omega}_{k,m} - \frac{J'_{Y_{k-1}}(\hat{\omega}_{k,m})}{J''_{Y_{k-1}}(\hat{\omega}_{k,m})} \tag{6.3.10}$$

where $J_{Y_{k-1}}(\omega) = \log I_{Y_{k-1}}(\omega)$ and $f'(.)$ denotes the derivative. Here,

$$J'_{Y_{k-1}}(\omega) = \frac{I'_{Y_{k-1}}(\omega)}{I_{Y_{k-1}}(\omega)} \tag{6.3.11a}$$

$$J''_{Y_{k-1}}(\omega) = \frac{I_{Y_{k-1}}(\omega)I''_{Y_{k-1}}(\omega) - I'_{Y_{k-1}}(\omega)^2}{I_{Y_{k-1}}(\omega)^2} \tag{6.3.11b}$$

Convergence is measured using the cost function:

$$CF\left(\hat{\omega}_{k,m+1}\right) = \left|\hat{\omega}_{k,m+1} - \hat{\omega}_{k,m}\right| \tag{6.3.12}$$

and once achieved, we obtain the k-th frequency estimate:

$$\hat{f}_k = \frac{\hat{\omega}_{k,m+1}}{2\pi}$$

Then having estimated the k-th harmonic parameters, we re-estimate the 1 to $(k-1)$-th frequency components from the intensity data with all previously estimated harmonic components removed except for the j-th one that is currently being re-estimated:

$$Y'_{k-1}(n) = I(n) - \tau_{CM}(n; \hat{\theta}_{0:k-1,\notin j}) \tag{6.3.13}$$

The process is repeated until K desired harmonic components have been estimated for the range bin of interest. Appropriate selection of K is in fact, a model order selection problem and model order methods such as (Stoica and Selén 2004) can be applied to find optimal values. This is not addressed here. Within the data sets investigated, we found that $K = 3$ to 5 minimised the difference between the texture predicted by our model and that obtained from a MW filter as further detailed in Section 6.5.4

6.4 Spatio-temporal methods for texture estimation

In this section we propose two methods for the estimation of clutter across a set of contiguous range bins. These methods exploit the spatial properties of the clutter to achieve a parsimonious texture estimate.

6.4.1 Frequency clustering of temporal texture parameters

Determination of the spatial relationship of the texture is performed by estimating the linear phase shift of common frequency components in each range bin from the set of range independent estimated texture parameters. Because of the nature of the texture model, the separation between the frequency estimates across the range bins can be quite small. This prevents us from using popular data clustering techniques such as k-means to identify common frequencies. Instead, we employ a modified form of subtractive clustering (Chiu 1994) that allows for some nearest neighbour exclusions as described in Algorithm 2.

We begin by grouping all of the frequency estimates together from the R range bins. We estimate the number of potential frequency clusters Q and their cluster centres $f_{1:Q}$ using subtractive clustering for cluster radius r_a which is used to define the neighbourhood around each data point. Starting with the cluster centre of the greatest density, we add the closest frequency estimate to the cluster centre from a neighbouring range cell if its squared distance

$$\Delta f_{r,k}^2 = |f_q - f_{r,k}|^2$$

Algorithm 2: RESTRICTED SUBTRACTIVE CLUSTERING

Input: $R \times K$-th order spectral estimate parameters $[\hat{\boldsymbol{\theta}}_{0:K}(1), \hat{\boldsymbol{\theta}}_{0:K}(2), \ldots, \hat{\boldsymbol{\theta}}_{0:K}(R)]$

Output: Clustered like frequency estimate parameters $\left[\hat{\boldsymbol{\theta}}_{R'}(1), \hat{\boldsymbol{\theta}}_{R'}(2), \ldots, \hat{\boldsymbol{\theta}}_{R'}(Q)\right]$ where $R' \subseteq \{1 : R\}, Q \leq RK$

`// Group all of the frequency components together`

$f_{1:R,1:K} \leftarrow [f_1, \ldots, f_R]_{1:K}$

`// Estimate the potential cluster centres`

$f_{1:Q} \leftarrow \mathrm{SubClust}(f_{1:R,1:K}, r_a)$

for $q \leftarrow 1$ ***to*** Q **do**

    `// Add the cluster centre to the cluster`

    $\hat{\boldsymbol{\theta}}_{r'}(q) \leftarrow f_q$

    remove f_q from $f_{1:R,1:K}$

    for $r \leftarrow 1$ ***to*** $R, f_r \notin f_q$ **do**

        if $\min \Delta f_{r,k} < \gamma$ **then**

            add $f_{r,k}$ to $\hat{\boldsymbol{\theta}}_{r'}(q)$

            remove $f_{r,k}$ from $f_{1:R,1:K}$

return $\left[\hat{\boldsymbol{\theta}}_{R'}(1), \hat{\boldsymbol{\theta}}_{R'}(2), \ldots, \hat{\boldsymbol{\theta}}_{R'}(Q)\right]$

is smaller than some test statistic:

$$\gamma = \left[\frac{r_a}{2\left[\max\{f_{r,k}\} - \min\{f_{r,k}\}\right]} \right]^2 \tag{6.4.1}$$

Once a frequency estimate has been added to a cluster, we remove the frequency from the set of estimates so as to limit the number of estimates from each range bin to just one potential cluster; a form of restricted nearest neighbour association. After the common frequency components have been clustered, we can reduce the series of individual texture parameter estimates to a single set of common frequency parameters of the texture across the range cells: $\bar{\boldsymbol{\theta}}_{0:Q} = \left[\bar{\theta}_0, \bar{\boldsymbol{\theta}}_1^T, \ldots, \bar{\boldsymbol{\theta}}_Q^T\right]^T$, $\bar{\boldsymbol{\theta}}_q = \left[\bar{A}_q, \bar{f}_q, \hat{\phi}_q, \bar{\psi}_q\right]^T$ where $\bar{A}_q$ is the average amplitude, $\bar{f}_q$ the average frequency, $\hat{\phi}_q$ the phase of the tone in the first range bin and $\bar{\psi}_q$ the estimated phase rate of the cluster.

Whilst this method reduces the complexity of the texture model to a single set of frequency estimates resulting in a parsimonious texture estimate, the frequency components can be difficult to accurately cluster. This technique also fails to address the difficulty of estimating closely spaced frequency components of the texture.

6.4.2 Joint range bin texture estimation

Using the texture model of (6.2.12) and estimating the parameters of the texture in 2-dimensional space across multiple range bins, we can increase the separation of the harmonics. This technique also provides a parsimonious estimate without condensing a series of independent texture estimates into a single set of parameters. Estimation of the texture parameters $\hat{\boldsymbol{\theta}}_{0:K}$ from the intensity cyclic mean follows Algorithm 1 with $\mathbf{z}$ defined as an $1 \times R$ vector of time-series clutter observations from adjacent range bins:

$$\mathbf{z} = [\mathbf{z}(1), \cdots, \mathbf{z}(R)]$$

where $\mathbf{z}(r) = [z(1,r), \dots, z(N,r)]^T$. In Algorithm 1, function $\mathbf{g}(\cdot)$ used to estimate the k-th texture parameter estimate $\hat{\boldsymbol{\theta}}_k$ is defined as:

$$\mathbf{g}(\mathbf{Y}_{k-1}) = \left[\hat{A}_k, \hat{f}_k, \hat{\phi}_k, \hat{\psi}_k\right]^T \tag{6.4.2}$$

where data

$$\mathbf{Y}_{k-1} = \begin{bmatrix} Y_{k-1}(1,1) & \cdots & Y_{k-1}(1,R) \\ & \ddots & \\ Y_{k-1}(N,1) & \cdots & Y_{k-1}(N,R) \end{bmatrix}$$

Estimates $\hat{\omega}_k, \hat{\psi}_k$ are obtained through joint maximisation of the cyclic mean in both frequency and phase rate as follows. The clutter intensity $I(n,r)$ is formed using (6.2.5) and $\hat{A}_0$ estimated as:

$$\hat{A}_0 = \frac{1}{NR}\sum_{r=1}^{R}\sum_{n=1}^{N} I(n,r) \tag{6.4.3}$$

By removal of lower frequency estimates from the intensity data:

$$Y_{k-1}(n,r) = I(n,r) - \tau_{CM}(n,r;\hat{\boldsymbol{\theta}}_{0:k-1}) \tag{6.4.4}$$

the 2-dimensional k-th spectral estimate of the cyclic mean $\hat{M}_{1Y_{k-1}}(\alpha,\beta)$ is computed from the zero-padded data $Y_{k-1}(n,r)$ as:

$$\hat{M}_{1Y_{k-1}}(\alpha,\beta) = \frac{1}{PQ}\sum_{m=1}^{Q}\sum_{n=1}^{P} Y_{k-1}(n,m)\mathrm{e}^{-j(\alpha n+\beta m)} \tag{6.4.5}$$

An initial joint estimate of the peak frequency and phase rate is performed using a coarse grid search:

$$\hat{\omega}_{k,0}, \hat{\psi}_{k,0} = \arg \max_{\alpha \in \mathcal{A}, \beta \in \mathcal{B}} \left| \hat{M}_{1Y_{k-1}}(\alpha, \beta) \right| \tag{6.4.6}$$

where $\mathcal{A} = \{2\pi p/P : p = 0, \ldots, (P-1)/2\}$ and $\mathcal{B} = \left\{\pi(2q-1) : q = 0, 1/Q - 1, 2/Q - 1, \ldots, 1\right\}$. Refinement of the initial estimate is performed again using Newton's method with joint maximisation of the log-periodogram performed according to:

$$\begin{bmatrix} \hat{\omega}_{k,m+1} \\ \hat{\psi}_{k,m+1} \end{bmatrix} = \begin{bmatrix} \hat{\omega}_{k,m} \\ \hat{\psi}_{k,m} \end{bmatrix} - \mathbf{J}''^{-1}_{Y_{k-1}} \mathbf{J}'_{Y_{k-1}} \tag{6.4.7}$$

until convergence is achieved by (6.3.12). $\mathbf{J}'_{Y_{k-1}}$ and $\mathbf{J}''_{Y_{k-1}}$ are defined by (6.3.11) and are derived in Appendix 6.A. Upon convergence we obtain the k-th frequency estimate:

$$\hat{f}_k = \frac{\hat{\omega}_{k,m+1}}{2\pi}, \quad \hat{\psi}_k = \hat{\psi}_{k,m+1}$$

The associated amplitude and phase of the estimate can be obtained as $\hat{A}_k = 2\left|\hat{M}_{1Y_{k-1}}(\hat{\omega}_k, \hat{\psi}_k)\right|$ and $\hat{\phi}_k = \angle \hat{M}_{1Y_{k-1}}(\hat{\omega}_k, \hat{\psi}_k)$ with the process iterated until K harmonic components have been estimated.

6.5 Validation

6.5.1 Radar

The sea clutter data used was collected at Osbourn Head Gunnery Range, Dartmouth, Nova Scotia, Canada by the McMaster University Intelligent PIXel (IPIX) X-band Polarimetric Coherent Radar during the OHGR - Dartmouth Campaign as shown in Figure 6.5.1. It is an experimental frequency agile, high-resolution radar originally developed for iceberg detection research featuring a 8 kW TWT operating at 8.9 GHz to 9.4 GHz. The parabolic dish antenna has a beamwidth of 0.9° with a cross-polarisation isolation greater than 33 dB.

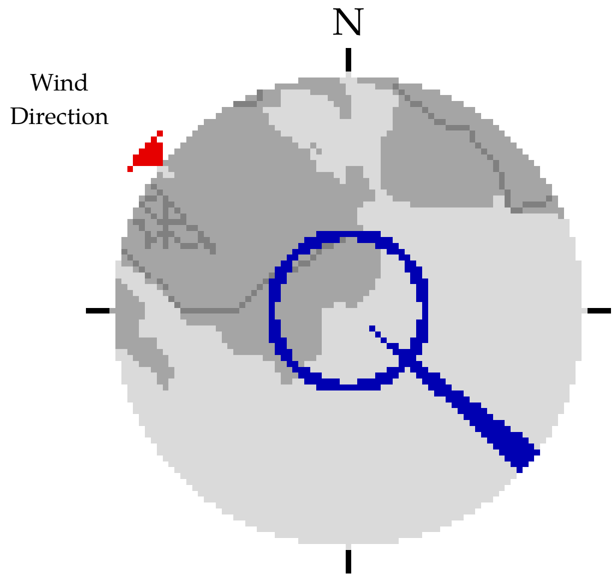

Figure 6.5.1: Radar data collection site at OHGR, Nova Scotia. Source: (Bakker and Currie 2001)

For validation purposes, we selected a measurement performed on the November 11th 1993 at 16:36:25, corresponding to the data file `19931111_163625_starea.cdf` (Bakker and Currie 2001). The radar was located on a cliff overlooking the Atlantic Ocean at a height of 30 m above mean sea level in a staring configuration at an azimuthal bearing of 129.5° over the open ocean. At the time of collection, the sea was reported to having a significant wave height of 0.7 m with a average wave period of 4.4 s. During the measurement period, the radar was operated at 9.39 GHz with a PRF of 1000 Hz and a range resolution 30 m, sampled at 15 m over a period of 131 s. We utilised measurements gathered in a VV polarisation from range bins 1 to 6, corresponding to ranges 2574 m to 2649 m.

The purpose of the analysis is to validate the cyclostationary sea clutter models presented and examine the performance of the algorithms used to perform estimation within these models. To do this, we first examine the validity of the spatial model used to establish the phase relationship between range bins for estimated harmonics. We then analyse the prediction error performance of the independent and joint range estimators. The results shown here apply to the CM-RELAX Newton algorithm being run over a a data set of length 120 s. For FFT computation of the intensity data Y_{k-1}, we found that padded lengths of $P = 2^{18}$ and $Q = 2^8$ provided sufficient resolution of initial estimates $\hat{\omega}_{k,0}$ and $\hat{\psi}_{k,0}$ to commence the Newton iteration. As the initial frequency estimate from the FFT only serves as an initiation point for the Newton iteration, artefacts from this process are inconsequential. Convergence was considered achieved when (6.3.12) $\leq \epsilon = 10^{-6}$. We have used a non-parametric MW-Filter texture estimate of length 2^{10} samples, equivalent to 1.024 s for comparison with our parametric estimates.

6.5.2 Validation of spatio-temporal clutter model

To validate the spatio-temporal clutter model, we compare the derived phase rate for a set of clustered frequency estimates and those from the gravity wave model in Section 6.2.2 using jointly estimated frequencies and phases. The application of Algorithm 2 to the range independent estimator parameters identified 5 common harmonics that were prevalent in at least 5 of the 6 range bins. These are shown in Figure 6.5.2, with the clustered phase estimates and their linear least-means square phase fits in Figure 6.5.3a. The associated coefficients of determination $R_q^2 = [0.930, 0.985, 0.988, 0.971, 0.881]$ provide good evidence of a linear fit to the phase rate of the clustered tones and that the harmonic components present in each range bin do exist across the contiguous range bins.

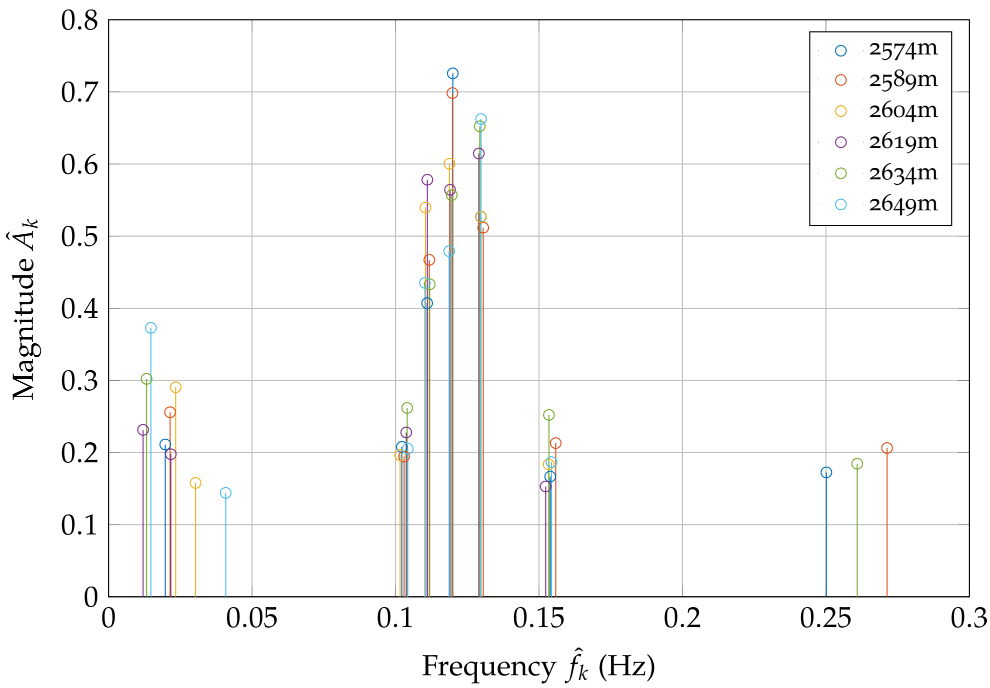

Figure 6.5.2: Set of independently estimated harmonics $\hat{\boldsymbol{\theta}}_{0:K,1:R}$ for $R = 6, K = 7$

Figure 6.5.3b shows the estimated phase across multiple range bins for the jointly estimated tones $\hat{f}_k, \hat{\phi}_k$ (Section 6.4.2) using the phase rate ($\psi_k = d/\lambda_k$) predicted by the gravity wave model (Section 6.2.2). This phase rate is based on the gravity wave phase velocity (Figure 6.5.4), where we can observe the reciprocal relationship between the predicted phase velocity and estimated wavelengths $\hat{\lambda}_k$ from the joint range estimates. In Figure 6.5.5, we see the fitted phase rate for independent and joint range bin estimators for $K = 7$ and those of the gravity wave model of Section 6.2.2 at clustered frequency components $\bar{f}_{1:Q}$. The resultant phase in Figure 6.5.3b is found by applying velocities $c_k(\hat{f}_k)$ from (6.2.9) to find associated phase rates $\phi_k(\hat{f}_k, r)$ for the gravity wave model in Figure 6.5.5 using the jointly estimated initial phases $\hat{\phi}_k$.

Comparison of the linear least-means square phase rate $\bar{\psi}_{q,r}(\hat{\phi}_{q,(1:R)})$ of Figure 6.5.3a and the gravity wave phase rate $\psi_k(\hat{f}_{(1:K)})$ in Figure 6.5.3b shows that that those independently estimated using CM-RELAX Newton for each range bin are similar to those predicted by the gravity wave model for the jointly estimated frequencies. This agrees with the notion that the estimated texture is the result of the sea swell travelling across the surface of the ocean in range over time. Additional jointly estimated frequencies $\hat{f}_6$ and $\hat{f}_7$ in Figure 6.5.3b have been shown for completeness.

6.5.3 Predictive texture sample length

In the interest of efficiency, we seek to identify both the quantity of data as well as the number of significant harmonic components required to accurately model the texture parsimoniously. We numerically compare the independent and joint range CM-RELAX Newton predictions as a function of the number of frequency components and the length of the observed data with the MW Filter texture estimate (6.3.1) (Gini *et al.* 2001) over a fixed period using the root means square deviation (RMSD). Define the predicted K-th space-time texture RMSD as:

$$RMSD(N, K) = \frac{1}{\sqrt{NR}} \left\| \boldsymbol{\tau}_{CM}(\hat{\boldsymbol{\theta}}_{0:K}) - \hat{\boldsymbol{\tau}}_{MW} \right\|_2 \tag{6.5.1}$$

where N is number of time samples we wish to predict forward and R is the number of range bins.

The predicted texture is generated from the same time samples for ease of comparison using (6.2.11) for the independent range estimator and (6.2.12) for the joint range estimator. In Figure 6.5.6 we see an improvement in the ability of the independent range estimator to predict the texture as we increase the duration of the measurement data. For smaller measurement samples, the joint range estimator outperforms the independent estimator presumably because of its improved ability to distinguish between closely spaced tones in 2-dimensional frequency space. Figure 6.5.6c indicates for both the independent and joint estimators a low optimal

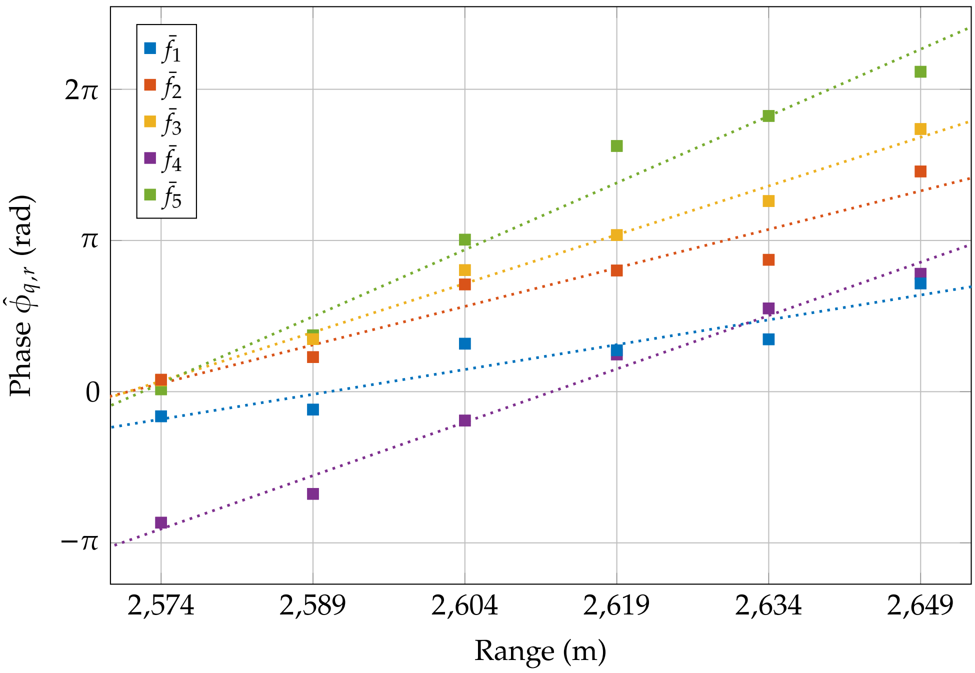

(a) Clustered phase estimates $\hat{\boldsymbol{\theta}}_{R',1:Q}$, $Q = 5$ and fitted phase $\bar{\phi}_q(r)$

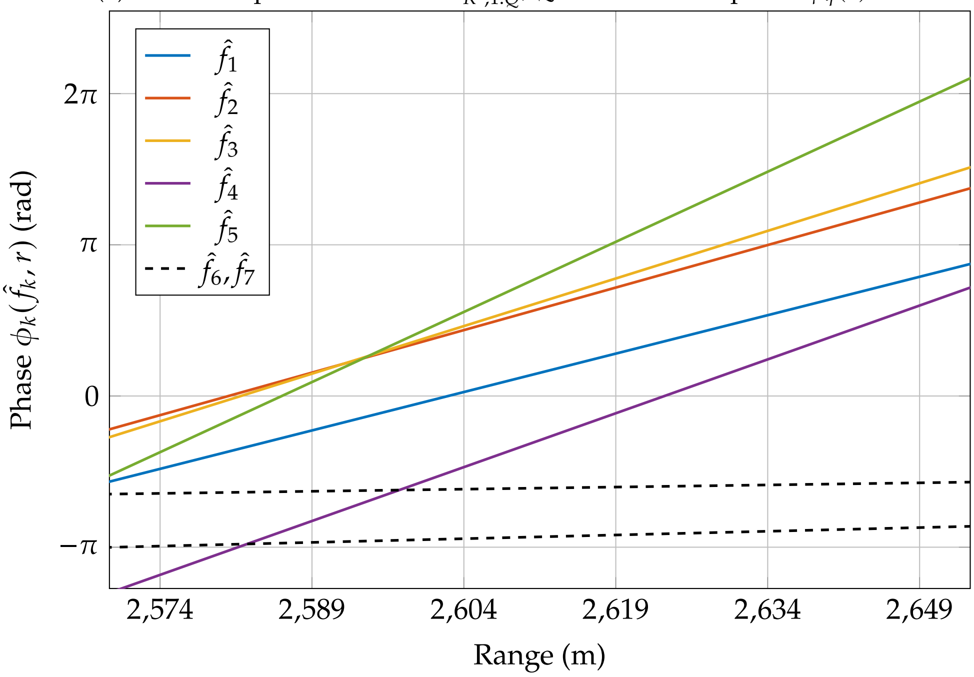

(b) Gravity wave phase for jointly estimated $\hat{f}_{1:K}$, $K = 7$

Figure 6.5.3: Similarities between the clustered and gravity wave phases indicate the spectral estimate comprises of gravity waves

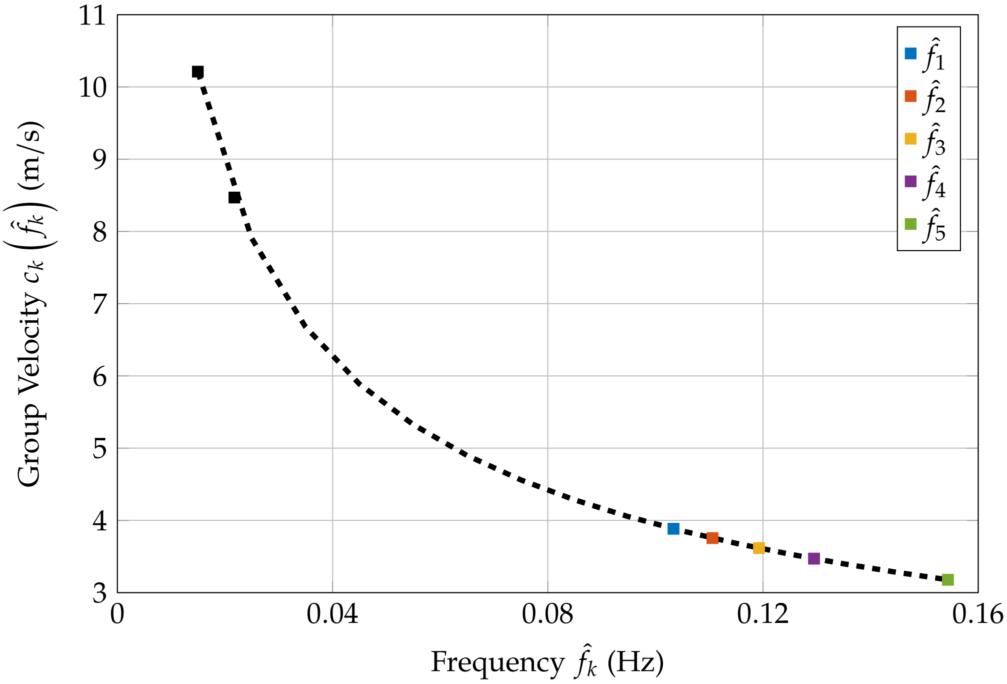

Figure 6.5.4: Gravity wave velocity for jointly estimated frequencies $\hat{f}_{1:K}$, $K = 7$

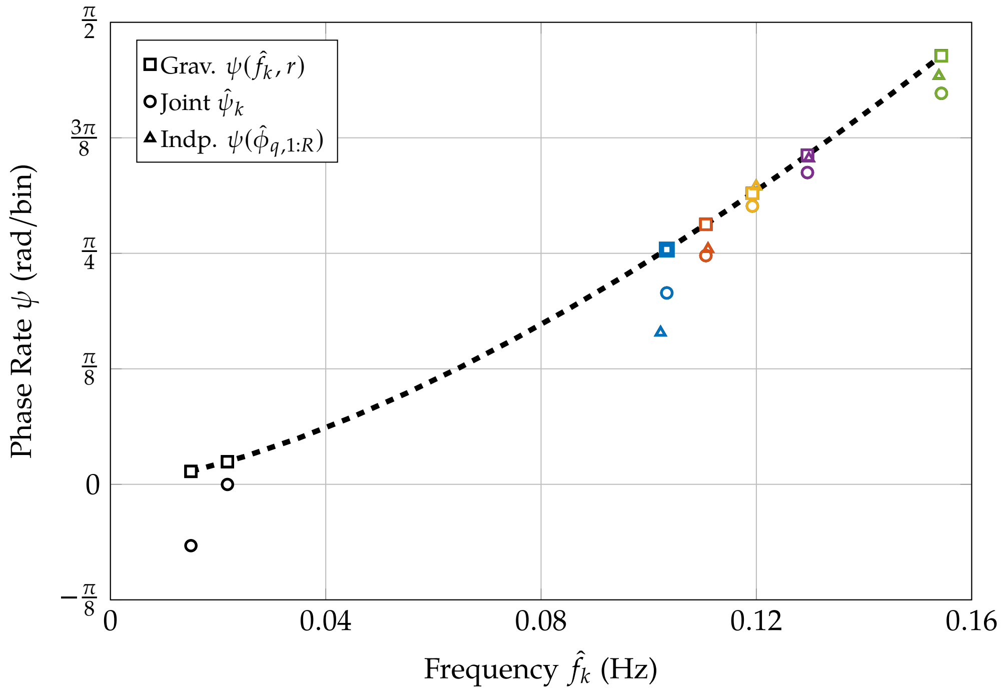

Figure 6.5.5: Gravity wave model, jointly estimated and fitted phase rates for common harmonics across 6 range bins

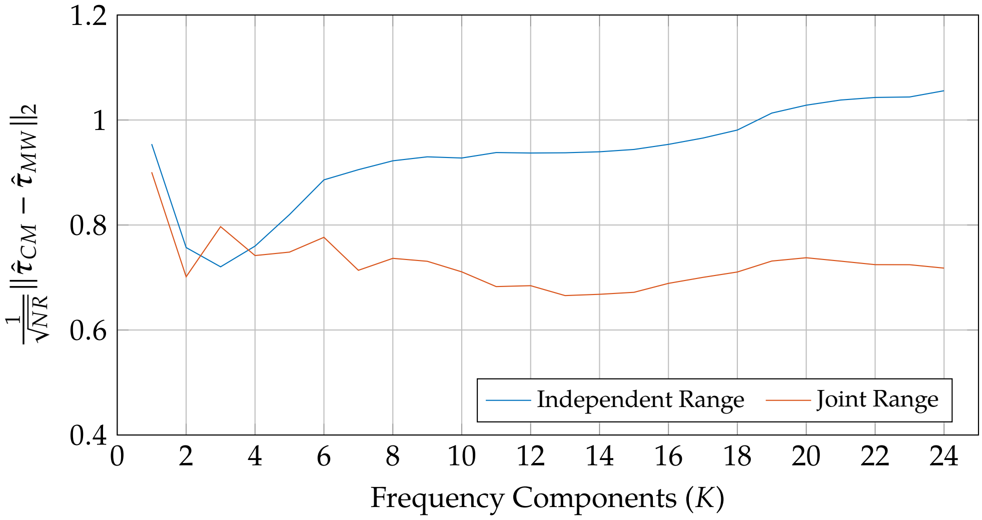

(a) 60 s of measurement data

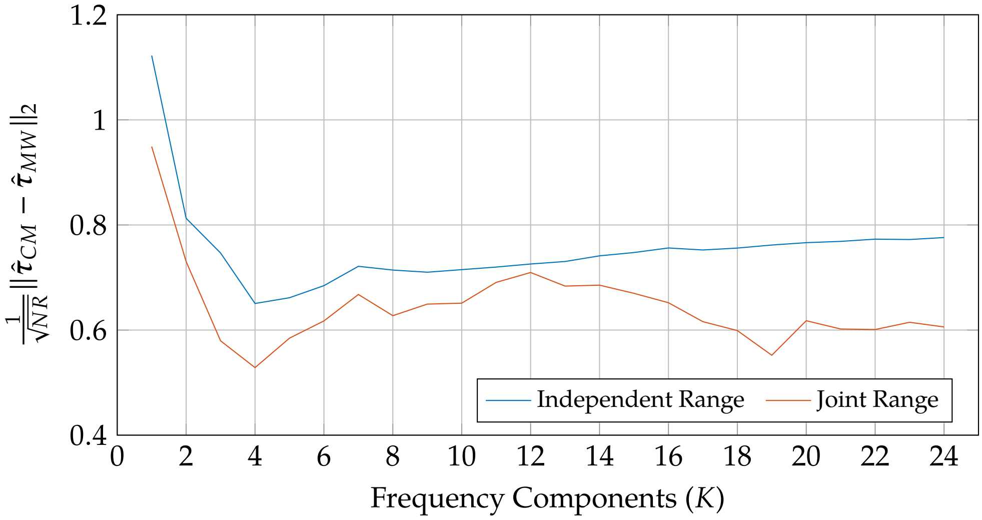

(b) 90 s of measurement data

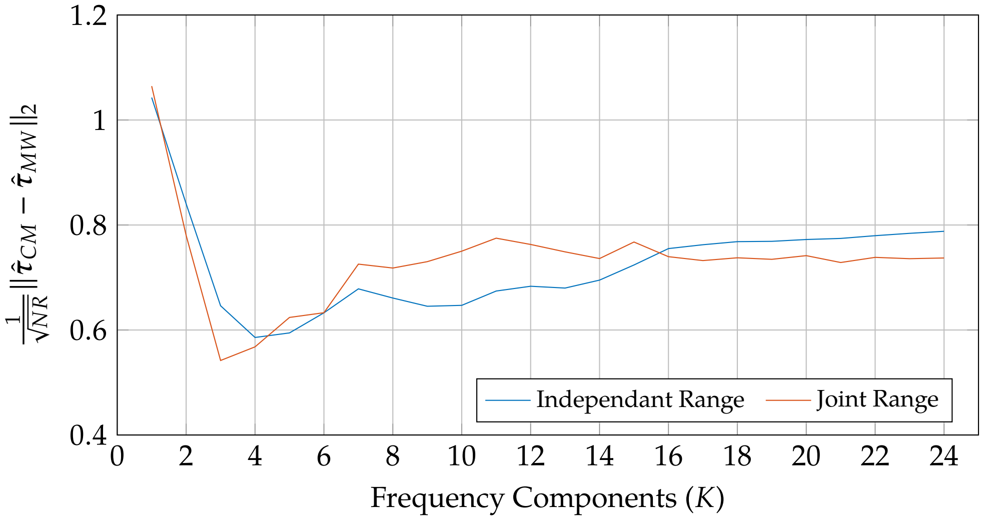

(c) 120 s of measurement data

Figure 6.5.6: *RMSD* of 10 s of predicted texture

model order of 3 to 6 harmonic components with our modified implementation of CM-RELAX, far less than in (Gini and Greco 2002). Figure 6.5.7 confirms that few tones persist across the contiguous range bins.

6.5.4 Time-average texture prediction performance

To quantify the degradation of the predicted texture with time we utilise the time-averaged error $RMSD_K(N)$ (6.5.1) where N is now the incremental number of time samples we predict the texture forward. Using 120 s of measurement data, we compare the prediction performance of a joint range estimate with a set of range independent CM-RELAX Newton estimates. Across 6 range bins, Figure 6.5.8a shows the RMSD is minimised for $K = 5$ to 8 using the range independent estimated texture and $K = 3$ to 6 for the joint range estimate in Figure 6.5.8b. We attribute this to the joint range estimator's ability to more reliably extract tones prevalent across all of the range bins compared with the temporal estimator. Prediction accuracy appears to degrade over a period of 2 s before remaining relatively steady for both estimators.

Predicted texture for both parametric estimators is compared with the MW Filter in Figure 6.5.9 showing that both techniques are able to successfully predict the periodic structure associated with the sea swell for varying values of $K \geq 3$. A macroscopic view of the estimated and predicted texture for both CM-RELAX techniques compared with the MW Filter in Figure 6.5.10 shows the characteristic periodic structure we commonly associate with the sea swell. Whilst both CM-RELAX estimators are able to recreate this structure with ease, we observe that the joint range estimator is unable to accommodate for the variances in $\hat{A}_k$ for each of the different range bins.

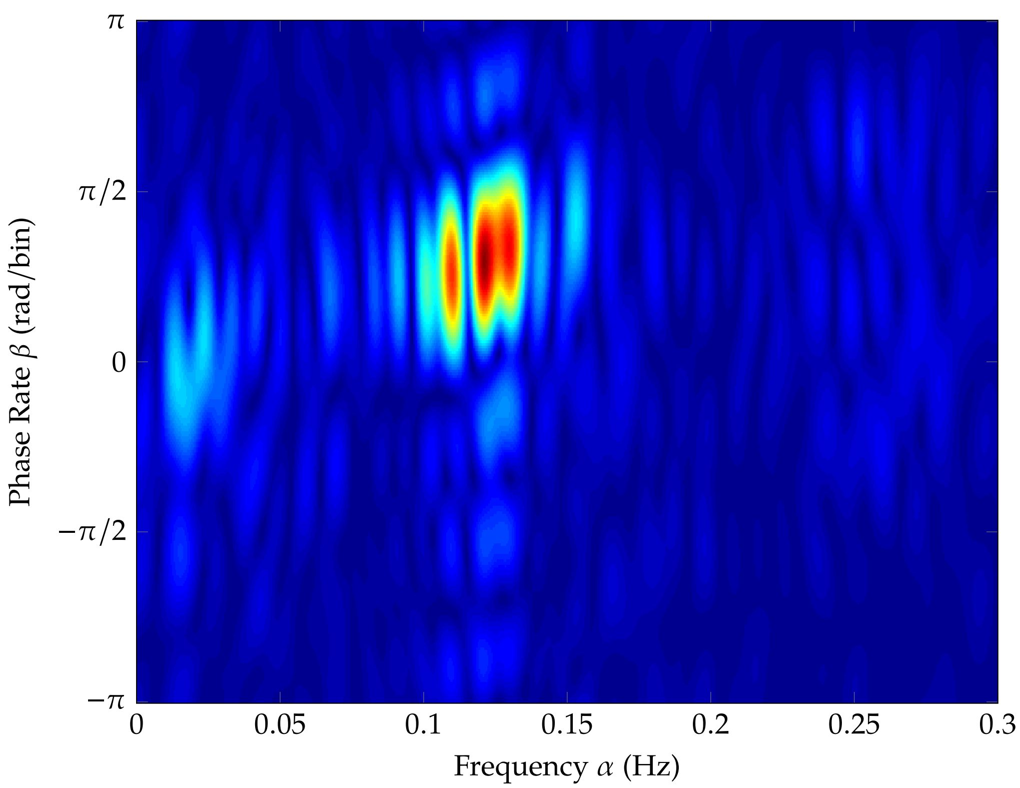

Figure 6.5.7: The clutter spectrum shows that few significant harmonics exist across the contiguous range bins

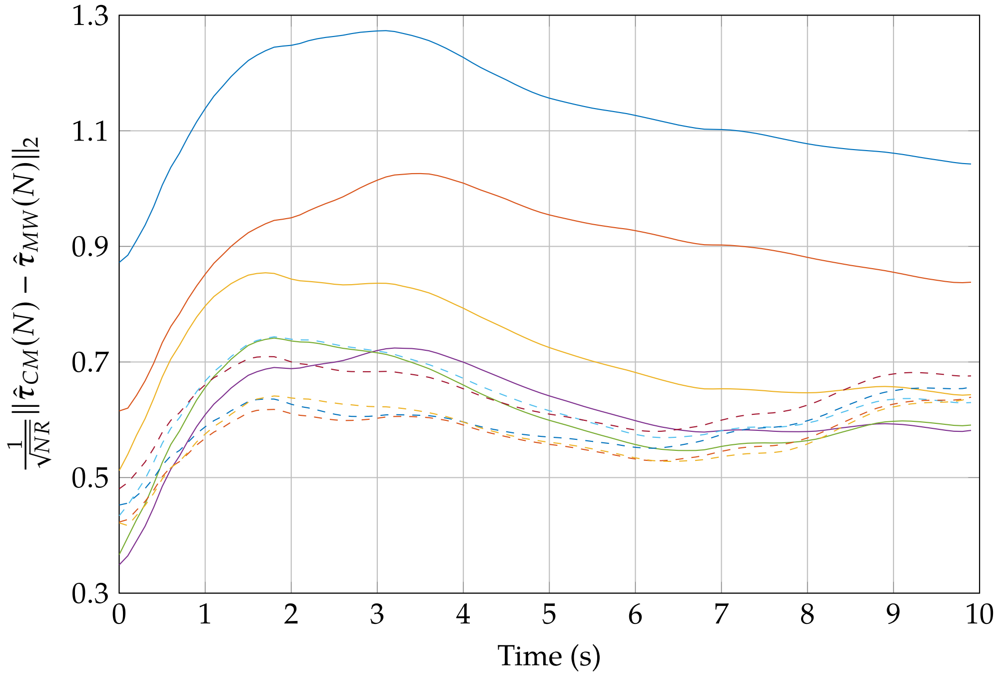

(a) Independent Range

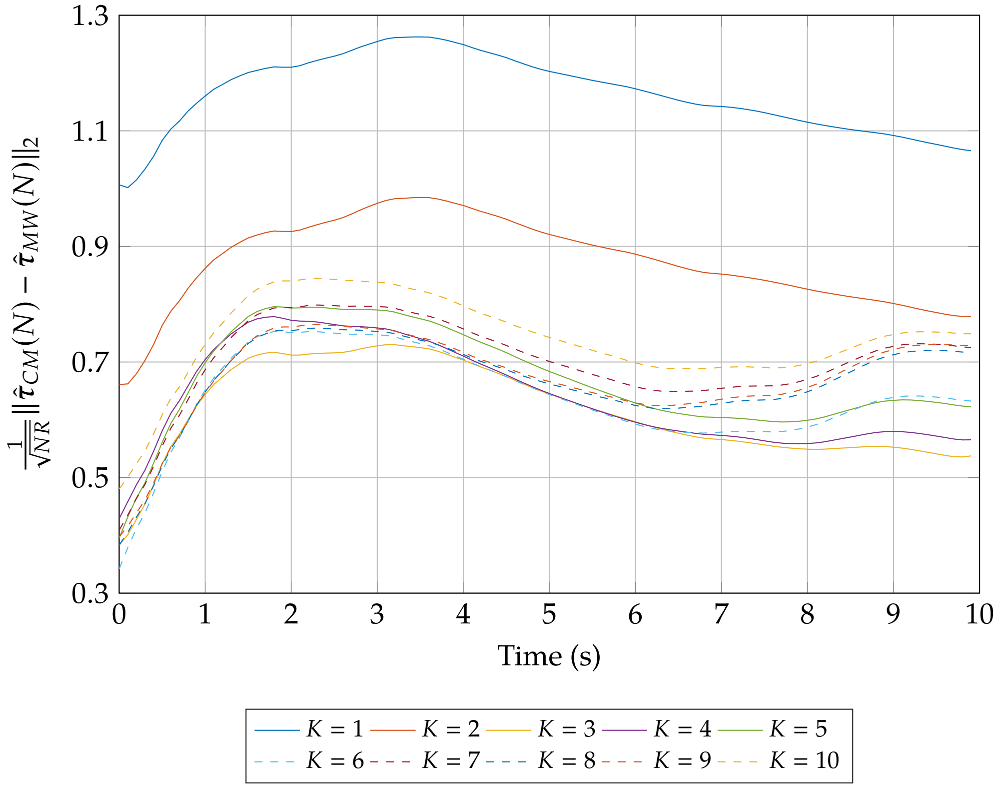

(b) Joint Range

Figure 6.5.8: Time averaged $RMSD$ of predicted texture using 120 s of measurement data for $R = 6$

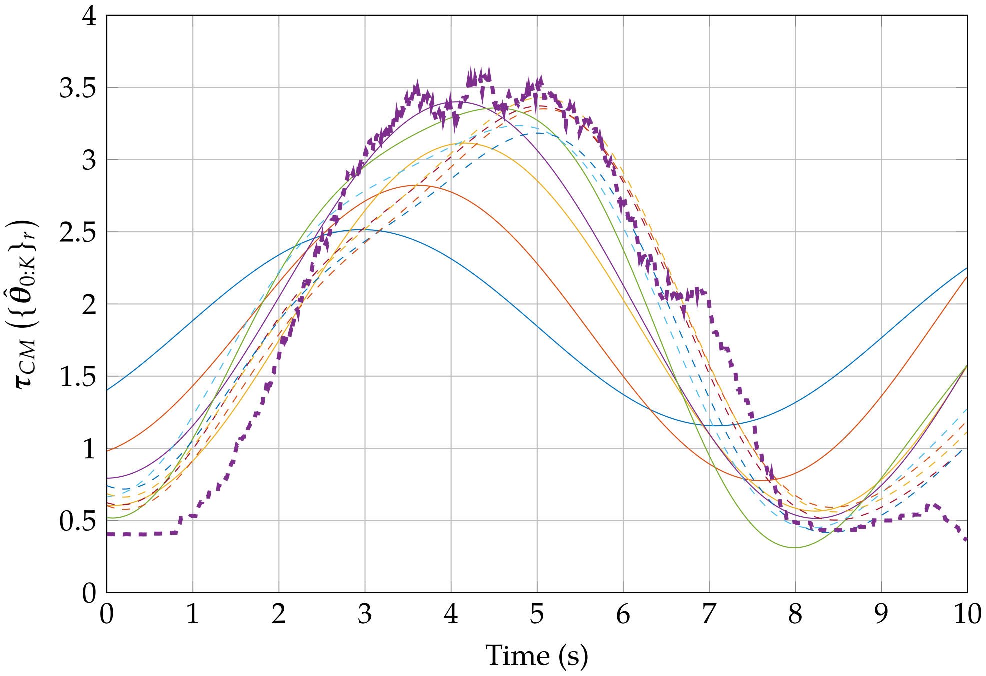

(a) Independent Range

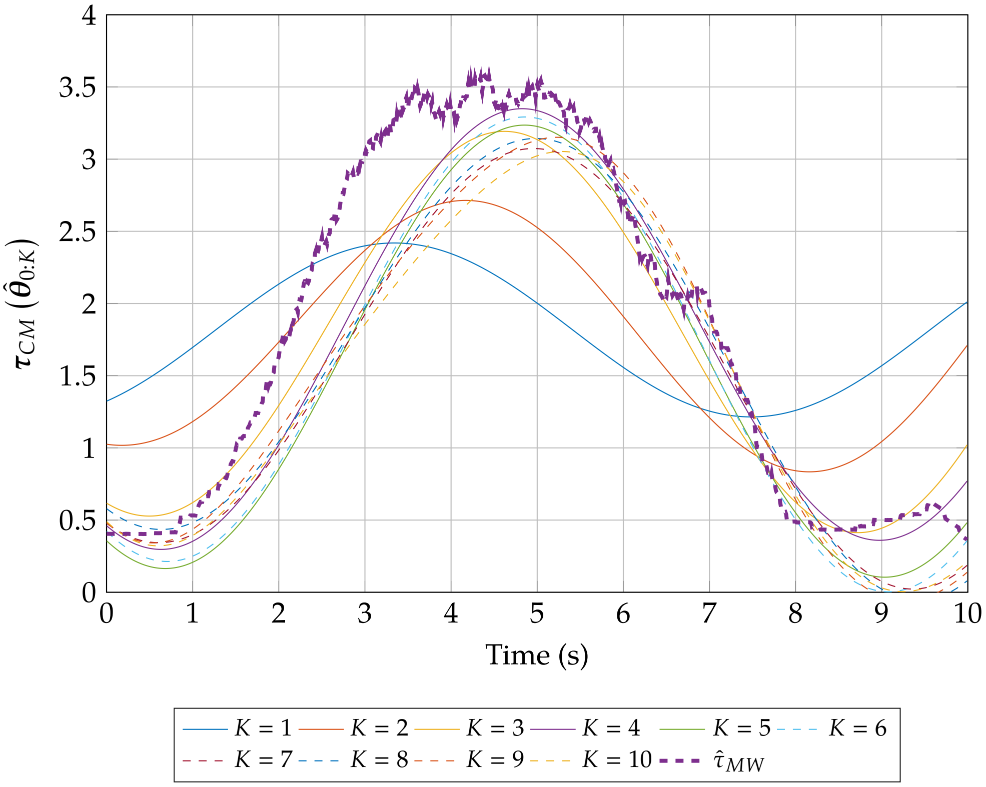

(b) Joint Range

Figure 6.5.9: CM-RELAX Newton predicted texture at r = 2589 m compared with non-parametric texture estimate for L = 1024

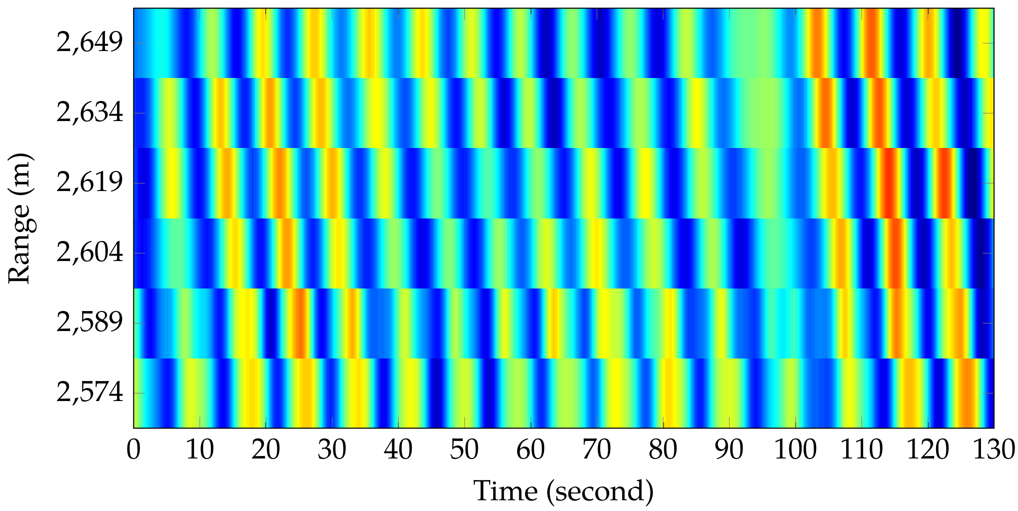

(a) Independently estimated and predicted texture $\boldsymbol{\tau}_{CM}\left(\{\hat{\boldsymbol{\theta}}_{0:K}\}_{1:R}\right)$

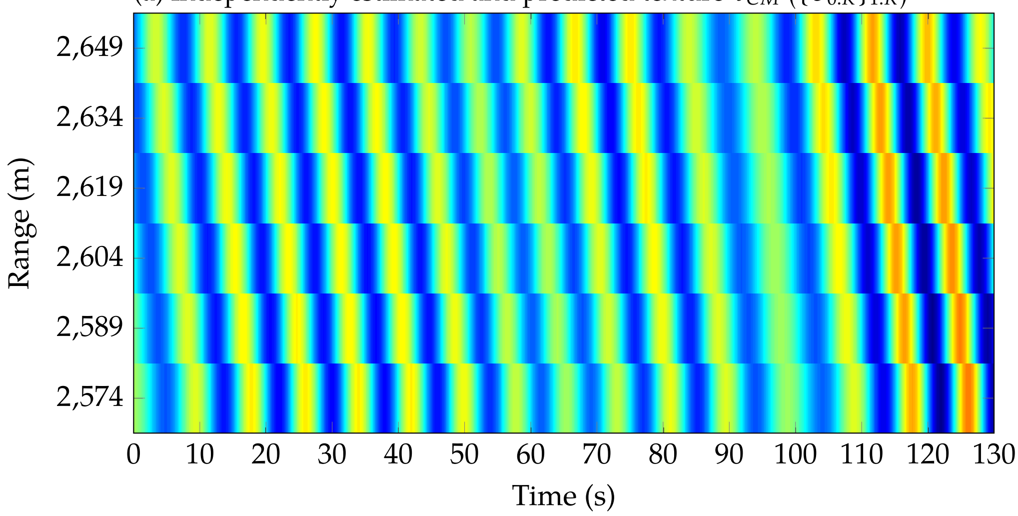

(b) Joint estimated and predicted texture $\boldsymbol{\tau}_{CM}\left(\hat{\boldsymbol{\theta}}_{0:K}\right)$

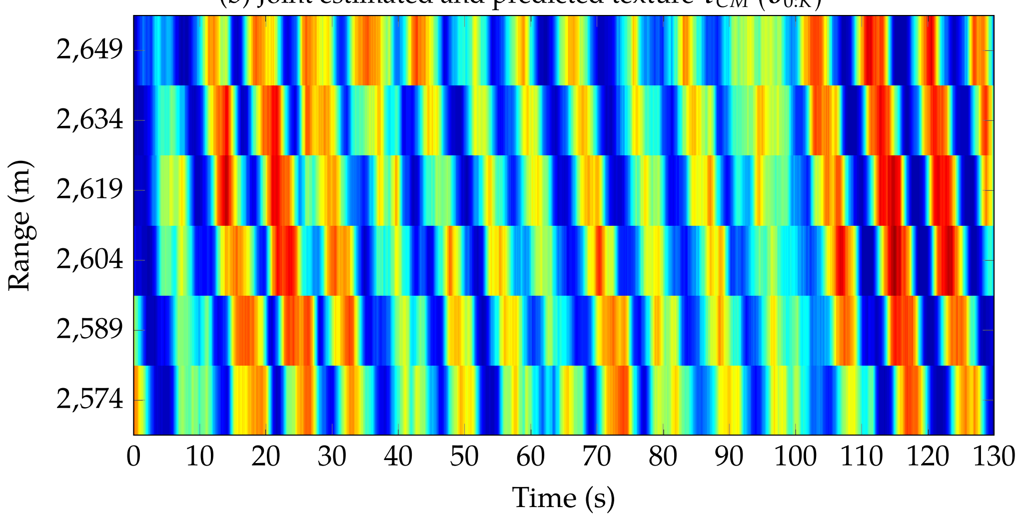

(c) MW estimated texture $\hat{\boldsymbol{\tau}}_{MW}$

Figure 6.5.10: CM-RELAX Newton estimated (120 s) predicted texture (10 s) for $K = 6$ (6.5.10a) and $K = 4$ (6.5.10a) for $R = 6$ compared with non-parametric estimate (6.5.10c) for $L = 1024$

6.6 Conclusion

In this chapter, we introduced a spatio-temporal model for parametric texture estimation and prediction that provided a better physical fit than existing temporal texture models. We adapted an existing texture estimation technique based on RELAX for estimation of closely spaced harmonics. We found that our spectral estimation algorithm was more efficient and robust for computing the harmonic estimates for a spatio-temporal parametric texture model compared with a series of temporal models through improved separation of the tones in 2-dimensional frequency space.

Predicted texture using parameters from a joint range and a set of range independent estimates computed by the CM-RELAX Newton algorithm were compared with a non-parametric texture estimator across a set of contiguous range bins. Whilst the texture prediction performance for both estimators was similar, our spatio-temporal estimator proved more reliable at identifying significant harmonic components resulting in a more parsimonious model with only 3 to 10 significant harmonic components across multiple ranges. We also found that the spatio-temporal model provided marginally improved texture predictive performance compared with a temporal model of similar order for a single range bin.

Texture prediction presents potential application in target detection and efficient radar scheduling algorithms particularly as prior knowledge of the texture and speckle correlation lengths are unrequired for our parametric texture model. Forecasting of the texture outside of the observation period allows the arrangement of future radar measurements about the periodicity of the estimated mean clutter with view to maximise signal to clutter ratios through simple scheduling.

The estimation of the spatial relationship the texture allows for the sea clutter to be modelled as a generalised spherically invariant random vector (SIRV) under the compound-Gaussian clutter model. The conventional cell-averaging constant false alarm rate (CA-CFAR) detector requires knowledge of the scale and shape of the distribution to set an appropriate detection threshold level (Watts 2000). The application of our spatio-temporal texture estimator could allow the formulation of spatially and temporally adaptive detector threshold levels. This could lead to the implementation of more spatially consistent P_{fa} thresholds toward the 'ideal CFAR' detector (Bucciarelli *et al.* 1996, Watts 1987) with improved consistency of target detection in the presence of sea clutter particularly for scenarios of high texture variance.

Appendices

6.A Newton-Raphson method for maximisation

This appendix presents the equations used for maximisation of the periodogram using Newton's method. Using (6.3.9) we compute the derivatives of the log-periodogram as:

$$\begin{aligned} I'_{Y_{k-1}}(\omega) &= \hat{M}_{1Y_{k-1}}(\omega)\hat{M}^{*\prime}_{1Y_{k-1}}(\omega) + \hat{M}'_{1Y_{k-1}}(\omega)\hat{M}^{*}_{1Y_{k-1}}(\omega) \\ &= \mathrm{Re}\left[\hat{M}'_{1Y_{k-1}}(\omega)\hat{M}^{*}_{1Y_{k-1}}(\omega)\right] \qquad (6.A.1a) \end{aligned}$$

$$I''_{Y_{k-1}}(\omega) = 2\left[\left|\hat{M}'_{1Y_{k-1}}(\omega)\right|^2 + \mathrm{Re}\left[\hat{M}''_{1Y_{k-1}}(\omega)\hat{M}^{*}_{1Y_{k-1}}(\omega)\right]\right] \qquad (6.A.1b)$$

where f^* denotes the complex conjugate.

For independent range bin texture estimation, from (6.2.6) the derivatives of spectrum of the cyclic mean estimate are:

$$\hat{M}'_{1Y_{k-1}}(\omega) = \frac{-j}{N}\sum_{n=1}^{N} nY_{k-1}(n)\mathrm{e}^{-j\omega n} \qquad (6.A.2a)$$

$$\hat{M}''_{1Y_{k-1}}(\omega) = \frac{-1}{N}\sum_{n=1}^{N} n^2Y_{k-1}(n)\mathrm{e}^{-j\omega n} \qquad (6.A.2b)$$

For the joint range estimation process in Section 6.4.2, the being the Jacobian and Hessian matrices of the localised 2-D cyclic mean estimate are:

$$\hat{\mathbf{M}}'_{1Y_{k-1}}(\omega,\psi) = \begin{bmatrix} \frac{\partial \hat{M}_{1Y_{k-1}}(\omega,\psi)}{\partial\omega} \\ \frac{\partial \hat{M}_{1Y_{k-1}}(\omega,\psi)}{\partial\psi} \end{bmatrix} \qquad (6.A.3a)$$

$$\hat{\mathbf{M}}''_{1Y_{k-1}}(\omega,\psi) = \begin{bmatrix} \frac{\partial^2 \hat{M}_{1Y_{k-1}}(\omega,\psi)}{\partial\omega^2} & \frac{\partial^2 \hat{M}_{1Y_{k-1}}(\omega,\psi)}{\partial\omega\partial\psi} \\ \frac{\partial^2 \hat{M}_{1Y_{k-1}}(\omega,\psi)}{\partial\omega\partial\psi} & \frac{\partial^2 \hat{M}_{1Y_{k-1}}(\omega,\psi)}{\partial\psi^2} \end{bmatrix} \qquad (6.A.3b)$$

where

$$\frac{\partial \hat{M}_{1Y_{k-1}}(\omega,\psi)}{\partial\omega} = \frac{-j}{NR}\sum_{r=1}^{R}\sum_{n=1}^{N} nY_{k-1}(n,r)\mathrm{e}^{-j(\omega n+\psi r)} \qquad (6.A.4a)$$

$$\frac{\partial \hat{M}_{1Y_{k-1}}(\omega,\psi)}{\partial\psi} = \frac{-j}{NR}\sum_{r=1}^{R}\sum_{n=1}^{N} rY_{k-1}(n,r)\mathrm{e}^{-j(\omega n+\psi r)} \qquad (6.A.4b)$$

and

$$\frac{\partial^2 \hat{M}_{1Y_{k-1}}(\omega,\psi)}{\partial \omega^2} = \frac{-1}{NR}\sum_{r=1}^{R}\sum_{n=1}^{N} n^2 Y_{k-1}(n,r)\mathrm{e}^{-j(\omega n+\psi r)} \tag{6.A.5a}$$

$$\frac{\partial^2 \hat{M}_{1Y_{k-1}}(\omega,\psi)}{\partial \omega \partial \psi} = \frac{-1}{NR}\sum_{r=1}^{R}\sum_{n=1}^{N} n r Y_{k-1}(n,r)\mathrm{e}^{-j(\omega n+\psi r)} \tag{6.A.5b}$$

$$\frac{\partial^2 \hat{M}_{1Y_{k-1}}(\omega,\psi)}{\partial \psi^2} = \frac{-1}{NR}\sum_{r=1}^{R}\sum_{n=1}^{N} r^2 Y_{k-1}(n,r)\mathrm{e}^{-j(\omega n+\psi r)} \tag{6.A.5c}$$

where n and r represent time delay and range bin indices.

Chapter 7

Conclusion

This thesis has focused its study in sensor scheduling, particularly the application of adaptive radar. The preceding chapters have extended this research area through a number of ways that address different implementation aspects of adaptive radar; firstly by deriving a maximum likelihood based method of range and range-rate estimation for pulse trains of diverse linear frequency modulation (LFM) pulses, secondly investigating the time costs and associated closed-loop sensor scheduling, and finally an efficient estimation methods and parsimonious model for radar sea clutter texture. This chapter summarises these contributions and provides some suggestions for areas of future investigation.

7.1 Summary of contributions

The following sections outline the contributions made in this thesis.

7.1.1 LFM waveform diversity

The analysis in Chapter 4 examined the range-Doppler coupling errors exhibited by matched filter receivers when using LFM pulse compression. By exploiting these errors, a maximum likelihood based method of jointly estimating target range and range-rate was proposed for diverse pulse trains. This also included a temporally aligned estimator, that accounted for the delay between successive pulses in the train. Low computational complexity methods for designing diverse optimal pulse trains were proposed for both control theoretic and information theoretic cost functions for moving targets. Simulations of the joint estimator were used to compare with pulse trains using conventional range bias compensation methods, such as alternating chirps and compensated pulse-Doppler processing for an adaptive radar in a manoeuvring target scenario.

Results showed that libraries of low bandwidth LFM pulses accentuate the range-Doppler coupling bias error, especially for trains that lack inter pulse waveform diversity in a linear target tracking scenario. Use of the adaptive waveform selection strategy and joint estimation method was found to significantly improve target track root mean square error (RMSE) for both linear and manoeuvring target tracking examples compared with conventional range-Doppler coupling error mitigation techniques.

7.1.2 Concurrent processing for adaptive tracking radar

By considered the requisite tasks required to implement an adaptive sensing system, particularly for a target tracking context, in Chapter 5 we proposed the use of decision time as a measure of the processing cost in a closed-loop scheduling process. Two parallel processing architectures, concurrent and delayed pipeline, were proposed for closed-loop radar scheduling based on processor pipelining to increase the available decision time with negligible impact to radar font-end duty.

To evaluate the alternate processing architectures for various processing costs, a tracking scenario involving multiple manoeuvring targets of varying radar cross section (RCS) is simulated with a minimax target selection criterion used to choose the order in which the radar interrogates the targets. When compared with a conventional (sequential) scheduling strategy the minimax scheduler was found to almost halve the required front-end duty required to attain the same position RMSE for this particular scenario. Both the pipeline processing architectures showed a significant improvement in the peak target track error compared with the conventional scheduling strategy, despite the long lag between measurement epochs and the future scheduled action being executed. For the delayed pipeline processor, a decision period of 9 cumulative coherent processing interval (CCPI) was found to be achieve equivalent track performance to the sequential processor with a decision period of only 6 pulse repetition interval (PRI). This is equivalent to a sensor front-end dead time of less than 20% of a coherent processing interval (CPI) between epochs. For the same decision period, overall target track RMSE improvement for both the concurrent and delayed pipeline processors was found to be similar.

7.1.3 Parametric sea clutter texture estimation and prediction

In Chapter 6, the work of Gini and Greco (2001; 2002) is extended to propose a deterministic parametric sea clutter texture model for high-resolution radar backscatter at low grazing angles in the open ocean. An algorithm is presented for the estimation of the two-dimensional spectral components of the parametric texture model. This algorithm is shown to be more computationally efficient that established methods by estimating texture model parameters across multiple contiguous range-bins simultaneously. Validation is performed by comparing the predictive fit for our estimator with a series of temporal estimators and a non-parametric estimator using measured sea clutter data from the Atlantic Ocean recorded by the IPIX radar of McMaster University in Canada.

Implementation of the spatio-temporal estimator results in a more parsimonious parametric model with improved reliability because to the increased separation of the tones in two-dimensional space. Results are shown to agree with an established physical model for the sea swell. The estimated and predicted sea clutter texture using our spatio-temporal method is compared with the estimated texture from an established parametric model and a non-parametric moving weighted filter method. For the examined dataset, we find that the sea clutter texture can be adequately represented using only 3-10 significant harmonic components across multiple range bins compared with up to 48 tones for the established parametric model. Our spatio-temporal model also offers the possibility of predicting future clutter texture with good accuracy unlike the non-parametric model.

7.2 Recommendations for future work

Sensor scheduling and adaptive radar are active areas of ongoing area of research, particularly in regards to the their application and implementation in real systems. The following sections describe some promising areas that may be suitable for future investigation activities that are related to the areas investigated in this thesis.

7.2.1 Joint estimation of target range and Doppler using LFM chirp diversity

The joint estimation method proposed in Chapter 4 exploits the use of LFM chirp diversity an range bias to correct the range error error and estimate the target range-rate. Additional work in this area could consider the further exploitation of this error and the waveform selection process.

Adaptive LFM chirp for multiple target separation and clutter mitigation

LFM range bias results in the shift of the measured target delay when using a matched filter receiver. Range bias may also be used to intentionally shift a moving targets range response through the careful selection of chirp rate. The intentional shifting of target range response may be useful when multiple reflectors such as targets and clutter of differing radial velocity simultaneously occupy a single range-bin. Whilst coherent processing methods such as range-Doppler processing already separate target responses in both range and Doppler, the proposed method in Chapter 4 is suitable for incoherent pulsed radar. The use of a clutter map in the waveform design process could help avoid unintentional placement of target responses in range-bins that may be otherwise be occupied by other genuine targets or clutter.

The lack of Doppler tolerance in low bandwidth LFM pulses means that although some waveforms can be unsuitable for targets that have large range-rates due to excess coupling, this could possibly be accounted for through use of mismatched receiver filters (McAulay and Johnson 1969, Niu *et al.* 2002, Xue *et al.* 2014).

Simultaneous diverse waveform selection for entire pulse trains

The suggested greedy pulse train scheduling method in Chapter 4 although efficient, is suboptimal. Although if we assume that resultant measurement covariance is small, the greedy solution can approach that of the optimal pulse train (Williams *et al.* 2007a;b). However, the complexity of evaluating a long pulse train can be prohibitive due to the curse of dimensionality.

For a waveform library that can be described using a discrete parameters, the waveform sequence can be described using a hierarchical tree structure. The efficient evaluation of the entire set of combinations or tree can be achieved using a depth-first-search approach. For longer pulse sequences or a non-myopic scheduling approach, a submodular optimisation approached could be used to prune candidate sequences without the need to evaluate the entire sequence.

7.2.2 Concurrent adaptive radar processing

In Chapter 6 we proposed the use of pipeline radar for adaptive radar. Future areas for this work could be directed towards further investigation on the understanding the application and implementation of this alternate close-loop scheduling process.

Concurrent processing for highly manoeuvrable and evasive targets

The results in Chapter 5 showed that the track error for concurrent and delayed pipeline processing architectures were similar for the same decision periods. This suggested that the additional information provided by the concurrent pipeline approach did not make significantly influence the prior in the pseudo-update.

It is possible that this may be a result of the target dynamics modelled in the simulated scenario. Scenarios where the mutual information between the prior and the puesdo-update is greater may be better candidates for this particular processing architecture. Such a scenario might include targets that are highly manoeuvrable or evasive. Partial measurements that are found to have low mutual information could be aborted part way through the pulse train and the puesdo-update instead used to inform the posterior. The remaining unused radar budget from the truncated epoch could then be reallocated to other targets or tasks instead.

Design of a time flexible adaptive radar processing architecture

Trends in radar hardware development has seen much analog hardware supplanted with digital technologies, particularly in the areas of signal generation processing. This trend is arguably seeing the implementation of some radars transition into a more generic hardware proposition comprising of a specialist radio frequency (RF) front end with a universal computational bank end.

The proposed parallel processing radar architecture in Chapter 5 was premised upon the use of fixed-time algorithms to simplify the timing between events in the processing loop. Whilst these strict lags can be achieved using real-time processing systems, the relaxation of real-time constraints on the radar processor could significant decrease the difficulty and cost in the implementation of radar. The three primary budgets managed by the radar resource manager (RRM) are time, energy and processing. The adoption of a time-flexible parallel processing architecture could allow the processor to perform tasks about a processing equilibrium point to maximise the radar utility. Flexible RRM scheduling is already commonplace in multi-function radar (MFR) task scheduling (Section 2.4). A similar but parallel or pipeline compatible process for the signal processing aspects of sensor scheduling radar could be adapted to achieve this task. Rewards or penalties could be attached to the computation costs of queued tasks to help prioritise them within the feedback cycle with thought given to the associated performance compromises for the selected radar objective.

7.2.3 Sea clutter texture estimation and prediction

Chapter 6 provided a method of estimating the parameters for a parametric sea clutter texture model. Extensions for this work could be centred about the application of this model in various settings.

Radar target detection in the presence of sea clutter

The detection and tracking of target on the sea surface can be challenging due to the sea clutter response masking target reflections. Target detection in high clutter environments such as maritime operations often utilise algorithms including constant false alarm rate (CFAR) to adaptively select the threshold levels for the detector to help cope with the fluctuating clutter. An application of this spatial-temporal model is to estimate the sea clutter in a measured radar scene and use this to formulate spatially and temporally adaptive detector threshold levels.

This could lead to the implementation of non-homogeneous clutter map and more spatially consistent probability of false alarm thresholds toward the 'ideal CFAR' detector with improved consistency in target detection particularly for scenarios of high texture variance between range bins (Bucciarelli *et al.* 1996, Watts 1987). Using the deterministic model, a future the clutter map could be predicted concurrently as the radar interrogates the scene, reducing the amount of processing required after the reflected signals have been received for target detection.

Adaptive scheduling for target detection

Adaptive radar scheduling using clutter mitigation has been previously proposed as method to improve target tracking (Song and Mušicki 2011). Estimation of the clutter map can provide information about density of the clutter response (Mušicki *et al.* 2005). Target surveillance in large swaths can take significant amount of time to process due to the requirement of the radar to 'stare' at any particular patch for a period of time until sufficient energy is reflected from the scene. Reducing the time required to interrogate any specific patch can be difficult to due to the energy budget, resolution requirements or some other operational criteria such ambiguous ranges, the employed Doppler ambiguity resolution algorithm.

As such, surveillance search patterns are normally pre-determined according to heuristics about the operating scene to accommodate these operational requirements. An application of a predictive spatio-temporal model for clutter could be to form a deterministic scaling property that aids in the adaptive design of target search patterns or waveform selection that minimises the expected clutter response in both space and time. This could be accomplished through a combination of beam steering, spatial task and waveform resource scheduling.

Bibliography

Abatzoglou T.J. and Gheen G.O. (**1998**). "Range, radial velocity, and acceleration MLE using radar LFM pulse train" IEEE Transactions on Aerospace and Electronic Systems **34**(4), 1070–1083. (Cited on page 69.)

Adas A. (**1997**). "Traffic models in broadband networks" IEEE Communications Magazine **35**(7), 82–89. (Cited on page 32.)

Antipov I. (**1998**a). "Analysis of sea clutter data" Technical Report DSTO-TR-0647, Defence Science and Technology Organisation. (Cited on pages 126 and 132.)

Antipov I. (**1998**b). "Simulation of sea clutter returns" Technical Report DSTO-TR-0679, Defence Science and Technology Organisation. (Cited on page 131.)

Athans M. and Schweppe F.C. (**1967**). "Optimal waveform design via control theoretic concepts" Information and Control **10**(4), 335–377. (Cited on page 61.)

Baker C.J. (**1991**). "K-distributed coherent sea clutter" in *IEE Proceedings F (Radar and Signal Processing)*, volume 138, 89–92. (Cited on page 126.)

Baker C.J., Griffiths H.D., and Papoutsis I. (**2005**). "Passive coherent location radar systems. Part 2: Waveform properties" IEE Proceedings - Radar, Sonar and Navigation **152**(3), 160. (Cited on page 31.)

Bakker R. and Currie B. (**2001**). "IPIX radar - Dartmouth database" URL `http://soma.ece.mcmaster.ca/ipix/dartmouth/index.html`. (Cited on pages xiv and 141.)

Bar-Shalom Y. (**2001**). "Negative correlation and optimal tracking with Doppler measurements" IEEE Transactions on Aerospace and Electronic Systems **37**(3), 1117–1120. (Cited on page 70.)

Bar-Shalom Y., Li X.R., and Kirubarajan T. (**2001**). *Estimation with applications to tracking and navigation: Theory, algorithms and software* (John Wiley & Sons). (Cited on page 59.)

Barbaresco F., Deltour J.C., Desodt G., Durand B., Guenais T., and Labreuche C. (**2009**). "Intelligent M3R radar time resources management: Advanced cognition, agility & autonomy capabilities" in *2009 International Radar Conference "Surveillance for a Safer World" (RADAR 2009)*, 1–6. (Cited on page 17.)

Barnes S.D. and Maharaj B.T. (**2011**). "Performance of a hidden Markov channel occupancy model for cognitive radio" in *IEEE Africon '11*, 1–6 (IEEE, Victoria Falls, Livingstone, Zambia). (Cited on page 32.)

Barton D.K. (**1988**). *Modern radar system analysis* (Artech House, Norwood, MA, USA). (Cited on page 111.)

Barton D.K. and Ward H.R. (**1969**). *Handbook of radar measurement*, Microwaves and Fields (Prentice-Hall, Englewood Cliffs, NJ, USA). (Cited on page 111.)

Belcher M.L. Jr. (**2013**). "Multifuncton phased array radar systems" in *Radar applications*, volume 3 of *Principles of modern radar*, 251–283 (IET). (Cited on page 17.)

Bell K., Smith G., Mitchell A., and Rangaswamy M. (**2018**). "Multiple task hierarchical fully adaptive radar" in *2018 52nd Asilomar Conference on Signals, Systems, and Computers*, 1344–1348. (Cited on page 36.)

Bell K.L., Baker C.J., Smith G.E., Johnson J.T., and Rangaswamy M. (**2014**a). "Fully adaptive radar for target tracking part I: Single target tracking" in *Radar Conference, 2014 IEEE*, 0303–0308. (Cited on page 35.)

Bell K.L., Baker C.J., Smith G.E., Johnson J.T., and Rangaswamy M. (**2014**b). "Fully adaptive radar for target tracking part II: Target detection and track initiation" in *Radar Conference, 2014 IEEE*, 0309–0314. (Cited on page 35.)

Bell K.L., Baker C.J., Smith G.E., Johnson J.T., and Rangaswamy M. (**2015**a). "Cognitive radar framework for target detection and tracking" IEEE Journal of Selected Topics in Signal Processing **9**(8), 1427–1439. (Cited on page 35.)

Bell K.L., Johnson J.T., Smith G.E., Baker C.J., and Rangaswamy M. (**2015**b). "Cognitive radar for target tracking using a software defined radar system" in *2015 IEEE Radar Conference (RadarCon)*, 1394–1399 (IEEE, Arlington, VA, USA). (Cited on page 97.)

Bell M. (**1993**). "Information theory and radar waveform design" IEEE Transactions on Information Theory **39**(5), 1578 –1597. (Cited on pages 23, 33, 55, 58, 63 and 65.)

Bell M.R. (**1999**). "Information theory of radar and sonar waveforms" in *Wiley Encyclopedia of Electrical and Electronics Engineering*, edited by J. G. Webster, 180–190 (John Wiley & Sons, Hoboken, NJ, USA). (Cited on page 63.)

Bello P. (**1960**). "Joint estimation of delay, Doppler, and Doppler rate" IRE Transactions on Information Theory **6**(3), 330–341. (Cited on page 69.)

Benoudnine H., Keche M., Ouamri A., and Woolfson M. (**2006**). "Fast adaptive update rate for phased array radar using IMM target tracking algorithm" in *2006 IEEE International Symposium on Signal Processing and Information Technology*, 277–282 (IEEE, Vancouver, BC, Canada). (Cited on page 24.)

Berry P. and Fogg D. (**2003**). "On the use of entropy for optimal radar resource management and control" in *2003 Proceedings of the International Conference on Radar*, 572–577 (IEEE, Adelaide, SA, Australia). (Cited on page 24.)

Beun S.L. (**2017**). "Cognitive radar: Waveform design for target detection" in *2017 IEEE MTT-S International Microwave Symposium (IMS)*, 330–332 (IEEE, Honolulu, HI, USA). (Cited on page 54.)

Billetter D.R. (**1989**). *Multifunction array radar*, Artech House Radar Library (Artech House, Norwood, MA). (Cited on page 17.)

Blackman S. and Popoli R. (**1999**). *Design and analysis of modern tracking systems*, Artech House Radar Library (Artech House). (Cited on page 111.)

Blair W.D., Richards M.A., and Long D.G. (**2010**). "Radar measurements" in *Principles of modern radar: Basic principles*, volume 1 of *Principles of modern radar*, 677–712 (SciTech Publishing). (Cited on page 111.)

Blom H.A. and Bar-Shalom Y. (**1988**). "The interacting multiple model algorithm for systems with Markovian switching coefficients" IEEE Transactions on Automatic Control **33**(8), 780–783. (Cited on page 106.)

Blom H.A.P. (**1984**). "An efficient filter for abruptly changing systems" in *The 23rd IEEE Conference on Decision and Control*, 656–658. (Cited on page 106.)

Bocquet S. (**2015**). "Parameter estimation for Pareto and K distributed clutter with noise" IET Radar, Sonar Navigation **9**(1), 104–113. (Cited on page 126.)

Bruno L., Braca P., Horstmann J., and Vespe M. (**2013**). "Experimental evaluation of the range-Doppler coupling on HF surface wave radars" Geoscience and Remote Sensing Letters, IEEE **10**(4), 850–854. (Cited on page 70.)

Bucciarelli T., Lombardo P., and Tamburrini S. (**1996**). "Optimum CFAR detection against compound Gaussian clutter with partially correlated texture" IEE Proceedings - Radar, Sonar and Navigation **143**(2), 95–104. (Cited on pages 152 and 160.)

Butler J.M. (**1998**). "Tracking and control in multi-function radar" Ph.D. thesis, University College London, London, UK. (Cited on pages xiii, 17 and 21.)

Butterfield A.S., Mitchell A.E., Smith G.E., Bell K.L., and Rangaswamy M. (**2016**). "Metrics for quantifying cognitive radar performance" in *2016 CIE International Conference on Radar (RADAR)*, 1–4 (IEEE, Guangzhou, China). (Cited on pages 99 and 114.)

Cabrera J.B. (**2013**). "Controlling modern radars: Challenges and opportunities" in *In Proceedings of the 16th Yale Workshop on Adaptive and Learning Systems*, 6 (New Haven, CT, USA). (Cited on page 17.)

Cabrera J.B.D. (**2014**). "Tracker-based adaptive schemes for optimal waveform selection" in *2014 IEEE Radar Conference*, 0298–0302 (IEEE, Cincinnati, OH, USA). (Cited on pages 59 and 70.)

Cabrera J.B.D. (**2015**). "Tracker-based selection of radar waveforms with range and range-rate measurements: Analytical results" in *2015 IEEE Radar Conference (RadarCon)*, 0767–0771 (IEEE, Arlington, VA, USA). (Cited on page 59.)

Calderbank A.R., Howard S.D., and Moran W. (**2009**). "Waveform diversity in radar signal processing" IEEE Signal Processing Magazine **26**(1), 32 –41. (Cited on pages 33, 45, 51 and 70.)

Casasent D. (**1980**). "Optical processing for adaptive phased-array radar" IEE Proceedings F Communications, Radar and Signal Processing **127**(4), 278. (Cited on page 36.)

Casasent D., Psaltis D., Vijaha Kumar B.V.K., and Carlotto M. (**1980**). "Optical processors for adaptive phased-array radar" in *Optical Signal Processing for C3I*, edited by W. J. Miceli, 47–52 (Boston, MA, USA). (Cited on page 36.)

Cassandra A.R., Littman M.L., and Zhang N.L. (**1997**). "Incremental pruning: A simple, fast, exact method for partially observable Markov decision processes" in *Proceedings of the Thirteenth Conference on Uncertainty in Artificial Intelligence*, 54–61 (Morgan Kaufmann, San Francisco, CA, USA). (Cited on page 60.)

Castañón D.A. (**1997**). "Approximate dynamic programming for sensor management" in *Proceedings of the 36th IEEE Conference on Decision and Control*, volume 2, 1202–1207 (IEEE, San Diego, CA, USA). (Cited on page 57.)

Challa S., Morelande M.R., Mušicki D., and Evans R.J. (**2011**). *Fundamentals of object tracking* (Cambridge University Press). (Cited on page 85.)

Charlish A., Woodbridge K., and Griffiths H. (**2011**). "Agent based multifunction radar surveillance control" in *2011 IEEE RadarCon (RADAR)*, 824–829 (IEEE, Kansas City, MO, USA). (Cited on page 22.)

Charlish A., Woodbridge K., and Griffiths H.D. (**2010**). "Information theoretic measures for MFR tracking control" in *2010 IEEE Radar Conference*, 987–992 (IEEE, Arlington, VA, USA). (Cited on page 64.)

Charlish A., Woodbridge K., and Griffiths H.D. (**2015**). "Phased array radar resource management using continuous double auction" IEEE Transactions on Aerospace and Electronic Systems **51**(3), 2212–2224. (Cited on page 23.)

Chavali P. and Nehorai A. (**2010**). "Cognitive radar for target tracking in multipath scenarios" in *2010 International Waveform Diversity and Design Conference*, 000110–000114 (IEEE, Niagara Falls, ON, Canada). (Cited on page 34.)

Chavali P. and Nehorai A. (**2012**). "Scheduling and power allocation in a cognitive radar network for multiple-target tracking" IEEE Transactions on Signal Processing **60**(2), 715–729. (Cited on page 34.)

Cheng Y., Wang X., Caelli T., Li X., and Moran B. (**2012**). "On information resolution of radar systems" IEEE Transactions on Aerospace and Electronic Systems **48**(4), 3084–3102. (Cited on page 58.)

Chiu S. (**1994**). "Fuzzy model identification based on cluster estimation" Journal of Intelligent and Fuzzy Systems **2**, 267–278. (Cited on page 137.)

Choudhary A., Liao W.K., Weiner D., Varshney P., Linderman R., and Linderman M. (**1998**). "Design, implementation and evaluation of parallel pipelined STAP on parallel computers" in *Proceedings of the First Merged International Parallel Processing Symposium and Symposium on Parallel and Distributed Processing*, 220–225. (Cited on pages 97 and 101.)

Choudhary A., Liao W.K., Weiner D., Varshney P., Linderman R., Linderman M., and Brown R. (**2000**). "Design, implementation and evaluation of parallel pipelined STAP on parallel computers" IEEE Transactions on Aerospace and Electronic Systems **36**(2), 528–548. (Cited on pages 97 and 101.)

Cochran D. (**2005**). "Waveform-agile sensing: Opportunities and challenges" in *Proceedings of IEEE International Conference on Acoustics, Speech, and Signal Processing, 2005. (ICASSP '05)*, volume 5, 877–880 (IEEE, Philadelphia, PA, USA). (Cited on pages 33, 36, 52 and 70.)

Cochran D., Suvorova S., Howard S., and Moran B. (**2009**). "Waveform libraries" IEEE Signal Processing Magazine **26**(1), 12 –21. (Cited on pages xiii, 23, 51, 52, 53, 60 and 70.)

Coetzee S., Woodbridge K., and Baker C. (**2003**). "Multifunction radar resource management using tracking optimisation" in *Proceedings of the 2003 International Conference on Radar*, 578–583 (IEEE, Adelaide, SA, Australia). (Cited on page 24.)

Conte E. and Longo M. (**1987**). "Characterisation of radar clutter as a spherically invariant random process" Communications, Radar and Signal Processing, IEE Proceedings F **134**(2), 191–197. (Cited on pages 127 and 129.)

Cook C.E. and Bernfeld M. (**1967**). *Radar signals: An introduction to theory and application*, Electrical Science (Elsevier, New York). (Cited on page 70.)

Cooley J.W. and Tukey J.W. (**1965**). "An algorithm for the machine calculation of complex Fourier series" Mathematics of Computation **19**(90), 297–301. (Cited on page 16.)

Cover T. and Thomas J. (**2006**). *Elements of information theory*, Wiley Series in Telecommunications and Signal Processing (Wiley). (Cited on pages 58 and 63.)

Daum F. and Fitzgerald R. (**1983**). "Decoupled Kalman filters for phased array radar tracking" IEEE Transactions on Automatic Control **28**(3), 269–283. (Cited on page 24.)

De Martino A. (**2012**). *Introduction to modern EW systems* (Boston Artech House). (Cited on page 111.)

DeBenedictis E.P. (**2017**). "It's time to redefine Moore's Law again" Computer **50**(2), 72–75. (Cited on page 101.)

Delano R. (**1953**). "A Theory of Target Glint or Angular Scintillation in Radar Tracking" Proceedings of the IRE **41**(12), 1778–1784. (Cited on page 112.)

Dempster A.P., Laird N.M., and Rubin D.B. (**1977**). "Maximum likelihood from incomplete data via the EM algorithm" Journal of the Royal Statistical Society. Series B (Methodological) **39**(1), 1–38. (Cited on page 54.)

Dennard R.H., Gaensslen F.H., Yu H.N., Rideout V.L., Bassous E., and Leblanc A.R. (**1999**). "Design of ion-implanted MOSFET's with very small physical dimensions" Proceedings of the IEEE **87**(4), 11. (Cited on page 101.)

Ding Z. (**2008**). "A survey of radar resource management algorithms" in *2008 Canadian Conference on Electrical and Computer Engineering*, 001559–001564 (IEEE, Niagara Falls, ON, Canada). (Cited on pages 16 and 19.)

Ding Z. (**2009**). "A literature survey of radar resources management algorithms" Technical Memorandum TM 2008-334, Defence R&D Canada, Ottawa, ON, Canada. (Cited on pages xiii, 16, 19 and 20.)

Ding Z. and Moo P. (**2017**). "Benefits of target prioritization for phased array radar resource management" in *2017 18th International Radar Symposium (IRS)*, 1–7 (IEEE, Prague, Czech Republic). (Cited on page 17.)

Dogandzic A. and Nehorai A. (**2001**). "Cramér–Rao bounds for estimating range, velocity, and direction with an active array" IEEE Transactions on Signal Processing **49**(6), 1122–1137. (Cited on page 71.)

Dong Y. (**2006**). "Distribution of X-band high resolution and high grazing angle sea clutter" Technical Report DSTO-RR-0316, Defence Science and Technology Organisation. (Cited on page 126.)

Dong Y. and Haywood B. (**2007**). "High grazing angle X-band sea clutter distributions" in *2007 IET International Conference on Radar Systems*, 1–5. (Cited on page 126.)

Ender J.H. and Bruggenwirth S. (**2015**). "Cognitive radar - Enabling techniques for next generation radar systems" in *2015 16th International Radar Symposium (IRS)*, 3–12 (IEEE, Dresden, Germany). (Cited on page 37.)

Evans R.J., Farrell P., Felic G., Duong H.T., Le H.V., Li J., Li M., Moran W., Morelande M., and Skafidas E. (**2013**). "Consumer radar: Technology and limitations" in *2013 International Conference on Radar*, 21–26 (IEEE, Adelaide, Australia). (Cited on page 17.)

Evans R.J., Farrell P.M., Felic G., Duong H.T., Le H.V., Li J., Li M., Moran W., and Skafidas E. (**2014**). "Consumer radar: Opportunities and challenges" in *2014 11th European Radar Conference*, 5–8 (IEEE, Italy). (Cited on page 17.)

Farina A., Gini F., Greco M.V., and Verrazzani L. (**1997**). "High resolution sea clutter data: Statistical analysis of recorded live data" IEE Proceedings - Radar, Sonar and Navigation **144**(3), 121–130. (Cited on pages 126 and 132.)

Farshchian M. and Posner F. (**2010**). "The Pareto distribution for low grazing angle and high resolution X-band sea clutter" in *2010 IEEE Radar Conference*, 789–793. (Cited on page 126.)

Feng X., Zhao Y.N., Zhao Z.F., and Zhou Z.Q. (**2018**). "Cognitive tracking waveform design based on multiple model interaction and measurement information fusion" IEEE Access **6**, 30680–30690. (Cited on page 60.)

Fitz M.P., Halford T.R., Hossain I., and Enserink S.W. (**2014**). "Towards simultaneous radar and spectral sensing" in *2014 IEEE International Symposium on Dynamic Spectrum Access Networks (DYSPAN)*, 15–19 (IEEE, McLean, VA, USA). (Cited on page 45.)

Fitzgerald R. (**1974**). "Effects of range-Doppler coupling on chirp radar tracking accuracy" IEEE Transactions on Aerospace and Electronic Systems **AES-10**(4), 528–532. (Cited on pages 69, 70, 72 and 80.)

Forsberg H., Svensson B., Ahlander A., and Jonsson M. (**2001**). "Radar signal processing using pipelined optical hypercube interconnects" in *Proceedings 15th International Parallel and Distributed Processing Symposium. IPDPS 2001*, 2043–2052 (IEEE Comput. Soc, San Francisco, CA, USA). (Cited on pages 97 and 101.)

Fuster J.M. (**2003**). *Cortex and mind: Unifying cognition* (Oxford University Press). (Cited on page 28.)

Fuster J.M. (**2006**). "The cognit: A network model of cortical representation" International Journal of Psychophysiology **60**(2), 125–132. (Cited on page 28.)

Gardner W.A., Napolitano A., and Paura L. (**2006**). "Cyclostationarity: Half a century of research" Signal Processing **86**(4), 639–697. (Cited on page 129.)

Garren D., Osborn M., Odom A., Goldstein J., Pillai S., and Guerci J. (**2001**). "Enhanced target detection and identification via optimised radar transmission pulse shape" IEE Proceedings - Radar, Sonar and Navigation **148**(3), 130. (Cited on pages 57 and 58.)

Genovese A.F. (**2001**). "The interacting multiple model algorithm for accurate state estimation of maneuvering targets" Johns Hopkins APL Technical Digest **22**(4), 614–623. (Cited on page 107.)

Ghosh A. and Ertin E. (**2010**). "Waveform agile sensing for tracking with collaborative radar networks" in *2010 IEEE Radar Conference*, 1197–1202 (IEEE, Arlington, VA, USA). (Cited on page 61.)

Ghosh S. (**2004**). "Scalable QoS-based resource allocation" Ph.D. thesis, Carnegie Mellon University, Pittsburgh, PA, USA. (Cited on page 22.)

Ghosh S., Hansen J., Rajkumar R., and Lehoczky J. (**2004**a). "Adaptive QoS optimizations with applications to radar tracking" in *Proceedings of the 10th International Conference on Real-Time and Embedded Computing Systems and Applications* (Gothenburg, Sweden). (Cited on page 22.)

Ghosh S., Hansen J., Rajkumar R., and Lehoczky J. (**2004**b). "Integrated resource management and scheduling with multi-resource constraints" in *Proceedings of 25th IEEE International Real-Time Systems Symposium, 2004.*, 12–22 (IEEE, Lisbon, Portugal). (Cited on page 22.)

Gini F. (**2000**). "Performance analysis of two structured covariance matrix estimators in compound-Gaussian clutter" Signal Processing **80**(2), 365–371. (Cited on page 126.)

Gini F., De Maio A., and Patton L.K., eds. (**2012**). *Waveform design and diversity for advanced radar systems*, number 22 in IET Radar, Sonar and Navigation Series (Institution of Engineering and Technology, London, United Kingdom). (Cited on page 45.)

Gini F., Giannakis G.B., Greco M.V., and Zhou G.T. (**2001**). "Time-averaged subspace methods for radar clutter texture retrieval" Signal Processing, IEEE Transactions on **49**(9), 1886–1898. (Cited on pages 127, 132, 134 and 143.)

Gini F. and Greco M.V. (**2001**). "Texture modeling and validation using recorded high resolution sea clutter data" in *Proceedings of the 2001 IEEE Radar Conference, 2001*, 387–392. (Cited on pages 127, 133, 134 and 156.)

Gini F. and Greco M.V. (**2002**). "Texture modelling, estimation and validation using measured sea clutter data" IEE Proceedings - Radar, Sonar and Navigation **149**(3), 115–124. (Cited on pages 125, 127, 134, 147 and 156.)

Gini F. and Rangaswamy M., eds. (**2008**). *Knowledge based radar detection, tracking, and classification* (John Wiley & Sons, Hoboken, NJ, USA). (Cited on page 33.)

Gittins J.C. (**1979**). "Bandit processes and dynamic allocation indices" Journal of the Royal Statistical Society, Series B **41**(2), 148–177. (Cited on page 21.)

Goodman N.A. (**2012**). "Adaptive waveform design for target classification" in *Waveform design and diversity for advanced radar systems*, edited by F. Gini, A. De Maio, and L. Patton, number 22 in IET Radar, Sonar and Navigation Series, 377–411 (The Institution of Engineering and Technology, London, United Kingdom). (Cited on page 58.)

Goodman N.A., Venkata P.R., and Neifeld M.A. (**2007**). "Adaptive waveform design and sequential hypothesis testing for target recognition with active sensors" IEEE Journal of Selected Topics in Signal Processing **1**(1), 105–113. (Cited on pages 34 and 58.)

Greco M.V., Bordoni F., and Gini F. (**2004**). "X-band sea-clutter nonstationarity: Influence of long waves" IEEE Journal of Oceanic Engineering **29**(2), 269–283. (Cited on pages 128 and 131.)

Greco M.V., Gini F., and Stinco P. (**2016**). "Cognitive radars: Some applications" in *2016 IEEE Global Conference on Signal and Information Processing (GlobalSIP)*, 1077–1082. (Cited on page 30.)

Greco M.V., Gini F., Stinco P., and Bell K.L. (**2018**). "Cognitive radars: On the road to reality: Progress thus far and possibilities for the future" IEEE Signal Processing Magazine **35**(4), 112–125. (Cited on page 30.)

Greenspan M. (**2014**). "Potential pitfalls of cognitive radars" in *2014 IEEE Radar Conference*, 1288–1290. (Cited on page 36.)

Griffiths H. and Baker C.J. (**2013**). "Towards the intelligent adaptive radar network" in *2013 IEEE Radar Conference (RadarCon13)*, 1–5 (IEEE, Ottawa, ON, Canada). (Cited on pages 32 and 37.)

Griffiths H.D. (**2010**). "Multistatic, MIMO and networked radar: The future of radar sensors?" in *The 7th European Radar Conference*, 81–84 (Paris, France). (Cited on page 31.)

Griffiths H.D. and Baker C. (**2005**). "Passive coherent location radar systems. Part 1: Performance prediction" IEE Proceedings - Radar, Sonar and Navigation **152**(3), 153. (Cited on page 31.)

Guerci J.R. (**2010**). "Cognitive radar: A knowledge-aided fully adaptive approach" in *2010 IEEE Radar Conference*, 1365–1370 (IEEE, Arlington, VA, USA). (Cited on pages 33 and 37.)

Guerci J.R. and Baranoski E.J. (**2006**). "Knowledge-aided adaptive radar at DARPA: An overview" IEEE Signal Processing Magazine **23**(1), 41–50. (Cited on page 37.)

Guerci J.R., Guerci R.M., Ranagaswamy M., Bergin J.S., and Wicks M.C. (**2014**). "CoFAR: Cognitive fully adaptive radar" in *2014 IEEE Radar Conference*, 0984–0989. (Cited on pages 36 and 37.)

Hansen J., Rajkumar R., Lehoczky J., and Ghosh S. (**2006**). "Resource management for radar tracking" in *2006 IEEE Conference on Radar*, 140–147 (IEEE, Syracuse, NY, USA). (Cited on page 22.)

Hansen J.P. and Lehoczky J. (**2004**). "Resource management of highly configurable tasks" in *18th International Parallel and Distributed Processing Symposium, 2004. Proceedings.*, 116–123 (IEEE, Santa Fe, NM, USA). (Cited on page 22.)

Haykin S. (**2005**). "Cognitive radar networks" in *1st IEEE International Workshop on Computational Advances in Multi-Sensor Adaptive Processing, 2005.*, 1–3 (IEEE, Puerto Vallarta, Mexico). (Cited on page 31.)

Haykin S. (**2006**). "Cognitive radar: A way of the future" IEEE Signal Processing Magazine **23**(1), 30–40. (Cited on pages 25, 26, 28, 29 and 33.)

Haykin S., Bakker R., and Currie B.W. (**2002**). "Uncovering nonlinear dynamics-The case study of sea clutter" Proceedings of the IEEE **90**(5), 860–881. (Cited on pages 127 and 128.)

Haykin S. and Puthusserypady S. (**1997**). "Chaotic dynamics of sea clutter" Chaos: An Interdisciplinary Journal of Nonlinear Science **7**(4), 777–802. (Cited on page 126.)

Haykin S., Xue Y., and Setoodeh P. (**2012**). "Cognitive radar: Step toward bridging the gap between neuroscience and engineering" Proceedings of the IEEE **100**(11), 3102–3130. (Cited on page 28.)

Haykin S., Zia A., Arasaratnam I., and Xue Y. (**2010**). "Cognitive tracking radar" in *2010 IEEE Radar Conference*, 1467–1470. (Cited on pages 33 and 100.)

Haykin S.S. (**2012**). *Cognitive dynamic systems: Perception–action cycle, radar, and radio* (Cambridge University Press, Cambridge ; New York), oCLC: ocn714728195. (Cited on pages 28 and 37.)

Henderson H.V. and Searle S.R. (**1981**). "On deriving the inverse of a sum of matrices" SIAM Review **23**(1), 53–60. (Cited on page 78.)

Hennessey G., Leung H., Drosopoulos A., and Yip P. (**2001**). "Sea-clutter modeling using a radial-basis-function neural network" IEEE Journal of Oceanic Engineering **26**(3), 358–372. (Cited on page 126.)

Hero A.O. III and Cochran D. (**2011**). "Sensor management: Past, present, and future" IEEE Sensors Journal **11**(12), 3064–3075. (Cited on pages xiii, 43, 44 and 63.)

Hero A.O. III, Kreucher C.M., and Blatt D. (**2008**). "Information theoretic approaches to sensor management" in *Foundations and applications of sensor management*, edited by A. O. Hero, III, D. A. Castañón, D. Cochran, and K. Kastella, 33–57 (Springer, Boston, MA, USA). (Cited on page 63.)

Hintz K.J. and McVey E.S. (**1991**). "Multi-process constrained estimation" IEEE Transactions on Systems, Man, and Cybernetics **21**(1), 237–244. (Cited on page 63.)

Hong S.M., Evans R.J., and Shin H.S. (**2005**). "Optimization of waveform and detection threshold for range and range-rate tracking in clutter" IEEE Transactions on Aerospace and Electronic Systems **41**(1), 17 – 33. (Cited on pages 23, 34, 51, 62 and 70.)

Hong S.M. and Jung Y.H. (**1998**). "Optimal scheduling of track updates in phased array radars" IEEE Transactions on Aerospace and Electronic Systems **34**(3), 1016–1022. (Cited on page 24.)

Horne C., Ritchie M., and Griffiths H.D. (**2018**). "Proposed ontology for cognitive radar systems" IET Radar, Sonar Navigation **12**(12), 1363–1370. (Cited on pages xiii, 25 and 26.)

Howard S.D., Suvorova S., and Moran W. (**2004**). "Waveform libraries for radar tracking applications" in *1st International Conference Waveform Diversity and Design* (Edinburgh, UK). (Cited on pages 23, 33, 34, 52, 60, 64, 65, 76 and 79.)

Huleihel W., Tabrikian J., and Shavit R. (**2012**). "Optimal sequential waveform design for cognitive radar" in *2012 IEEE International Conference on Acoustics, Speech and Signal Processing (ICASSP)*, 2457–2460 (IEEE, Kyoto, Japan). (Cited on page 70.)

Huleihel W., Tabrikian J., and Shavit R. (**2013**). "Optimal adaptive waveform design for cognitive MIMO radar" IEEE Transactions on Signal Processing **61**(20), 5075–5089. (Cited on page 70.)

Hurtado M., Gogineni S., and Nehorai A. (**2012**). "Adaptive polarization design for target detection and tracking" in *Waveform design and diversity for advanced radar systems*, edited by F. Gini, A. De Maio, and L. Patton, 454–496 (IET, Stevenage, UK). (Cited on page 56.)

Hyun E., Kim S.D., Choi J.H., Yeom D.J., and Lee J.H. (**2015**). "Parallel and pipelined hardware implementation of radar signal processing for an FMCW multi-channel radar" Elektronika ir Elektrotechnika **21**(2), 65–71. (Cited on pages 97 and 101.)

Ing K., Morelande M.R., Suvorova S., and Moran W. (**2016**). "Parametric texture estimation and prediction using measured sea clutter data" IET Radar, Sonar & Navigation **10**(3), 449–458. (Cited on page v.)

Inggs M. (**2009**). "Passive coherent location as cognitive radar" in *2009 International Waveform Diversity and Design Conference*, 229–233 (IEEE, Kissimmee, FL, USA). (Cited on page 31.)

Inggs M. (**2010**). "Passive coherent location as cognitive radar" IEEE Aerospace and Electronic Systems Magazine **25**(5), 12–17. (Cited on pages 25 and 31.)

Ioannidis G.A. and Hammers D.E. (**1979**). "Optimum antenna polarizations for target discrimination in clutter" IEEE Transactions on Antennas and Propagation **27**(3), 357–363. (Cited on page 56.)

Izquierdo-Fuente A. and Casar-Corredera J. (**1994**). "Optimal radar pulse scheduling using a neural network" in *Proceedings of 1994 IEEE International Conference on Neural Networks (ICNN'94)*, volume 7, 4588–4591 (IEEE, Orlando, FL, USA). (Cited on page 19.)

Joshi S. and Boyd S. (**2009**). "Sensor selection via convex optimization" IEEE Transactions on Signal Processing **57**(2), 451–462. (Cited on page 36.)

Jung Y.H. and Hong S.M. (**1999**). "Optimal scheduling of detection and tracking parameters for a phased array radar" in *Proceedings of the 38th SICE Annual Conference (SICE '99)*, 1111–1116 (Soc. Instrum. & Control Eng, Morioka, Japan). (Cited on page 24.)

Kalman R.E. (**1960**). "A new approach to linear filtering and prediction problems" Journal of Basic Engineering **82**(1), 35–45. (Cited on pages 77 and 106.)

Katsilieris F., Charlish A., and Boers Y. (**2012**). "Towards an online, adaptive algorithm for radar surveillance control" in *2012 Workshop on Sensor Data Fusion: Trends, Solutions, Applications (SDF)*, 66–71 (IEEE, Bonn, Germany). (Cited on page 22.)

Kay S.M. (**1993**). *Fundamentals of statistical signal processing: Estimation theory*, volume 1 of *Prentice Hall Signal Processing Series* (Prentice Hall, Englewood Cliffs, NJ, USA). (Cited on page 73.)

Kelly E.J. (**1961**). "The radar measurement of range, velocity and acceleration" IRE Transactions on Military Electronics **MIL-5**(2), 51–57. (Cited on page 69.)

Kershaw D.J. and Evans R.J. (**1994**). "Optimal waveform selection for tracking systems" IEEE Transactions on Information Theory **40**(5), 1536 –1550. (Cited on pages 23, 25, 29, 33, 50, 51, 59, 61, 62, 63, 70, 71, 93, 100 and 109.)

Kershaw D.J. and Evans R.J. (**1996**). "A contribution to performance prediction for probabilistic data association tracking filters" IEEE Transactions on Aerospace and Electronic Systems **32**(3), 1143–1148. (Cited on page 62.)

Kershaw D.J. and Evans R.J. (**1997**). "Waveform selective probabilistic data association" IEEE Transactions on Aerospace and Electronic Systems **33**(4), 1180–1188. (Cited on pages 23, 34, 59 and 100.)

Keuk G.v. and Blackman S.S. (**1993**). "On phased-array radar tracking and parameter control" IEEE Transactions on Aerospace and Electronic Systems **29**(1), 186–194. (Cited on page 24.)

Kim H.S., Goodman N., Lee C., and Yang S.I. (**2017**). "Improved waveform design for radar target classification" Electronics Letters **53**(13), 879–881. (Cited on page 58.)

Kim Y. and Ling H. (**2009**). "Human activity classification based on micro-Doppler signatures using a support vector machine" IEEE Transactions on Geoscience and Remote Sensing **47**(5), 1328–1337. (Cited on page 57.)

Kirk B.H., Narayanan R.M., Martone A.F., and Sherbondy K.D. (**2016**). "Waveform design for cognitive radar: Target detection in heavy clutter" in *Radar Sensor Technology XX*, volume 9829 (SPIE, Baltimore, MD, USA). (Cited on page 55.)

Kirk B.H., Owen J.W., Narayanan R.M., Blunt S.D., Martone A.F., and Sherbondy K.D. (**2017**). "Cognitive software defined radar: Waveform design for clutter and interference suppression" in *Radar Sensor Technology XXI*, volume 1018818 (SPIE, Anaheim, CA, United States). (Cited on page 56.)

Klauder J.R., Price A.C., Darlington S., and Albersheim W.J. (**1960**). "The theory and design of chirp radars" Bell Labs Technical Journal **39**(4), 745–808. (Cited on page 46.)

Kolodziej K.E., Perry B.T., and Herd J.S. (**2015**). "Simultaneous Transmit and Receive (STAR) system architecture using multiple analog cancellation layers" in *2015 IEEE MTT-S International Microwave Symposium*, 1–4 (IEEE, Phoenix, AZ, USA). (Cited on page 45.)

Komorniczak W. and Pietrasinski J. (**2000**). "Selected problems of MFR resources management" in *Proceedings of the Third International Conference on Information Fusion*, volume 2, 3–8 (IEEE, Paris, France). (Cited on page 20.)

Kreucher C.M. and Hero A.O. III (**2005**). "Non-myopic approaches to scheduling agile sensors for multistage detection, tracking and identification" in *Proceedings of the IEEE International Conference on Acoustics, Speech, and Signal Processing, 2005 (ICASSP '05)*, volume 5, 885–888 (IEEE, Philadelphia, PA, USA). (Cited on page 36.)

Kreucher C.M., Hero A.O. III, and Kastella K. (**2005**a). "A comparison of task driven and information driven sensor management for target tracking" in *Proceedings of the 44th IEEE Conference on Decision and Control*, 4004–4009 (IEEE, Seville, Spain). (Cited on page 61.)

Kreucher C.M., Kastella K., and Hero A.O. III (**2005**b). "Sensor management using an active sensing approach" Signal Processing **85**(3), 607–624. (Cited on page 34.)

Krishnamurthy V., Mickova J., and Evans R.J. (**1999**). "Beam scheduling for electronically scanned array tracking systems using multi-arm bandits" in *Proceedings of the 38th IEEE Conference on Decision and Control*, volume 1, 1039–1044 (IEEE, Phoenix, AZ, USA). (Cited on page 21.)

Krishnan K., Schwering T., and Sarraf S. (**2016**). "Cognitive dynamic systems: A technical review of cognitive radar" arXiv preprint . (Cited on page 28.)

La Scala B., Rezaeian M., and Moran W. (**2005**). "Optimal adaptive waveform selection for target tracking" in *2005 7th International Conference on Information Fusion*, volume 1 (IEEE, Philadelphia, PA, USA). (Cited on pages 34 and 59.)

La Scala B.F. and Moran W. (**2006**). "Optimal target tracking with restless bandits" Digital Signal Processing **16**(5), 479–487. (Cited on page 21.)

La Scala B.F., Moran W., and Evans R.J. (**2003**). "Optimal adaptive waveform selection for target detection" in *Proceedings of the International Radar Conference, 2003*, 492–496 (IEEE, Adelaide, SA, Australia). (Cited on pages 21, 54 and 56.)

LaManna M. (**2015**). "Frequency sharing techniques in a cognitive radar" in *2015 IEEE Radar Conference*, 379–382 (IEEE, Johannesburg, South Africa). (Cited on page 33.)

Lamb H. (**1932**). *Hydrodynamics*, Cambridge Mathematical Library, 6 edition (Cambridge University Press, London, UK). (Cited on page 130.)

Lee C., Lehoczky J., Siewiorek D., Rajkumar R., and Hansen J. (**1999**). "A scalable solution to the multi-resource QoS problem" in *Proceedings 20th IEEE Real-Time Systems Symposium (Cat. No.99CB37054)*, 315–326. (Cited on page 22.)

Leighton T.G., Meers S.D., and White P.R. (**2004**). "Propagation through nonlinear time-dependent bubble clouds and the estimation of bubble populations from measured acoustic characteristics" Proceedings of the Royal Society of London. Series A: Mathematical, Physical and Engineering Sciences **460**(2049), 2521–2550. (Cited on page 26.)

Leshem A., Naparstek O., and Nehorai A. (**2007**). "Information theoretic adaptive radar waveform design for multiple extended targets" IEEE Journal of Selected Topics in Signal Processing **1**(1), 42–55. (Cited on page 65.)

Leshem A. and Nehorai A. (**2006**). "Information theoretic radar waveform design for multiple targets" in *2006 40th Annual Conference on Information Sciences and Systems*, 1408–1412 (IEEE, Princeton, NJ). (Cited on page 65.)

Leung H. (**1995**). "Applying chaos to radar detection in an ocean environment: An experimental study" IEEE Journal of Oceanic Engineering **20**(1), 56–64. (Cited on page 126.)

Leung H., Dubash N., and Xie N. (**2002**). "Detection of small objects in clutter using a GA-RBF neural network" IEEE Transactions on Aerospace and Electronic Systems **38**(1), 98–118. (Cited on page 126.)

Leung H. and Lo T. (**1993**). "Chaotic radar signal processing over the sea" IEEE Journal of Oceanic Engineering **18**(3), 287–295. (Cited on page 126.)

Levanon N. and Mozeson E. (**2004**). *Radar signals* (John Wiley & Sons, Hoboken, NJ, USA), oCLC: 702600061. (Cited on pages 14, 46, 47 and 71.)

Li C., Dai H., and Li H. (**2009**a). "Adaptive quickest change detection with unknown parameter" in *2009 IEEE International Conference on Acoustics, Speech and Signal Processing*, 3241–3244. (Cited on page 54.)

Li J. and Stoica P. (**1996**). "Efficient mixed-spectrum estimation with applications to target feature extraction" IEEE Transactions on Signal Processing **44**(2), 281–295. (Cited on page 133.)

Li J., Stoica P., and Zheng D. (**1995**). "Angle and waveform estimation in the presence of colored noise via RELAX" in *Proceedings of The Twenty-Ninth Asilomar Conference on Signals, Systems and Computers*, volume 1, 433–437 (IEEE Comput. Soc. Press, Pacific Grove, CA, USA). (Cited on page 133.)

Li J., Zheng D., and Stoica P. (**1997**). "Angle and waveform estimation via RELAX" IEEE Transactions on Aerospace and Electronic Systems **33**(3), 1077–1087. (Cited on page 133.)

Li M., Evans R.J., Skafidas E., and Moran W. (**2010**). "Radar-on-a-chip (ROACH)" in *Radar Conference, 2010 IEEE*, 1224–1228. (Cited on page 17.)

Li X.R. and Jilkov V.P. (**2003**). "Survey of maneuvering target tracking. Part I: Dynamic models" IEEE Transactions on Aerospace and Electronic Systems **39**(4), 1333–1364. (Cited on pages 40 and 112.)

Li Y., Krakow L., Chong E., and Groom K. (**2006**). "Dynamic sensor management for multisensor multitarget tracking" in *2006 40th Annual Conference on Information Sciences and Systems*, 1397–1402 (IEEE, Princeton, NJ, USA). (Cited on page 60.)

Li Y., Krakow L., Chong E., and Groom K. (**2009**b). "Approximate stochastic dynamic programming for sensor scheduling to track multiple targets" Digital Signal Processing **19**(6), 978–989. (Cited on page 60.)

Liao W.K., Choudhary A., Weiner D., and Varshney P. (**2005**). "Performance evaluation of a parallel pipeline computational model for space-time adaptive processing" The Journal of Supercomputing **31**(2), 137–160. (Cited on pages 97 and 101.)

Littman M.L., Cassandra A.R., and Kaelbling L.P. (**1995**). "Efficient dynamic-programming updates in partially observable Markov decision processes" Technical Report, Brown University, Providence, RI, USA. (Cited on page 57.)

Logothetis A. and Isaksson A. (**1999**). "On sensor scheduling via information theoretic criteria" in *Proceedings of the 1999 American Control Conference*, volume 4, 2402–2406 (IEEE, San Diego, CA, USA). (Cited on page 63.)

Mahafza B.R. (**2013**). *Radar systems analysis and design using MATLAB*, 3 edition (CRC Press). (Cited on page 47.)

Martone A.F. (**2014**). "Cognitive radar demystified" URSI Radio Science Bulletin **2014**(350), 10–22. (Cited on pages xiii, 29 and 30.)

Mazor E., Averbuch A., Bar-Shalom Y., and Dayan J. (**1998**). "Interacting multiple model methods in target tracking: A survey" IEEE Transactions on Aerospace and Electronic Systems **34**(1), 103–123. (Cited on page 106.)

McAulay R. and Johnson J. (**1969**). "Optimal mismatched filter design for radar ranging and resolution" Technical Note 1969-6, Lincoln Laboratory MIT, Lexington, MA, USA. (Cited on pages 92 and 158.)

Meng H., Wei Y., Gong X., Liu Y., and Wang X. (**2012**). "Radar waveform design for extended target recognition under detection constraints" Mathematical Problems in Engineering **2012**, 1–15. (Cited on page 34.)

Metcalf J., Blunt S., and Himed B. (**2014**). "A machine learning approach to distribution identification in non-Gaussian clutter" in *2014 IEEE Radar Conference*, 0739–0744 (IEEE, Cincinnati, OH, USA). (Cited on page 55.)

Metcalf J., Blunt S.D., and Himed B. (**2015**). "A machine learning approach to cognitive radar detection" in *2015 IEEE Radar Conference (RadarCon)*, 1405–1411 (IEEE, Arlington, VA, USA). (Cited on pages 29 and 55.)

Miranda S.L.C., Baker C.J., Woodbridge K., and Griffiths H.D. (**2004**a). "Phased array radar resource management: A comparison of scheduling algorithms" in *Proceedings of the IEEE Radar Conference, 2004*, 79–84 (IEEE, Philadelphia, PA, USA). (Cited on page 22.)

Miranda S.L.C., Baker C.J., Woodbridge K., and Griffiths H.D. (**2004**b). "Simulation methods for prioritising tasks and sectors of surveillance in phased array radars" International Journal of Simulation: Systems, Science and Technology **5**(1), 8. (Cited on page 20.)

Miranda S.L.C., Baker C.J., Woodbridge K., and Griffiths H.D. (**2006**). "Knowledge-based resource management for multifunction radar: A look at scheduling and task prioritization" IEEE Signal Processing Magazine **23**(1), 66–76. (Cited on pages 20 and 21.)

Mitchell A.E., Smith G.E., Bell K.L., and Rangaswamy M. (**2017**). "Single target tracking with distributed cognitive radar" in *2017 IEEE Radar Conference (RadarConf)*, 0285–0288 (IEEE, Seattle, WA, USA). (Cited on page 35.)

Moo P.W. and Ding Z. (**2015**). *Adaptive radar resource management* (Elsevier Science). (Cited on page 19.)

Moore G. (**1998**). "Cramming more components onto integrated circuits" Proceedings of the IEEE **86**(1), 82–85. (Cited on page 98.)

Moran W., Suvorova S., and Howard S. (**2008**). "Application of sensor scheduling concepts to radar" in *Foundations and applications of sensor management*, edited by A. O. Hero, III, D. A. Castañón, D. Cochran, and K. Kastella, 221–256 (Springer US, Boston, MA, USA). (Cited on pages 62 and 63.)

Mušicki D. and Evans R. (**2004**). "Clutter map information for data association and track initialization" IEEE Transactions on Aerospace and Electronic Systems **40**(2), 387–398. (Cited on page 62.)

Mušicki D., Suvorova S., and Challa S. (**2004**). "Multi target tracking of ground targets in clutter with LMIPDA-IMM" in *Proceedings of the Seventh International Conference on Information Fusion (FUSION'04)*, 1104–1110 (ISIF, Stockhom, Sweden). (Cited on page 56.)

Mušicki D., Suvorova S., Morelande M.R., and Moran W. (**2005**). "Clutter map and target tracking" in *2005 7th International Conference on Information Fusion*, volume 1, 69–76 (IEEE, Philadelphia, PA, USA). (Cited on pages 62 and 160.)

Nalecz M., Kulpa K., Piatek A., and Wojdolowicz G. (**1997**). "Scalable hardware and software architecture for radar signal processing system" in *Radar Systems (RADAR 97)*, 720–724 (IEE, Edinburgh, UK). (Cited on page 17.)

Ng G. and Ng K. (**2000**). "Sensor management - What, why and how" Information Fusion **1**(2), 67–75. (Cited on pages 18 and 43.)

Nguyen N.H., Doğançay K., and Davis L. (**2015**). "Adaptive waveform selection for multistatic target tracking" IEEE Transactions on Aerospace and Electronic Systems **51**(1), 688–701. (Cited on pages 100 and 109.)

Nguyen N.H., Doğançay K., and Davis L.M. (**2014**). "Adaptive waveform selection and target tracking by wideband multistatic radar/sonar systems" in *Proceedings of the 22nd European Signal Processing Conference (EUSIPCO), 2014*, 1910–1914 (IEEE, Lisbon, Portugal). (Cited on page 100.)

Nieh J.Y. and Romero R.A. (**2013**). "Ambiguity function and detection probability considerations for matched waveform design" in *2013 IEEE International Conference on Acoustics, Speech and Signal Processing*, 4280–4284 (IEEE, Vancouver, BC, Canada). (Cited on page 55.)

Nieh J.Y. and Romero R.A. (**2014**). "Adaptive waveform for integrated detection and identification of moving extended target" in *2014 48th Asilomar Conference on Signals, Systems and Computers*, 1473–1478 (IEEE, Pacific Grove, CA, USA). (Cited on page 55.)

Niu R., Willett P., and Bar-Shalom Y. (**1999**). "From the waveform through the resolution cell to the tracker" in *Proceedings of the 1999 IEEE Aerospace Conference*, volume 4, 371–385 (IEEE, Aspen, CO, USA). (Cited on page 59.)

Niu R., Willett P., and Bar-Shalom Y. (**2002**). "Tracking considerations in selection of radar waveform for range and range-rate measurements" IEEE Transactions on Aerospace and Electronic Systems **38**(2), 467–487. (Cited on pages 34, 59, 70, 74, 80, 92 and 158.)

O'Connor A.C. (**2009**). "Control of observation systems with application to radar" in *2009 Chinese Control and Decision Conference*, 2140–2145 (IEEE, Guilin, China). (Cited on pages 62 and 70.)

Orman A.J. and Potts C.N. (**1997**). "On the complexity of coupled-task scheduling" Discrete Applied Mathematics **72**(1), 141–154. (Cited on page 21.)

Orman A.J., Potts C.N., Shahani A.K., and Moore A.R. (**1996**). "Scheduling for a multifunction phased array radar system" European Journal of Operational Research **90**(1), 13 – 25. (Cited on page 21.)

Papoulis A. (**1977**). *Signal analysis*, Electrical and Electronic Engineering (McGraw-Hill, New York). (Cited on page 71.)

Patini M. and Vigilante D. (**2008**). "Adaptive waveforms selection for IMM-UKF tracking architecture: Application to multifunctional radar systems in heavy cluttered scenario" in *2008 International Conference on Radar*, 536–540 (IEEE, Adelaide, Australia). (Cited on page 33.)

Perry R.P., DiPietro R.C., and Fante R.L. (**1999**). "SAR imaging of moving targets" IEEE Transactions on Aerospace and Electronic Systems **35**(1), 188–200. (Cited on page 73.)

Pillai S., Oh H., Youla D., and Guerci J. (**2000**). "Optimal transmit-receiver design in the presence of signal-dependent interference and channel noise" IEEE Transactions on Information Theory **46**(2), 577–584. (Cited on pages 57 and 58.)

Quinn B.G., McKilliam R.G., and Clarkson I.V.L. (**2008**). "Maximizing the Periodogram" in *IEEE Global Telecommunications Conference, 2008 (IEEE GLOBECOM 2008)*, 1–5 (IEEE, New Orleans, LA, USA). (Cited on page 136.)

Rago C., Willett P., and Bar-Shalom Y. (**1998**). "Detection-tracking performance with combined waveforms" IEEE Transactions on Aerospace and Electronic Systems **34**(2), 612–624. (Cited on page 54.)

Raj R.G. and Bovik A.C. (**2012**). "A nonlinear compound representation of sea clutter" in *2012 IEEE Radar Conference (RadarCon)*, 0196–0201 (IEEE, Atlanta, GA, USA). (Cited on page 127.)

Rajkumar R., Lee C., Lehoczky J., and Siewiorek D. (**1997**). "A resource allocation model for QoS management" in *Proceedings Real-Time Systems Symposium*, 298–307. (Cited on page 22.)

Rangarajan R., Raich R., and Hero A.O. III (**2006**). "Single-stage waveform selection for adaptive resource constrained state estimation" in *2006 IEEE International Conference on Acoustics Speed and Signal Processing Proceedings*, volume 3, 672–675 (IEEE, Toulouse, France). (Cited on page 36.)

Rihaczek A.W. (**1996**). *Principles of high-resolution radar*, The Artech House Radar Library (Artech House, Boston). (Cited on page 70.)

Ritchie M., Griffiths H., Watts S., and Rosenberg L. (**2014**). "Statistical comparison of low and high grazing angle sea clutter" in *Radar Conference (Radar), 2014 International*, 1–5. (Cited on page 126.)

Romero R.A., Bae J., and Goodman N.A. (**2011**). "Theory and application of SNR and mutual information matched illumination waveforms" IEEE Transactions on Aerospace and Electronic Systems **47**(2), 912–927. (Cited on page 55.)

Romero R.A. and Goodman N.A. (**2009**a). "Improved waveform design for target recognition with multiple transmissions" in *2009 International Waveform Diversity and Design Conference*, 26–30 (IEEE, Kissimmee, FL, USA). (Cited on page 55.)

Romero R.A. and Goodman N.A. (**2009**b). "Waveform design in signal-dependent interference and application to target recognition with multiple transmissions" IET Radar, Sonar & Navigation **3**(4), 328. (Cited on page 58.)

Rosenberg L. and Bocquet S. (**2013**). "The Pareto distribution for high grazing angle sea-clutter" in *2013 IEEE International Geoscience and Remote Sensing Symposium*, 4209–4212 (IEEE, Melbourne, Australia). (Cited on page 126.)

Sabatini S. and Tarantino M. (**1994**). *Multifunction array radar: System design and analysis*, Artech House Radar Library (Artech House, Boston, MA, USA). (Cited on page 17.)

Sarunic P.W. and Evans R.J. (**1997**). "Adaptive update rate tracking using IMM nearest neighbour algorithm incorporating rapid re-looks" IEE Proceedings - Radar, Sonar and Navigation **144**(4), 195–204. (Cited on page 24.)

Savage C.O. and Moran W. (**2007**). "Waveform selection for maneuvering targets within an IMM framework" IEEE Transactions on Aerospace and Electronic Systems **43**(3), 1205–1214. (Cited on pages 60 and 62.)

Scharf L.L. and Demeure C. (**1991**). *Statistical signal processing: Detection, estimation, and time series analysis*, Electrical and Computer Engineering (Addison-Wesley, Reading, MA, USA). (Cited on page 73.)

Schikorr M., Fuchs U., and Bockmair M. (**2016**). "Radar resource management study for multifunction phased array radar" in *2016 European Radar Conference (EuRAD)*, 213–216 (IEEE, London, UK). (Cited on page 17.)

Schweppe F. and Gray D. (**1966**). "Radar signal design subject to simultaneous peak and average power constraints" IEEE Transactions on Information Theory **12**(1), 13–26. (Cited on page 61.)

Selvi E., Buehrer R.M., Martone A., and Sherbondy K. (**2018**). "On the use of Markov decision processes in cognitive radar: An application to target tracking" in *2018 IEEE Radar Conference (RadarConf18)*, 0537–0542 (IEEE, Oklahoma City, OK, USA). (Cited on page 35.)

Setlur P. and Devroye N. (**2012**). "Adaptive waveform scheduling in radar: An information theoretic approach" in *Radar Sensor Technology XVI*, edited by K. I. Ranney and A. W. Doerry, volume 8361 (SPIE, Baltimore, MD, USA). (Cited on page 66.)

Setlur P., Devroye N., and Cheng Z. (**2012**). "Waveform scheduling via directed information in cognitive radar" in *2012 IEEE Statistical Signal Processing Workshop (SSP)*, 864–867 (IEEE, Ann Arbor, MI, USA). (Cited on page 66.)

Shaghaghi M. and Adve R.S. (**2018**). "Machine learning based cognitive radar resource management" in *2018 IEEE Radar Conference (RadarConf18)*, 1433–1438 (IEEE, Oklahoma City, OK, USA). (Cited on page 29.)

Shin H.J., Hong S.M., and Hong D.H. (**1995**). "Adaptive-update-rate target tracking for phased-array radar" IEE Proceedings - Radar, Sonar and Navigation **142**(3), 137–143. (Cited on page 24.)

Sira S., Papandreou-Suppappola A., Morrell D., and Cochran D. (**2006**). "Waveform-agile sensing for tracking multiple targets in clutter" in *40th Annual Conference on Information Sciences and Systems, 2006*, 1418–1423 (IEEE, Princeton, NJ, USA). (Cited on pages 23, 33, 45 and 100.)

Sira S.P., Cochran D., Papandreou-Suppappola A., Morrell D., Moran B., Howard S., and Calderbank R. (**2007**a). "Improving detection in sea clutter using waveform scheduling" in *IEEE International Conference on Acoustics, Speech and Signal Processing, 2007. (ICASSP 2007)*, volume 3, 1241–244 (IEEE, Honolulu, HI). (Cited on page 126.)

Sira S.P., Cochran D., Papandreou-Suppappola A., Morrell D., Moran W., Howard S.D., and Calderbank R. (**2007**b). "Adaptive waveform design for improved detection of low-RCS targets in heavy sea clutter" IEEE Journal of Selected Topics in Signal Processing **1**(1), 56–66. (Cited on page 54.)

Sira S.P., Li Y., Papandreou-Suppappola A., Morrell D., Cochran D., and Rangaswamy M. (**2009**a). "Waveform-agile sensing for tracking" IEEE Signal Processing Magazine **26**(1), 53–64. (Cited on pages 29, 34, 59 and 61.)

Sira S.P., Papandreou-Suppappola A., and Morrell D. (**2007**c). "Dynamic configuration of time-varying waveforms for agile sensing and tracking in clutter" IEEE Transactions on Signal Processing **55**(7), 3207–3217. (Cited on pages 23, 62 and 70.)

Sira S.P., Papandreou-Suppappola A., and Morrell D. (**2009**b). *Advances in waveform-agile sensing for tracking*, number 2 in Synthesis Lectures on Algorithms and Software in Engineering (Morgan & Claypool). (Cited on page 59.)

Skolnik M.I. (**2001**). *Introduction to radar systems*, McGraw-Hill Electrical Engineering Series, third edition edition (McGraw Hill, Boston, MA, USA). (Cited on page 45.)

Smith G.E., Cammenga Z., Mitchell A., Bell K.L., Johnson J., Rangaswamy M., and Baker C. (**2016**). "Experiments with cognitive radar" IEEE Aerospace and Electronic Systems Magazine **31**(12), 34–46. (Cited on page 35.)

Smits F., Huizing A., van Rossum W., and Hiemstra P. (**2008**). "A cognitive radar network: Architecture and application to multiplatform radar management" in *2008 European Radar Conference*, 312–315 (IEEE, Amsterdam, Netherlands). (Cited on page 31.)

Song T.L. and Mušicki D. (**2011**). "Adaptive clutter measurement density estimation for improved target tracking" IEEE Transactions on Aerospace and Electronic Systems **47**(2), 1457–1466. (Cited on page 160.)

Sowelam S.M. and Tewfik A.H. (**1994**). "Optimal waveform selection in range-Doppler imaging" in *Proceedings of 1st International Conference on Image Processing*, volume 1, 441–445 (IEEE, Austin, TX, USA). (Cited on pages 25 and 51.)

Sowelam S.M. and Tewfik A.H. (**1997**). "Optimal waveform selection for radar target classification" in *Proceedings of International Conference on Image Processing*, volume 3, 476–479 (IEEE Comput. Soc, Santa Barbara, CA, USA). (Cited on pages 57 and 64.)

Sowelam S.M. and Tewfik A.H. (**2000**). "Waveform selection in radar target classification" Information Theory, IEEE Transactions on **46**(3), 1014–1029. (Cited on pages 57 and 64.)

Stafford W.K. (**2007**). "MESAR, Sampson & radar technology for BMD" in *2007 IEEE Radar Conference*, 437–442 (IEEE, Waltham, MA, USA). (Cited on pages xiii and 18.)

Steinberg A.N. and Bowman C.L. (**2004**). "Rethinking the JDL data fusion levels" in *Proceedings of National Symposium on Sensor Data Fusion*, volume 38 (Johns Hopkins University Applied Physics Laboratory). (Cited on page 31.)

Stinco P., Greco M., Gini F., and Himed B. (**2014**a). "Channel parameters estimation for cognitive radar systems" in *2014 4th International Workshop on Cognitive Information Processing (CIP)*, 1–6 (IEEE, Copenhagen, Denmark). (Cited on page 33.)

Stinco P., Greco M.S., Gini F., and Himed B. (**2016**). "Cognitive radars in spectrally dense environments" IEEE Aerospace and Electronic Systems Magazine **31**(10), 20–27. (Cited on pages xiii, 32 and 33.)

Stinco P., Greco M.V., Gini F., and La Manna M. (**2014**b). "Compressed spectrum sensing in cognitive radar systems" in *2014 IEEE International Conference on Acoustics, Speech and Signal Processing (ICASSP)*, 81–85 (IEEE, Florence, Italy). (Cited on page 33.)

Stoica P. and Selén Y. (**2004**). "Model-order selection: A review of information criterion rules" IEEE Signal Processing Magazine **21**(4), 36–47. (Cited on page 137.)

Strömberg D. (**1996**). "Scheduling of track updates in phased array radars" in *Proceedings of the 1996 IEEE National Radar Conference*, 214–219 (IEEE, Ann Arbor, MI, USA). (Cited on page 19.)

Strömberg D. and Grahn P. (**1996**). "Scheduling of tasks in phased array radar" in *Proceedings of International Symposium on Phased Array Systems and Technology*, 318–321 (IEEE, Boston, MA, USA). (Cited on page 19.)

Suvorova S., Howard S.D., and Moran B. (**2009**). "Generalized frequency modulated waveform libraries for radar tracking applications" in *Conference Record of the Forty-Third Asilomar Conference on Signals, Systems and Computers*, 151–155 (IEEE, Pacific Grove, CA, USA). (Cited on page 24.)

Suvorova S., Howard S.D., and Moran W. (**2006**a). "Beam and waveform scheduling approach to combined radar surveillance & tracking — The Paranoid tracker" in *Proc. IEEE International Waveform Diversity and Design Conference*, 1–5 (IEEE, Lihue, HI, USA). (Cited on pages 34 and 56.)

Suvorova S., Howard S.D., and Moran W. (**2013**). "Application of Reed-Müller coded complementary waveforms to target tracking" in *2013 International Conference on Radar*, 152–156 (IEEE, Adelaide, Australia). (Cited on page 61.)

Suvorova S., Howard S.D., Moran W., Calderbank A.R., and Pezeshki A. (**2007**). "Doppler resilience, Reed-Müller codes and complementary waveforms" in *Conference Record of the 41st Asilomar Conference on Signals, Systems and Computers, 2007. (ACSSC 2007)*, 1839–1843 (IEEE, Pacific Grove, CA, USA). (Cited on page 61.)

Suvorova S., Howard S.D., Moran W., and Evans R.J. (**2006**b). "Waveform libraries for radar tracking applications: Maneuvering targets" in *40th Annual Conference on Information Sciences and Systems*, 1424–1428 (IEEE, Princeton, NJ, USA). (Cited on pages 34, 65, 70, 79 and 100.)

Suvorova S., Moran B., Kalashyan E., Zulch P., and Hancock R.J. (**2006**c). "Radar performance of temporal and frequency diverse phase-coded waveforms" in *2006 International Waveform Diversity & Design Conference*, 1–8 (IEEE, Lihue, HI, USA). (Cited on page 61.)

Suvorova S., Mušicki D., Moran W., Howard S.D., and La Scala B.F. (**2005**). "Multi step ahead beam and waveform scheduling for tracking of manoeuvering targets in clutter" in *Proceedings. IEEE International Conference on Acoustics, Speech, and Signal Processing, 2005.*, volume 5, 889–892 (IEEE, Philadelphia, PA, USA). (Cited on page 59.)

Swerling P. (**1960**). "Probability of detection for fluctuating targets" IRE Transactions on Information Theory **6**(2), 269–308. (Cited on pages 11 and 112.)

Tang B. and Tang J. (**2016**). "Robust waveform design of wideband cognitive radar for extended target detection" in *2016 IEEE International Conference on Acoustics, Speech and Signal Processing (ICASSP)*, 3096–3100 (IEEE, Shanghai, China). (Cited on page 55.)

Tichavsky P., Muravchik C.H., and Nehorai A. (**1998**). "Posterior Cramér-Rao bounds for discrete-time nonlinear filtering" IEEE Transactions on Signal Processing **46**(5), 1386–1396. (Cited on page 85.)

Turin G. (**1960**). "An introduction to matched filters" IEEE Transactions on Information Theory **6**(3), 311–329. (Cited on page 14.)

Unsworth C., Cowper M., McLaughlin S., and Mulgrew B. (**2002**). "Re-examining the nature of radar sea clutter" Radar, Sonar and Navigation, IEE Proceedings - **149**(3), 105–114. (Cited on page 127.)

Van Trees H.L. (**1968**). *Detection, estimation and linear modulation theory*, number Part 1 in Detection, estimation and modulation theory (Wiley, New York, NY, USA). (Cited on page 85.)

Van Trees H.L. (**2001**). *Radar-sonar signal processing and aussian signals in noise*, number 3 in Detection, Estimation, and Modulation Theory (John Wiley & Sons). (Cited on pages 47, 50, 51, 71 and 93.)

Vannicola V.C. (**1980**). "Optical processing for adaptive radar systems" in *Optical Signal Processing for C3l*, volume 209, 32–37 (SPIE, Boston, MA, USA). (Cited on page 36.)

Vannicola V.C. (**1990**). "Expert system for sensor resource allocation" in *Proceedings of the 33rd Midwest Symposium on Circuits and Systems*, 1005–1008 (IEEE, Calgary, Alberta, Canada). (Cited on page 20.)

Vespe M., Jones G., and Baker C. (**2009**). "Lessons for radar" IEEE Signal Processing Magazine **26**(1), 65–75. (Cited on pages 3 and 26.)

Ville J. (**1948**). "Théorie et applications de la notion de signal analytique" Câbles et Transmissions **2**(1), 61–74. (Cited on page 47.)

Vine M. (**2001**). "Fuzzy logic in radar resource management" in *IEE Multifunction Radar and Sonar Sensor Management Techniques*, volume 5, 1–4 (IEE, London, UK). (Cited on page 20.)

Wang H., Shi L., Wang Y., and Ben D. (**2013**a). "A novel target detection approach based on adaptive radar waveform design" Chinese Journal of Aeronautics **26**(1), 194–200. (Cited on page 54.)

Wang J., Dogandzic A., and Nehorai A. (**2006**). "Maximum likelihood estimation of compound-Gaussian clutter and target parameters" IEEE Transactions on Signal Processing **54**(10), 3884–3898. (Cited on page 127.)

Wang J., Qin Y., Wang H., and Li X. (**2013**b). "Dynamic waveform selection for manoeuvering target tracking in clutter" IET Radar, Sonar & Navigation **7**(7), 815–825. (Cited on page 62.)

Wang L., Wang H., Cheng Y., Qin Y., and Brennan P.V. (**2013**c). "Adaptive waveform design for maximizing resolvability of targets" in *2013 18th International Conference on Digital Signal Processing (DSP)*, 1–6 (IEEE, Fira, Santorini, Greece). (Cited on pages 58 and 64.)

Wang L., Wang H., and Qin Y. (**2014**). "Adaptive waveform design for multi-target classification in signal-dependent interference" in *2014 19th International Conference on Digital Signal Processing*, 167–172 (IEEE, Hong Kong, Hong Kong). (Cited on page 58.)

Wang L., Wang H., Qin Y., Cheng Y., and Brennan P.V. (**2013**d). "Adaptive waveform design for target classification" in *Science and Information Conference (SAI), 2013*, 680–684 (IEEE, London, UK). (Cited on pages 58 and 64.)

Ward K.D., Baker C., and Watts S. (**1990**). "Maritime surveillance radar. I. Radar scattering from the ocean surface" Radar and Signal Processing, IEE Proceedings F **137**(2), 51–62. (Cited on page 126.)

Ward K.D., Watts S., and Tough R.J.A. (**2006**). *Sea clutter: Scattering, the K-distribution and radar performance*, number 20 in IEE Radar, Sonar and Navigation Series (Institution of Engineering and Technology, London, UK), oCLC: ocm63400145. (Cited on page 126.)

Watts S. (**1987**). "Radar detection prediction in K-distributed sea clutter and thermal noise" IEEE Transactions on Aerospace and Electronic Systems **AES-23**(1), 40–45. (Cited on pages 126, 152 and 160.)

Watts S. (**1989**). "Empirical models for radar performance prediction in sea clutter" in *IEE Colloquium on Radar Clutter and Multipath Propagation*, volume 12, 1–4 (IET, London, UK). (Cited on page 126.)

Watts S. (**2000**). "The performance of cell-averaging CFAR systems in sea clutter" in *Record of the IEEE 2000 International Radar Conference*, 398–403 (IEEE, Alexandria, VA, USA). (Cited on page 152.)

Watts S. and Ward K.D. (**1987**). "Spatial correlation in K-distributed sea clutter" IEE Proceedings F Communications, Radar and Signal Processing **134**(6), 526–532. (Cited on page 126.)

Wei Y., Meng H., Liu Y., and Wang X. (**2010**). "Extended target recognition in cognitive radar networks" Sensors **10**(11), 10181–10197. (Cited on page 34.)

White K., Williams J., and Hoffensetz P. (**2008**). "Radar sensor management for detection and tracking" in *11th International Conference on Information Fusion*, volume IEEE, 1–8 (Cologne, Germany). (Cited on page 34.)

Whittle P. (**1980**). "Multi-armed bandits and the Gittins index" Journal of the Royal Statistical Society, Series B **42**(2), 143–149. (Cited on page 21.)

Wicks M.C., Mokole E.L., Blunt S.D., Schneible R.S., and Amuso V.J., eds. (**2011**). *Principles of waveform diversity and design*, Radar, Sonar & Navigation (Institution of Engineering and Technology). (Cited on pages 36 and 45.)

Williams J.L. (**2007**). "Information theoretic sensor management" Ph.D. thesis, Massachusetts Institute of Technology, Cambridge, MA, USA. (Cited on page 66.)

Williams J.L. (**2011**). "Search theory approaches to radar resource allocation" in *Proc. 7th US/Australia Joint Workshop on Defense Applications of Signal Processing (DASP)* (Coolum, Australia). (Cited on page 21.)

Williams J.L., Fisher J. III, and Willsky A.S. (**2007**a). "Performance guarantees for information theoretic active inference" in *Proceedings of the Eleventh International Conference on Artificial Intelligence and Statistics*, 620–627 (San Juan, Puerto Rico). (Cited on pages 66 and 158.)

Williams J.L., Fisher J. III, and Willsky A.S. (**2007**b). "Performance guarantees for information theoretic sensor resource management" in *2007 IEEE International Conference on Acoustics, Speech and Signal Processing (ICASSP '07)*, volume 3, 933–936 (IEEE, Honolulu, HI, USA). (Cited on pages 66 and 158.)

Willis N.J. and Griffiths H.D., eds. (**2007**). *Advances in bistatic radar* (Institution of Engineering and Technology). (Cited on page 31.)

Wintenby J. and Krishnamurthy V. (**2006**). "Hierarchical resource management in adaptive airborne surveillance radars" IEEE Transactions on Aerospace and Electronic Systems **42**(2), 401–420. (Cited on pages 19 and 36.)

Wong W. and Blair W.D. (**2000**). "Steady-state tracking with LFM waveforms" IEEE Transactions on Aerospace and Electronic Systems **36**(2), 701–709. (Cited on page 70.)

Woodbury M.A. (**1950**). "Inverting modified matrices" Memorandum Report 42, Princeton University, Princeton, NJ, USA. (Cited on page 78.)

Woodward P.M. (**1967**). "Radar ambiguity analysis" Technical Note 731, Royal Radar Establishment. (Cited on pages 23, 47, 71 and 93.)

Wright J.W. (**1968**). "A new model for sea clutter" IEEE Transactions on Antennas and Propagation **16**(2), 217–223. (Cited on page 128.)

Xiang Y., Akcakaya M., Sen S., Erdogmus D., and Nehorai A. (**2019**). "Target tracking via recursive Bayesian state estimation in cognitive radar networks" Signal Processing **155**, 157–169. (Cited on page 35.)

Xue F., Chen Q., and Zhang Y. (**2014**). "A Doppler frequency estimation algorithm based on band mismatch" in *2014 International Conference on Orange Technologies*, 77–80 (IEEE, Xi'an, China). (Cited on pages 92 and 158.)

Yang Y. and Blum R.S. (**2006**). "Waveform design for MIMO radar based on mutual information and minimum mean-square error estimation" in *40th Annual Conference on Information Sciences and Systems, 2006*, 111–116 (IEEE, Princeton, NJ, USA). (Cited on page 65.)

Yang Y. and Blum R.S. (**2007**). "MIMO radar waveform design based on mutual information and minimum mean-square error estimation" IEEE Transactions on Aerospace and Electronic Systems **43**(1), 330–343. (Cited on page 65.)

Zasada D.M., Santapietro J.J., and Tromp L.D. (**2014**). "Implementation of a cognitive radar perception/action cycle" in *2014 IEEE Radar Conference*, 0544–0547 (IEEE, Cincinnati, OH, USA). (Cited on page 98.)

Zhang H., Xie J., Shi J., Fei T., Ge J., and Zhang Z. (**2019**). "Joint beam and waveform selection for the MIMO radar target tracking" Signal Processing **156**, 31–40. (Cited on page 35.)

Zhang X., Gao Y., Wang K., and Liu X. (**2017**). "Optimal waveform design for target tracking and estimation in cognitive radar" in *2017 IEEE Radar Conference (RadarConf)*, 0175–0179. (Cited on pages 58, 61 and 100.)

Zhang X., Willett P., and Bar-Shalom Y. (**2006**). "Uniform versus nonuniform sampling when tracking in clutter" IEEE Transactions on Aerospace and Electronic Systems **42**(2), 388–400. (Cited on page 24.)

Zhao Q. and Principe J.C. (**2001**). "Support vector machines for SAR automatic target recognition" IEEE Transactions on Aerospace and Electronic Systems **37**(2), 643–654. (Cited on page 57.)

Zhu B., Gao Y., Wang K., and Liu X. (**2016**). "Optimal radar waveform design for moving target" Journal of Applied Remote Sensing **10**(3). (Cited on page 55.)

Zoutendijk G. (**1970**). *Methods of feasible directions: A study in linear and non-linear programming* (Elsevier). (Cited on page 35.)